

DUCTILITY OF THIN EXTENDED ENDPLATE CONNECTIONS

Israel Oludotun Adegoke

A thesis submitted to the Faculty of Engineering and the Built Environment,
University of the Witwatersrand, Johannesburg, in fulfilment of the requirements
for the degree of Doctor of Philosophy.

DECLARATION

I declare that this thesis is my own unaided work. It is being submitted for the Degree of Doctor of Philosophy to the University of the Witwatersrand, Johannesburg. It has not been submitted before for any degree or examination to any other University.

(Signature of Candidate)

_____ day of _____ year _____

Abstract

A model of the extended endplate behaviour has been developed in this thesis, which allows the prediction of the endplate contribution to the connection rotation in terms of the connection strength (moment capacity) and ductility (rotation capacity). The extended endplate strength model developed in this thesis is unique in that it addresses the possibility of strain hardening and membrane action in the endplate. These phenomena are shown to be critical for the ductility and strength of thin endplates, but they have not previously been modelled by other researchers. Because the leading models of the day have not catered for these effects, they seriously underestimate the strength of thin extended endplates.

The model is bi-linear, with the strength and ductility evaluated at two points – the swivel and maximum strain points. The flush region strength behaviour is based on a yield-line analysis of the endplate flush region at the swivel point, and an analysis for a plate supported on three sides and with a central point load, at the maximum strain point. The deformation of the flush region is based on the plate model. The strength and deformation of the extended region is based on uni-axial double-curvature bending of the portion between the bolt line and the weld line, for both the swivel and maximum strain points. Strain hardening and membrane action are catered for in the model by adjusting the material properties from elastic values to strain-hardening values, and by applying solutions for the deformation that takes account of large deflections and thick member theory. This makes the model developed here unique.

This thesis model is also unique in that the ductility of the endplate is measured directly by the model in a mechanical analogy. There are existing FEA and mathematical models of the moment-rotation curve, but these tend to be mostly empirical and completely opaque to the user. Comparisons with connection tests and published test results show that the ductility model developed here provides an excellent assessment of the ultimate rotations of a thin extended endplate connection.

DEDICATION

Thine, Oh Lord, is the greatness & power. Thine is the glory.

Thank you Lord God Almighty!

My deep gratitude and heartfelt thanks to my wife, Ros
and to our children, Ife, Buki & Sheba.

Thank you for being so supportive, patient and caring.

Thank you also Ojo.

You've each sown into this thesis

Acknowledgements

My supervisor Professor AR Kemp, for all his assistance over the years, and for his invaluable guidance and direction.

Mummy and Daddy and my brother and sisters for constantly supporting and encouraging me.

All my brethren in SA, Nigeria, Canada and US who have prayed for me, encouraged, cajoled, nagged or bullied me to complete this thesis. Thanks and God bless you all.

My thanks to all the individuals who assisted me with this research at some point or contributed in some fashion.

My former colleagues at the then Technikon Witwatersrand, especially Des Lange, Junior Butler, Fred Otieno, Thomas Auf der Heyde and the late Geoff Hartzenberg.

In the Wits labs: Andy Hofmeyr, Gideon Ntoagae & the late John Dyer. The late Geoff Scott, and the late Duccio Milo – my equipment suppliers.

My former students Vitor Albuquerque and ‘Sethu.

Cheryl Lombard at the National Research Foundation.

Former fellow postgrads who lent a helping hand: Sola Ilemobade and Paolo Trinchero

Professor Taigbenu, and all the others who encouraged me along the way.

Roy Mackenzie, formerly at the Steel Institute, for his support.

I gratefully acknowledge that the research in this thesis was supported financially by the following organisations at different times:

- The Southern African Institute for Steel Construction.
- The National Research Foundation.
- Technikon Witwatersrand Research Fund.
- Fluor Daniel South Africa (Pty) Ltd.

Contents

DECLARATION	I
ABSTRACT	II
ACKNOWLEDGEMENTS	IV
LIST OF FIGURES	IX
LIST OF TABLES	XIII
1. INTRODUCTION	1
1.1 BACKGROUND TO THE PROBLEM	1
1.2 PROBLEM STATEMENT	3
1.3 COMPONENTS OF EXTENDED ENDPLATE CONNECTIONS	4
1.4 DEFINITION OF KEY TERMS	6
1.5 THE CLASSIFICATION OF CONNECTIONS	7
1.6 THE LIMITATIONS OF THE STUDY	9
2. LITERATURE REVIEW	10
2.1 EARLY EXTENDED ENDPLATE MODELS	10
2.1.1 Sherbourne's Model	10
2.1.2 Surtees & Mann	13
2.2 TEE-STUB PRYING FORCE MODELS	15
2.2.1 Douty & McGuire	16
2.2.2 Nair, Birkemoe & Munse	18
2.2.3 Agerskov (1976)	19
2.2.4 Understanding the Early Research	21
2.3 COLUMN FLANGE STUDIES	22
2.3.1 Zoetemeijer's Work at Delft	22
2.3.2 Packer & Morris (1977)	26
2.3.3 Tarpy & Cardinal	27
2.3.4 Discussion of the Column Flange Studies	28
2.4 EXTENDED ENDPLATE STUDIES IN THE EIGHTIES	29
2.4.1 Krishnamurthy's Finite Element Studies	29
2.4.2 Kennedy's Split Tee Analogy	33

2.4.3	Murray's Research at Virginia Polytechnic	37
2.4.4	Some Other Relevant Models	37
2.5	THE SHIFT TO MODELLING BY COMPONENTS	41
2.5.1	By Components - Yee & Melchers' Moment-Rotation Model	41
2.5.2	Studies by Zandonini and Co-investigators	44
2.6	EUROCODE 3 ENDPLATE MODELS	50
2.6.1	Extended Endplate Model of Eurocode 3 Annex J	50
2.6.2	The Revised Annex J Model	57
2.6.3	The SCI Moment Connections Manual	61
2.6.4	The Model of BS EN 1993-1-8	62
2.7	SOUTH AFRICAN EXTENDED ENDPLATE STUDIES	65
3.	EXPERIMENTAL WORK	68
3.1	SETUP OF CONNECTION TESTS	68
3.2	THE TEST SPECIMENS	72
3.2.1	Beam and Column Material Properties	74
3.2.2	Bolt Material Properties	77
3.3	THE TEST INSTRUMENTATION	81
3.4	THE TEST PROCEDURE	85
4.	CONNECTION TEST RESULTS	87
4.1	OBSERVATIONS IN CONNECTION TESTS	87
4.1.1	Test 1 Observations	87
4.1.2	Test 2 Observations	90
4.1.3	Test 3 Observations	93
4.1.4	Discussion of Test Observations and Endplate Failure Modes	96
4.2	BEAM ROTATION DATA FROM THE CONNECTION TESTS	100
4.2.1	Moment-Rotation Curves for Connection Test 1	101
4.2.2	Moment-Rotation Curves for Connection Test 2	103
4.2.3	Moment-Rotation Curves for Connection Test 3	106
4.2.4	Discussion of Test Rotation Data	107
4.3	BOLT STRAIN GAUGE DATA	114
4.3.1	Bolt Strains and Bolt Forces Measured in the Connection Tests	114
4.3.2	Bolt Strains in Connection Test 1	117
4.3.3	Bolt Strains in Connection Test 2	120
4.3.4	Bolt Strains in Connection Test 3	122
4.3.5	Bolt Forces in the Connection Tests	124
4.3.6	Discussion of Bolt Forces	128
4.4	ENDPLATE STRAIN GAUGE DATA	131
4.4.1	Endplate Strain Gauge Data	132
4.4.2	Discussion of Endplate Strains	140

4.5	STRAIN DATA ON THE BEAM WEBS AND FLANGES	144
4.5.1	Description of Beam Web and Flange Strain Gauge Data	145
4.5.2	Discussion of Beam Web and Flange Strain Gauge Data	152
4.6	SUMMARY OF DEDUCTIONS FROM THE CONNECTION TESTS	155
5.	FE ANALYSES OF CONNECTION TEST ENDPLATES	159
5.1	FINITE ELEMENT MODELLING APPROACH	159
5.1.1.	Modelling the Endplate Geometry	159
5.1.2.	The FEA Material Models	161
5.2	RESULTS FROM THE FEA MODELS	164
5.2.1.	The FEA Model Moment-Rotation Curves	164
5.2.2.	Stresses and Deformations in the 10mm Endplate FEA Model	166
5.2.3.	Stresses and Deformations in the 12mm Endplate FEA Model	171
5.2.4.	Stresses and Deformations in the 14mm Endplate FEA Model	174
5.3	DISCUSSION OF FEA MODELS	176
6.	A MODEL OF ENDPLATE DUCTILITY	179
6.1.	INTRODUCTION	179
6.2.	THE ENDPLATE MATERIAL MODEL	182
6.2.1.	The Endplate Stress-Strain Curve in Uniaxial Tension	182
6.2.2.	The Endplate Moment-Curvature Relation	184
6.3.	DEVELOPING THE DUCTILITY MODEL EQUATIONS	188
6.3.1.	The Endplate Flush Region at the Swivel Point	188
6.3.2.	The Endplate Flush Region at the Maximum Point	197
6.3.3.	The Endplate Extended Region Flange Force	201
6.4.	AN ENDPLATE DUCTILITY MODEL	209
6.4.1.	The Stress-block Approach	209
6.4.2.	A Summary of the Ductility Model	211
7.	DISCUSSION OF DUCTILITY MODEL	214
7.1.	JUSTIFICATION OF ASPECTS OF THE DUCTILITY MODEL	214
7.1.1.	Introduction	214
7.1.2.	The Endplate Yield-line Pattern	214
7.1.3.	The Deflection of the Flush Region	217
7.1.4.	The Beam End and Bolt Contributions to Connection Rotation	224
7.2.	PARAMETERS INFLUENCING ENDPLATE BEHAVIOUR	226
7.3.	DUCTILITY MODEL COMPARISON WITH THE THESIS EXPERIMENTS	230
7.4.	MODEL COMPARISON WITH PUBLISHED TEST RESULTS	235
7.4.1.	Comparison with Test Results from Bernuzzi et al (1991)	235

7.4.2.	Comparison of Ductility Model with Eurocode 3 Model Predictions	237
7.4.3.	Comparison with Test Results from Jenkins et al (1986)	239
8.	CONCLUSION	243
8.1.	SUMMARY	243
8.2.	AREAS FOR FURTHER STUDY	245
	REFERENCES	247
	ANNEXURE A	253
A.1	MATERIAL TEST DATA	253

List of Figures

Chapter 1

Figure 1.1 – Types of endplate beam-to-column connections	4
Figure 1.2 – Components of a typical extended endplate beam-to-column connection	5
Figure 1.3 – The distinction between the connection and the joint	6
Figure 1.4 – The classification of joints in Eurocode 3	7

Chapter 2

Figure 2.1 – Sherbourne’s fixed-ended beam model	10
Figure 2.2 – Yield-line mechanism adopted in Surtees & Mann (1970)	13
Figure 2.3 – The tee-stub analogy for extended endplates	15
Figure 2.4 – Conceptualising a tee stub as a simply supported beam	16
Figure 2.5 – Tee-stub failure modes in Douty & McGuire (1965)	18
Figure 2.6 – Zoetemeijer’s parameters	24
Figure 2.7 – Zoetemeijer (1974)’s column flange collapse mechanisms	25
Figure 2.8 – Endplate geometry in Krishnamurthy (1978)	32
Figure 2.9 – Physical Parameters in Yee & Melchers (1986)	42
Figure 2.10 – Parameters Characterizing Moment-Rotation Curves (Zandonini & Zanon, 1988)	44
Figure 2.11 – Moment-Rotation Parameters in Tri-linear Representation (Bernuzzi et al, 1991)	46
Figure 2.12 – Permanent Deformation Pattern in Thin Endplates (Bernuzzi et al, 1991)	48
Figure 2.13 – Mechanism A in Bernuzzi et al (1991)	48
Figure 2.14 – Nomenclature used in Eurocode 3 (1992) Annex J	53
Figure 2.15 – Forces acting on tee-stub stiffness model in Revised Annex J	59
Figure 2.16 – Yield-line Pattern of Truby (1995), from Bernuzzi et al (1991)	65

Chapter 3

Figure 3.1 – Setup for the Connection Tests	69
Figure 3.2 – Lateral restraint of the column	70
Figure 3.3 – Supports at Test Beam ends	72
Figure 3.4 – Typical Stress-Strain Curve from an Endplate Coupon	75
Figure 3.5 – Layout of Bolt Yoke	77
Figure 3.6 – Bolt Material Test in progress	78

Figure 3.7 – Strain gauging the bolt	78
Figure 3.8 – Bolt Stress-Strain Curves	79
Figure 3.9– Test Instrumentation	81
Figure 3.10 – Strain Gauges on the Endplate and Beam End	83

Chapter 4

Figure 4.1 – Pilot Test A in progress	87
Figure 4.2 – Fractured endplate from Test 1	88
Figure 4.3 – Beams 10A and 10B after the test	89
Figure 4.4 – Cracking in Beam 12A endplate	90
Figure 4.5 – Endplate for Beam A from 12 mm Endplate Test 2	91
Figure 4.6 – 14mm endplate Test 3 in progress	93
Figure 4.7 – Endplate 14B from Test 3	94
Figure 4.8 – Extent of yielding observed in Test 2	96
Figure 4.9 – Cracks on far-side of 10mm endplate in Pilot test A	97
Figure 4.10 – Yield-line Pattern proposed in this thesis	98
Figure 4.11 – Fractured Extended Region Bolt from Pilot Test A	100
Figure 4.12 – Moment Rotation Curves for Beam 10A, Test 1	102
Figure 4.13 – Moment Rotation Curves for Beam 10B, Test 1	103
Figure 4.14 – ‘Raw’ Moment Rotation Curve for Beam 12A at joint, Test 2	104
Figure 4.15 – Moment Rotation Curves for Beam 12A, Test 2	104
Figure 4.16 – ‘Raw’ Moment Rotation Curve for Beam 12B at joint, Test 2	105
Figure 4.17 – Moment Rotation Curves for Beam 12B, Test 2	105
Figure 4.18 – Moment Rotation Curves for Beam 14A, Test 3	106
Figure 4.19 – Moment Rotation Curves for Beam 14B, Test 3	107
Figure 4.20 – Comparison of Moment Rotation Curves - Beams 10A and 10B	108
Figure 4.21 – Comparison of Moment Rotation Curves - Beams 12A and 12B	109
Figure 4.22 – Comparison of Moment Rotation Curves - Beams 14A and 14B	110
Figure 4.23 – Moment Rotation Curves for Tests 1 – 3 at the ‘Joint’	113
Figure 4.24 - Section through instrumented bolt, with strain gauge positions	114
Figure 4.25 – Orientation of Bolt Strain Gauges on Endplate	115
Figure 4.26 – Calculating the bolt ‘down’ strain	116
Figure 4.27 – Bolt Strains in Connection Test 1	119
Figure 4.28 – Bolt Strains in Connection Test 2	121
Figure 4.29 – Bolt Strains in Connection Test 3	123

Figure 4.30 – Bolt Forces for Connection Test 1	125
Figure 4.31 – Bolt Forces for Connection Test 2	127
Figure 4.32 – Bolt Forces for Connection Test 3	128
Figure 4.33 – Locations of Strain Gauges in the Endplate Extended Region	133
Figure 4.34 – Locations of Strain Gauges in the Endplate Flush Region	133
Figure 4.35 – Endplate Strains in Connection Test 1 – Beam 10A	134
Figure 4.36 – Endplate Strains in Connection Test 1 – Beam 10B	135
Figure 4.37 – Endplate Strains in Connection Test 2 – Beam 12A	138
Figure 4.38 – Endplate Strains in Connection Test 2 – Beam 12B	139
Figure 4.39 – Endplate Strains in Connection Test 3 – Beam 14A	141
Figure 4.40 – Endplate Strains in Connection Test 3 – Beam 14B	142
Figure 4.41 – Locations of Strain Gauges on the Beam Web and Flanges	144
Figure 4.42 – Strains in the Beam Webs and Flanges from Connection Test 1	146
Figure 4.43 – Strains in the Beam Webs and Flanges from Connection Test 2	148
Figure 4.44 – Strains in the Beam Webs and Flanges from Connection Test 3	151
Figure 4.45 – Strain Distribution across Beam Profile in Tests 1 and 2	155

Chapter 5

Figure 5.1 – FEA Model of Endplate Geometry	160
Figure 5.2 – Moment-Rotation Curve for 10mm Endplate FEA Model	164
Figure 5.3 – Moment-Rotation Curve for 12mm Endplate FEA Model	165
Figure 5.4 – Moment-Rotation Curve for 14mm Endplate FEA Model	166
Figure 5.5 – FEA Model Stresses in 10mm Endplate at Maximum Moment	167
Figure 5.6 – Yield-lines inferred from FEA Stresses in 10mm Endplate	168
Figure 5.7 – FEA Model Deformations in 10mm Endplate at Max Moment	169
Figure 5.8 – FEA Model Stresses in 12mm Endplate at Maximum Moment	171
Figure 5.9 – FEA Model Stresses in 12mm Endplate at Swivel Moment	172
Figure 5.10 – FEA Model Deformations in 12mm Endplate at Max Moment	173
Figure 5.11 – FEA Model Stresses in 14mm Endplate at Maximum Moment	174
Figure 5.12 – FEA Model Deformations in 14mm Endplate at Max Moment	175

Chapter 6

Figure 6.1 – Typical Bilinear Model of a Moment-Rotation Curve	180
Figure 6.2 – Idealized Material Stress-Strain Curve	182

Figure 6.3 – Changes in Stress Distribution on Member Section under Increasing Bending Moment	184
Figure 6.4 – Proposed Bi-linear Moment-Curvature Relation for the Endplate Material	187
Figure 6.5 – Idealized Yield-line Pattern Adopted for Flush Region at Swivel	188
Figure 6.6 – Detail of Assumed Yield-line Pattern	189
Figure 6.7 – Longitudinal Section through Flush Region at Swivel	191
Figure 6.8 – Transverse Section through Flush Region (Sect. X-X in Fig 6.7)	192
Figure 6.9 – Square plate model for flush region deflection	195
Figure 6.10 – Bending Moment Distribution across extended region	201
Figure 6.11 – Location of yield-lines in Extended Region	203
Figure 6.12 – Longitudinal Section through Endplate at Swivel	203
Figure 6.13 – Conceptual Model of Extended Region	205
Figure 6.14 – Longitudinal Section through Endplate at Swivel	207
Figure 6.15 – Forces and Stresses across the endplate in the Stress-block approach	209
Figure 6.16 – Nomenclature for endplate geometry in ductility model	210
Chapter 7	
Figure 7.1 – The Governing Yield-line Pattern for the Endplate	215
Figure 7.2 – Square plate model for flush region deflection	217
Figure 7.3 – Deflections for 10mm rectangular and square plate models	220
Figure 7.4 – Deflections for 12mm rectangular and square plate models	221
Figure 7.5 – Deflections for 14mm rectangular and square plate models	222
Figure 7.6 – Nomenclature for endplate geometry in ductility model	231
Figure 7.7 – Ductility Model Results for Connection Test 1	233
Figure 7.8 – Ductility Model Results for Connection Test 2	234
Figure 7.9 – Ductility Model Results for Connection Test 3	234
Figure 7.10 – Endplate Geometry in Bernuzzi et al (1991)	235
Figure 7.11 – Comparison of Ductility Model with Test EP 1-1 of Bernuzzi et al, 1991	236
Figure 7.12 – Comparison of Ductility Model with Test EP 1-2 of Bernuzzi et al, 1991	237
Figure 7.13 – Endplate Geometry in Jenkins et al (1986)	239
Figure 7.14 – Comparison of Ductility Model with Tests 4 & 15 of Jenkins et al, 1986	241
Figure 7.15 – Comparison of Ductility Model with Test 9 of Jenkins et al, 1986	241

List of Tables

Chapter 3

Table 3.1 – Nominal Dimensions for Test Section Sizes	73
Table 3.2 – Material Properties for Connection Tests	74
Table 3.3 – Actual Section Properties for Test Specimens	76
Table 3.4 – Measured Material Properties for Bolts	80

Chapter 4

Table 4.1 – Moments and rotations in connection tests 1 -3	112
Table 4.2 – Specimen Material Properties Relevant to Endplate & Beam Strains	132

Chapter 5

Table 5.1 – Material Properties for FEA Models of Endplate Behaviour	162
Table 5.2 – Comparison between FEA Results and Experimental Values	177

Chapter 6

Table 6.1 – Material Properties in Connection Tests as Dimensionless Parameters	183
---	-----

Chapter 7

Table 7.1 – Material Properties for FEA Deflection Models	219
Table 7.2 – Deflections Measured for Rectangular and Square Plate FEA Models	223
Table 7.3 – Relative Contributions of Connection Components to Maximum Rotation, in Bernuzzi et al (1991)	224
Table 7.4 – Connection Test Endplate Geometry for the Ductility Model	230
Table 7.5 – Results of the Ductility Model for the Connection Tests	231
Table 7.6 – Comparison between Ductility Model and Connection Test Results	232
Table 7.7 – Comparison between Ductility Model and Eurocode 3 Model Predictions	238
Table 7.8 – Comparison between Ductility Model and Jenkins et al Test Results	242

Annexure A

Table A.1 – Test Specimen Material Properties from Tensile Tests	254
--	-----

1. INTRODUCTION

1.1 BACKGROUND TO THE PROBLEM

From the thirties, structural engineers have been aware that the behaviour of steel-framed structures is greatly influenced by the connections (Steel Structures Research Committee, 1936). In everyday design practice however, structures are analysed either as though the connections are unable to resist any bending moment at all, (nominally ‘pinned’ connections) or as though they will carry the full moment at the end of the beam without any rotation (nominally ‘fixed’ connections). More appropriate terms for these idealisations as used in the SCI Moment Connections Manual (SCI, 1995) are ‘simple frames’ where the connections are conceptualised as pinned, and ‘continuous frames’ where the connections are considered fixed. However, many practical connections can not be considered completely pinned or fully fixed, and the SCI Manual refers therefore to ‘semi-continuous’ frames as well.

If a frame is being analysed elastically, the key property of the connection is its stiffness. For a semi-continuous frame this stiffness is finite i.e. neither zero stiffness (pinned) nor infinite stiffness (rigid), and such connections are then described as *semi-rigid*. If a frame is being analysed plastically however, the connection strength is the key property, and the semi-continuous connection is then neither zero strength (pinned) nor full strength (fixed). The connection strength of a semi-continuous connection in a plastic analysis must be less than that of all connected members, so that the connection fails first. Such a connection is said to be *partial-strength*. A partial-strength connection could also be semi-rigid in terms of its stiffness, but this is not an essential requirement. In an elastic-plastic analysis, the connections will either be semi-rigid or partial-strength, or both, for the frame to be considered semi-continuous.

The use of partial-strength connections in a plastic analysis is an attractive design option. The beam-end hinges are induced to form in the connection, which can lead to reduced beam sizes by comparison with fixed-end beams. Moreover, joint resistance is possibly independent of column size, reducing the design effort, as failure is easily guaranteed to be by a beam mechanism. Furthermore, fabricating a connection to be full strength and rigid is labour-intensive and so costly. The details could potentially be simpler and cheaper however, if the designer is able to accommodate flexibility in the connection and if the connection is partial-strength.

Partial-strength connections can lead to cost savings over pinned beams as well, as the available moment at the connection reduces the mid-span moments and so leads to a reduced beam depth. Steenhuis (1992) reported a 9% cost savings from shallower beams, due to the use of partial-strength rather than pinned connections, in a braced frame study.

The extended endplate connection is a widely used moment-resisting connection in South Africa and worldwide. It is usually assumed to be full-strength and fixed, but given the right configuration of endplate details, bolt size and beam/column sizes, this connection can behave in a semi-rigid or/and partial-strength manner. Designing the connection as semi-rigid or partial-strength could allow the use of lower beam mass or/and depth. The South African Code of Practice for steel structures, SANS 10162 (2005), provides for design based on semi-rigid or partial-strength construction, but requires the designer to show that the connection moment-rotation properties are suitable by experiments or from published experimental results. Thus, there are no established design models in the South African context.

Global (frame) elastic analysis with semi-rigid connections requires accurate knowledge of the connection stiffness as well as its moment capacity. A lot of international research effort has gone therefore into predicting semi-rigid connection stiffness and strength. Plastic frame analysis with partial-strength connections however, rather requires a knowledge of the moment capacity and the

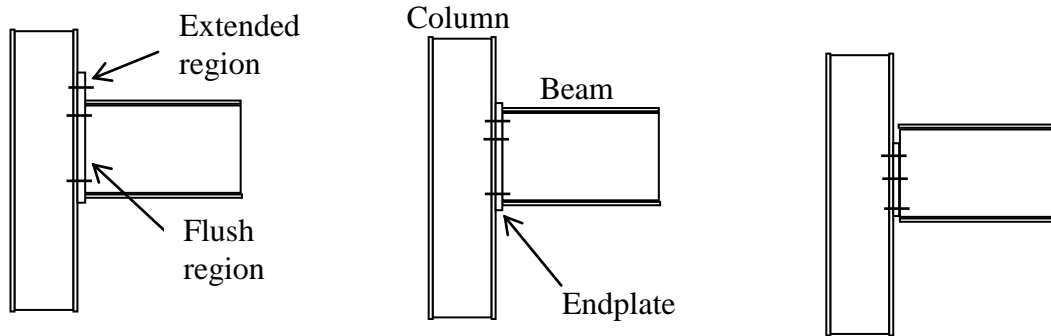
connection ductility or rotation capacity. This latter aspect of ductility has not been researched to the same degree as strength and stiffness.

Because of the popularity of the connection type, extended endplates have been extensively studied in the last thirty-five years or so. However, as shown in the next chapter, most such studies have been from a full-strength semi-rigid paradigm rather than a partial-strength paradigm. For the plastic failure of a connection to be safe, it must fail by gradual deformation (excessive rotation), rather than by brittle fracture. Ideally, therefore, failure should not be initiated in the bolts or welds, since bolt and weld fractures may be brittle and sudden, and are often catastrophic. It is preferable also to achieve the expected deformation in the endplate rather than the column flange, since it may be difficult to predict the effects that column flange deformation could have upon the carrying capacity of the column – especially in terms of buckling instability. Thus, the remaining option is to force ductile deformation of the endplate itself. The objective here therefore, is to study the ductility of a partial-strength extended endplate connection where failure initiates in the endplate.

1.2 PROBLEM STATEMENT

The problem is to develop a model of the partial-strength extended endplate beam-to-column connection that enables prediction of the ductility or rotation capacity of the connection, when the connection failure is initiated by inelastic deformation of the endplate.

1.3 COMPONENTS OF EXTENDED ENDPLATE CONNECTIONS



(a) Extended Endplate (b) Flush Endplate (c) Partial-depth

Figure 1.1 – Types of endplate beam-to-column connections

Endplate beam-to-column connections consist of a plate (the endplate) that is welded to the end of the beam profile. The endplate is then bolted on site to the column flange or web, using pre-drilled holes. In an extended endplate connection, the endplate is welded to both beam flanges as well as the web, and the endplate extends beyond one or both flanges so that some bolts lie outside the beam profile. This is illustrated in Figure 1.1(a). If the endplate covers the entire beam depth but does not extend beyond the beam, it is known as a flush endplate connection. If it does not extend beyond the full depth of the beam, it is known as a partial-depth endplate connection. In the flush and partial-depth endplates, all bolts lie generally within the beam section profile.

This study considers only extended endplate connections. The bolts lying within the beam profile are said to be in the ‘flush’ region while the bolts in the endplate extension are in the ‘extended’ region. The extended endplate of Figure 1.1 (a) is extended on one side only, and this would then be on the beam tension flange side. Where an extended endplate connection could be subjected to moments in both directions, it could be extended on both sides. Bernuzzi et al (1991) carried out tests of extended endplate connections extended on one side and nominally

identical connections extended on both sides. Their results show that for connections with identical geometry, the moment-rotation curves of the singly extended and doubly extended endplates are very similar. It has been decided here to consider only the case where the endplate is extended on one side.

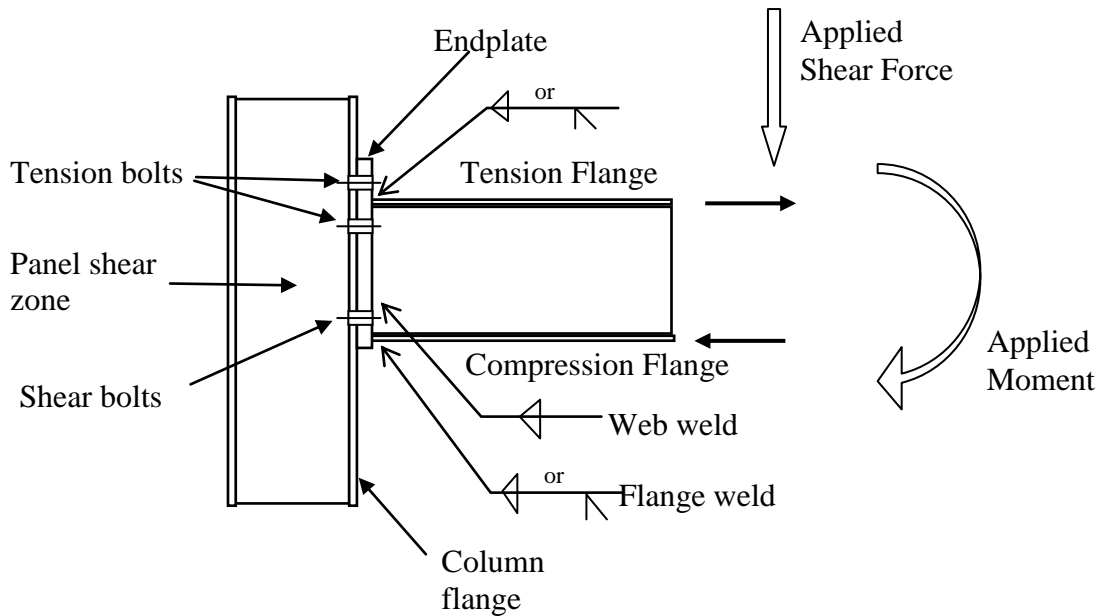


Figure 1.2 –Components of a typical extended endplate beam-to-column connection

The components of a typical extended endplate are shown in Figure 1.2. This thesis is limited to extended endplates extended on one side only, with four tension bolts disposed more or less symmetrically about the beam tension flange.

The bolt rows adjacent to the beam tension flange on either side are loaded in tension, while the lowermost (compression area) bolt row resists the shear forces. It is sometimes necessary to have an additional row for shear. There could also be more than one tension bolt row in the flush region. These other configurations are not common in SA practice and so are not considered here. It is typical to have two bolts per row (on either side of the beam web), though four bolts may sometimes be used for larger beam sizes. This study considers only the case of

two bolts per row, as this is again more common. As shown in Figure 1.2, the beam flange-to-endplate welds could be butt or fillet welds depending on moment requirements.

1.4 DEFINITION OF KEY TERMS

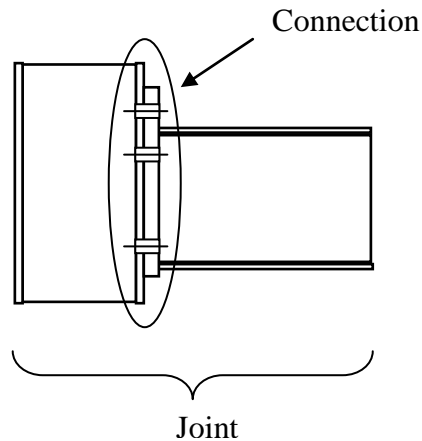


Figure 1.3 –The distinction between the connection and the joint

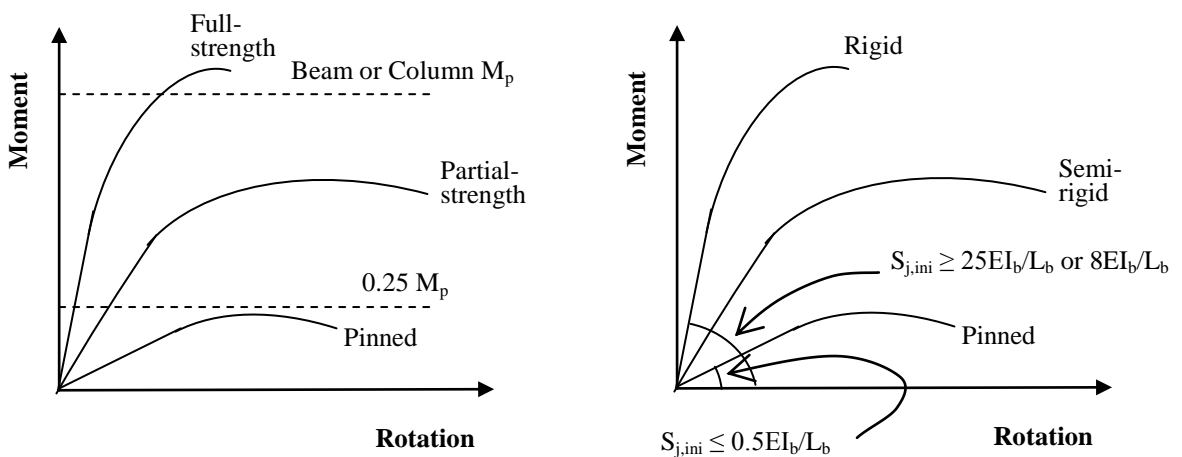
Connection vs. Joint: The term ‘connection’ properly refers to the interface between connected members. In an extended endplate beam-to-column connection, that would refer to the endplate, the column flange, the welds and the bolts. The term ‘joint’ refers to the connection as well as those parts of the connected members that are adjacent to the connection and which affect the connection. See for example, clause 1.4 of Part 1-8 of Eurocode 3 (Eurocode 3, 2005). The distinction between the two terms is illustrated in Figure 1.3. In this thesis, the joint is taken to include the portion of beam immediately adjacent to the connection up to a distance of about a beam depth from the connection. The joint is also taken to include that length of column about a beam depth and centred on the beam centreline. The terms joint and connection are however used interchangeably here, as this is in line with everyday usage.

Ductility: In a uniaxial tension test, ductility is used to refer to the deformability or extensibility of a metal. By analogy, it may be used in the case of a connection

to refer to its rotation capacity. The two terms are used interchangeably in this study. The rotation capacity of a connection is not limited to inelastic strains only, as in the uniaxial test, but all deformations of the connection components will contribute.

Endplate thickness: In this study an endplate is said to be ‘thick’ or ‘thin’ depending on whether or not the endplate undergoes elastic or plastic deformations prior to failure of the connection. In this usage, which is based on Grundy et al (1980) and Packer & Morris (1977), a connection with a ‘thick’ endplate fails from fracture of some other component (bolts or welds), before the endplate has yielded. In a connection with a ‘thin’ endplate, the endplate yields extensively prior to fracture of any connection component. An endplate may also be intermediate in behaviour between the two, with some limited yielding before a bolt or weld fractures.

1.5 THE CLASSIFICATION OF CONNECTIONS



(a) Strength classification

(b) Stiffness classification

Figure 1.4 – The classification of joints in Eurocode 3

In Eurocode 3 (Eurocode 3, 2005), joints are classified in terms of stiffness or strength. The joint stiffness criterion – pinned, rigid or semi-rigid - is applicable to elastic frame analyses, while the strength criterion – pinned, full-strength or partial-strength - is applicable to a rigid plastic frame analysis. If the frame analysis is elastic-plastic, a combination of both stiffness and strength is required for joint classification.

- Strength: Connections may be full-strength, partial-strength or nominally pinned. A full strength beam-to-column connection is able to transfer either 100% of the full beam design moment to the column or 100% of the column design moment to the beam, while a nominally pinned connection transfers less than 25% of the beam or column design moment. Thus, a joint is full-strength if the joint design moment resistance $M_{j,Rd} \geq$ the lesser of the beam plastic resistance moment capacity and the column plastic resistance moment capacity. Where the column continues to the floor above the joint, the column moment is doubled to cater for the contribution of the upper column. Likewise, a joint is defined as pinned if it transmits 25% or less of the full-strength criterion, and in addition has sufficient rotation capacity. The partial-strength connection lies between those two limits i.e. it transmits between 100 - 25% of the full-strength criterion. This is illustrated in Figure 1.4 (a).
- Stiffness or rigidity: A connection is classified as rigid, semi-rigid or nominally pinned depending on the initial rotational stiffness $S_{j,ini}$. $S_{j,ini}$ is the slope of the initial portion of the moment-rotation curve where the connection still behaves elastically. For a braced non-sway frame, a joint is considered rigid if $S_{j,ini} \geq 8EI_b/L_b$. The corresponding limit for an unbraced frame or a sway frame is $25EI_b/L_b$. I_b and L_b refer to the beam second moment of area and span, and non-sway braced frames are those where the bracing reduces the horizontal displacement by more than 80%. In relation to stiffness, a joint is considered pinned if the initial stiffness $S_{j,ini} \leq 0.5EI_b/L_b$. This applies to both sway and non-sway frames. Semi-rigid joints are defined as all joints falling between the limits for rigid and pinned joints (Figure 1.4b).

- Ductility or rotation capacity: Eurocode 3 (2005) does not classify joints in terms of rotation capacity. The rotation capacity of the joint is not calculated directly for extended endplates, but instead rules-of-thumb are given for situations where the rotation capacity may be assumed satisfactory. Following Surtees & Mann (1970) and Bose & Hughes (1995), this thesis assumes that any connection achieving a rotation of 30×10^{-3} radians is sufficiently ductile for global plastic analysis. This forms therefore, a 'limit state' threshold for ductility. Connections achieving lower rotations than this will be regarded as non-ductile. In current practice, global plastic analysis is only permitted if the frame members are Class 1 and Class 2 sections, and the members in which the plastic hinges form (except the last hinge) should be Class 1. This definition of a ductile connection implies that the need for a Class 1 section can be relaxed if the connection is ductile (achieves a rotation of 30×10^{-3} radians), as long as the plastic hinges form in the connection.

1.6 THE LIMITATIONS OF THE STUDY

This study is limited to extended endplate connections with the extension only on the side of the beam tension flange. It is also limited to the case where there are two shear bolts and four tension bolts – two in the flush region and two in the extended region – as shown in Figure 1.2. These are all assumed to be Grade 8.8 high-strength bolts. This study would therefore not apply to those large section size beams, for which four tension bolts and two shear bolts would not be adequate to transfer the load.

This study is limited to connections under static or quasi-static loads, excluding dynamic, cyclic and seismic loads.

2. LITERATURE REVIEW

Previous investigations of extended endplate behaviour are reviewed in this chapter. For consistency and ease of reference, a uniform notation is used throughout the thesis rather than the original symbols used by the respective authors. This uniform notation is based on Part 1-8 of Eurocode 3 (Eurocode 3, 2005) and on SCI (1995). Each symbol is defined at the first point of usage.

2.1 EARLY EXTENDED ENDPLATE MODELS

2.1.1 Sherbourne's Model

Sherbourne (1961) proposed an early model of the extended endplate connection. His investigation was in the context of the global plastic analysis of a frame, and he assumed that optimum economy would be obtained by allowing the connection to fail plastically at the same time as the beam. Thus, his objective was for the connection to develop exactly the full plastic moment M_p of the beam, with sufficient rotation capacity for other required plastic hinges to develop elsewhere. In other words, he wanted a model to design full-strength and ductile extended endplate connections.

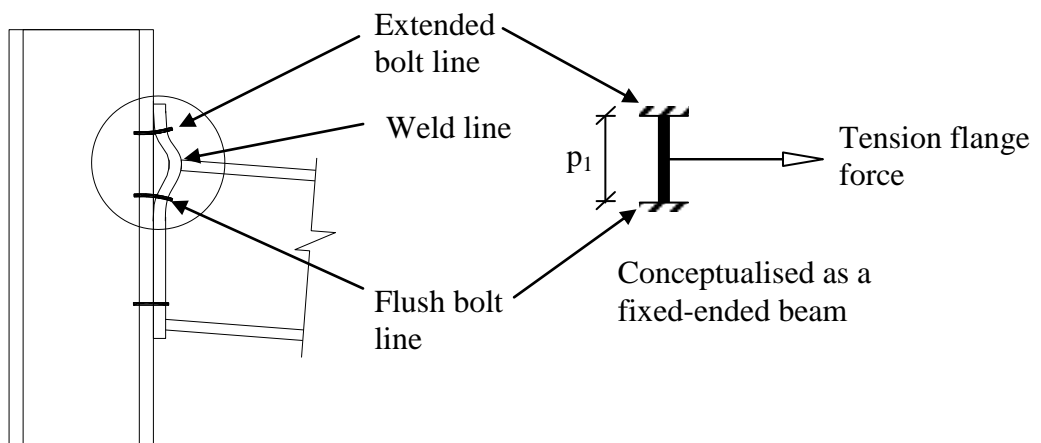


Figure 2.1 – Sherbourne's fixed-ended beam model

Sherbourne tested five extended endplate connections with varying thickness from approximately 19mm (¾") to 32mm (1¼"). Stiffener and bolt sizes were also varied. Based on his observations, Sherbourne proposed a design model for the endplate, in which the endplate was assumed to behave as a fixed ended beam spanning from the flush region tension bolt line to the extended region bolt line, with a line load at the centre applied by the beam tension flange. The model assumes a plastic collapse for this fixed-ended beam, with plastic hinges forming at the extended and flush bolt lines, and at the endplate-to-beam flange weld line. A plastic modulus is used for the internal moment of resistance but modified for shear using a Von Mises criterion. Thus, the endplate parameters taken into account are the bolt pitch p_1 , the endplate width b_p , and the endplate thickness t_p . b and t_f are the breadth and thickness respectively of the beam flange, and f_y is the material yield stress for both the beam flange and endplate.

The resulting equation (Sherbourne, 1961) is:

$$f_y b t_f \frac{p_1}{8} = \frac{b_p t_p^2}{4} \sqrt{f_y^2 - \frac{3f_y^2}{4} \left(\frac{b t_f}{b_p t_p} \right)^2} \quad \text{Eqn 2.1}$$

in which $f_y b t_f$ on the left hand side represents the force required to cause yielding of the beam tension flange. Thus, the left hand side is the theoretical collapse load (plastic beam theory) for a fixed-ended beam with span p_1 and a central point load. The right hand side of the equation represents the moment to cause plastic collapse across the breadth of the endplate, modified for shear.

The beam flange yield stress (f_y on the left) is taken equal to the endplate yield stress (f_y on the right), so that the equation can be simplified to:

$$\left(\frac{b t_f}{b_p t_p} \right)^2 \left[\left(\frac{p_1}{2 t_p} \right)^2 + \frac{3}{4} \right] = 1 \quad \text{Eqn 2.2}$$

The bolts on either side of the tension flange are assumed to restrain the endplate completely, and the bolts are sized by assuming them all to be equally stressed

and to be fully loaded (proof or yield load) at the same time as the beam tension flange. Hence the bolt thread area A_s is given by:

$$A_s = \frac{bt_f}{4} \cdot \frac{f_y}{f_{yb}}$$

where f_{yb} is the proof stress for the bolts.

Thus, the bolts yield as the plate plastic hinge is formed.

It seems then that Sherbourne's model is essentially a one-dimensional plastic beam model assuming double curvature in both the extended and flush regions. This is illustrated by the longitudinal profile of the endplate in Figure 2.1. Since the flush and extended regions are assumed to behave identically, the stiffening effect of the beam web is ignored and the endplate tension area is effectively considered a tee-stub (though Sherbourne did not use that term). The use of a simple plastic hinge implies a rigid-perfectly plastic material model, so that strain-hardening effects are excluded. Sherbourne noted in his experiments with thin endplates that the tension bolts in the flush region may attract more load than the bolts in the extended region. However, he made no attempt to account for this in the model formulated. Neither did he make any mention of prying forces in the bolts.

A criticism of Sherbourne's model is that it can seriously underestimate the flange tension force at the plastic moment M_p of the beam, since it is quite evident that the maximum tension force at M_p may greatly exceed the force $f_y \cdot bt_f$ to cause yield in the tension flange. Besides the fact that the contribution of the web is ignored, the beam flange may sustain loads well beyond the first yielding condition, until the beam forms a plastic hinge adjacent to the connection or the compression flange fails in local buckling.

Despite stating the need for the connection to be full-strength, Sherbourne recognised the value of designing the connection to fail inelastically rather than the beam end, so that he was really catering for a partial-strength connection. As

endplate due to the presence of the web. In their model, they assumed the flush yield-lines to extend a distance of $0.5d_f$, where d_f is as shown in Figure 2.2. This would imply that the ‘neutral axis’ for bending of the endplate is at that depth.

They recorded carbon-backed imprints of the endplate-column contact surface during tests, which showed indeed that the compression zone was triangular with a base along the beam compression flange and an apex along the lower web. However, in the photograph provided in their paper, the apex only extended to the level of the shear bolts.

Surtees and Mann proposed equations for obtaining the endplate thickness and the bolt sizes. Sherbourne’s model served as their point of departure, but they omitted the shear modification in the expression for M_p in Sherbourne’s equation for endplate thickness. They also calculated the maximum tension force as the ratio M_p/d_f rather than equating it to the beam flange tension capacity at yield. d_f is the depth between centres of the beam flanges i.e. the beam total depth D minus the beam tension flange thickness t_f . The most radical difference however was that Surtees and Mann based the internal moment of resistance on a plate yield-line mechanism rather than on Sherbourne’s beam analysis, though they still assumed the extended bolts to restrain the endplate completely. Thus, they effectively treated the extended region as half of a fixed-ended beam.

Their resulting equation (Surtees & Mann, 1970) for endplate thickness t_p was:

$$t_p = \sqrt{\frac{M_p}{16d_f \left(\frac{2b_p}{p_1} + \frac{d_f}{p_2} \right)}} \quad \text{Eqn 2.3}$$

where d_f is the depth between centres of the beam flanges and p_2 is the bolt gauge distance. They explained that this equation leads to generally thinner endplates than Sherbourne’s. A second radical change in Surtees & Mann from Sherbourne’s proposals was that they considered the possibility of prying action, catering for this with an empirical 30% increase in the bolt load. Thus, the bolts are to be sized for a force P , where:

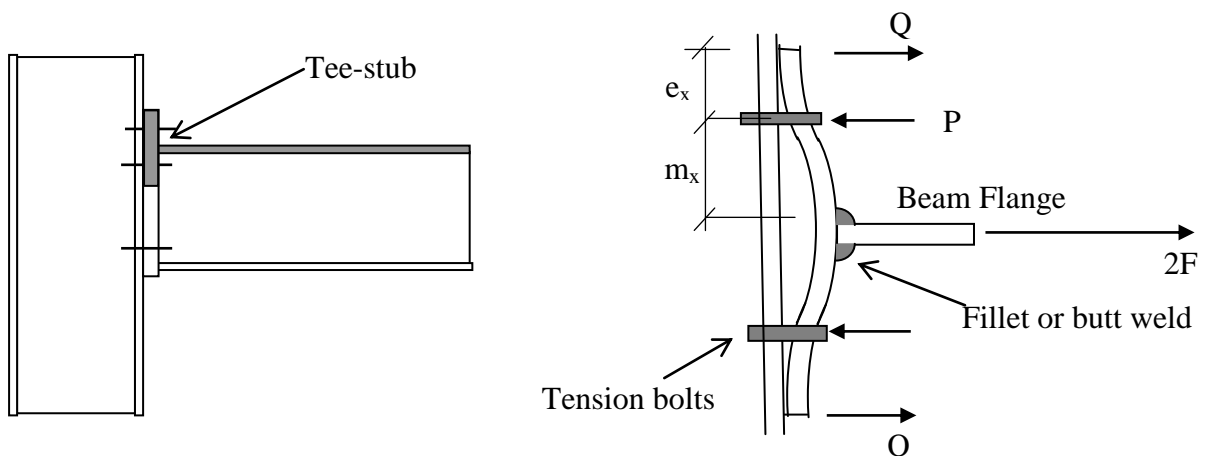
$$P = \frac{M_p}{4d_f} \times 1.3 \approx \frac{M_p}{3d_f} \quad \text{Eqn 2.4}$$

However, they also recommended that this bolt load be equated to the ultimate tensile capacity of the bolt rather than the proof load as suggested by Sherbourne. This would mean an effective increase of about 22% in bolt size as compared to Sherbourne's model. The adoption of an ultimate criterion was considered better as it leads to an earlier redistribution of forces between the tension bolt rows.

Surtees & Mann (1970) demonstrated that a connection rotation of 30×10^{-3} radians is a reasonable value for the required connection rotation for plastic analysis of a structure failing in a beam mechanism. That value is therefore adopted in this thesis as the limit value for the ductile – non-ductile distinction.

2.2 TEE-STUB PRYING FORCE MODELS

Working at about the same time as Surtees & Mann, other investigators were researching the assessment of prying forces. Most of this research was based on an analogy between the extended region of the endplate and tee-stubs, since it is easier to conceptualise and estimate prying action with tee-stubs.



(a) Idealisation of tension region as a tee-stub.

(b) Enlarged view of 'tee-stub', in flexure under load. Flange force is $2F$, prying force is Q , and bolt force is P .

Figure 2.3 – The tee-stub analogy for extended endplates

The extended region of the endplate, or/and the column flange in the tension region, is considered to behave like a tee profile with four bolts placed symmetrically around the stem. This is illustrated in Figure 2.3.

2.2.1 Douty & McGuire

In the United States, Douty & McGuire’s investigation at Cornell University (Douty & McGuire, 1965) was initially into tee-stub connections. However, they recognised the close resemblance between the tee-stub and the tension part of the extended endplate, and drew an analogy between both connections. Their tee-stub model led to the computation of the prying force in the extended bolt – either at working load or at ultimate load. Their prying force derivation is involved, based on the initial elastic deformation of the endplate around the bolts due to the bolt pretension, and also including the initial bolt elongations. This analytical model was derived from an assumption of the tee flange behaving as a simply supported elastic beam, spanning across the flange ends, with the equations derived from compatibility of deformation principles, but modified for design based on their observations. This is shown in Figure 2.4.

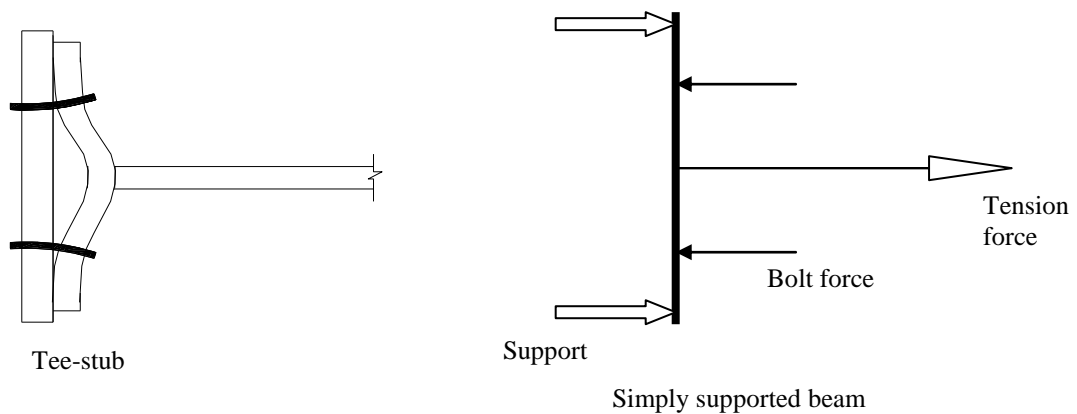


Figure 2.4 – Conceptualising a tee stub as a simply supported beam

The semi-empirical prying force Q at ultimate load was given by Douty & McGuire (1965) as:

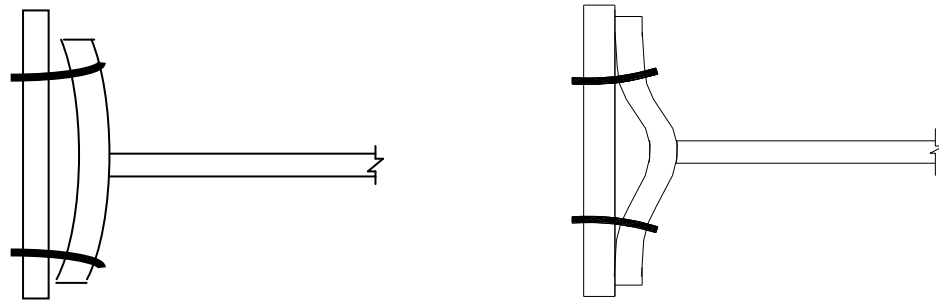
$$Q = \left[\frac{\frac{1}{2} - \frac{b_p t_p^4}{30e_x m_x^2 A_s}}{\frac{e_x}{m_x} \left(\frac{e_x}{3m_x} + 1 \right) + \frac{b_p t_p^4}{6e_x m_x^2 A_s}} \right] F_u = k_2 F_u \quad \text{Eqn 2.5}$$

in which Q is the prying force, and b_p and t_p are the width and thickness respectively of the endplate. The end distance e_x for the extended bolt row, and the effective distance m_x between the extended bolts and the weld line, are as shown in Figure 2.3. A_s is the bolt effective area and F_u is the ultimate force in the beam flange.

Once the prying forces were obtained, the total bolt forces could be checked to ensure that bolt fracture does not govern failure. The endplate (or tee-stub flange) thickness was then checked to ensure that the maximum bending stress does not exceed the plastic value of $4M_p/t_p^2$, in which the bending moment M is taken at the bolt line or the weld line, whichever is higher. The bolt and weld line moments are calculated by taking moments for the prying force Q about the bolt line and for Q and the total bolt force about the weld line. Thus, their inelastic endplate model was derived from the assumption of a simply supported beam, but with a maximum plate moment of M_p either at the bolt line or the weld line, or at both.

Like Sherbourne in England, Douty & McGuire (1965) were essentially applying a one-dimensional yield mechanism model, assuming double-curvature bending in the inelastic phase - though Douty & McGuire did not include Sherbourne's modification of the plastic moment for shear. Their external applied moment however is based on the calculated prying force and the corresponding restraining couple, rather than on an assumption of full fixity at the bolt lines. As in Sherbourne, the maximum connection load would occur when the bolt-line and weld line moments are both at M_p so that a mechanism forms. Douty & McGuire pointed out that much higher endplate (or flange) moments than M_p were observed in practice, and this was thought to be due to strain hardening. However, their model ignores this strain hardening effect. The prying force value was also rather sensitive to the assumed location of the prying forces, which location was

found to be rather uncertain. Douty & McGuire clearly differentiated between two failure modes in the tee-stub flange – one in which the two tee-stubs separated before yielding of the flange set in, and a second where yielding took place before the stubs separated, so that a mechanism formed. These are shown in Figure 2.5. They considered the first a condition to be avoided as it led to ‘thick’ endplates, and their aim was for the connection to fail in the second mode as a ‘thin’ endplate.



(a) Tee-stubs separate first

(b) Tee-stubs yield first

Figure 2.5 – Tee-stub failure modes in Douty & McGuire (1965)

2.2.2 Nair, Birkemoe & Munse

Nair et al (1974) investigated the sensitivity of prying action in tee-stubs to changes in the bolt pitch and the end distance, and also considered the effect of cyclic fatigue loads. They found that the prying forces in the bolts increased with the bolt pitch, particularly at intermediate values of end distance. The prying was also more pronounced for A490 bolts than for A325 bolts (higher strength steel). They went on to carry out a 2-dimensional FEA study of the connection to further study the parameters. Based on the FEA results, a semi-empirical model was derived for the prying force. By idealizing the connection as a simply supported beam with the prying forces as reactions at the edges of the tee-stub flange, and the web load and bolt forces as applied loads, a model was derived. The model assumed that bolt failure would be critical at a bolt load including prying, such that the prying force Q (Nair et al,1974) would be obtained from:

$$\text{Prying ratio} = \left(\frac{Q}{P} \right) = \frac{\frac{p_1}{2} - \beta \frac{b_p t_p^2}{d^2}}{e_x + \beta \frac{b_p t_p^2}{d^2}} \quad \text{Eqn 2.6}$$

In this equation, β is an empirically-derived constant for a given endplate yield stress and bolt type, b_p and t_p are the width and thickness respectively of the plate, and d is the bolt diameter. P is the bolt force from the flange loading only, and e_x is the end distance from the bolt line to the edge of the tee flange, measured perpendicular to the web. Q , P and e_x are as illustrated in Figure 2.3. The distance p_1 is the span from the bolt line on one side to the bolt line on the other i.e. the bolt pitch.

Once the prying ratio is obtained, the ultimate load P_u per bolt is calculated as:

$$P_u = \frac{F_{ub}}{1 + \left(\frac{Q}{P} \right)_u} \quad \text{Eqn 2.7}$$

where F_{ub} is the ultimate capacity of each bolt in tension.

An obvious drawback of this model is that it is based on bolt failure as the critical failure mode, and this brittle failure mode is of course not desirable. It seems therefore that these researchers took for granted that the resulting connection from their model would only be applied as a full-strength connection. The research of Nair, Birkemoe & Munse was incorporated in the design model of the seventh edition of the American AISC Manual.

2.2.3 Agerskov (1976)

In Europe, Agerskov (1976) reported on an investigation of tee-stubs and beam-to-beam endplate connections, in which the theory presented by Douty & McGuire (1965) was used as a point of departure. By measuring the bolt forces in his experiments, Agerskov determined the moments on the bolt line and on the weld line. He came to the conclusion that after an initial yielding of the endplate on the weld line, the moment increases there due to strain hardening, but the bolt

line moment does not increase due to a drop in prying force - the prying force dropping as a result of reduced stiffness from the endplate yielding. He therefore rejected the mechanism model that had been advocated by earlier authors, rather conceptualising failure as first yield on the weld line.

To develop a model, Agerskov also treated the tee-stub as a simply supported beam spanning across the flange ends, but with a hinge developing only at the center (weld line). The unknown bolt and prying forces were obtained from equilibrium conditions, and by considering compatibility of deformation at the bolt locations in a similar manner to Douty & McGuire. For the deformation equation, Agerskov went to considerable effort to include the deformations of the washer, nut and bolt shank, equating these to the elastic deformation of the endplate at that location, using elastic bending theory for a simply supported beam. In deriving the yield moment at the weld line, Agerskov referred back to Sherbourne and included a reduction for shear, also using the Von Mises criterion.

In essence, Agerskov was really considering a third failure mode, different from and intermediate between the two considered by Douty & McGuire (1965). Such an intermediate mode would apply if the bolt sizes were not large enough to restrain the endplate sufficiently for a hinge to form at the bolt line, but yet the bolts were too strong for the tee-stubs to separate before the weld line and bolt line yielded. It seems very unlikely though that the elastic beam deformation equations assumed by Agerskov would be applicable over such small spans, particularly after the weld line moment approaches or exceeds the yield moment M_y . This is probably why Agerskov defined failure as the onset of yielding on the weld line. Nevertheless his model is conceived as an elastic one rather than a plastic one (in terms of the connection components) and so there is a large reserve of strength due to the observed strain hardening, which is ignored.

2.2.4 Understanding the Early Research

By now two distinct streams of enquiry or research were emerging. On the one hand there were researchers such as Sherbourne and Surtees and Mann, who tried to model endplate connections directly, and who conceptualised the extended region of the endplate as half of a fixed ended beam terminating at the bolt line. On the other hand, there were researchers such as Nair et al and Agerskov, who concentrated more on tee-stubs and the tee-stub analogy, and who tended to conceptualise this as a simply supported beam extending to the edge of the plate. The former group of researchers tended to ignore prying forces or to assess them using simple rules of thumb, while the latter group went to considerable trouble to calculate the prying forces exactly on tee-stubs. The prying action assumptions for tee-stubs were then ‘extrapolated’ to extended endplates.

A fundamental difference between Sherbourne, Surtees and Mann on the one hand, and the other researchers developing prying force models on the other, was the objective in design. Sherbourne and Surtees and Mann started from an ultimate strength paradigm in which plastic collapse of the endplate was the goal. The prying force researchers were more in a working load paradigm, though trying to account for ultimate load conditions. Douty & McGuire derived their prying force equation using an elastic formulation, but then applied these elastic prying forces to the inelastic endplate model. As shown by Agerskov, prying forces are significant in the elastic phase but not after the endplate has yielded. For Sherbourne and his colleagues, a plastic mechanism in the endplate was the fundamental starting point - and if one assumes that there is a plastic hinge along the bolt line as assumed by both Sherbourne and Surtees & Mann, there would be no need to measure the prying force to calculate the bolt line moment. There is therefore also no need to investigate beyond the area bounded by the weld line and the bolt line in the extended region.

Of course, Sherbourne's approach is only valid if the endplate is thin enough to allow the endplate to yield sufficiently on the bolt line (see the two failure modes identified by Douty & McGuire). Moreover, the assumption of a plastic hinge at the bolt line is only feasible at ultimate load. If the behaviour at working loads is considered important (in order to assess initial stiffness and limit deflections, or to allow a semi-continuous analysis of the frame) then a model that includes the prying force may be more appropriate. In the prying force literature, all these researchers showed experimentally that the moment on the bolt lines may not reach M_p under certain conditions, which would invalidate the assumptions of Sherbourne and Surtees and Mann. This implies that there is more than one failure mechanism. It would seem that the failure mechanism is linked to how thin the endplate is and how strong the bolts are. Thus, the important questions at this stage were to determine the conditions under which the bolt line moment will attain M_p , and the conditions under which the weld line moment remains at M_p or increases through strain hardening. A third question of interest prompted by Surtees & Mann's yield-line pattern is whether or not a tee-stub adequately represents the flush region behaviour in the endplate.

2.3 COLUMN FLANGE STUDIES

Parallel to the developments in understanding the contribution of the endplate, other researchers were emphasising the effects of column deformation in their investigations. The next three papers reviewed made major contributions in assessing the column flange deformation.

2.3.1 Zoetemeijer's Work at Delft

Zoetemeijer (1974) reported on a detailed investigation of tee-stub connections in which the connections are initially symmetrical about the contact surface of each individual tee-stub. His model of the tee-stub flange was a one-dimensional collapse analysis, idealized as a simply supported beam with a plastic hinge of magnitude M_p at the weld line, and with a second plastic hinge possibly

developing at the bolt line. He considered two possible patterns of failure – collapse Mechanism A in which the bolt line plastic hinge does not develop (although the weld line one does) and failure is by fracture of the bolts, and Mechanism B in which both plastic hinges develop and failure is by excessive deformation of the tee-stub flange. Thus, Mechanism A is similar to Agerskov's (1976) failure mode. Douty & McGuire's (1965) first mode is subsumed in Mechanism A as a third possibility, in which the endplate is so thick that the tee-stub flanges separate before any flange yielding, and the assembly fails by bolt fracture.

From a consideration of static equilibrium of the forces on the tee-stub, Zoetemeijer found that at one extreme when the prying force is zero (collapse Mechanism A – Douty & McGuire, 1965), then:

$$T_u \times m = M_p \Rightarrow t = 2 \sqrt{\frac{T_u m}{b f_y}} \quad \text{Eqn 2.8}$$

where $m = p_1/2$ (half the bolt pitch) and b is the width of the tee-stub. T_u is the ultimate tension load on half of the tee-stub and t is the tee-stub thickness.

At the other extreme, when the prying force is at a maximum (collapse Mechanism B), then:

$$T_u \times m = M_p + M'_p \Rightarrow t = 1.41 \sqrt{\frac{T_u m}{b f_y}} \quad \text{Eqn 2.9}$$

The first equation corresponds to the minimum plate thickness for the smallest bolt size at a given connection load (no prying), while the second equation corresponds to the maximum plate thickness to ensure plate failure for the same connection load, but using the largest bolt diameter. (M_p and M'_p are plastic moments at the weld and bolt lines respectively). In the first case bolt diameter is obtained from $\Sigma F_{ub} \leq T$, but in the latter from $\Sigma F_{ub} \geq T + M_p/e$ - where F_{ub} is the ultimate capacity of a bolt and e is the edge distance to the edge about which prying is taking place. Thus, Zoetemeijer demonstrated that the designer can control the failure mode quite easily by varying the plate thickness and bolt size for a given plate and beam geometry. He also demonstrated that larger (stronger)

bolts combined with thin plates are required to develop M_p in the plate for double curvature plate collapse, but thicker plates will eliminate prying and cause failure by bolt fracture.

For cases where the prying force is between these extremes, the two conditions to be satisfied (Zoetemeijer, 1974) are:

$T_u \times m - (\sum F_{ub} - T)e \leq M_p$ where $(\sum F_{ub} - T) \geq 0$ else $T = \sum F_{ub}$ if bolt fracture is the determining factor, and

$T_u \times m \leq M_p + M'_p$ if excessive plate deformation is the determining factor.

When a tee-stub is connected to a column flange however, the connection is not symmetrical about the connected faces, for though the portion of the column in contact may be idealized as a second tee-stub, this second tee-stub is rotated at 90 degrees to the first. Thus, the above equations that were developed for the symmetrical case cannot be applied without careful consideration.

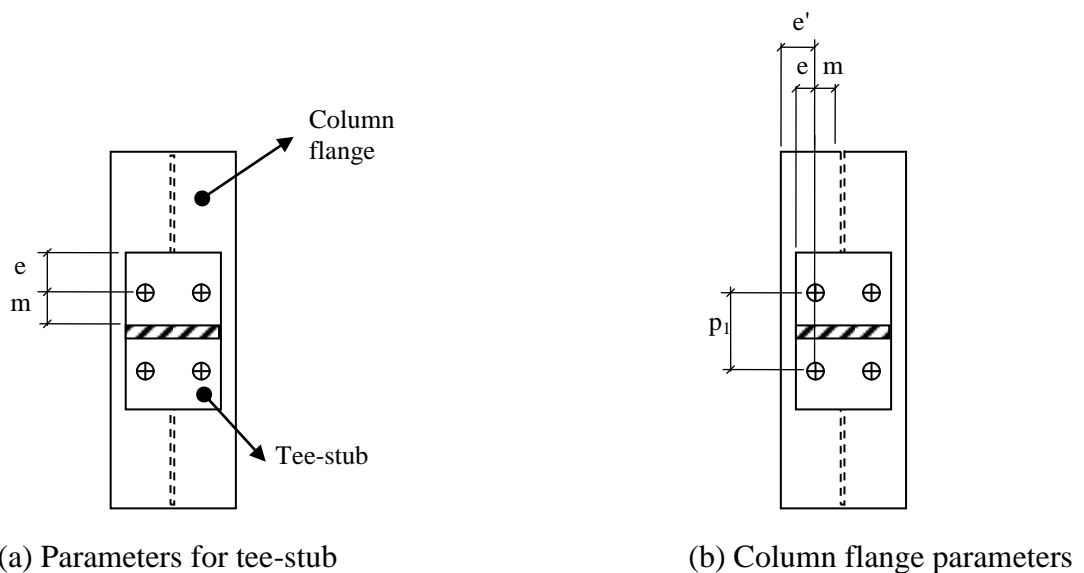


Figure 2.6 – Zoetemeijer’s parameters

Nevertheless, Zoetemeijer showed that these equations could be applied to the column flange and the tee-stub independently, to obtain separate values for the limiting value of T_u for a mechanism to form. The mechanism would form first in

whichever component has the more flexible flange – the column or the tee-stub. Thus, the flange with the lower value of T_u would be the critical one for failure.

The column flange is always wider than the tee-stub flange, and this raised a question about what would be an acceptable value for e (now the edge distance from the bolt holes on the column flange) to use in the above equation. The assumption that prying would take place at the edge of the tee-stub parallel to the column flange edge dictated that that distance be used to mark e . Zoetemeijer suggested that e should not be taken as greater than $1.25m$. To distinguish e in the equations from the actual edge distance, the edge distance was denoted e' (see Figure 2.6). Also, because the column flange has a fillet of radius r at the flange-web junction, m was taken as being from the face of the web but minus $0.8r$.

To apply his two equations above to column flanges, Zoetemeijer needed to calculate M_p for the column flange. This required a decision as to what length of the column was actually yielding. He used the concept of a participating or ‘effective length’ of column flange, which was decided by energy considerations from studying the yield-line mechanisms for collapse of the column flange.

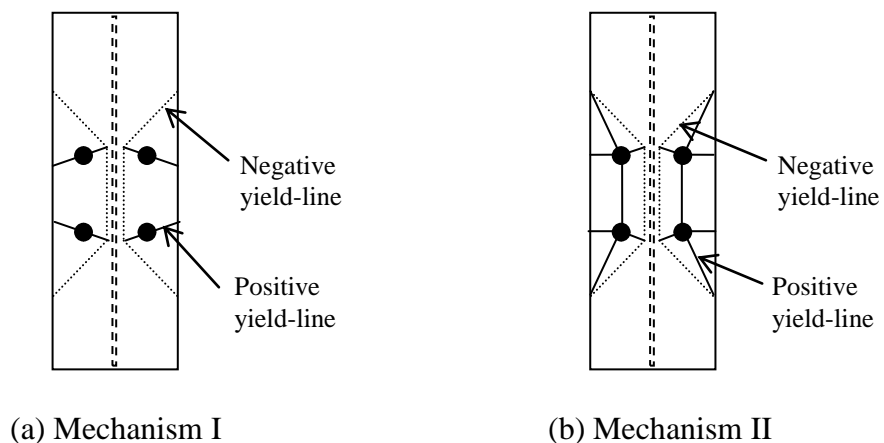


Figure 2.7 – Zoetemeijer (1974)'s column flange collapse mechanisms

Two collapse mechanisms were considered for the column flange (see Figure 2.7), which he tagged Mechanism I and II. Mechanism I was analogous to Mechanism

A in the tee-stub and resulted in bolt fracture. Mechanism II was analogous to Mechanism B in the tee-stub and resulted in excessive deformation of the column flange. The resulting participating column length he proposed was a value of:

$$\text{Participating length} = p_1 + 4m + 1.25e'$$

where p_1 is the bolt pitch. This participating length is then multiplied by the plastic moment per unit length to obtain M_p .

Zoetemeijer then investigated the effect of stiffening the column flanges with backing plates to reduce column flange deformations. He showed that the two possible collapse mechanisms in the column flange would not be altered by the presence of backing plates, though the plastic moment per unit length would change on some of the yield-lines. He did not attempt to justify this approach analytically, but argued that the predictions of this equation were in accordance with experiments conducted.

2.3.2 Packer & Morris (1977)

Packer & Morris (1977) took a similar approach to Zoetemeijer (1974) and concentrated on the column flange deformation, also assuming that shear deformations were negligible. They separated Zoetemeijer's tee-stub Mechanism A into two failure modes. Thus, their own Mechanism A was for really thick tee-stubs where there is no tee-stub yielding at all, and the bolts fail in fracture. Their Mechanism B was then the case where the tee-stub flange yields along the weld line but not the bolt line, and then the bolts fracture. Finally, the case where both weld line and bolt line yield, and the tee-stub collapses, was referred to as Mechanism C. The equation for Mechanism A was that:

Bolt ultimate capacity = the total tension force divided by 4 i.e. $F_{ub} = T/2 = F/4$.

For Mechanisms B and C they retained the tee-stub equations proposed by Zoetemeijer.

In applying the equations for Mechanisms B and C to column flanges (referred to as Mechanisms I and II respectively by Zoetemeijer), Packer & Morris adopted circular yield-lines in the corners of the patterns, rather than the straight lines

investigated by Zoetemeijer. The basis for this was that their experimental observations showed a circular rather than a straight pattern. For Mechanism B they obtained the equation:

$$F = 2T = t_{fc}^2 \cdot f_{yc} \{3.14 + 0.5p_1 / (m + e)\} + 2F_{ub} \cdot e / (m + e) \quad \text{Eqn 2.10}$$

where p_1 is the vertical bolt pitch, and t_{fc} and f_{yc} are the thickness and yield strength respectively for the column flange. They suggested F_{ub} could be multiplied by 0.8 to provide a safety factor against undesirable bolt fracture.

In the case of Mechanism C in the column flange, Packer & Morris considered several yield-line patterns. In a further refinement to Zoetemeijer's proposals, Packer & Morris also investigated yield patterns for a column flange with transverse stiffeners, where the stiffeners are midway between the tension bolts. In all their equations they neglected strain hardening and membrane action.

2.3.3 Tarpy & Cardinal

Tarpy and Cardinal (1981) also considered the deformation of the column flange, limiting their studies to unstiffened flanges and using finite element analyses rather than yield-lines. They modelled 97 connections using standard sections, and then derived prediction equations for the column flange displacement and web stress, using multiple linear regression. The displacement δ was given in inches (Tarpy & Cardinal, 1981) as:

$$\delta = \frac{1.54 \times 10^{-6} b_{fc}^{0.76} p_2^{2.09} M^{1.31}}{p_1^{0.84} t_{fc}^{2.38} t_p^{1.84} D^{0.74}} \quad \text{Eqn 2.11}$$

where D	= beam depth	t_{fc}	= column flange thickness
p_2	= gage	b_{fc}	= column flange width
p_1	= pitch	M	= applied beam end moment
t_p	= endplate thickness		

In the equation for δ the dominant parameters are the bolt gage, and the endplate and column thicknesses. By assuming the centre of rotation to act at the bottom

flange of the beam, they could then derive an equation for the applied beam moment in terms of the beam end rotation.

Tarpy and Cardinal found in comparative studies that with what they considered to be thin endplates ($t_p = 1.5t_{fc}$), the column flange was the stronger bending element, while with thick endplates ($t_p = 4t_{fc}$), the endplate was stronger.

2.3.4 Discussion of the Column Flange Studies

Zoetemeijer's paper provides a means of differentiating between three failure modes in tee-stubs (and by inference, in endplates), and he also shows how these tee-stub failure modes can interact with the column flange thickness. He introduced the very important concept of a participating length for the column flange yield lines, and illustrated how this could be used in practical design. He also showed that the tee-stub/endplate and the column flange could in fact be analysed separately, though using the same principles.

Zoetemeijer showed a relationship between 'thin' and 'thick' endplate behaviour, and the bolt size/ strength. In order for the connection to fail by excessive endplate yielding and deformation, and so be 'thin', larger and stronger bolts are required.

Packer & Morris extended this by analysing several yield-line patterns for column flanges and defining participating lengths for these. Interestingly though, in their extended endplate connection tests, Packer & Morris found that those tests that failed by endplate Mechanism C (double curvature collapse) behaved differently from the tee-stub tests that failed by the same mechanism. Their use of Zoetemeijer's equations led to a consistent overestimate of connection strength for the extended endplate, but to a consistent underestimate for the tee-stubs. Thus, they concluded that thin endplate behaviour is not quite analogous to tee-stub behaviour, though Zoetemeijer's equation led to better predictions than any of the other models available to them such as Surtees and Mann's. Their measurements of bolt forces indicated that the value of $M'_p/3d_f$ suggested by Surtees and Mann,

and which includes a 30% estimate of prying, was a good approximation to the bolt force.

A second major contribution by Zoetemeijer is that he showed the importance of the interaction between the endplate and the column flange, by demonstrating that the location and magnitude of the prying forces depends on the relative ‘thickness’ of the endplate compared to the column flange. Tarpay and Cardinal confirmed this interaction using a different approach. The column flange behaviour is affected by the presence of stiffeners as shown by Packer & Morris.

At this stage in the review, it is clear from Packer & Morris that there are three failure modes in endplates – one of which is the ‘thin’ endplate behaviour. The other two modes (intermediate – bolt fracture after endplate yielding, and ‘thick’ – bolt fracture prior to endplate yielding) are undesirable from the viewpoint of ductility since they involve the brittle failure of bolts. It is also clear that an endplate is ‘thin’ in relation not only to its own thickness, but also in relation to the bolt size/strength and the column flange thickness. Clearly also, the tee-stub analogy is not really applicable to ‘thin’ endplates in which the flush region exhibits complex bending behaviour. The presence of strain-hardening in ‘thin’ endplates has been acknowledged by several researchers (leading to different plastic moments on the weld and bolt lines), but has not been accounted for. The column flange and endplate can be ‘uncoupled’ from each other and analysed separately at the ultimate limit state. The elastic behaviour of the endplate and the column flange are linked together via prying forces, but this is de-emphasised once either component has formed a yield mechanism.

2.4 EXTENDED ENDPLATE STUDIES IN THE EIGHTIES

2.4.1 Krishnamurthy’s Finite Element Studies

Krishnamurthy (1978) carried out an extensive FEA study of extended endplate connections, and came up with a model of behaviour for these connections. He

suggested that the actual behaviour of the end plate in the extended region differed from Sherbourne's model in that the force transferred to the extended region is not necessarily half of the beam tension flange force, but depends on the relative stiffness of the extended region and the flush region (between the flanges). His analyses showed that the extended region typically accounted for between 30 – 50% of the beam flange force. He hypothesized that the beam web transfers some of the force that goes into the flush region, so that the tension force in the beam is not limited to the tension flange.

Sherbourne had assumed that the tension bolts in the extended region would restrain the plate completely and so modelled it as a fixed-ended beam. That meant that at collapse the point of inflexion in the endplate moment diagram would be halfway between the weld and bolt lines if the maximum moment is M_p at both lines. Krishnamurthy pointed out that the bolts do not restrain the plate completely and will also bend and stretch under load. All this leads to less stiffness at the bolt line so that the point of inflexion shifts towards the bolt line. His analyses showed that the inflexion point could be anywhere from halfway between the weld and bolt lines, right up to the bolt line itself. (He also showed that the weld line position is approximately at the toe of the beam tension flange to endplate fillet weld, rather than at the face of the flange). Thus, by allowing the inflexion point to shift, he was catering for the possibility of a different failure mechanism such as Packer & Morris' Mechanism B, in which the weld line moment is M_p but the bolt line moment $< M_p$.

Thirdly, Krishnamurthy pointed out that the prying forces and the bolt forces on the extended region are not concentrated forces as commonly assumed, but form curved pressure bulbs. On the basis of these observations, he proposed that the moment for which the endplate is sized, i.e. the design moment M_d , could be considered a modification of the theoretical moment M_t for a fixed-ended beam with concentrated loads resisting half the flange force, as follows:

$$M_d = \alpha_m M_t = C_1 C_2 C_3 M_t$$

where the C coefficients each cater for one of the three effects described above (ratio of the flange force resisted, shift in inflexion point and non-concentrated loads), and are all summarized in the α coefficient. Krishnamurthy was unable to suggest a physical approach for modeling these coefficients directly, and resorted to a regression analysis of the FEA generated results. Based on the statistical analysis, Krishnamurthy (1978) came up with the following formula for the plate design moment (the moment at the weld line):

$$\begin{aligned}
 M_d &= 1.29 \left(\frac{f_y}{f_{bu}} \right)^{0.4} \left(\frac{f_{bt}}{f_p} \right)^{0.5} \left(\frac{b}{b_p} \right)^{0.5} \left(\frac{A_f}{A_w} \right)^{0.32} \left(\frac{p_e}{d} \right)^{0.25} \times M_t \\
 &= \alpha_m M_t = C_a C_b \left(\frac{A_f}{A_w} \right)^{0.32} \left(\frac{p_e}{d} \right)^{0.25} \times M_t \quad \text{Eqn 2.12} \\
 &\left[C_a = 1.29 \left(\frac{f_y}{f_{bu}} \right)^{0.4} \left(\frac{f_{bt}}{f_p} \right)^{0.5} ; C_b = \left(\frac{b}{b_p} \right)^{0.5} \right]
 \end{aligned}$$

In this equation, f_p and f_y are the working and ultimate stresses in the endplate, while f_{bt} and f_{bu} are the corresponding working and ultimate values for the bolt. b and b_p are the beam flange and plate widths respectively, and A_f and A_w are the areas of the beam flange and beam web. The nominal bolt diameter is d and m_x is the effective span (between the bolt and weld lines), taken as $p_e = p_f - 0.25d - s_{wf}$. p_f is the distance from the bolt centre-line to the face of the flange, and s_{wf} is the throat size of the fillet weld. These parameters are shown in Figure 2.8.

According to Krishnamurthy, the design moment obtained by the above equation could be used as a basis for obtaining the endplate thickness (Krishnamurthy equated the design moment to the endplate yield moment of resistance rather than the plastic moment of resistance), while the bolts were sized on the basis of working load by dividing the total flange force by the total number of tension bolts. The effective plate width was restricted to the maximum value obtained by assuming a 45-degree dispersion from the flange-to-plate weld toe. Thus, b_p could not be taken as greater than $b + 2(p_f - s_{wf})$.

While Krishnamurthy's model adds valuable information to the body of work on extended endplates, it is an empirical model and thus the key parameters have no physical meaning such as would aid conceptual understanding of the connection behaviour. The use of a yield criterion for failure (in deriving endplate thickness) meant that the model still led to fairly thick endplates, and since the model does not explicitly recognise the different failure modes, it does not provide guidance for a designer on when the connection will fail in one mode or the other.

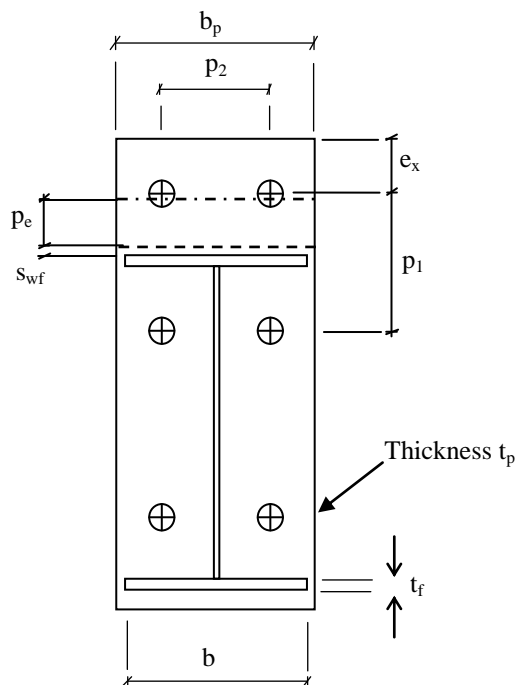


Figure 2.8 – Endplate geometry in Krishnamurthy (1978)

His model allows indirectly for the possibility that a yield line does not form at the bolt line but there is no guidance as to when this happens. His work also shows that the tee-stub analogy may be really weak in some cases and his model accounts for the increased load in the flush region. However there is no attempt to cater for the strain hardening of the weld line since he was using a yield failure criterion. Since his equations are based on regression analyses, the units become quite important. Nevertheless, Krishnamurthy is important in demonstrating that the restraint effect of the beam web cannot be ignored as it increases the flush bolt forces over the extended region significantly. Moreover, his insight into the shift

in the inflexion point provides a reasonable explanation for Zoetemeijer's observation that the moments can differ on the bolt and weld lines.

In Krishnamurthy & Oswalt (1981), the earlier work by Krishnamurthy was extended to include the effect of the bolt heads and the fillet welds in the extended region of the connection. These had not been modelled previously in the FEA analyses of the earlier work and there was a consistent underestimate of the connection stiffness measured in tests, when compared to predictions by the previous model. Krishnamurthy concluded that this underestimate was because the bolt head and weld detail had been omitted. Besides the design moment equation described in the previous publication, Krishnamurthy & Oswalt referred to an equation for the connection rotation, which had been derived as part of the same work. That equation was:

$$\theta = \frac{0.00124\beta_r \mu_r p_f^{2.048} f_b^{1.731}}{t_p^{1.558} a_b^{1.130}} \quad \text{Eqn 2.13}$$

where f_b is the extreme fibre stress in the beam, t_p is the endplate thickness, and a_b is the net area of the bolt shank.

Krishnamurthy & Oswalt found that the inclusion of the bolt head and weld did give more accurate results. The problem was then how to account for these details in the previous equations for M_d and θ . This was solved by changing the equation for the effective bolt (vertical) pitch, p_e , so that:

$$\begin{aligned} p_{er} &= p_f - 0.125d - 0.5 s_{wf}, \text{ and} & \text{Eqn 2.14} \\ p_{em} &= p_f - 0.25d - 0.707s_{wf} \end{aligned}$$

where the subscripts r and m denote different values for the rotation and moment equations, and s_{wf} is the weld size. They suggested that it would be easier to use a single value for p_e and that p_{em} would then be more appropriate.

2.4.2 Kennedy's Split Tee Analogy

Kennedy et al (1981) presented an important study of endplate connections, in which they concentrated on the analogy between the extended region of the

endplate and the tee-stub – the so-called “split-tee analogy”. Kennedy and his co-investigators follow Packer and Morris (1977) in considering three failure mechanisms in the tee-stub – the ‘thick’ endplate which fails by bolt fracture and no endplate yielding; the ‘thin’ endplate that fails by yielding at the weld and bolt lines; and the intermediate case that fails by bolt fracture but only after yielding of the weld line. Unlike Packer and Morris however, Kennedy et al conceived of these three endplate types, not simply as fixed failure mechanisms, but also as modes of behaviour such that an endplate could move from one behaviour mode to another, at different levels of loading.

Kennedy et al’s conceptualisation of the endplate load level is that initially the loads are low and so every endplate is effectively behaving as though it is thick i.e. no yielding and very low prying forces – assumed zero. As the load increases, if the bolts are large enough so that bolt fracture is precluded, the thick behaviour ceases when the weld line yields. At that point the plate would be behaving as though in the intermediate range. If the load increases further and a second hinge forms at the bolt line, then the plate would be behaving as though thin. Thus, the challenge for them was to ensure that the load, at which the transition from one mode to the other takes place, could be correctly predicted. In their words “*for ideal design the end plate should be thick under service loads, intermediate under factored loads and function as a thin plate at ultimate load.*”

In the model presented by these authors, the transition from one behaviour mode to the other was dictated by the endplate thickness for a given geometry. Thus, for a thick plate, the endplate thickness t_p is set at t_1 the ‘thick’ behaviour cut-off point, where t_1 is given by:

$$t_1 = \sqrt{\frac{2bt_f f_{yf} p_f}{b_p \sqrt{f_y^2 - 3 \left[\frac{bt_f}{2b_p t_1} \cdot f_{yf} \right]^2}}} \approx \sqrt{2.11 \times p_f t_f \cdot \frac{b}{b_p} \cdot \frac{f_{yf}}{f_y}} \quad \text{Eqn 2.15}$$

In this equation:

b , t_f and f_{yf} are the width, thickness and yield stress respectively, of the beam flange; p_f is the distance from the bolt line to the face of the beam flange; b_p is the endplate width, and f_y is the endplate yield stress.

The first exact equation for t_1 has to be solved iteratively but the second provides a quick approximation. The beam flange force is set at its elastic limit F_{max}

(Kennedy et al, 1981), where $F_{max} = \frac{bt_f f_{yf}}{2}$

When the endplate thickness t_p exceeds t_1 , the endplate cannot yield before the beam flange force exceeds F_{max} , so the endplate fails in the ‘thick’ mode and the prying force Q is zero.

Kennedy et al also defined a ‘thin’ behaviour cut-off when the endplate thickness is t_{11} , such that:

$$t_{11} = \frac{\sqrt{2\left(bt_f f_{yf} p_f - \frac{\pi}{16} d_b^3 f_{yb}\right)}}{\sqrt{b_p \sqrt{f_y^2 - 3\left[\frac{bt_f}{2b_p t_{11}} \cdot f_{yf}\right]^2} + b_p' \sqrt{f_y^2 - 3\left[\frac{bt_f'}{2b_p' t_{11}} \cdot f_{yf}\right]^2}}}$$

Eqn 2.16

$$\approx \frac{\sqrt{2\left(bt_f f_{yf} p_f - \frac{\pi}{16} d_b^3 f_{yb}\right)}}{\sqrt{(0.85b_p + 0.80b_p') f_y}}$$

where d_b is the bolt diameter and b_p' is the endplate width minus the bolthole diameters.

Again the exact form is iterative and the approximate solution may be used to obtain a first approximation. This equation is derived by taking moments with the maximum bolt line and weld line moments at M_p , but with the bolt line moment (width) reduced for the bolt holes. Thus, while the endplate width at the weld line is b_p , the width at the boltholes is taken as b_p' . In their formulation of M_p , a shear

correction is included as in Sherbourne (1961). The equilibrium equation includes the resisting moment of the bolt M_b , where $M_b = \frac{\pi d_b^3 f_{yb}}{32}$.

When the endplate thickness t_p is less than t_{11} , the endplate is ‘thin’ at ultimate load and the prying force is at its maximum value, Q_{max} . The value of Q_{max} is given by:

$$Q_{max} = \frac{b_p' t_p^2}{4e_x} \sqrt{f_y^2 - 3 \left(\frac{F}{b_p' t_p} \right)^2} \quad \text{Eqn 2.17}$$

in which e_x is the edge distance from the bolt line to the endplate edge, and F is the flange force which has its maximum at the elastic limit as F_{max} . The authors placed a limit on e_x , such that $2d_b \leq e_x \leq 3d_b$.

For intermediate plates, $t_1 \leq t_p \leq t_{11}$, the maximum value of the reduced prying force Q'_{max} is taken to occur when $F = F_{max}$, and is then given by:

$$- Q'_{max} = \frac{b_p t_p^2}{4e_x} \sqrt{f_y^2 - 3 \left(\frac{F_{max}}{b_p t_p} \right)^2} + \frac{\pi d_b^3}{32e_x} f_{yb} - \frac{F_{max} p_f}{e_x} \quad \text{Eqn 2.18}$$

The bolt is sized to be stronger than $(F+Q)_{max}$ to achieve ductile failure.

The approach of Kennedy et al (1981) is very similar to Zoetemeijer (1974), but is more sophisticated in that the three endplate modes are explicitly recognised and are treated as behaviour modes in the endplate load level rather than simply failure modes. Moreover, Kennedy et al include the bolt resisting moment M_b and a shear adjustment for M_p . The work by Kennedy et al highlights the fact that the endplate behaviour is in relation to the applied load on the connection, but fails to emphasise the possibility that under certain conditions an endplate cannot go beyond the thick limit or thin limit because another component (such as the bolt) has failed.

The main criticisms of Kennedy et al (1981) are that at both the endplate thick and thin limits, F_{\max} is taken to be the elastic limit of the flange force. A ‘thin’ endplate is inelastic, and there is no justification then for limiting the beam tension flange force to an inelastic criterion. As is shown later also, the inclusion of a prying force in analysing a ‘thin’ endplate is unnecessary. Secondly, the split-tee analogy ignores the fact that the flush region may not really behave in the same manner as the extended region. Finally the strain hardening of the weld line and bolt line is ignored.

2.4.3 Murray’s Research at Virginia Polytechnic

Murray and his co-investigators at Virginia Polytechnic have adapted the work of Kennedy et al into a design model (Abel & Murray, 1992). They use the yield-line mechanism of Surtees & Mann (1970), but with the location of the centre of rotation as a variable. The endplate thickness is based on solving the resulting work equation, with the centre of rotation located so as to minimise the internal work. The bolt forces however are determined from the Kennedy et al (1981) equations, with the prying force assumed to be located at a distance a from the bolt centreline, where a is given as:

$$a = 3.682 \left(\frac{t_p}{d_b} \right)^3 - 0.085 \quad \text{Eqn 2.19}$$

This equation, which was empirically obtained, relates the distance ‘ a ’ to the endplate thickness and the bolt diameter. All dimensions are in inches. Murray has also investigated the extension of this design approach to extended endplates with more than two tension bolt rows or with more than two bolts in each row, as in for example, Murray and Borgsmiller (1996).

2.4.4 Some Other Relevant Models

In Australia, Grundy et al (1980) proposed a detailed design procedure, also based on Sherbourne’s model, suitable for different variations of the extended endplate

connection. The bolts were sized as in Surtees & Mann (1970) but with a twenty percent addition rather than thirty percent. The endplate thickness was decided as in Sherbourne (1961) but without the shear correction, and the internal moment of resistance was for an elastic rather than a plastic failure criterion.

Grundy et al went on to suggest a detailed model for the column flange behaviour. For unstiffened flanges they used a participating length concept as introduced by Zoetemeijer, and for transversely stiffened flanges they suggested a plastic interaction formula. Unfortunately, they only reported two connection experiments, and these experiments did not test their hypotheses about the column flange behaviour. Interestingly, in one of their tests, they reported the development of a crack in the endplate-to-beam-web weld in the tension zone. They pointed out quite correctly that this showed a failure in Sherbourne's model to consider compatibility of deformation between the beam flange and web.

Bahia et al (1981) tested 4 tee-stubs and 12 extended endplate connections. In their tee-stub tests, they found that the measured bolt forces did not end up in equilibrium with the assumed pattern of moments if the weld line moment was assumed to be M_p . Thus, they corroborated the findings of Agerskov, also on tee-stubs. Bahia et al hypothesized that the out-of-balance moment could be explained either by a moment on the bolt line (possibly due to prying of the head), or due to a reduction in the dimension m_x (the distance between bolt line and weld line), or by increasing the resistance of the plastic hinge at the weld line. They rejected the first hypothesis on the basis that the bolts failed at the full tensile strength so that the bolt moments did not appear to be significant. They also rejected the second hypothesis on the basis that their observations of the deformed endplate shape did not support a reduction in m_x . They therefore decided that the explanation had to be an increase in the hinge moment due to strain hardening.

In order to investigate the strain hardening further, Bahia et al carried out bending tests on simply supported strips of the endplate material (yield stress of 229 MPa), applying a central point load and measuring the load deflexion curve. The span of

the steel strip was conceptualised as being the same as the span from the bolt line on one side of the tee-stub flange to the bolt line on the other side. They found that for the smaller span to strip thickness ratios, there was evidence of strain hardening with the plastic hinge forming at moments much higher than theoretically predicted. For a typical value of a plate thickness of 15,9 mm, the hinge formed at $2.2M_p$ – the difference was considered to be due to strain hardening. Bahia et al (1981) suggested therefore that the load-deflection curve could be represented as a bi-linear curve with the strain-hardening moment of resistance m_{ph} at the discontinuity being empirically determined to be:

$$m_{ph} = m_p \left[2.65 - 0.275 \left(\frac{l}{t} \right) \right]; \quad 2 < \left(\frac{l}{t} \right) < 6 \quad \text{Eqn 2.20}$$

In this formula, m_p is the unit width theoretical plastic moment of resistance, l is half the span of the simply supported strip and t is the thickness of the strip.

Bahia et al suggested a formula for the bolt prying force in tee stubs from similar considerations as Douty & McGuire (1965). Based on the prying force formula and the above expression for strain hardening moment, and defining failure of a component as the point at which its load-deformation curve ceases to be linear, they established equations for the maximum moment at the weld line in the endplate and for the equivalent moment in the column flange. For the column flange they used an effective width derived from Timoshenko (1959) to allow them to apply the prying force formula, based on the understanding that the column flange behavior would remain elastic up to the discontinuity. The tensile bolts were all assumed to be equally loaded and to have equal prying forces. These prying forces had been noticed to be twice as large at separation as at ultimate loads. It was then possible to establish the beam moment as at ultimate load (when the weld line or the column flange is at the point where the load-deformation becomes non-linear).

Bahia et al's study is particularly interesting as it includes an attempt to explicitly cater for the strain hardening effect at the weld line. It uses Douty & McGuire's

(1965) prying force formula as the departure point but adopts the moment of resistance m_{ph} for the weld line, rather than m_p . This model is much more sophisticated however, in that the deformation of the column flange is considered, as in Zoetemeijer (1974) for example. But there are questions as to the limits of applicability of Douty & McGuire's formula, which is based on the initial elastic deformation of the endplate around the bolts due to the bolt pretension, and which also includes the initial bolt elongations. Moreover, Douty & McGuire's formula is semi-empirical. A further criticism is that the formula for m_{ph} is empirical and does not consider the material strength; moreover the simple-support span tests used to determine m_{ph} were inconsistent with the assumptions made by Douty & McGuire regarding spanning across the tee-stub flange edges. Their value for m_x does not take the effect of the weld into account as Krishnamurthy does. In accordance with classical mechanics, their simply-supported strip plate tests (equation 2.20) showed a relationship between the level of strain hardening on the one hand, and the plate thickness relative to the bending span on the other hand. The possibility of strain hardening on the bolt line was not considered.

Nevertheless, the findings of Bahia et al about the bolt forces not balancing the weld moment are consistent with the findings of Agerskov, who had concluded that the bolt line does not really yield but the weld line strain-hardens. They are also consistent with the findings of Krishnamurthy in the sense that he also accepted that the bolt line would not yield due to what he referred to as a shift in the inflexion point. Krishnamurthy did not consider strain hardening as a critical contributor. However, any strain hardening effects would be masked and included in his regression-analysis-derived coefficients. Krishnamurthy, Agerskov and Bahia et al were all implicitly considering a mechanism in which the bolts fractured after yielding of the weld line but before yielding of the bolt line. This differs from the thin endplate behaviour revealed by Zoetemeijer (1974).

Bahia et al focused on tee-stubs, and ignored the weld effect on the effective span between weld and bolt lines, but they clearly demonstrated that strain hardening does play an important role under certain circumstances.

2.5 THE SHIFT TO MODELLING BY COMPONENTS

2.5.1 By Components - Yee & Melchers' Moment-Rotation Model

Some early researchers had been working on including the connection non-linearity into non-linear frame analyses. For such researchers, the emphasis was not on the connection proportions but on correctly modelling the connection moment-rotation characteristic, and preferably in a manner amenable to easy inclusion in a frame analysis. Thus, some of the initial research developed mathematical expressions for the moment-rotation curves of specific connections, by fitting polynomials (Frye & Morris, 1975) or power functions (Krishnamurthy et al, 1979 for example), to experimental data. The problems with such attempts are that there is often a wide variation in test connections, the parameters in fitted polynomials typically have no physical meaning, and the moment-rotation curves therefore cannot be adjusted for changes in connection geometry and layout.

Yee and Melchers (1986) proposed a mathematical model for extended endplate moment-rotation curves, in which the moment M and the rotation θ at a point in the curve are related by the expression:

$$M = M_p \left\{ 1 - \exp \left[\frac{-(K_i - K_p + C\theta)\theta}{M_p} \right] \right\} + K_p \theta \quad \text{Eqn 2.21}$$

where M_p is the maximum moment transferred by the connection before strain-hardening sets in, K_i is the tangential initial stiffness of the moment-rotation curve, and K_p is the tangential strain hardening stiffness. The parameter C was introduced to control the rate of decay of the slope. The physical parameters are illustrated in Figure 2.9.

In order to determine the moment M_p , Yee and Melchers suggested that six failure modes be investigated to establish the lowest load at which one of these would occur and the connection would begin to behave non-linearly. The failure modes were:

- ❑ Bolt failure in tension
- ❑ Formation of an endplate plastic mechanism
- ❑ Formation of the column flange plastic mechanism
- ❑ Shear yielding of the column web
- ❑ Web buckling, and
- ❑ Web crippling

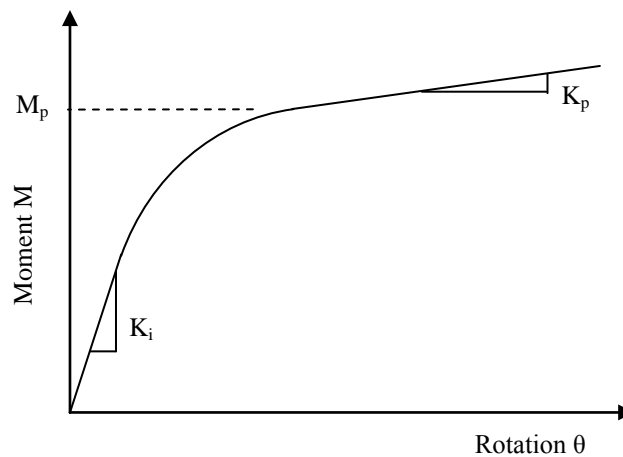


Figure 2.9 – Physical Parameters in Yee & Melchers (1986)

Their model for determining the endplate failure load was derived from Whittaker and Walpole (1982), an adaptation of Surtees and Mann (1970). Their column flange load was based on Packer and Morris (1977).

To evaluate K_i and K_p , Yee and Melchers suggested a ‘by components’ approach, in which the connection rotation was expressed in terms of the deflection at the level of the tension flange, and the connection deflection was determined by summing up the deflections of the component parts – endplate and column flange flexure, bolt extension, column web panel shear, and column web compression. Thus, Yee and Melchers had to derive expressions for the component deflections. They applied simple beam bending theory and drew on the work of Agerskov (1976) for the endplate and column flange contributions, and for bolt elongation. The beam tension force was assumed to be concentrated in the tension flange, and

the compression force in the compression flange. The rotation was assumed to be around the compression flange centroid.

The work of Yee and Melchers was significant in that most of the parameters in their model were physical ones. Moreover, their suggested models such as Packer and Morris or Agerskov, for establishing M and θ , were directly based on the geometry of the connection. A really interesting aspect was the use of the ‘components’ approach, in which they demonstrated the usefulness of summing up deflections to obtain the connection stiffness. Unfortunately however, their model still included the non-physical parameter, C , and the simple bending theory they utilised may not really be applicable for some of the small connection components.

Jenkins et al (1986) also produced a design model that was based on moment-rotation characteristics. Their model was for flush endplates (endplates having no extension beyond the beam tension flange – see Section 1.3), rather than extended endplates, but it is mentioned here because of certain similarities to Yee and Melchers’ proposals. Jenkins et al suggested a bi-linear moment-rotation curve defined by three points – the origin, the point at the end of the linear elastic section, and the ‘ultimate’ point at the onset of strain hardening. They also applied a ‘by components’ approach, considering endplate flexure, column flange flexure and bolt extension. However, rather than evaluate deflections to obtain rotations as in Yee and Melchers, they evaluated the stiffness of each component and calculated the connection stiffness by summing the inverse of component stiffnesses. Moreover, instead of determining the moment and stiffness of each component from behavioural models as in Yee and Melchers, they drew up design charts for various beam and column sections and for different endplate thicknesses. These charts were based on Finite Element analyses of various configurations, calibrated with experimental results. Rather intriguingly, they reported that they could not get the FE analyses results to match the experimental ones until they allowed for an enhanced material yield stress in the heat affected zone area adjacent to the endplate welds.

2.5.2 Studies by Zandonini and Co-investigators

Zandonini and Zanon (1988) reported on a study at the University of Trento, in which they tested 10 extended endplate connections – five were extended on one side only and the other five on both sides. The Trento researchers approached the problem of characterizing the moment-rotation curve from the same premise as Yee and Melchers (1986), assuming that the joint rotation could be broken down into the component parts. In this particular study however, they focused only on the contribution of the connection – endplate and bolts - and the beam end. Bolting the endplate to a very rigid counter-beam eliminated the column flange contribution.

Zandonini and Zanon took measurements of deflections at three points:

- Deflections of the endplate at the levels of the beam flanges.
- Deflections of the tension bolt heads away from the counter-beam, and
- Deflections of beam flanges at a point 300mm from the endplate surface.

They also measured the tension bolt axial forces by measuring the extensions of the bolts.

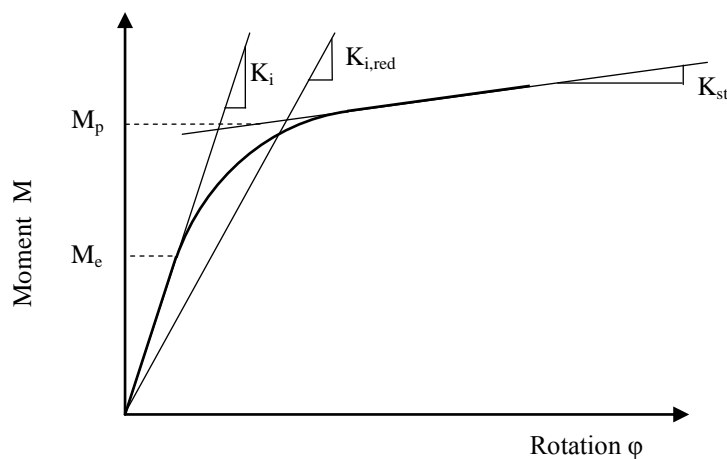


Figure 2.10 – Parameters Characterizing Moment-Rotation Curves (Zandonini & Zanon, 1988)

The connections tested by Zandonini and Zanon were identical except for the endplate thickness, which ranged from 12 mm to 25 mm. As would be expected,

the connections with thinner endplates had much higher rotations but lower ultimate strengths – nevertheless they were all able to resist the full beam moment so that the beam end buckled locally in each test. In the 12mm endplate connections, endplate deformation accounted for as much as 90% of the total rotation. In no case however was the bolt contribution negligible. The contribution of the beam was high in the thick endplates but very small in the thin endplates. Each connection was tested to failure in multiple load cycles.

Based on their very careful observations, Zandonini and Zanon arrived at several important conclusions about the behaviour of the connection as follows: The initial pretension force in the bolts (snug-tight – set at 40% of the bolt's nominal yield strength) tended to disappear after a few loading cycles. This was thought to be due to the fact that the washers deformed plastically. (It could also be due to burrs or high spots on the bolt head or nuts leading to lack of fit. This possibility was apparently not considered by Zandonini and Zanon.) The consequence of this was that the initial stiffness of the elastic part of the moment-rotation curve was consistently much higher in the first loading cycle than in subsequent cycles. This is illustrated in Figure 2.10, in which the $M-\phi$ curve for subsequent loading cycles is shown superimposed on the $M-\phi$ curve for the first load cycle. The elastic stiffness of the first cycle is K_i , while that for subsequent cycles is $K_{i,red}$. The stiffness of the strain-hardening part of the curve is shown as K_{st} .

Secondly, Zandonini and Zanon found that there was consistently a difference between the axial bolt forces in the flush region and those in the extended region, and concluded that the effect of the beam web in restraining the flush region cannot be ignored. This was especially true for the thinner endplates. They found moreover that the bolts in the thinner endplates were subject to appreciable bending moments as well as the axial forces, and this was more pronounced for the extended region than the flush region. Because of the beam web effect, Zandonini and Zanon rejected the tee-stub analogy and suggested that the extended region could rather be modelled as a cantilever and the flush region as a plate with a point load.

Zandonini and his associates concluded that a first step towards describing the moment-rotation curve would be to establish the five parameters k_i , $k_{i,red}$, k_{st} , M_e and M_p shown in Figure 2.10. Thus, they would have a benchmark against which to compare the predictions of any analytical model of the connection moment-rotation curve. M_e is the connection moment at the limit of elastic behaviour on the first loading cycle, and M_p is the connection moment when the connection is fully plastic. In order to determine M_p on their experimentally-obtained curves (to facilitate comparison with later-to-be-developed analytical curves), they initially suggested that M_p be defined as the average point between the intersection of the k_{st} and k_i lines and the intersection of the k_{st} and $k_{i,red}$ lines (see Figure 2.10). Zandonini and Zanon (1988) suggested further research to establish mechanical models for determining these five parameters analytically.

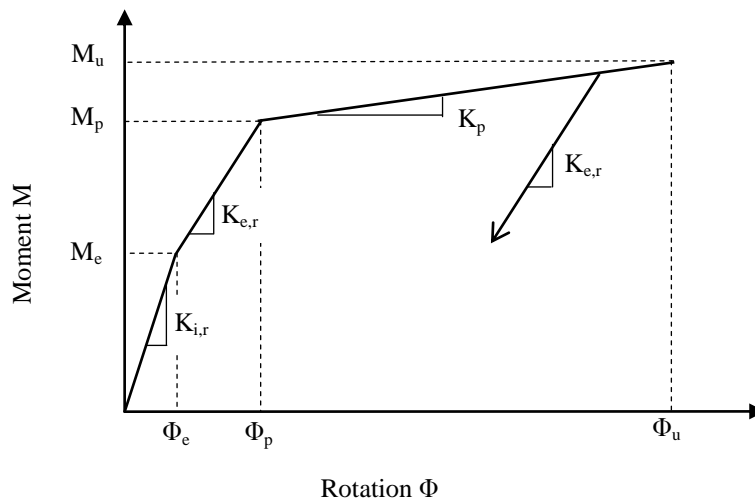


Figure 2.11 – Moment-Rotation Parameters in Tri-linear Representation (Bernuzzi et al, 1991)

In Bernuzzi et al (1991), Zandonini and his colleagues continued to examine the same data from their experiments. However, they changed their approach to the evaluation of moment-rotation parameters from experimental data. They now suggested a tri-linear representation as shown in Figure 2.11, with an initial elastic

portion, then a second phase with a reduced but still elastic stiffness, and finally a third plastic portion. The slope for unloading was taken as being the same as for the second phase, as shown in the Figure. With this new representation, the characterisation of the moment-rotation curve from experimental data now became dependent on the determination of the strength parameters M_e , M_p and M_u , and the stiffness parameters $K_{e,i}$, $K_{e,r}$ and K_p . Bernuzzi et al determined these parameters from their test results, using linear regression to establish the locations of the three lines in the tri-linear representation. The slopes of the lines were then obtained from the regression analyses, and the values of M_e and M_p were obtained from the intersections of the lines; M_u was measured directly in each test.

The development of the analytical models for estimating these parameters was based on yield-line analyses of the endplate. In order to better understand the endplate behaviour, Bernuzzi et al described a photogrammetric study of the permanent deformations in the endplate surface, drawing contour lines and establishing the positions of maximum gradient. Based on this study, they concluded that there were three possible failure mechanisms in the endplate. Like other researchers before them they noted that the extended region of the thin endplates failed in double curvature by the development of two parallel transverse yield-lines - across the bolt-line and adjacent to the weld-line. The flush region however was clearly more complex, and resembled a partially circular pattern as shown in Figure 2.12

Bernuzzi et al chose to represent the pattern in the flush region by one very similar to that used in Surtees & Mann (1970). However, the centre of rotation for the endplate (transition from compression to tension), was taken as either being at the level of the compression bolts (Mechanism A) or as being at the inside edge of the compression flange (Mechanism B). In Surtees & Mann (1970) the centre of rotation was assumed to be at a point halfway along the depth of the beam. Bernuzzi et al's Mechanism A is shown in Figure 2.13. A second difference was that Bernuzzi et al took the extended region bolt yield-line as eccentric to the bolthole axis by a quarter of the bolt diameter.

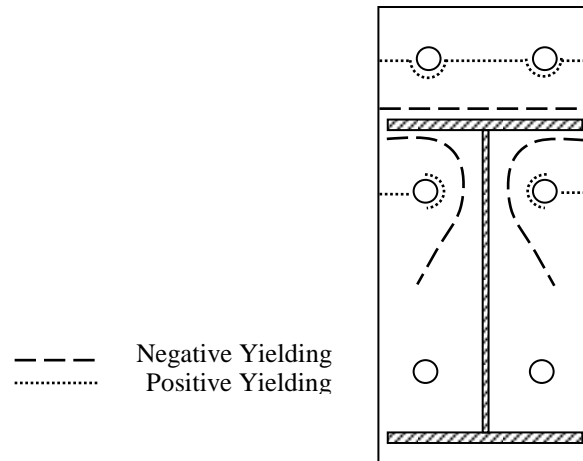


Figure 2.12 – Permanent Deformation Pattern in Thin Endplates (Bernuzzi et al, 1991)

They also considered a third mechanism for thick plates (Mechanism C), in which the only yield-line was in the extended region along the weld.

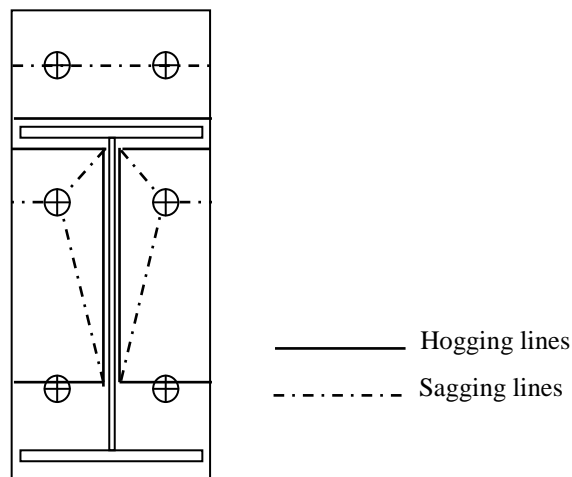


Figure 2.13 – Mechanism A in Bernuzzi et al (1991)

In order to validate the mechanisms assumed, Bernuzzi et al calculated the M_p strength parameter for each of the tested connections using the three different mechanisms. They found that for the 12mm endplate the M_p calculated for

Mechanism A had a good agreement with the experimental value, while the Mechanism C values showed good agreement with experimental values for the other connections with thicker endplates. However, Bernuzzi et al did not include the details of the yield-line equations, nor did they attempt to analytically derive the other strength or stiffness parameters.

Finally, in Bernuzzi and Zandonini (1990), the Trento researchers reported on four additional connection tests carried out to extend the data to include partial strength connections. These connection details were identical to those from the first series of tests, except that the beam material was chosen to be much stronger so that the connections were partial strength, and secondly, in these tests the bolt moments were measured. The results from Bernuzzi and Zandonini (1990) confirmed their earlier results. As expected, the connection strength was reduced since the beam material was weaker. The thicker plates also exhibited a changed stiffness in the plastic region. They found moreover that the bolt moments were significant in the thin endplates.

The work by Zandonini and his associates is valuable because of the detailed and meticulous nature of their experimental observations, which give insight into the behaviour of the connection in its component parts. The tri-linear approximation used to evaluate parameters of the moment-rotation curve is useful and relatively straightforward in application. It is clear though that initial stiffness is a variable phenomenon, being affected by bolt pre-tension and the connection lack of fit. There is also a question as to whether or not the middle portion of the tri-linear curve is actually a 'reduced elastic stiffness' region as they term it. There is already yielding taking place on some yield-lines at that point, so the slope of that line is not simply an elastic portion minus the effects of pre-tension and lack of fit. That would be true for the unloading portion of the curve, but not for the middle line in the tri-linear loading curve.

In the test instrumentation used by Zandonini and his associates, the connection rotations were measured at the beam flanges so that the rotations measured for the

thin endplates (where the rotation axis would have been between the flanges), possibly underestimate the connection component and correspondingly overestimate the beam component. This would not however affect the qualitative validity of the majority of their conclusions. It is problematic though that their analytical calculations of M_p were reportedly based on the assumption that the rotation axis was at the compression flange, as this is at variance with the yield-line position in Mechanism A.

2.6 EUROCODE 3 ENDPLATE MODELS

Part 1 of Eurocode 3 was initially released in 1992 as DD ENV 1993-1-1, which was a draft for development with voluntary usage in EU member states (Eurocode 3, 1992). In this document, beam-to-column connections were covered in Annex J, which was revised in 1994. That revision is referred to here as ‘Revised Annex J of DD ENV 1993-1-1: 1992’ (Revised Annex J, 1994). In the final version of Eurocode 3 which is a mandatory standard, joints are treated as a separate sub-part – 1.8 – rather than as an annex to sub-part 1.1. This was published in Britain in 2005 as BS EN 1993-1-8: 2005 (Eurocode 3, 2005). Thus, there have been three models for extended endplate connections in Eurocode 3 to date. These are discussed below.

2.6.1 Extended Endplate Model of Eurocode 3 Annex J

The ‘by components’ approach was refined and codified in Eurocode 3 (1992). In DD ENV1992 the connection was introduced into the global analysis of the frame as pinned, rigid or semi-rigid based on stiffness; and as pinned, full strength or partial strength based on strength. The connection was considered conceptually as a rotational spring with a known secant stiffness S_j acting to some moment resistance M_{Rd} . Thus, the emphasis was on predicting the moment resistance and the stiffness.

Connection Strength

The tension bolt forces were determined first - either as a plastic distribution (all bolts at yield) or as a linear triangular distribution (furthest bolt from compression flange at yield and others resisting forces proportional to ratio of the distances from the compression flange). These bolt forces could then be adjusted to a value compatible with the forces transmitted by each component, checking each bolt row individually and as part of the group of bolts. The chosen distribution was maintained – plastic or triangular. The connection moment was then derived from the bolt forces in each component, taking the lever arm at the centroid of the beam compression zone. For a triangular bolt distribution the extended and flush tension bolt forces would first be assumed at particular levels, and then adjusted to be compatible with the component failure forces.

The difference in the plastic method was that the bolt forces corresponding to failure of the endplate and column flange were determined first, and then checked against yielding of the bolts. The bolt forces had to be compatible with the strength of five components – the endplate strength in bending, the column flange strength in bending, the column web in tension, the column web in compression, and the column web in shear. The bolt itself was the sixth component under consideration.

The bending strength of the endplate was determined based on a yield-line model using the tee-stub analogy. Following Zoetemeijer (1974), an effective tee-stub length concept was used as a means to relate the possible yield-line patterns in the endplate (and the column flange), to that of a tee-stub. The flush and extended regions were considered separately, with the beam flange taken as the tee-stub web for the extended region (half of a tee-stub really), and with the beam web taken as the tee-stub web for the flush region.

The effective or participating length of the analogous tee-stub would depend on the yield-line pattern being considered. Though the yield-line patterns were not described in Eurocode 3 (1992), the participating length values were given in

clauses J.3.5.5 and J.3.5.7 of the code, for column flanges and endplates respectively. The yield-line patterns assumed could then be easily deduced. The participating lengths in the code and the yield-line patterns implied by these are given below for the extended endplate with four tension bolts. The participating length considered for each region was the least of:

<u>l_{eff} in extended region</u>	<u>Yield pattern implied</u>
1. $0.5b_p$	Two straight lines at weld and bolt lines.
2. $0.5w + 2m_x + 0.625e_x$	Half-circular pattern around both bolt-holes as a group, interrupted at free edge.
3. $4m_x + 1.25e_x$,	Half-circular pattern around each bolt-hole, interrupted at free edge.
4. $2\pi m_x$	Circular pattern with bolt-hole as centre.

l_{eff} in flush region

1. αm	Half-circular pattern, interrupted at free edge, but constrained by the beam tension flange.
2. $2\pi m$	Circular pattern with bolt-hole as centre.

In these expressions (see Figure 2.14),

m_x is the distance between the extended bolt centreline and the nearest face of the beam flange, less 0.8 times the leg length of the beam flange – endplate weld.

e_x is the distance from the extended region bolt centreline to the end of the endplate, measured perpendicular to the beam tension flange.

e is the distance from the bolt centreline to the nearest edge of the endplate, measured parallel to the beam tension flange.

w is the bolt pitch.

b_p is the endplate width.

α is determined using a graph, and is a function of two ratios: λ_1 and λ_2

$$\lambda_1 = \frac{m_1}{m_1 + e}; \quad \lambda_2 = \frac{m_2}{m_1 + e}$$

m_1 or m is the distance between the flush tension bolt centreline and the nearest face of the beam web, less 0.8 times s_{ww} (the leg length of the beam web – endplate weld).

m_2 is the distance between the flush bolt centreline and the nearest face of the beam flange, less 0.8 times s_{wf} (the leg length of the beam flange – endplate weld).

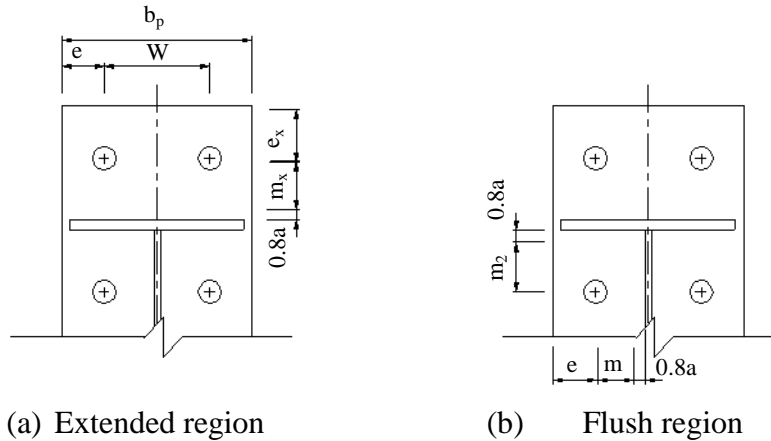


Figure 2.14 – Nomenclature used in Eurocode 3 (1992) Annex J

In Eurocode 3 the strength of these analogous tee-stubs is based on three tee-stub failure modes, similar to Kennedy et al (1981). Thus, mode 1 failure assumes two parallel yield-lines on either side of the web of an equivalent tee-stub – one yield-line at the bolt line and the other at the weld line - with complete yielding of the flange on the four yield-lines. Mode 2 is bolt failure combined with yielding of the flange on the weld lines, while mode 3 is bolt failure only with no endplate yielding. The Eurocode 3 (1992) equations for the design tension force $F_{t,Rd}$ in the tee-stub web are:

$$\text{Mode 1: } F_{t,Rd} = \frac{4M_{pl,Rd}}{m} \quad \text{Eqn 2.22}$$

$$\text{Mode 2: } F_{t,Rd} = \frac{2M_{pl,Rd} + n \sum B_{t,Rd}}{m + n} \quad \text{Eqn 2.23}$$

$$\text{Mode 3: } F_{t,Rd} = \sum B_{t,Rd} \quad \text{Eqn 2.24}$$

n is the smaller of the edge distances for the endplate and the column flange but $n \leq 1.25m$.

$B_{t,Rd}$ is the design tension resistance for a bolt.

$M_{pl,Rd}$ is the plastic moment of resistance per each yield line, which is given by:

$$M_{pl,Rd} = 0.25 \frac{l_{eff} t^2 f_y}{\gamma_{MO}}$$

This is the familiar expression for plastic moment per unit length of material, multiplied by the participating length of the yield-line and divided by a material partial safety factor.

Endplate Stiffness

The secant stiffness S_j of the connection at a given moment M , was to be calculated as:

$$S_j = \frac{E h_1^2 t_{wc}}{\sum \frac{\mu_i}{k_i} \left[\frac{F_i}{F_{i,Rd}} \right]^2} \quad \text{Eqn 2.25}$$

where $M < M_{Rd}$ and M_{Rd} is the connection design resistance moment.

h_1 is the distance from the flush tension bolt row to the centre of resistance of the compression zone.

μ_i and k_i are the modification and stiffness factors respectively for component i .

F_i and $F_{i,Rd}$ are the applied force and the design resistance respectively for component i .

t_{wc} is the column web thickness.

The subscript i referred to the six components that had to be considered, numbered as follows:

1. Column web shear zone
2. Column web tension zone
3. Column web compression zone
4. Column flange tension zone
5. Bolts tension zone

6. Endplate tension zone

The endplate stiffness was based on the formula:

$$k_6 = \frac{t_p^3}{12\lambda_2 m^2 t_{wc}} \quad \text{but } k_6 \geq \frac{t_p^3}{4m^2 t_{wc}}$$

in which $\lambda_2 = \frac{m_2}{m+e}$ as before

The factor μ_1 was taken as 1 for the first three components and $= \frac{h_1 F_{1.Rd}}{M_{Rd}}$ for the

others.

Since S_j could be calculated at any value of M , it meant that a designer could determine a point on the moment-rotation curve corresponding to M . In effect therefore, Annex J was providing a means to predict the moment-rotation characteristic for the connection. The designer could however choose to apply a bi-linear or multi-linear simplification instead.

Rotation Capacity

The ductility or rotation capacity of the connection was to be assessed via rules of thumb. Thus, a connection was considered to have adequate ductility for plastic analysis purposes, either if the moment resistance was governed by column panel shear or by bending of the endplate or column flange. The latter was subject to the condition that either the column flange or the endplate was governed by a mode 1 failure in bending. The failure mode could be confirmed by the check $\beta \leq \frac{2\lambda}{1+2\lambda}$ for mode 1, where β is the ratio of $4M_{pl.Rd}/m$ to the sum of bolt forces, calculated for both the column flange and endplate at each bolt row. $\lambda = n/m$

If the endplate and column flange were governed by mode 2 failures

however $\left(\frac{2\lambda}{1+2\lambda} < \beta \leq 2 \right)$, the rotation capacity θ_{Cd} was to be calculated as:

$$\theta_{Cd} = \frac{10,6 - 4\beta_{cr}}{1,3h_1} \quad \text{Eqn 2.26}$$

The subscript cr on β indicates the lower of the two values calculated for the endplate and the column flange. The extended region was to be excluded in calculating β_{cr} . The rotation capacity θ_{Cd} refers to the rotation of the entire connection, and includes both elastic and plastic contributions.

Criticisms of DD ENV 1993-1-1: 1992 Annex J

The Eurocode 3 (1992) approach to connection resistance effectively extended Kennedy's split-tee analogy and Zoetemeijer's participating (effective) length concept, by applying the split-tee to the flush region as well. As mentioned earlier, the yield-line pattern in the flush region is actually quite complex and bears no resemblance to a tee-stub. There is no allowance for strain-hardening in this strength model, even though the code explicitly allows for ductile partial-strength joints. The allowed option of adopting a triangular linear bolt distribution is difficult to justify since that implies a thick (and inefficient) elastic endplate, leading to bolt failure.

The stiffness model of Eurocode 3 (1992) was particularly criticised in the literature. In SCI (1995) for example, it was reported that the stiffness model of Eurocode 3 Annex J "does not give accurate predictions, and designers are warned against reliance on it in critical cases". In their paper on the need for the Annex J revision, Weynand et al (1996) mention that the model led to contradictory results – an unstiffened endplate was predicted to be stiffer than a stiffened endplate.

There is no ductility (rotation capacity) model in Eurocode 3 (1992) for mode 1 failures. Moreover, the limits for checking mode 1 failure are again based on the tee-stub analogy, and bear little resemblance to actual behaviour in the flush region. The formula for θ_{Cd} in mode 2 failure seems to have a semi-empirical basis, and no ductility limit is given to provide a basis for accepting or rejecting the calculated θ_{Cd} . The inclusion of elastic components in θ_{Cd} is problematic given the criticisms of the initial stiffness model, and given that initial stiffness has been known to vary for nominally identical connections (see Chapter four).

2.6.2 The Revised Annex J Model

In the Revised Annex J (1994), the strength model was unaltered in its philosophy except that the (elastic) triangular bolt force distribution was taken out. Some other changes were as follows:

An alternative expression was included for calculating the tee-stub design tension force in Mode 1 failure, as follows (Revised Annex J, 1994):

$$\text{Mode 1: } F_{T,Rd} = \frac{(8n - 2e_w)M_{pl1,Rd}}{2mn - e_w(m + n)} \quad \text{Eqn 2.27}$$

where e_w is $d_w/4$ and d_w is the diameter of the bolt head (or nut) across points.

This alternative equation was derived by assuming that the forces at the bolt line are not concentrated at the centreline but are uniformly distributed under the bolt head or nut. It leads to a higher bolt force for mode 1.

There was an attempt to determine the limits of modes 1 and 2 failure in terms of the endplate geometry in Eurocode 3 (1992), but this was taken out of the Revised Annex J. The chart used to determine α (for the yield-line case of semi-circular yielding in the flush region next to the stiffener) was also extended to include more values of α .

The number of yield-line patterns checked for a 4-bolt extended endplate increased for the extended region, so that the participating lengths were now:

<u>l_{eff} in extended region</u>	<u>Yield pattern implied</u>
1. $4m_x + 1.25e_x$,	Half-circular pattern around each bolt-hole, interrupted at free edge on end of plate.
2. $e + 2m_x + 0.625e_x$	Corner patterns around each bolt-hole, in a 'quarter-circle' shape
3. $0.5b_p$	Two straight lines at weld and bolt lines.
4. $0.5w + 2m_x + 0.625e_x$	Half-circular pattern around both bolt-holes as a group, interrupted at free edge on end of plate.

- | | |
|-------------------|---|
| 5. $2\pi m_x$ | Circular pattern with bolt-hole as centre. |
| 6. $\pi m_x + w$ | Circular patterns around both bolt-holes but with portion between holes also yielded. |
| 7. $\pi m_x + 2e$ | Half-circular pattern around each bolt-hole, interrupted at free edge on edge of plate. |

l_{eff} in flush region

- | | |
|---------------|--|
| 1. αm | Half-circular pattern, interrupted at free edge, but constrained by the beam tension flange. |
| 2. $2\pi m$ | Circular pattern with bolt-hole as centre. |

In these participating lengths the smallest value was adopted for each region, and the symbols mean the same as before.

The stiffness model was where most of the changes to Annex J took place. The basic formula for the stiffness S_j at a moment $M_{j,sd}$ less than the design moment resistance $M_{j,Rd}$, was now given (Revised Annex J, 1994) as:

$$S_j = \frac{Ez^2}{\mu \sum_i \frac{1}{k_i}} \quad \text{Eqn 2.28}$$

with k_i = stiffness coefficient for component i

z = lever arm

μ = a stiffness ratio $S_{j,ini}/S_j$, and

$S_{j,ini}$ = the initial tangential value of the stiffness S_j

$$\mu \text{ was to be determined from } \mu = \left[\frac{1.5M_{j,sd}}{M_{j,Rd}} \right]^\psi \text{ but } \mu \geq 1 \quad \text{Eqn 2.29}$$

For a bolted endplate, $\psi = 2.7$.

Thus, the definition of μ implies a constant ratio between the initial tangential stiffness on the moment-rotation curve, and the secant stiffness of the curve at failure. This ratio was defined as equal to 3 for an endplate connection. Weynand et al (1996) explained that the μ values were semi-empirical, based on tests and

parameter studies. From comparing the equations for μ and S_j , it is evident that the implicit formula for $S_{j,ini}$ would then be (Revised Annex J, 1994):

$$S_{j,ini} = \frac{Ez^2}{\sum_i \frac{1}{k_i}} \quad \text{Eqn 2.30}$$

For an extended endplate, the components whose stiffness coefficients k_i were to be considered included the column flange in bending, the endplate in bending, and the tension bolts. The endplate stiffness for each tension bolt row was given as:

$$k_5 = \frac{0.85 \cdot l_{eff} \cdot t_p^3}{m^3} \quad \text{Eqn 2.31}$$

where l_{eff} is the participating (effective) length for an equivalent tee-stub as determined for the strength model.

In Weynand et al (1996), the same formula is given as $k_5 = \frac{l_{eff,ini} \cdot t_p^3}{m^3}$ where $l_{eff,ini}$ is the value of participating length required to establish the initial stiffness from a tee-stub model. Thus, $l_{eff,ini} = 0.85 l_{eff}$. The participating length l_{eff} of course relates to the *strength* model. Their model for k_5 is shown in Figure 2.15.

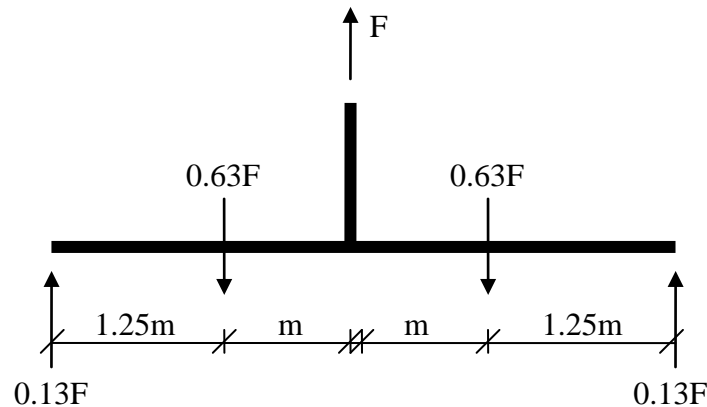


Figure 2.15 – Forces acting on tee-stub stiffness model in Revised Annex J (based on Weynand et al, 1996)

Secondly, when the first plastic hinge formed on the tee-stub flange, this was assumed to form at the weld line, and to have a value of $0.322F \cdot m$. (When this

value is scrutinized however, it implies a 28.5% prying force rather than 26%). By equating this moment to the plastic moment of resistance for a flange width of $l_{\text{eff,ini}}$, Weynand et al (1996) calculated the bolt force F_{el} corresponding to this

$$\text{moment of } 0.322F_y m \text{ as } F_{\text{el}} = \frac{l_{\text{eff,ini}} \cdot t^2}{1.288m} \cdot f_y \quad \text{Eqn 2.32}$$

They then obtained the bolt force at the (ultimate) design value by multiplying F_{el} by 3/2.

Clearly, there are inconsistencies in this stiffness model, with the use of a 28.5% prying force in one area and a prying force of 26% in another area. In the material model used in Revised Annex J strain-hardening is omitted, so that there cannot be prying forces on the tee-stub at ultimate collapse from the model, or the plate moment of resistance on the bolt line would exceed the plastic moment. It seems questionable to simply scale up bolt forces derived on the assumption of maximum prying, so as to obtain ultimate bolt forces that occur when prying forces are very low (and are here implicitly assumed to be zero). But this is what happens when F_{el} is multiplied by 3/2 above.

In the ductility or rotation capacity model of Revised Annex J (1994), a bolted connection was again considered to have adequate rotation capacity for plastic analysis purposes if the moment resistance was governed by a mode 1 failure in bending of either the endplate or the column flange. In addition however, the endplate thickness t_p was limited to a value:

$$t_p = 0.36d \sqrt{f_{\text{ub}}/f_y} \quad \text{Eqn 2.33}$$

where d is the nominal bolt diameter, f_{ub} is the bolt ultimate tensile strength, and f_y is the endplate yield strength.

This appears to be a semi-empirical rule. The calculation for rotation capacity θ_{Cd} in mode 2 failure was now omitted.

2.6.3 The SCI Moment Connections Manual

In 1995, the British Steel Construction Institute published a design guide on moment connections (SCI, 1995). This guide and Revised Annex J were in preparation at the same time period, and it was based partly on Eurocode 3 (1992) and partly on BS 5950: Part 1 (1990).

The resistance moment or strength model was again based on the use of effective tee-stubs with all the yield line patterns of Revised Annex J being allowed for to determine the participating length l_{eff} . Unlike Eurocode 3 (1992), but similar to the revised Annex J, the SCI manual considered only the possibility of a plastic distribution of bolt forces, omitting the triangular bolt distribution. SCI (1995) however included a triangular distribution upper limit on the bolt forces, where the endplate may be too thick to deform sufficiently to allow the full plastic distribution.

SCI (1995) did not include the Annex J stiffness models – neither the original nor the revised version. Instead, the rule was adopted that full-strength connections used in braced or single-storey portal frames and designed according to the guide could be considered rigid. For multi-storey unbraced frames, the designer was encouraged to adopt thick, full-strength and rigid endplates. These endplates would fail in mode 3, but as full-strength connections, the beam would fail first.

In order to determine if the endplate was ‘thin’ enough for a full plastic distribution (mode 1 failure), SCI introduced a similar rule of thumb to that in Revised Annex J:

$$t \leq \frac{d}{1.9} \sqrt{f_{ub}/f_y} = 0.53d \sqrt{f_{ub}/f_y} \quad \text{Eqn 2.34}$$

Thus, the acceptable endplate thickness for mode 1 was 46% more than the corresponding limit in Revised Annex J. The two limits apply to different aspects of the model however, with the Revised Annex J limit referring to the tee-stub

model for a single bolt-row, and the SCI limit applying to the behaviour of multiple rows in the actual connection.

There was however a section of the guide dealing with wind-moment connections for unbraced frames. These are connections that are assumed to be pinned when designing for gravity loads, but assumed to be rigid under wind loads. This philosophy leads to partial-strength connections which must be sufficiently ductile. SCI (1995) suggested as a rule of thumb that these connections be proportioned so that the endplate thickness is about 60% of the bolt diameter, to establish the right balance of strength, stiffness and ductility. The strength model to be used in design would be the same as for the full strength connections, but with the designer limited to connections that fail in mode 1. SCI (1995) presented standard connections for which the ductility had been confirmed by testing.

Thus, we find that the philosophy of SCI (1995) was similar to Eurocode 3 (1992) Annex J but with additional checks taken from BS 5950. As in Eurocode 3 (1992), there was only limited guidance in the area of ductility, however standard details were presented which had been verified by tests.

2.6.4 The Model of BS EN 1993-1-8

BS EN 1993-1-8 (Eurocode 3, 2005) was published in 2005 and replaces Annex J. The design philosophy for extended endplate connections is unchanged, with the strength and stiffness being calculated by components, using the analogy with tee-stubs. The possibility of a triangular bolt distribution (which was criticised in SCI, 1995) is retained. However, it is reserved now for slip-resistant connections and connections subject to impact, vibration and load reversal (except due to wind).

The strength model of Revised Annex J has been retained, with the three failure modes and the tee-stub participating lengths. As in Revised Annex J, an alternative equation is given for Mode 1, which takes the width of the bolt head into consideration. The equations for Modes 1 and 2 are unchanged from Revised

Annex J. A variation from Revised Annex J however, is that the possibility is now considered of an endplate failing in a combination of Modes 1 and 2 without prying forces. The criterion for this fourth ‘no-prying’ mode to apply is that:

$$L_b > \frac{8.8m^3 A_s}{\sum l_{\text{eff},1} t_f^3} \quad \text{Eqn 2.35}$$

where,

as before, m is the distance from the bolt centreline to the nearest face of the tee-stub web, less 0.8 times the leg length of the weld,

A_s is the tensile stress area of the bolt,

L_b is the bolt elongation length (grip length + ½ bolt head height + ½ nut height),

$l_{\text{eff},1}$ refers to the effective tee-stub length l_{eff} for mode 1, and

t_f is the thickness of the tee-stub flange.

The participating lengths (and so the yield-line patterns) considered for endplates and column flanges in bending, are the same as those considered in Revised Annex J (1994) – seven for the extended region, and two for the flush region when there is only one row of flush tension bolts.

The stiffness model of Eurocode 3 (2005) is again the same as for Revised Annex J. However, the factor of 0.85 in the value of $l_{\text{eff},\text{ini}}$ has been altered to 0.9, so that $l_{\text{eff},\text{ini}} = 0.9 l_{\text{eff}}$. That effectively resolves the inconsistency in Revised Annex J where a prying force of 25% is implied in one equation and a value of 28.5% is implied in another equation. The prying force applied in both cases is now 26%.

Eurocode 3 (2005) also gives a simplified method for the stiffness of extended endplates with only two tension bolt-rows. Rather than calculate $k_{\text{eff},r}$ and k_{eq} for each bolt-row from

$$k_{\text{eff},r} = \frac{1}{\sum_i \frac{1}{k_{i,r}}}, \text{ and } k_{\text{eq}} = \frac{\sum_r k_{\text{eff},r} h_r}{z_{\text{eq}}};$$

Instead, $k_{\text{eff},r}$ is calculated for the extended bolt-row, and k_{eq} is then calculated using twice that value for each bolt-row, and taking z_{eq} as the average value of h_r

for both bolt-rows. This simplification is said to lead to a lower value for the rotational stiffness S_j .

As in Revised Annex J, there is no model given for rotation capacity of extended endplates, but the same rule of thumb is provided. Thus, the rotation capacity is assumed satisfactory when the design resistance is governed by (mode 1) bending of the endplate or bending of the column flange, as long as either the column flange or the endplate has a thickness t such that $t < 0.36d\sqrt{f_{ub}/f_y}$, where d is the nominal bolt diameter, f_{ub} is the bolt ultimate tensile strength, and f_y is the endplate or column flange yield strength.

Discussion of Eurocode 3 models

Eurocode 3 (2005) is open to the same criticisms as Revised Annex J (1994) and DD ENV 1993-1-1 (Eurocode 3, 1992) before it. The yield-line pattern in the flush region is actually quite complex and bears no resemblance to a tee-stub, so that the use of an equivalent length is questionable. As reported later, experiments suggest that the yield-line pattern distribution may change as the flush region becomes inelastic, so that a participating length that is suitable at the early onset of inelastic behaviour may not be suitable for the entire range of behaviour.

Eurocode 3 allows certain joints to be designed as ductile, but the underlying material model excludes strain-hardening. This is contradictory as ductile inelastic strains imply that there must be strain-hardening. The tee-stub model for stiffness is based on an assumed geometry that is not explicitly stated in the code itself (edge distance $e = 1.25m$ – see Figure 2.15 in Section 2.6.2), and the model implicitly assumes large prying forces at collapse – a further contradiction.

From the perspective of this work, the most important criticism however, is the lack of a suitable model for estimating rotation capacity, which would be required for serviceability calculations on partial strength connections for example. In Eurocode 3 (1992) the possibility of a mode 2 endplate failure being sufficiently ductile for plastic analysis was accepted. However, this was removed in the

subsequent revisions. In effect therefore, the ductility criterion became more stringent in Revised Annex J by comparison with Eurocode 3 (1992), and mode 2 has now been excluded from plastic analyses. For the connection tests reported later in this thesis (chapter four), with an M20 Grade 8.8 bolt (average $f_{ub} = 788$ MPa) and Grade 300WA endplate (average $f_y = 309$ MPa), the Revised Annex J and Eurocode 3 (1995) rule-of-thumb would lead to a maximum endplate thickness of 11.5mm. This limit is rather conservative as shown later. For the same connection tests (M20 bolt, average $f_{ub} = 788$ MPa, average $f_y = 309$ MPa), the SCI rule-of-thumb would lead to a maximum endplate thickness of 16.9mm. This is much less conservative than the Eurocode 3 (2005) requirement. For use in partial-strength (wind moment) connections however, SCI (1995) limits the endplate thickness to 60% of d_b . For an M20 bolt that would mean a maximum endplate thickness of 12mm.

2.7 SOUTH AFRICAN EXTENDED ENDPLATE STUDIES

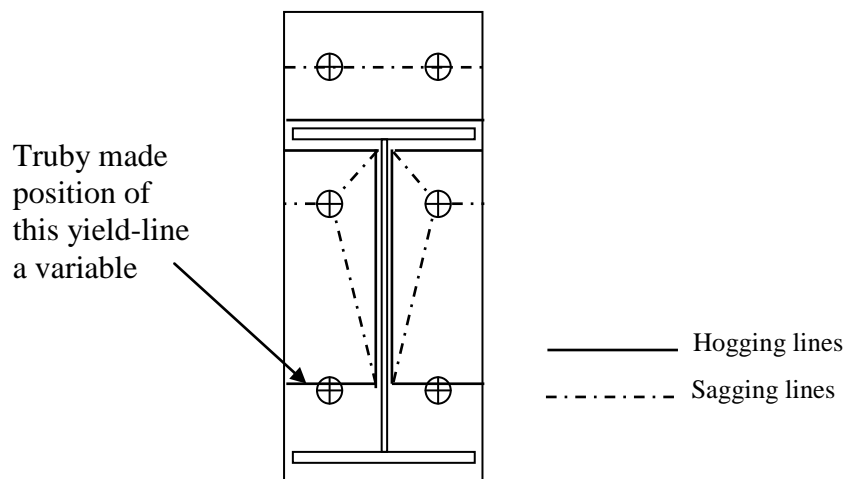


Figure 2.16 – Yield-line Pattern of Truby (1995), from Bernuzzi et al (1991)

Dekker (1986) carried out an investigation of extended endplates at the University of Pretoria. Dekker applied simple beam theory to the endplate tension region, and used a numerical method (finite differences) to obtain a solution for the flush region as a plate. The endplate geometry was taken into account using a flexibility

approach. Dekker's model was then compared with test results. Dekker's work was limited to the elastic range however, and neither his model nor his tests considered inelastic behaviour. Thus, his model is not really applicable to the emphasis in this thesis.

Truby (1995) proposed a model of extended endplate connections to establish the connection ultimate moment and the corresponding rotation, for a thin extended endplate connection. Truby carried out a yield-line analysis of the Mechanism A yield-line pattern of Bernuzzi et al (1991) to obtain the endplate tension bolt forces. This pattern was illustrated in Figure 2.13 and is reproduced here again for convenience as Figure 2.16. Truby however made the location of the lowest hogging line a variable in his model, so that the model could only be solved iteratively using a purpose-written computer programme. In Truby's programme the effect of tension bolt elongations was included as an option. The possibility of assessing bolt forces in the extended region as a fixed proportion of forces in the flush region was also included as an option.

To establish the corresponding rotation at the endplate yielded moment, Truby considered the deflection of only the extended region of the endplate from the assumption that this portion of the endplate yields first. His deflection is obtained by assuming that the portion from the bolt line to the weld line is in double curvature bending, with equal moments at the bolt line and weld line. He then assumed a moment-curvature relationship across a section of the endplate from the bolt line to the weld line, and determined the deflection from the moment of the areas of the curvature diagram.

There are two key criticisms of Truby's work. The yield-line formulation is complex and could only be solved iteratively with a computer model. This would not be suitable for everyday applications. The output from his computer simulations are useful however as they show that the inclusion of the bolt elongations does not significantly affect the yield-line analyses. The second criticism is fundamental and relates to the calculation of rotations. He assumes

that the endplate deflection is governed by the deformation of the extended region. Observation would suggest however, that the endplate rotation is governed by the deformation of the flush region. This is further discussed in Chapter five.

Truby did attempt to cater for strain hardening in the material model assumed in his computer programme, but he conceded that large strains would be incompatible with the yield-line analysis. Truby also did not attempt to determine the connection rotation capacity, but only the rotation at the fully yielded point – taken as the ultimate moment in his formulation.

3. EXPERIMENTAL WORK

In order to have a better understanding of the ductility behaviour of relatively thin extended endplates, five connection tests were carried out as part of this study. The first test with 12mm endplates and a second with 10mm endplates were pilot tests carried out to verify the test setup and to rectify problems with the instrumentation. Three other tests were then carried out with two connections per test, involving the testing to failure of 10mm, 12mm and 14mm endplates. The intention in these tests was to gain insights into thin extended endplates and increase the available data to include endplates as thin as 10mm.

Thus, there were five connection tests in total as follows:

- Pilot Test A – 10 mm endplates
- Pilot Test B – 12 mm endplates
- Test 1 – 10 mm endplates
- Test 2 – 12 mm endplates
- Test 3 – 14 mm endplates

3.1 SETUP OF CONNECTION TESTS

A cruciform arrangement was adopted in the tests, with two beams connected into each flange of the column at the same level. Thus, two beam-to-column connections were tested simultaneously. Figure 3.1 shows the cruciform arrangement used. The test specimen beams were supported at their far ends on beams running perpendicularly on trestles. The load was then applied to the top of the column stub using a hydraulic jack. In this way, the lower beam flanges were in tension while the upper flanges were in compression. The load was applied to the column top with a square load button screwed onto the ram of the jack, with the button bearing on a recess in a load plate welded to the column. Thus, the load point was restrained against lateral and longitudinal displacement.

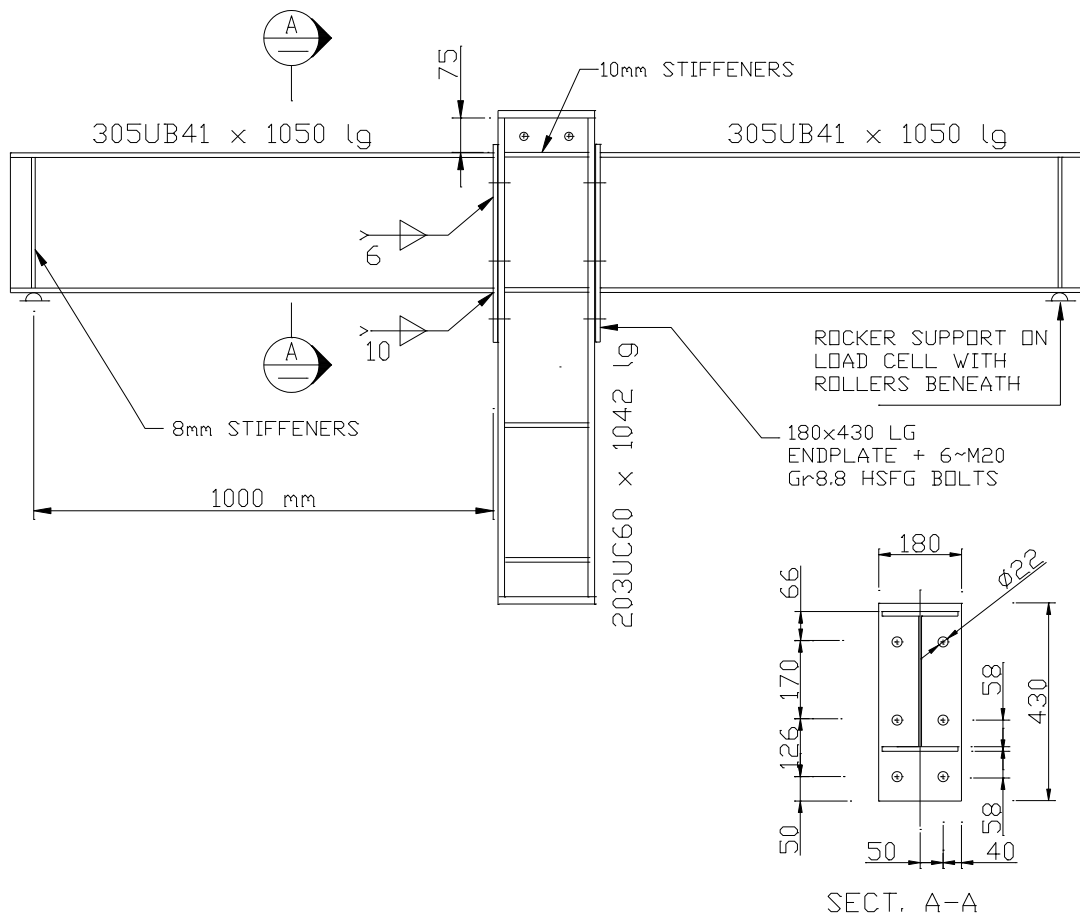


Figure 3.1 – Setup for the Connection Tests

The column web was also laterally restrained against out-of-plane rotation just above the beam tension flanges, using struts of adjustable length, with rollers at their far ends that fitted into guides fixed to the load frame. These restraints were necessary to prevent out-of-plane rotation of the column (leading to unwanted secondary effects), and to prevent instability under load. The column had two pairs of 10mm web stiffeners at locations opposite the beam flanges at the joint. There was also a 16 mm plate welded to the top of the column where the load would be applied, to distribute the load evenly through the cross-section and prevent bearing failure. It was our aim to test the endplate in isolation while minimizing the interaction with the column flange. In order to replicate a practical connection we chose not to use an unrealistically stiff column, but rather to provide stiffeners at the flange levels and accept minor column deformations.

During the pilot test the column was instrumented with an inclinometer to measure any in-plane column rotations. In the latter tests this measurement was discarded and the bottom part of the column was instead restrained with snug fitting vertical guides to prevent any in-plane rotation. The column restraints are shown in Figure 3.2. At the beam-to-column connection end, each beam was welded to its endplate with E70XX 10 mm fillet welds (flanges - both sides) and 6 mm fillet welds (web - both sides). These welds were chosen to exclude the possibility of the connections failing by weld fracture.

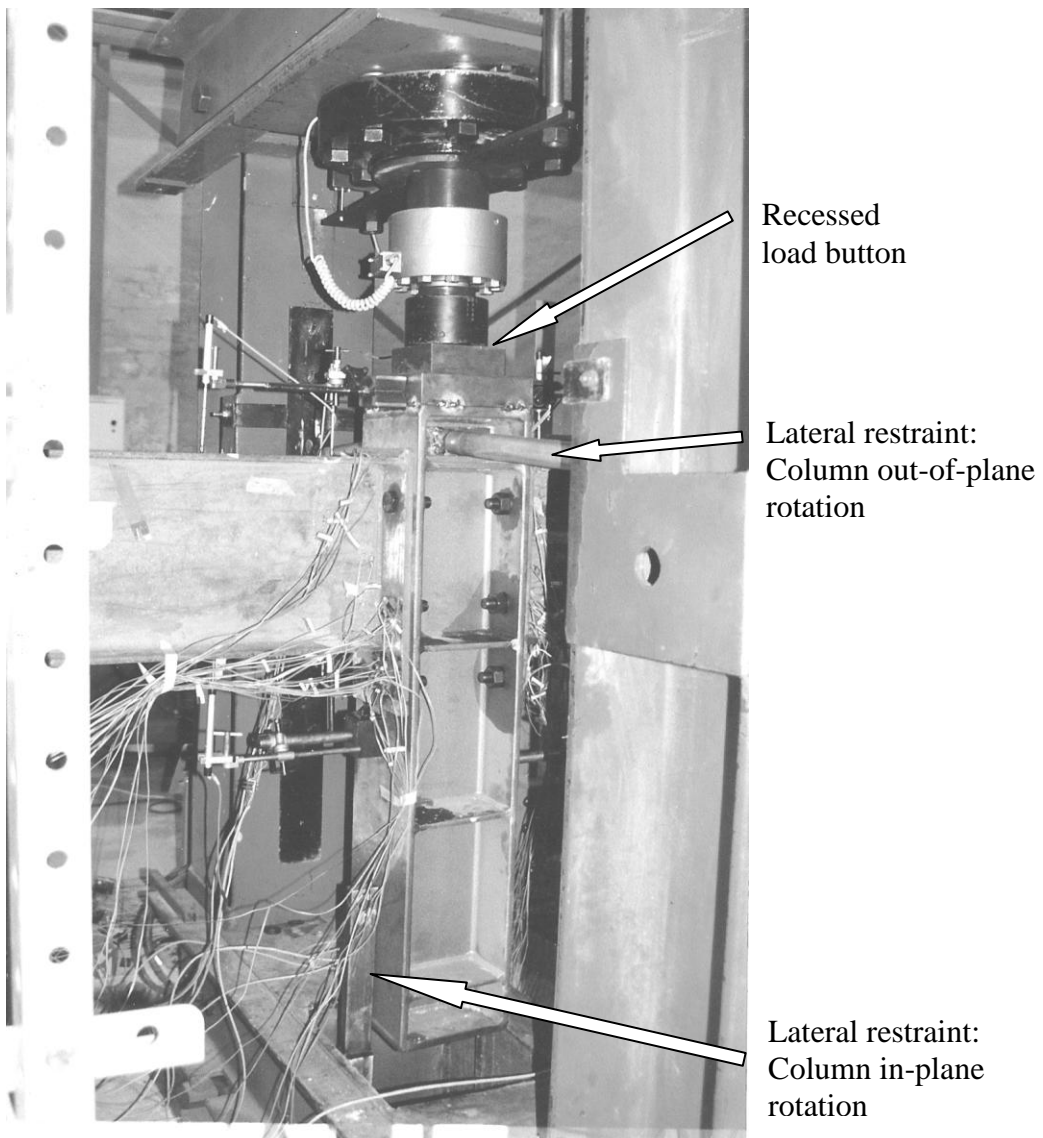


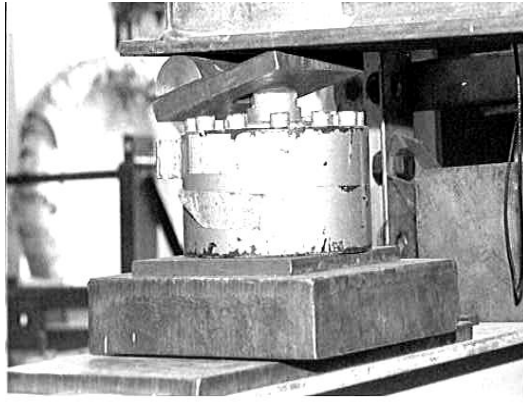
Figure 3.2– Lateral restraint of the column

At the simply supported end, each beam was supported on back-to-back double channel cross-beams, which were supported in turn on laced and battened ‘towers’ secured to the ground. Above the support, each beam had its (upper) compression flange restrained against lateral movement but not against rotation. This was done by providing a pair of ribbed bar ‘guides’ fitting snugly on either side of the beam flange. Thus, the beams were laterally restrained but allowed to move longitudinally and to rotate. This was to prevent the development of extraneous axial forces and end moments due to rotational restraint, during tests. Rotational and longitudinal freedom was ensured using a rocker consisting of a half-round bar supported on needle roller bearings, with a load cell between the half-round and the rollers. The rollers allowed the beam to move longitudinally.

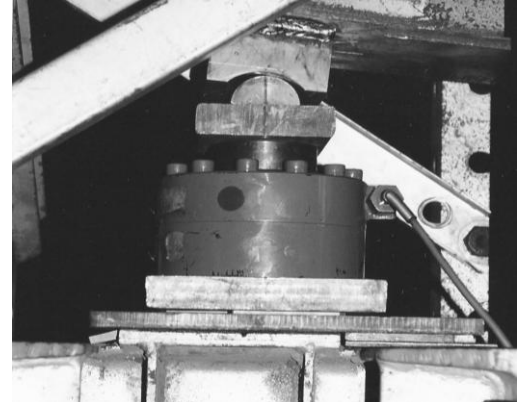
The beam end had a recess welded on with the same shape as the rocker, to reduce the likelihood of the rocker shifting from beneath the beam during testing. Essentially therefore, the beam end was on a line support. In the first pilot test we supported the half-round on the button of a load cell so as to have a point support at each beam. This proved to be unsuitable as the arrangement became unstable at large deflections. This realisation was brought home in dramatic fashion as during the test a load cell at one end suddenly shot out from its position. We therefore changed to the line support described above. The two support arrangements are shown in Figure 3.3.

The choice of endplate geometry was made to reflect typical South African practice and also to facilitate comparison with the predictions and tests of other researchers. The endplate dimensions and geometrical details are given in Figure 3.1. The plate was 430 x 180 mm wide, with 22 mm diameter bolt holes for M20 Grade 8.8 HSFG bolts. The bolt holes were located at a gauge of 100 mm symmetrically about the plate centreline, with an edge distance of 40 mm on each side. The extended region row of bolts was 50 mm from the plate end as can be calculated from the dimensions in Figure 3.1. The distance from the tension bolts centre to the beam flange surface was made as small as feasible for tightening of

bolts (58mm). Thus, the tension bolt pitch is not a round figure but rather 126.2 mm, which is $58 + 58 + 10.2$ (nominal flange thickness).



(a) Initial unstable point support



(b) Stable line support

Figure 3.3 – Supports at Test Beam ends

3.2 THE TEST SPECIMENS

My choice of section sizes for the tests was based on the following considerations:

- The use of ‘average’-sized sections/details that would be applicable in a wide variety of situations.
- Section sizes and details that are relatively commonly used in South Africa, and which are typically used together.
- The need for failure of the test specimens to be initiated by the endplate rather than by failure of the beam flanges or column flange.

Based on these considerations, I elected to use a 305 x 165 x 41 I section (305 UB 41) as the beam in all the tests, with a 203 x 203 x 60 H column (203 UC 60) – both in Grade 300WA. The use of a 305 series beam facilitates comparison with several well-documented published test results using similar sized beams (Bernuzzi et al (1991), Zandonini & Zanon (1988) and Jenkins et al (1986). It was

considered that the 305 UB 41 and 203 UC 60 sections could typically go together, and would be suited to a medium load in a commercial or industrial structure. These parallel-flange section sizes are in common usage in South Africa. The intention in the tests is to limit bending of the column flange so the column flange contribution to connection deformation is small or negligible. The 203 UC 60 has a 14mm flange, and web stiffeners are introduced at the beam compression and tension flange levels, to achieve this.

Both sections are Class 1 – plastic design sections (both flange and web) under the provisions of SANS 10162 (2005). The beam web is Class 1 in bending but not in axial compression. From the South African Institute of Steel Construction’s Handbook (SAISC, 1997), these section sizes have the following nominal dimensions:

Table 3.1 – Nominal Dimensions for Test Section Sizes

Designation	m	D	b	t _w	t _f	r ₁	h _w	A
mm x mm x kg/m	kg/m	mm	mm	mm	mm	mm	mm	10 ³ mm ²
305x165x41 I	40.5	303.8	165.1	6.1	10.2	8.9	266	5.16
203x203x60 H	59.7	209.6	205.2	9.3	14.2	10.2	161	7.60

In Table 3.1, D is the overall depth of the section, b is the breadth, t_w is the web thickness and t_f is the flange thickness. The dimension r₁ is the root radius at the web-flange joint, and h_w is the clear distance from the top of the root radius above the bottom flange to the bottom of the root radius below the top flange. The beam mass is denoted as m in kg/m and the cross-sectional area as A. Three endplate thicknesses were used in the tests – 10mm, 12mm and 14mm. These were all in Grade 300WA steel. A 14 mm endplate was taken as the upper limit, since this was the maximum value at which I expected to find the endplate behaving as ‘thin’, based on the literature reviewed. 10mm was selected as a lower limit as there are few tests reported in the literature with thinner endplates than 12mm.

Thus, the 10mm endplate test would help extend the range of available endplate test results. I did not extend the lower limit to 8mm as an 8mm endplate would be considered unreasonably thin, relative to the beam size, in current practice.

Typical South African practice is to standardize connection bolts on M20 and M24 sizes for Grade 8.8 HSFG. I therefore used M20 Grade 8.8 HSFG bolts in all the tests.

3.2.1 Beam and Column Material Properties

Table 3.2 – Material Properties for Connection Tests

	Young's Modulus GPa	Yield stress MPa	Yield strain 10^{-3}	Hard'g strain 10^{-3}	Hard'g Modulus GPa	Ultimate Stress MPa
Col flange	209.6	299.1	1.43	16.60	3.82	483.0
Col web	201.9	333.9	1.65	12.20	4.01	494.7
Bm flange (1)	209.7	324.4	1.55	17.75	5.09	494.9
Bm web (1)	213.6	365.3	1.71	21.10	3.91	525.4
Bm flange (2)	205.7	318.9	1.55	16.80	4.91	493.7
Bm web (2)	212.1	381.8	1.80	14.55	3.88	534.6
10 plate (pilot)	212.1	304.5	1.44	11.60	5.84	537.6
12 plate (pilot)	219.1	306.0	1.40	13.50	5.04	510.2
10mm plate (Test 1)	202.2	331.3	1.64	13.45	3.50	505.7
12mm plate (Test 2)	219.1	306.0	1.40	13.50	5.04	510.2
14mm plate (Test 3)	213.0	295.0	1.39	13.60	4.58	478.3

The beam and column material was donated by fabricator member companies of the Southern African Institute for Steel Construction, and fabricated by them in their shops to typical tolerances and standards. The beams and columns were taken from one length each, and the endplates from one plate each for a given thickness. Off cuts were obtained and used to determine the material properties, in tensile tests. Two coupons were taken per beam or column flange (for each flange), and two coupons per beam web. Also a minimum of four coupons were taken per plate – two in the longitudinal direction and two from the transverse direction. The material test data is included in Appendix A, and the averages of the properties determined are summarized in Table 3.2:

The material properties measured in the tensile tests were essentially tri-linear with a linear elastic portion, then a flat yielding plateau with zero slope, and finally a strain-hardening region with a reduced but non-zero slope. Thus the material behaviour has been summarized by the moduli of the elastic and strain-hardening regions, and the stresses at which yielding commenced and at which strain-hardening commenced. We were unable to measure the strain-weakening behaviour because of the likelihood of causing damage to the extensometer, however we did determine the fracture load and so the ultimate stress in each test. A typical stress-strain curve derived in one of the material tests is shown in Figure 3.4 to illustrate the tri-linear nature.

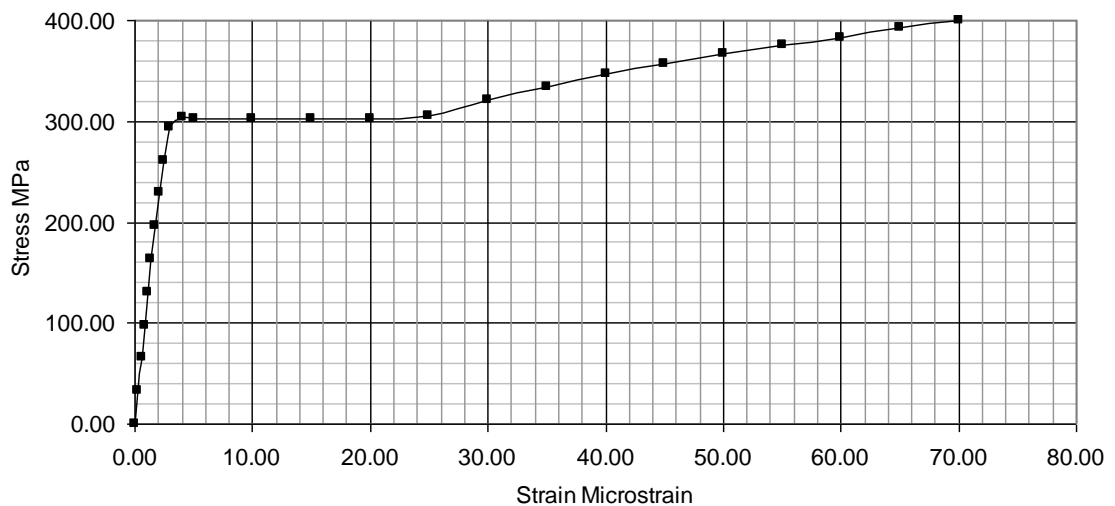


Figure 3.4 – Typical Stress-Strain Curve from an Endplate Coupon

As can be seen in Table 3.2, the material for the beams came from two sources. The ones marked (2) were used in the 10mm endplate tests, while the ones marked (1) were used in all other tests, including the 10mm pilot tests. The actual dimensions of the beams, columns and plates were measured, and these and the material properties above have been used to compute the actual beam and column section properties, which are reported in Table 3.3.

The yield moment M_y for the column and beams has been derived from the following equation:

$$M_y = \frac{\sum I_{xx} \cdot f_y}{y} \quad \text{Eqn 3.1}$$

where the summation is for the flanges and web; I_{xx} is the second moment of area, f_y is the yield stress and y is half the section depth. M_y and M_p both refer to bending of the beam (and column) about the strong axis. The values given for the plates are calculated per meter length.

Table 3.3 – Actual Section Properties for Test Specimens

	Flange thickness mm	Web thickness mm	Elastic Modulus $\times 10^3$ mm^3	Plastic Modulus $\times 10^3$ mm^3	Yield Moment M_y kN-m	Plastic Moment M_p kN-m
203UC60 Col	14.03	8.88	575.20	644.14	173.75	195.48
305UB41 Bm (1)	9.95	5.89	549.84	610.96	181.75	203.44
305UB41 Bm (2)	10.19	6.24	564.30	628.81	185.40	209.00
10 mm plate/m	10.24	-	17.48	26.21	5.79	8.68/m
12mm plate/m	11.83	-	23.33	34.99	7.14	10.71/m
14mm plate/m	13.86	-	32.02	48.03	9.45	14.17/m

3.2.2 Bolt Material Properties

All the bolts used in the material and connection tests were M20 Grade 8.8 HSFG bolts taken from a single production batch. In order to determine the material properties for the bolts, samples were tested to failure in pure tension, while recording the applied load and corresponding strains. Strain is measured as a surrogate for the bolt extension. The literature suggested that bolt strains would be related to the bolt grip length i.e. the total thickness of plies (column flange, endplate and washer) gripped between the bolt head and the nut. Thus, I needed to determine stress-strain characteristics for the different grip lengths to be used in the actual connection tests. These corresponded to the 10mm, 12mm and 14mm endplate thicknesses.

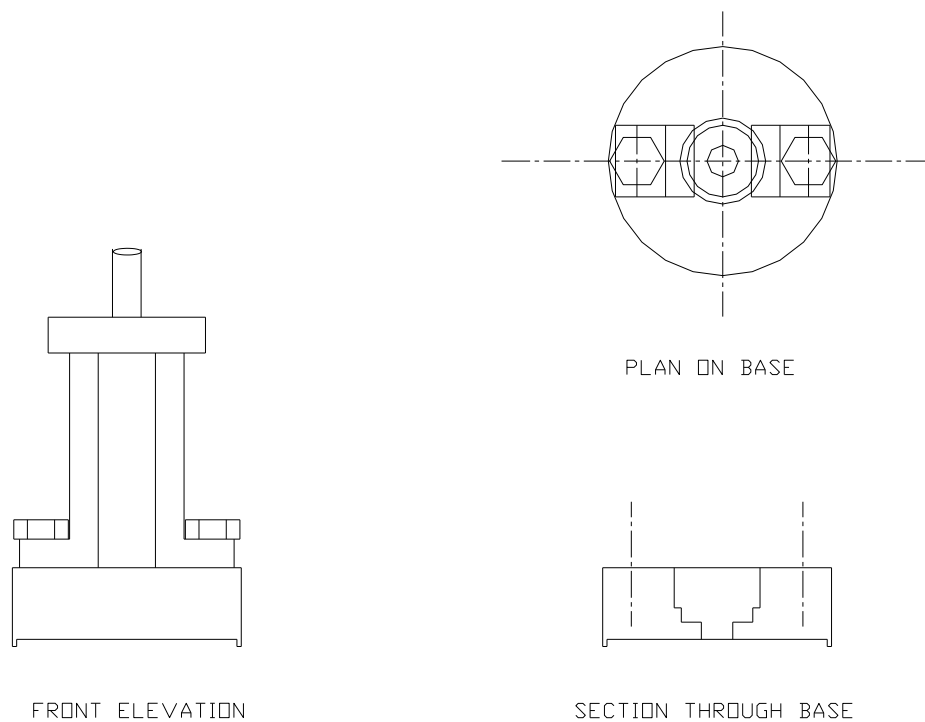


Figure 3.5 – Layout of Bolt Yoke

We designed a ‘yoke’ that could be gripped in the Amsler tensile testing machine, and which would allow the bolt and nut assembly to be pulled apart in pure tension. The layout of one of the symmetrical halves of the yoke is shown in Figure 3.5, and a picture of the test is shown in Figure 3.6. The yoke consists of

two symmetrical halves with each half having a base and an upper part attached to a rod. The base has a recessed hole in which the tested bolt with its washer and nut is fitted, and the rods for both halves are then clamped into the tensile testing machine so the bolt can be pulled apart. Three yokes with different recess depths were used to simulate three different grip lengths.

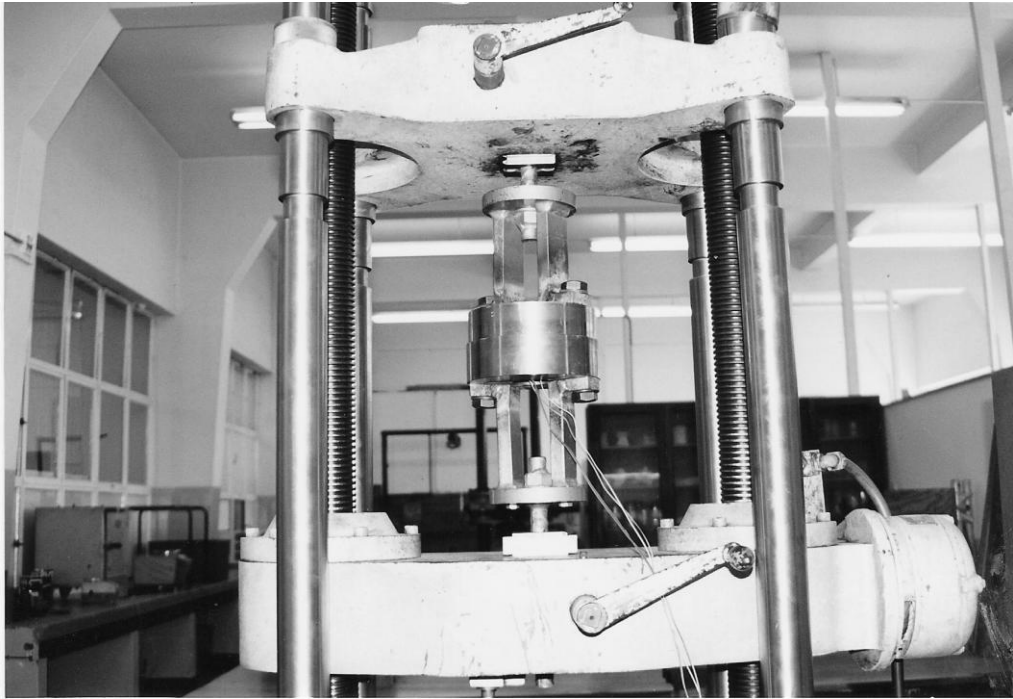


Figure 3.6 – Bolt Material Test in progress

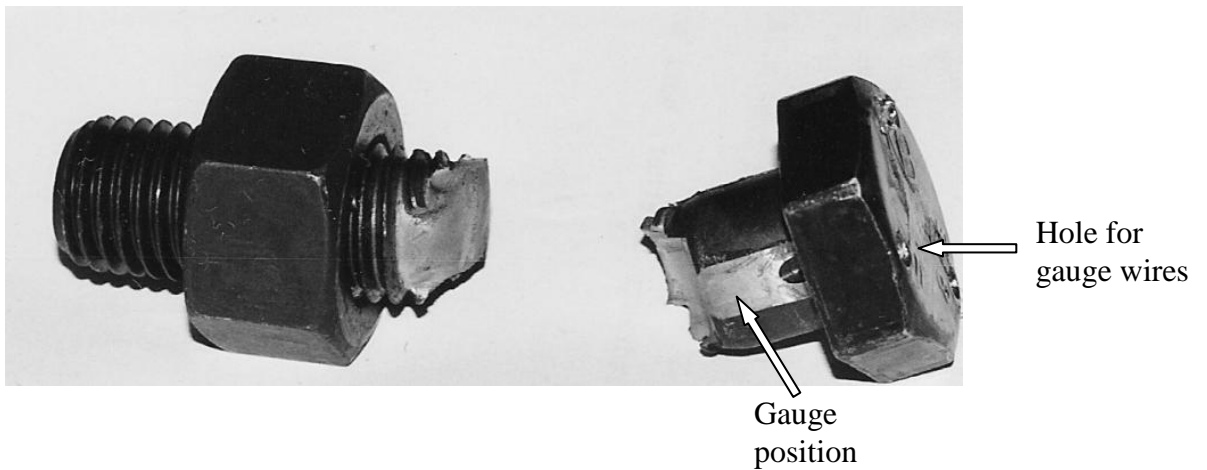


Figure 3.7 – Strain gauging the bolt

The bolt strains were measured by putting strain gauges onto the bolt shank, just adjacent to the threaded region. The gauges were placed to measure longitudinal strains along the length of the bolt. In order to ensure that bending effects could be eliminated, three gauges were used on each bolt, with the gauges at 120 degrees around the bolt circumference. It was necessary to machine the bolt surface flat at the position of each gauge, to prepare a flat surface for the gauge and to prevent the gauge from damage during tests. The machined region was 6mm wide and 10mm long, so that the nominal bolt diameter was reduced locally by 0.46mm and the area reduced by 1.38 mm². The actual shank diameter and actual machined area was measured for each bolt, and the actual areas were calculated and used to convert forces to stress. Holes were drilled into the bolt head to pass the gauge wires through without damaging them, and the installed wires and gauges were all coated with non-conducting lacquer. The drilled holes had to continue as a groove into the shank for a short length so the gauge wires did not ‘pinch’ with bolt tightening. The bolt modification for strain gauges can be seen in Figure 3.7.

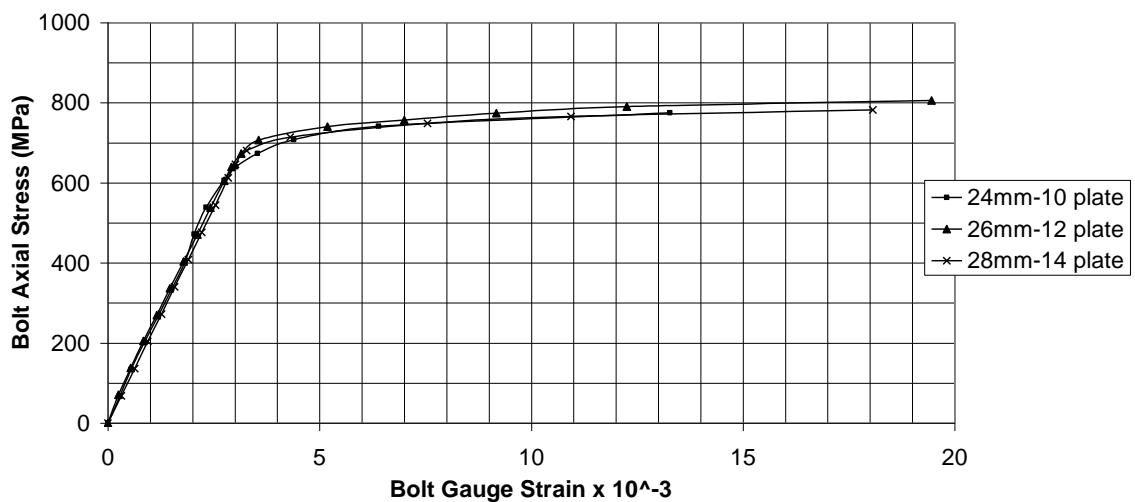


Figure 3.8 – Bolt Stress-Strain Curves

Two bolts were tested for each of the three required grip lengths. Each test was carried out to failure. The stress rate was kept at about 3 MPa/sec, and the strain was kept to about 0.0025/s from the yield point to fracture. In all tests, the bolts failed in tension by fracturing across the threads. The exact yield point was

determined graphically. The stress-strain curves for the bolts are essentially bilinear with no intermediate plateau. These are shown in Figure 3.8. The curves can therefore each be represented in terms of the initial elastic modulus and the strain-hardening modulus, together with the yield point and the ultimate fracture point. The measured bolt properties are summarized in Table 3.4 for each of the tested grip lengths. These bolt properties provide a means of converting bolt strains measured in the connection tests, into actual bolt forces.

The average yield stress measured was 725.58 MPa, versus the nominal yield value of 640 MPa. The average ultimate stress measured was 788.22 MPa versus the nominal value of 800 MPa (but there would be stress concentrations at the threads). The ratio of yield to ultimate stress is 92% rather than the nominal 80%. Thus, a bolt failure would be more brittle and unexpected and possibly more catastrophic.

The change in grip length from one test to another did not appear to have a consistent effect. Therefore, although the measured values for each endplate thickness are used wherever appropriate, grip length was not considered as a variable after these tests.

Table 3.4 – Measured Material Properties for Bolts

Grip Length (Excluding washer thickness)	Young's Modulus (GPa)	Yield Stress (MPa)	Yield Strain (10 ⁻³)	Harden Modulus (GPa)	Ultimate Stress (MPa)	Ultimate Capacity (kN)
24mm (10mm plate grip)	228.53	725.26	3.174	4.90	773.39	238.3
26mm (12mm plate grip)	223.21	729.03	3.266	7.09	808.50	239.5
28mm (14mm plate grip)	215.13	722.44	3.358	5.21	782.78	229.9

3.3 THE TEST INSTRUMENTATION

In order to understand the behaviour of the connections tested, we needed to determine the following parameters for each test beam connection to the column.

1. The connection moment and the corresponding rotation.
2. The tension bolt forces in the extended and flush regions.
3. The stress distribution patterns along and across the endplate, and in the beam adjacent to the connection.

The connection moment could be determined from the load applied to the connection. The load transferred into each of the two connections was measured from a load cell at each far end beam support, with the jack load being monitored as a check on the load cell measurements.

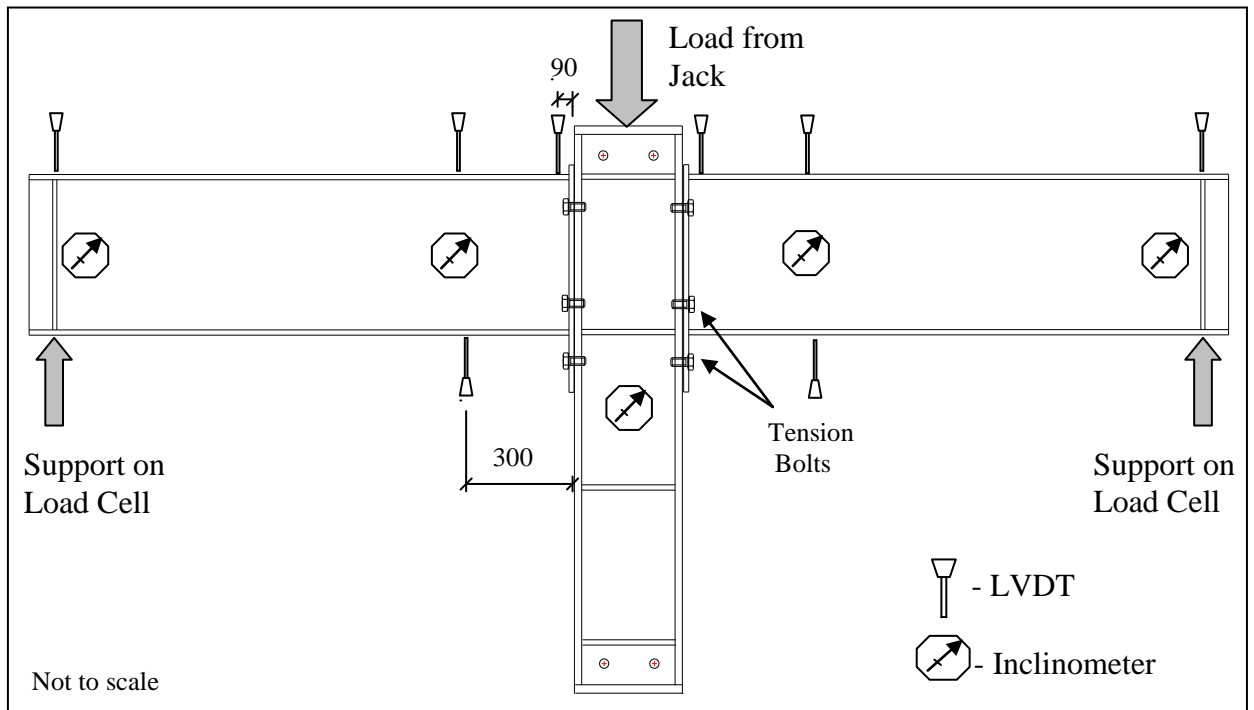


Figure 3.9– Test Instrumentation

The rotation measurements were made with linear voltage-displacement transducers (LVDTs) and with inclinometers (see Figure 3.9). LVDTs actually

measure displacement but this is easily converted to rotation once the exact distance from the column axis is known. Inclinometers measure angles directly. The positions of some LVDTs and inclinometers were changed after the first test, and Figure 3.9 shows positions that were constant for all the connection tests.

Each beam had an inclinometer at the beam support and another at 300mm from the endplate face. A fifth (dual-axis) inclinometer on the column web was used to monitor in plane and out of plane column rotations. Similarly, each beam had an LVDT on the beam column flange adjacent to the column face (90mm from the column face – the closest distance practicable), a second on the compression flange at 300mm from the column face, and a third at the beam support. There was also an LVDT on the tension flange at 300mm from the column face, as a check on the compression flange LVDT. The measurement at 300mm approximates a distance equal to the beam depth away from the column face. This is commonly taken as the extent of the joint region. These LVDTs at the column face and at the joint limit were mounted off the column face, so that they measured beam displacement parallel to the column axis, while the beam support LVDT was mounted off the support steelwork and measured displacement of the beam support under load.

The displacement transducers were intended as a check on the inclinometer readings. However, problems with faulty inclinometers led to us discarding the inclinometer readings and using the LVDT data only. The column inclinometer readings became redundant after the pilot test and were discontinued, as lateral restraints were introduced to prevent in-plane and out-of-plane rotation of the column. Guides were introduced at the level of the beam compression flanges to prevent out-of-lane rotation. Other supports were fixed in place at the base of the test rig to guide the lower part of the column and prevent in-plane rotation.

In order to determine tension bolt axial forces, bolt strains were measured with three strain gauges at 120° per bolt, as in the bolt material tests. Two of the four tension bolts were instrumented per connection – one in the tension flush region

(immediately above the beam tension flange in Figure 3.9) and the second in the extended region of the connection – making four instrumented bolts in each test. These measured bolt strains could then be converted to stresses and axial force, using the stress-strain curves obtained in the bolt material property tests for the given grip length, and the measured bolt diameter, to effect the conversion.

In the two pilot tests and in the Test 2 (12mm endplate test), I attempted to measure the deflection of the endplate away from the column at the level of the beam tension flange. In order to do this, a hole was drilled through the column flange and horizontal slots were cut into the column web, to allow an LVDT to bear on the endplate surface. Cover plates were therefore welded across the column from flange toe to flange toe, to counteract any weakening effect due to the cuts. This measurement was discontinued after the first test because it was difficult to manoeuvre the LVDT into position. Thus, the column web cut-outs and cover plates were not used in the 10mm and 14mm tests.

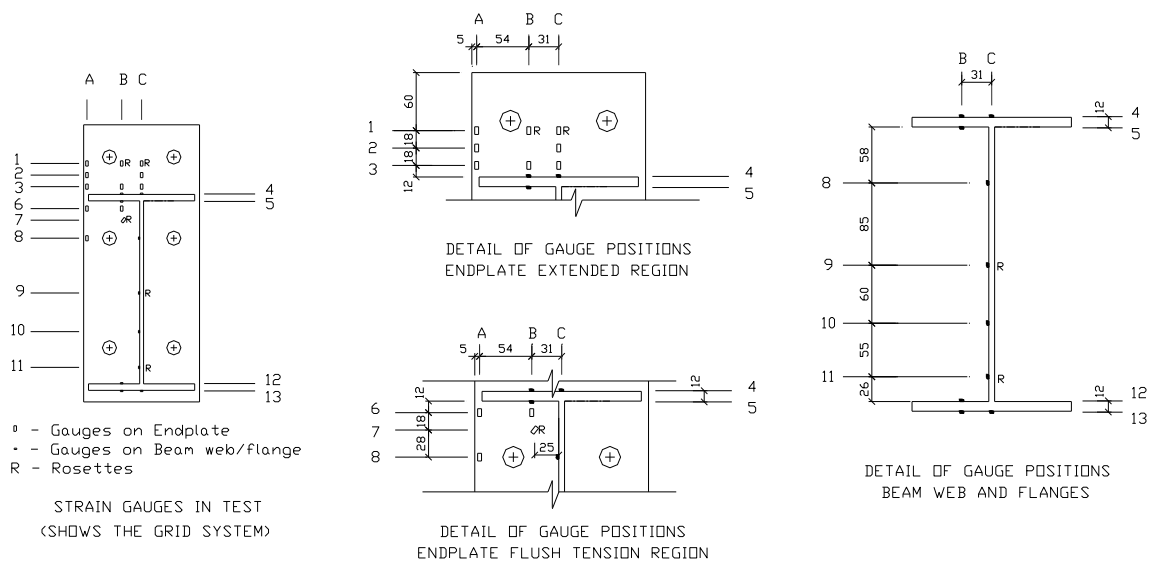


Figure 3.10 – Strain Gauges on the Endplate and Beam End

Strain gauges were placed on the endplate and beam ends as shown in Figure 3.10. There were 13 gauges on each endplate including three 0-45-90 rosettes, and 10 gauges on each beam including two rosettes. The beam gauges were placed

with their axes along the beam length, at 5mm from the end of the beam-endplate weld. When the strain gauges on the bolts are included, a total of 58 strain gauges were monitored during each test, for both beams, with ten of these being rosettes.

For convenience of referral, the endplate gauges are labelled using a grid system as shown in Figure 3.10. Thus, for example the uppermost gauge on the left in the figure is referred to as gauge A1. Gauges A1-3, B1, B2, and C1-3 are in the extended region of the endplate; gauges A6, A8, B6-7 are in the tension part of the flush region, while gauges B4-5, B12-13, C4, C8-11, and C13 are on the beam end web and flanges.

By comparison with Figure 3.1 which gives the endplate dimensions, Figure 3.10 has been rotated to have the beam tension flange above the compression flange, as this is the more typical presentation in literature.

The strain gauges used on the bolts, endplates and beam ends were mostly Kyowa single gauges KFG-2-120-C1-11 bonded with CC-13A glue – a room-temperature-setting cyanoacrylate. These are self-temperature-compensating (SELCOM) gauges designed to operate around ambient temperature on steel specimens with a linear expansion coefficient of $11 \times 10^{-6}/\text{degree Centigrade}$. All the tests were carried out in an indoors laboratory environment with no exposure to direct sunlight. Ambient temperatures indoors during tests varied by only a few degrees Centigrade, with 20 degrees Centigrade as an average value, and there were no temperature gradients across the specimens. SELCOM gauges are completely self-compensating under those conditions, from about room temperature up to about 60 degrees Centigrade. Thus, temperature compensation measures were not required in the tests.

The three gauges marked as rosettes in Figure 3.10 were KFG-2-120-D17-11. These are 0-45-90 rosettes with the three resistive elements being similar to the element in the KFG-2-120-C1-11. Thus, the behaviour is similar.

Strain measurement was carried out for each gauge, using a 1-gauge Wheatstone bridge i.e. a bridge with the active gauge on one gauge arm and three precision resistors (120 Ω) on the other three arms. Little portable bridges were manufactured for this purpose, each with its potentiometer. To reduce errors from noise in long lead wires (3m length) the Wheatstone bridge output was amplified before being fed into the recording multiplexer.

Calibration of the strains was based on the specified gauge factors, which ranged from 2.05 to 2.15 for different batches. For the KFG-2-120-C1-11 the use of a specified gauge factor rather than a calibrated gauge factor leads to an estimated 5% error for plastic strains i.e. above 8 000 to 10 000 μ strains. This was considered an acceptable error range. The resistive element in the KFG-2-120-C1-11 is 2mm long, which means the measured strains are really averaged over a 2mm length. This was also considered a reasonable level of accuracy.

3.4 THE TEST PROCEDURE

Each test was carried out in three steps as follows:

1. The bolts were initially made finger-tight, then load was applied slowly via the jack to approximately 30 kN at the jack (15 kN-m per connection), and then unloaded, to allow the endplates to 'bed' in and seat properly.
2. The bolts were then made 'snug tight' and bolt strain readings were taken. Clause 21.12.2 of the South African structural steel design code SANS 10162-1:2005 requires bolts in a slip-critical connection (which would be a typical application for an extended endplate), to be pretensioned. The pretension for an M20 Grade 8.8 HSFG bolt should be at least 142 kN (Table 7). The code provides for the pretension to be measured by the turn of the nut (Table 8) or with the use of a direct indicator. This approach is endorsed in Clause 4.5.3.2 of SANS 2001-CS1:2005. We have chosen to use the turn of the nut method as this is more typical in everyday South African practice, and we consider this to be better than the other methods. Thus, the bolt pretension was applied by

applying a third turn to each bolt. The bolt strains were again recorded after the pretension was applied.

3. The load was applied until a connection failed. In the loading we initially controlled the test based on the load applied (a constant rate of load application), but then moved to displacement-based control once it was clear that the connection had begun to yield and/or deform.

In test 2 (which was the first test chronologically), the load application was actually carried out in four load cycles of load and unload – an elastic cycle first, then three plastic ones with the last cycle continued to failure. In these tests, failure was defined as either the connection becoming incapable of sustaining a load any longer, or as fracture of a connection component.

4. CONNECTION TEST RESULTS

The results for Tests 1 – 3 are given below in the rest of this chapter. The Pilot Test results are only included in the qualitative descriptions of section 4.1 as the instrument readings for the pilot tests are not available. The data from each test can be distinguished into four categories – the observations and failure modes, the connection rotation data, the bolt strain gauge data, and the endplate and beam strain gauge data. I have distinguished between the data for both beams in each test, differentiating them as a Beam A and a Beam B. Thus, in Test 2 for example, Beam 12A refers to the A beam in the 12mm endplate test.

4.1 OBSERVATIONS IN CONNECTION TESTS

4.1.1 Test 1 Observations

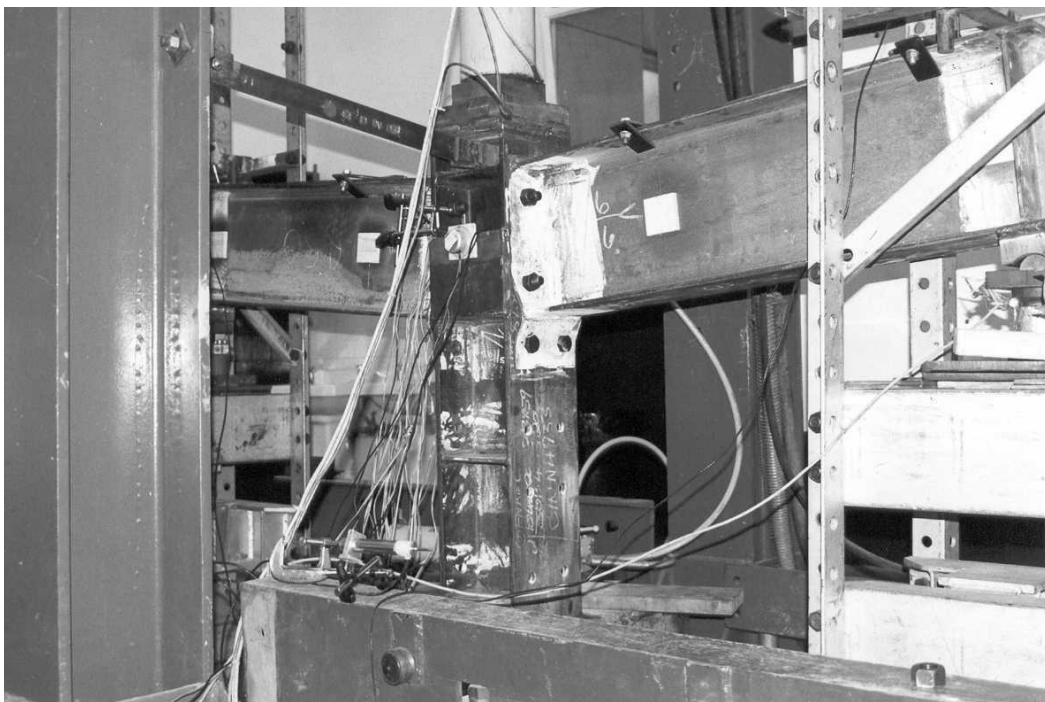


Figure 4.1 – Pilot Test A in progress

Figure 4.1 shows the specimen in Pilot Test A during the conduct of the test. In both Pilot Test A (the pilot 10mm test) and Test 1 (the actual 10mm test), the bending of the endplate was about two axes. There was considerable bending along the length of the endplate, especially about the beam tension flange. There was also clearly transverse bending across the width of the endplate, with this being particularly evident in the flush tension region.



(a) Endplate fracture & deformation (b) Buckle in compression flange

Figure 4.2 – Fractured endplate from Test 1

The endplate yielding started around the extended and flush region tension bolts and initially appeared to be rotationally symmetrical around each bolt-head, thus suggesting a circular yield-line pattern. As the test progressed however, the yielding, the progression of which could be distinguished by the flaking off of mill scale, became similar to that described for thin endplates in Surtees & Mann (1970) and Mechanism A of Bernuzzi et al (1991). As the test progressed further,

the yielding progressed into straight lines rather than the initial circular pattern, until the endplate fractured in the flush tension region with straight longitudinal cracks running parallel to and adjacent to the beam web welds. There were also transverse cracks in the endplate extended region, parallel to and adjacent to the beam tension flange weld. The longitudinal cracks are apparent in Figure 4.2 (a). In Figure 4.2 (a) it is also possible to see a ‘kink’ in the beam profile where it is welded to the endplate, at the shear bolt level. Thus, the beam profile is in compression to the shear bolt level. In Test 1 the test was stopped only when the crack next to the beam tension flange weld developed into a complete transverse fracture across the endplate width on one connection, so that the endplate tore into two pieces.



Figure 4.3 – Beams 10A and 10B after the test

The fracture of the endplate in Test 1 was almost lamellar in nature, tearing at a shallow angle through the endplate, rather than in a clean break – see Figure 4.2 (a). (In Pilot Test A, which was on a nominally identical sample, the test was stopped when a bolt in the extended region fractured on one connection). The arrows on Figure 4.2 (a) show the transverse fracture and the longitudinal crack

on the endplate. Prior to the endplate fracture, the beam compression flange had developed a local buckle. This is shown in Figure 4.2 (b). By comparison with beam 10B that failed, the local buckling in beam 10A was less noticeable. Figure 4.3 shows both beams 10A and 10B after testing. The more pronounced local buckle in 10B is evident, as also the greater permanent deformation.

In Figure 4.3, we notice that each endplate is permanently deformed such that there is a bulge away from the column flange, between the level of the flush tension bolts and the shear bolts.

4.1.2 Test 2 Observations



Figure 4.4 – Cracking in Beam 12A endplate

In Test 2 with the 12mm thick endplates, there was noticeable flaking of the endplate as early as the first plastic cycle – starting first on the transverse line adjacent to the weld in the extended region, then in a transverse line around the bolts. The bending of the endplates was initially quite slight, and only became

pronounced in the second plastic cycle. There was more noticeable buckling of the beam compression flanges towards the end of the test. There were loud cracking noises at 300 kN (approximately 150 kN-m per connection) and 308 kN, and the actuator load began to drop shortly afterwards, going from a recorded maximum of 311 kN to about 305 kN at failure.

Test 2 was terminated when the endplate on beam 12A sheared - fracturing into two pieces - on the weld line in the extended region. On examination, endplate 12B was seen to have also cracked on the weld line. In addition, both endplates had fine cracks at the root of the beam web weld, on both sides. These longitudinal cracks extended from the tension flange to about half the beam depth.

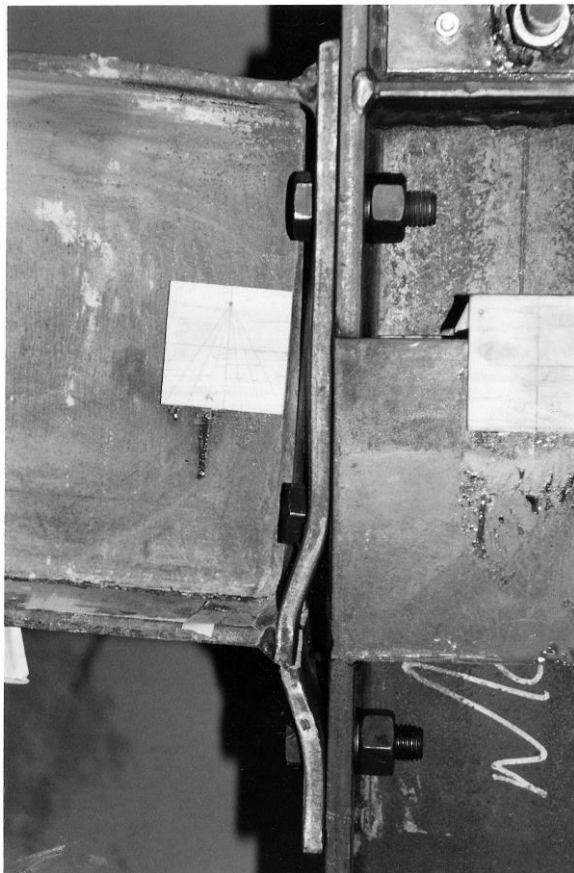


Figure 4.5 – Endplate for Beam A from 12 mm Endplate Test 2

The transverse fracture is clearly visible in Figure 4.4 and the longitudinal crack can just be seen in that figure. There were also fine cracks in the beam flange weld on the flush side, also visible in Figure 4.4. The failure mode was identical to that observed in pilot test B. As with the 10mm endplates in Test 1, the deformation pattern during the tests was similar to that described by Bernuzzi et al (1991) for thin endplates (Mechanism A).

Again, the beam that failed (12A) appeared to have more pronounced local buckling in the compression flange than beam 12B. By comparison with the 10mm endplates, the 12mm endplates deformed less – both longitudinally at the beam tension flange, and transversely across the endplate width, about the beam web. The cracks along the beam web were finer but the buckling of the beam compression flange was more pronounced and there was a slight but noticeable curvature of the tension flange adjacent to the endplate as well. The flush side cracks in the beam flange weld which were reported for the 12mm endplates, were not visible in the 10mm endplates.

The local buckle in the beam compression flange can be seen in Figure 4.5 for beam 12A. The same bulge is observable in the endplate, between the flush tension bolts and the shear bolts.

4.1.3 Test 3 Observations



Figure 4.6 – 14mm endplate Test 3 in progress

Figure 4.6 shows the deformation of the endplate during the course of the 14mm endplate test - Test 3. In Test 3 the endplate deformation differed from that in tests 1 and 2. There was very little of the transverse bending about the beam web that was evident in the other tests, and the partial circular pattern in the flush region about the tension bolts, was not discernible. Nevertheless, there was significant bending in the endplate longitudinal direction, about the tension flange.

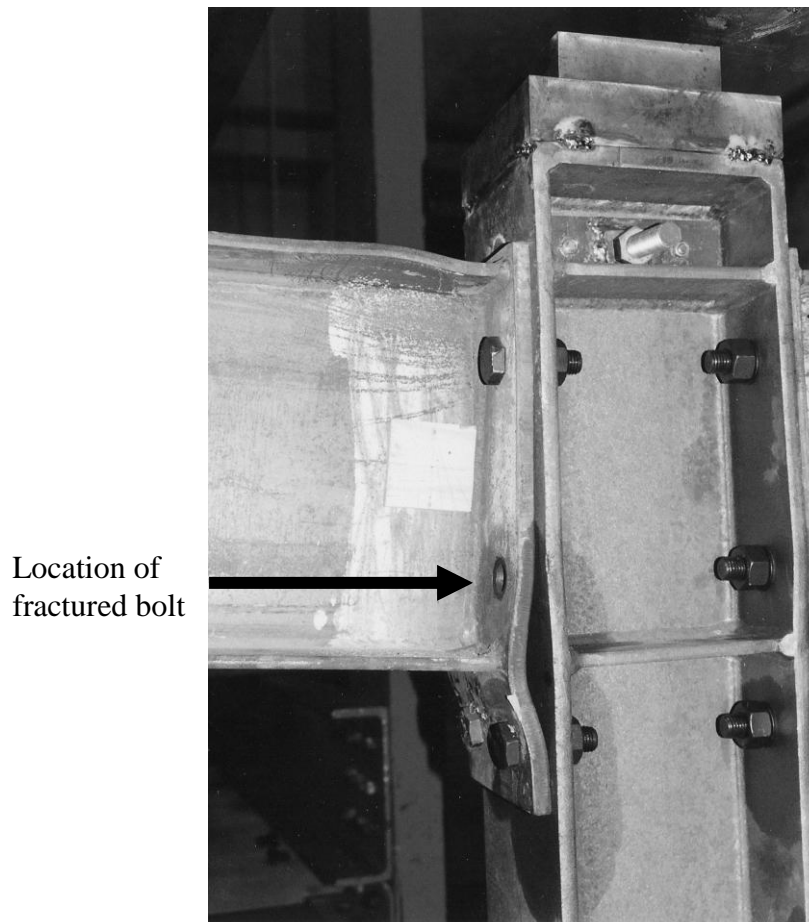


Figure 4.7 – Endplate 14B from Test 3

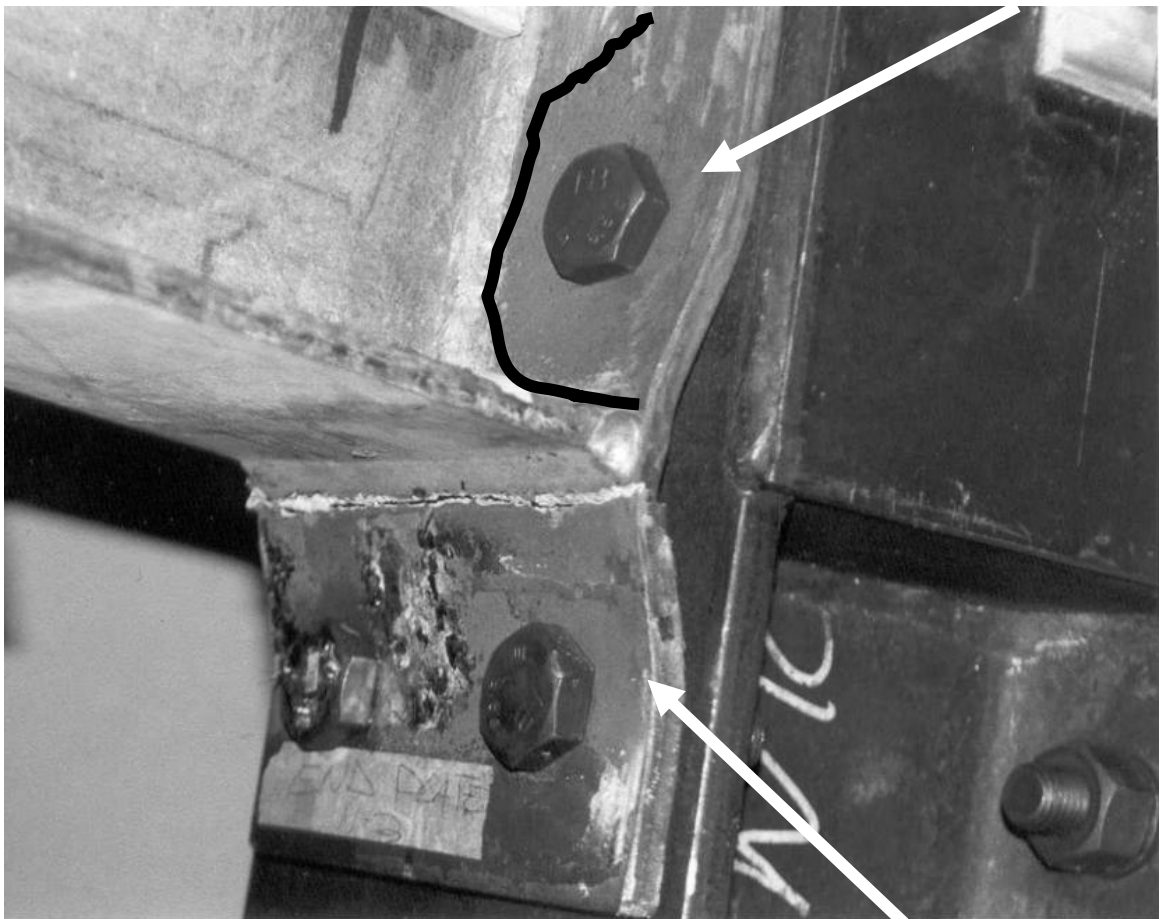
There were fine longitudinal cracks along the beam web but there was no sign of cracking adjacent to the beam tension flange. The buckling of the beam compression flange was pronounced (see Figure 4.7), but there was no discernible curvature in the tension flange adjacent to the endplate. The test was stopped when a bolt fractured suddenly in the tension flush region of Beam 14B. The endplate with a missing flush region bolt can be seen in Figure 4.7. By comparison with tests 1 and 2, the 14mm test endplates did not deform as readily, and as mentioned above there was little cracking and little apparent transverse bending. The bulge in the endplate between the flush tension bolts and the shear bolts was also observed here but was less pronounced than in the other two tests.

It can be seen in Figure 4.6 that the column flange has deformed noticeably at the flush bolt level. In Figure 4.7 taken after completion of the test, the residual plastic deformation of the column flange is much less. It is evident therefore that most of the column flange deformation in Figure 4.6 was elastic. By comparison with Test 1 and Test 2 (Figures 4.2 a and 4.5), there was only a very slight plastic deformation of the column flange at the flush bolt level in Test 1. In Test 2 there was no deformation of the column flange – probably because of the additional stiffener.

4.1.4 Discussion of Test Observations and Endplate Failure Modes

On the near-side face of the endplate (the face visible on the connection), the 10mm and 12mm endplates fractured in the same locations – adjacent and parallel to the beam web, and at the beam tension flange on the extended side. The location of the cracks in the flush region seem to suggest that the initial semi-circular pattern grows in size as the yielded area spreads, until it is restrained by the web and the beam flange, and then becomes more or less straight lines. The initial circular yield area and the subsequent restraint by the beam web/flange can be seen in the photograph of Figure 4.8 for beam 12A.

Yielding evident in a circle around bolt head



Yielding evident in transverse band across the bolt line

Figure 4.8 – Extent of yielding observed in Test 2

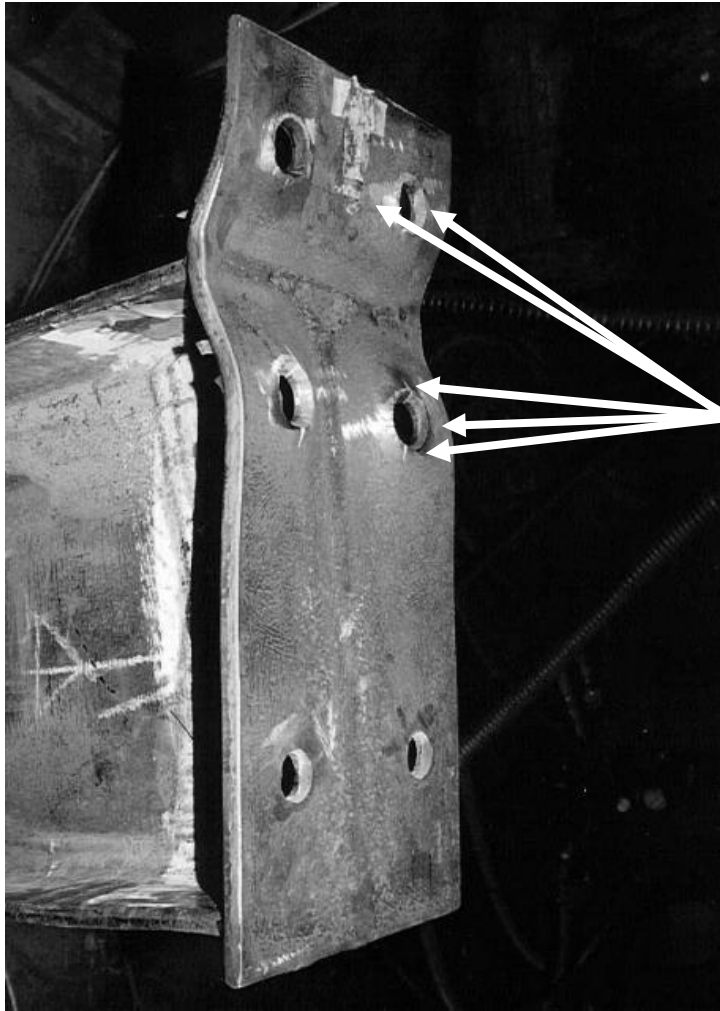


Figure 4.9 – Cracks on far-side of 10mm endplate in Pilot test A

When the 10mm and 12mm connections were unbolted after the tests, cracks were observed on the far-side of the connections around the tension bolt holes, in a radial pattern. This is shown in Figure 4.9 for beam 10A from Pilot test A. These cracks suggest that negative yield lines are developing radially from the bolt holes. They support the observation that the pattern was initially circular and centred around the bolt holes.

The 14mm endplates did not behave in the classical ‘thin’ manner. There was yielding on the weld line of the extended region, and that region behaved like the tee-stub Mode 2 of Eurocode 3. The bolt failure was in the flush region rather than the extended region. The flush region had signs of the same circular yielding

around the tension bolt-heads as in the other tests, but these did not develop into the semi-circular pattern. Thus, instead of considering it a Mode 2 tee-stub, the behaviour of the flush region is probably better regarded as similar to the thin plates, but with the bolt being too weak to develop the full yield pattern.

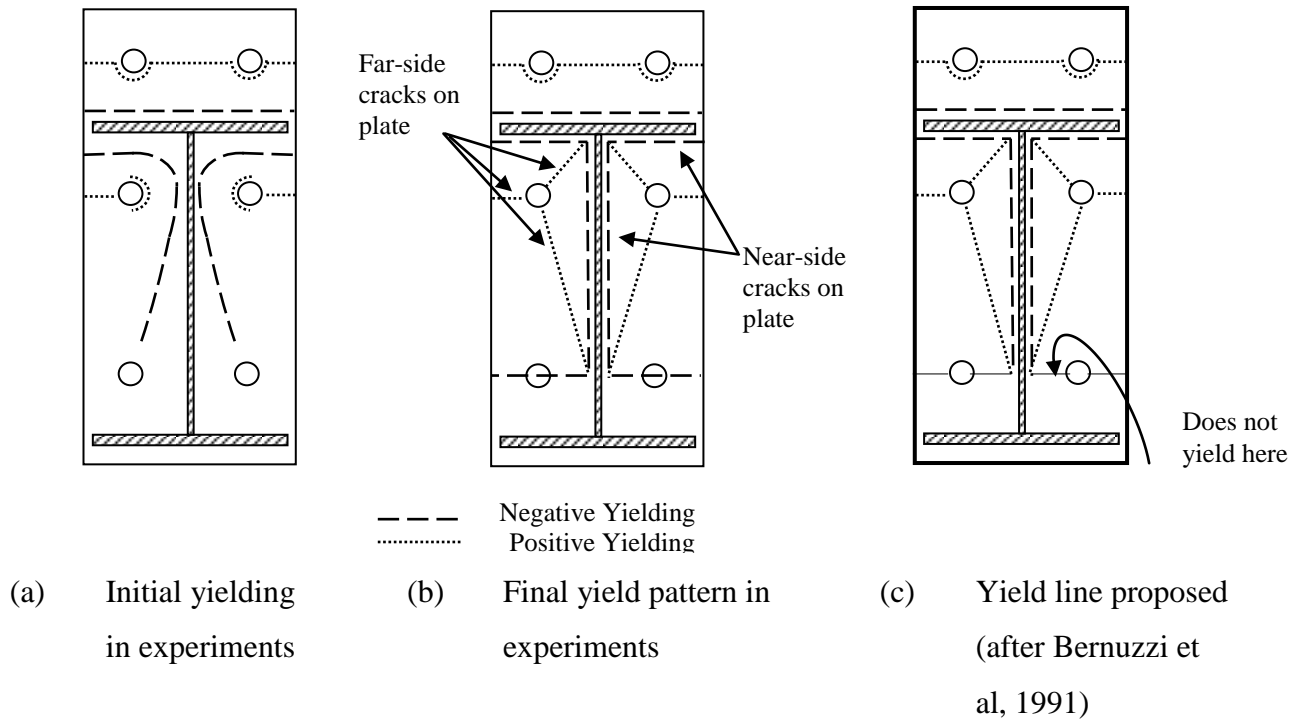


Figure 4.10 – Yield-line Pattern proposed in this thesis

We conclude that the yielding in the flush region is initially in a semi-circular pattern, but this develops into straight lines along the web and flange as the test continues. For reasons that become clear later out emphasis is the final pattern rather than the initial. It means then that the yield line pattern of Bernuzzi et al (1991) for thin endplates (12mm and 15mm), which they referred to as Mechanism A, is relevant here. On close examination however, it is evident that the positive yield line shown at the level of the shear bolts in Figure 4.10b cannot develop. There is no evidence of yielding or cracking at that level in any of the tests, and deformation of the endplate in that region cannot be large enough for the yield line to develop. Thus, in this thesis, the proposal of Bernuzzi et al (1991) has been modified as shown in Figure 4.10c. We note that the largest cracks on the far side of the endplate around the bolt holes (Figure 4.9) coincide with the positions

where negative yield lines are located in the proposed yield line pattern of Figure 4.10c. This further confirms the appropriateness of the chosen yield line pattern.

It should be noted that the yield line pattern proposed here is also very similar to the earlier proposal by Surtees & Mann (1970), but with the yielding extending to the shear bolt level. Thus, the validity and relevance of this pattern is well-established.

Some observations that were common to all three tests are as follows:

- In all cases, yielding (as inferred from the flaking of mill scale) started on the bolt line in the extended region. Subsequently, there was yielding on the weld line in the extended region as well as around the flush bolt.
- The greatest endplate deformation was around the beam tension flange. The curvature was higher in the extended region adjacent to the beam flange than on the flush side, and no doubt this is why those endplates that fractured did so in the extended region.
- Cracks in the endplate consistently developed in the stiffer flush region first, around the bolt-holes and adjacent to the beam web.
- There appears to be a relationship between larger local buckling curvatures in the beam compression flange, and the failure of the connection.
- Under moment, the beam profile initially rotates about a point in the compression flange depth. At large moments approaching the connection moment capacity however, some of the beam web seems to come into compression also to about the shear bolt level. This can be seen clearly in Figures 4.2 and 4.7. The endplate remains flat against the column flange between the beam compression flange and the shear bolt level.
- There was a slight permanent curvature (bulge) of the endplate between the level of the flush tension bolts and the shear bolts.

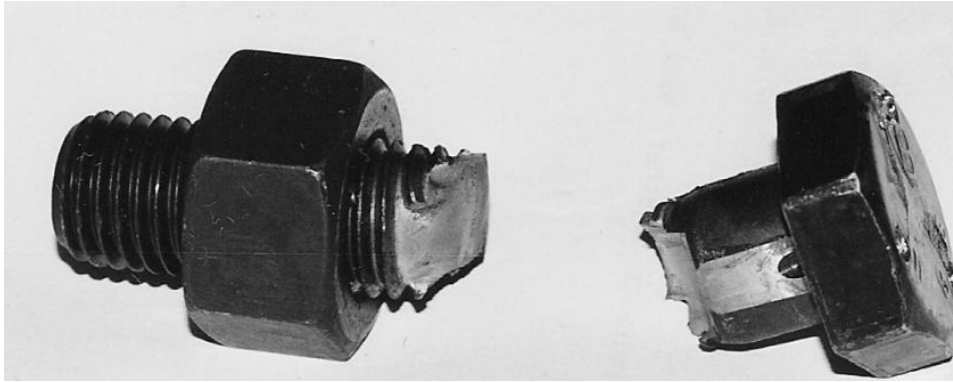


Figure 4.11 – Fractured Extended Region Bolt from Pilot Test A

An interesting issue for consideration is the difference in failure modes between pilot test A and test 1. The test endplates and bolts were nominally identical, nevertheless pilot test A failed by fracture of the extended bolt while beam 10B in test 1 failed by endplate fracture. The fractured bolt from pilot test A is shown in Figure 4.11. We notice that it was the instrumented bolt that failed. As a matter of interest, the flush region bolt that fractured in test 3 was not an instrumented bolt.

4.2 BEAM ROTATION DATA FROM THE CONNECTION TESTS

In the connection tests, beam rotations were measured using LVDTs and inclinometers. Each beam had three LVDTs that measured beam rotation directly - immediately adjacent to the column (90mm from the endplate face), at 300 mm from the endplate face, and at the beam support 1000mm from the endplate face. The value of 300mm is approximately the beam depth, and it represents the point commonly accepted as the limit of the beam to column joint. The measurement at 300mm was carried out to allow comparison of the results with other published work. Previous investigators have defined the boundary of the joint at a beam depth away from the column face, and many have taken their rotation measurements at that distance from the endplate face, in order to establish the total joint rotation. However, since beam end rotations could be quite large in some cases, it was considered desirable to also measure the rotations adjacent to

the endplate – hence the LVDT at 90 mm from the face. The 90mm value reflects the practical difficulty of mounting the LVDT magnetic clamp on the column face while resting the needle-point off the beam flange immediately adjacent to the endplate. The LVDTs at the beam supports were mounted off the supporting steelwork while the others were mounted off the column face. Besides the LVDTs, inclinometers were mounted on each beam at the same positions as the LVDTs (300mm from the face and at the beam support). There was also a dual-axis inclinometer on the column stub itself to measure in-plane and out-of-plane rotations of the column stub.

However, the inclinometer readings at the beam support and at 90mm from the column face tended to be erratic in Test 3 (14mm test). The LVDT readings were generally less erratic than the inclinometer readings. I have therefore focused more on LVDT measurements of joint rotations at a beam depth from the column face, and these are used for comparison purposes.

The beam rotation data is reported as moment-rotation curves in subsequent sections. The ‘raw’ moment–rotation curves for test 2 have been cleaned-up into ‘loading envelope’ versions. This was necessary as the load in test 2 was applied through four load and unload cycles. The load envelope versions have been obtained by removing the unloading readings for each cycle, thus obtaining an ‘envelope’ of readings.

4.2.1 Moment-Rotation Curves for Connection Test 1

The moment-rotation curves for test 1 are shown in Figures 4.12 and 4.13 below. In the Beam 10A curve, as one would expect, the rotations at the joint are much higher than those for the column face (90mm), and those for the beam support are again higher than those for the joint. The same situation occurs in the Beam 10B graph, however the difference between the joint and the column face readings is now less, while the difference between the joint and beam support readings is higher.

Using joint values, the highest moment recorded for Beam 10A was 157.9 kN-m or 75.6% of the beam M_p (209 kN-m), at a rotation of 87.2 milli-radians. The corresponding value for Beam 10B was 158.1 kN-m at 100.4 milli-radians. The ‘swivel point’ is the moment at which the transition knee between the initial linear elastic region and the next linear inelastic region occurs. For beam 10A the swivel was at 81.1 kN-m, and for 10B it was at 79.5 kN-m. In this test, it was beam 10B that failed by fracture of the endplate, so that the test had to be terminated. It seems likely therefore that the connection on beam 10A could have supported a higher rotation.

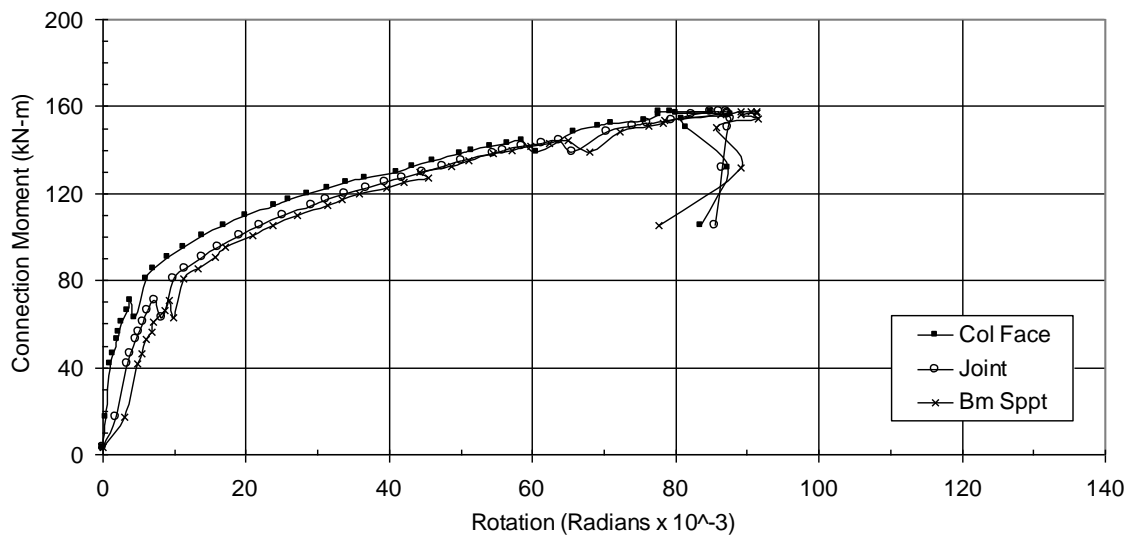


Figure 4.12 – Moment Rotation Curves for Beam 10A, Test 1

The dip in connection moment, at about 70 kN-m on beam 10A, is thought to be due to slip at the bolts. The M20 bolts with a nominal diameter of 20mm were in 22mm holes. Thus, a maximum 2mm slip could occur of the endplate when the endplate friction is overcome. The later dip, at about 140 kN-m in the same beam, could be due to cracks developing in the endplate. The difference in rotations at similar load levels, between both beams, is possibly due to differences in bolt pre-tension forces or slight column rotations.

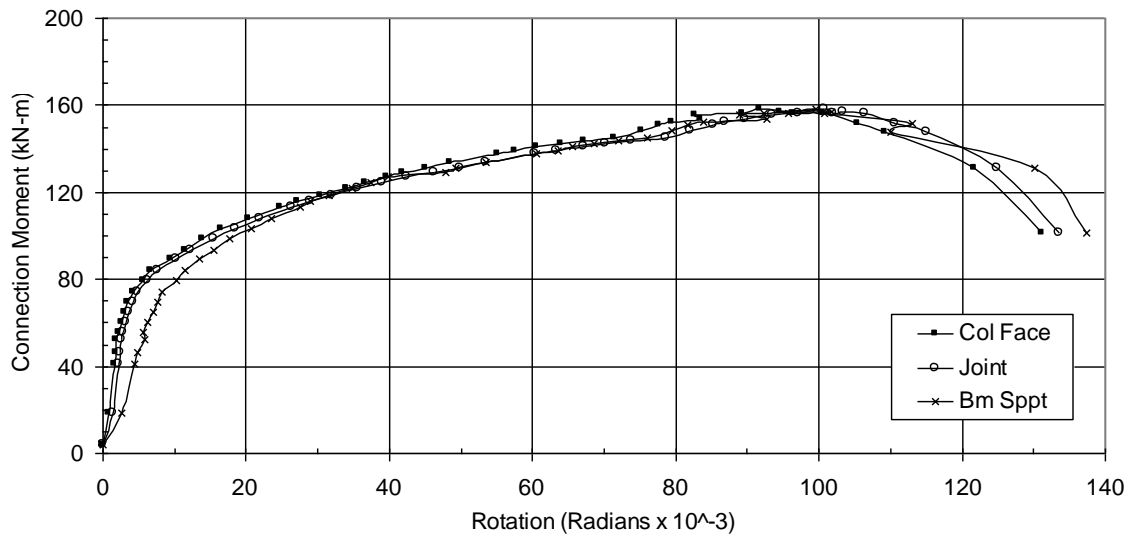


Figure 4.13 – Moment Rotation Curves for Beam 10B, Test 1

4.2.2 Moment-Rotation Curves for Connection Test 2

In Test 2, the load was applied in four load cycles. Hence, the experimental curves include unloading and re-loading portions. These had to be ‘cleaned-up’ for readability and ease of comparison with the other tests. To illustrate, the ‘raw’ results are given below for the joint readings in Figures 4.14 and 4.16, along with the ‘clean’ versions for the column face, joint and beam support in Figures 4.15 and 4.15. The first reading in each test was a non-zero moment. This was retained as is without adjustment, but a zero reading is included in the ‘clean’ graphs.

In this test also, unlike in the other tests, the column was reinforced with plates welded across the flange tips in the tension area. It seems clear from the literature that the bulk of the inelastic rotations are contributed by the endplate (e.g. see Bernuzzi et al, 1991). Therefore the effect of this reinforcement on moment-rotation is considered negligible.

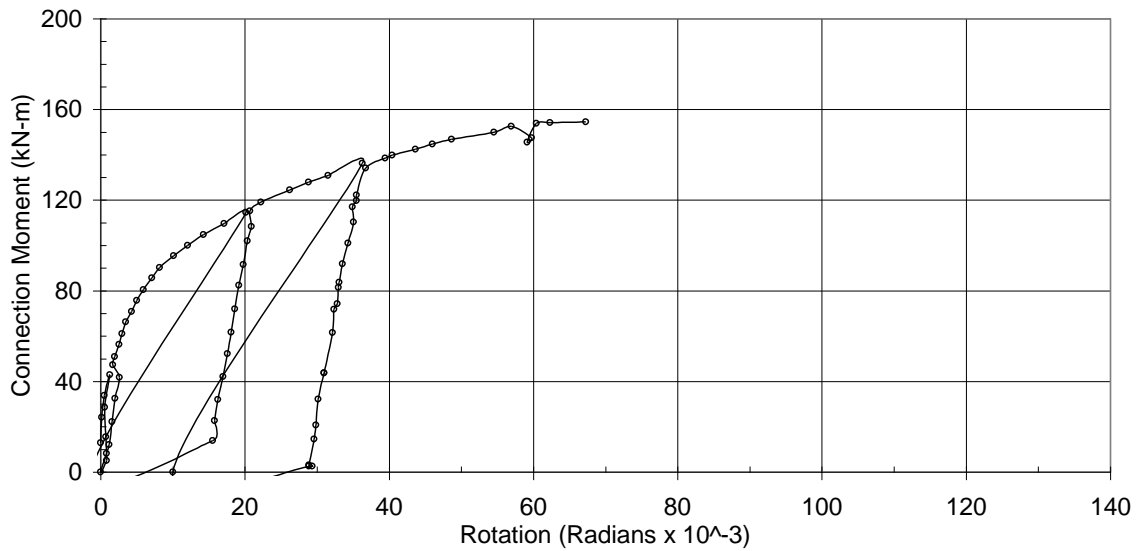


Figure 4.14 – ‘Raw’ Moment Rotation Curve for Beam 12A at joint, Test 2

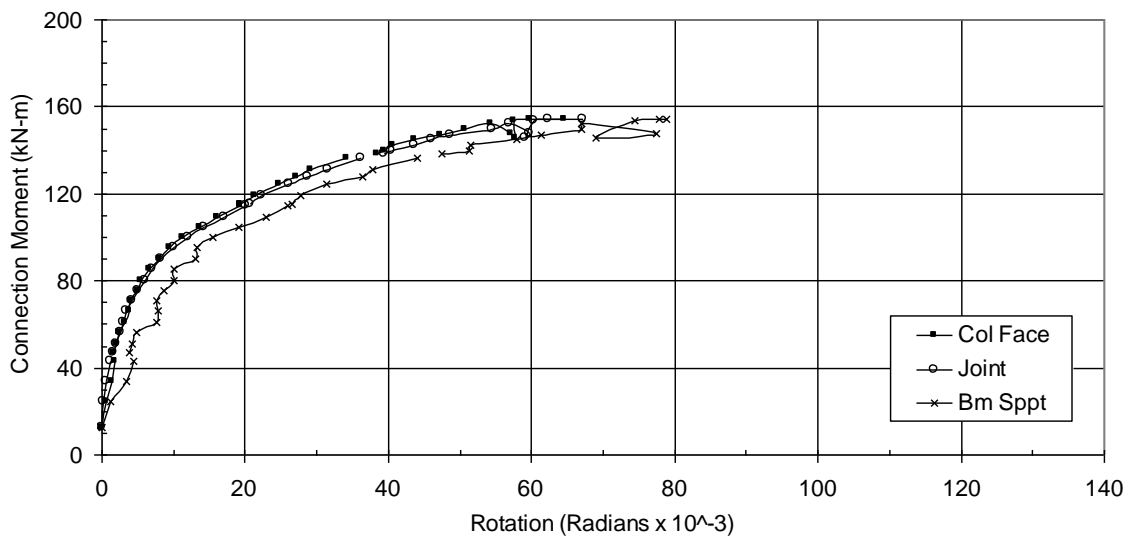


Figure 4.15 – Moment Rotation Curves for Beam 12A, Test 2

The swivel moment for beams 12A and 12B respectively was 95.4 kN-m and 97.1 kN-m. The highest connection moment measured for 12A was 154.5 kN-m, at a rotation of 67.3 milli-radians (joint values). The corresponding value for beam 12B was 149.7 kN-m at 47.3 milli-radians. However, at the final rotation of 77.5 milli-radians the load was still increasing. The plastic moment M_p calculated for the beam in this test was 203.44 kN-m. Thus, the highest connection moments of

154.5 kN-m on beam A, and 149.7 kN-m on beam B, are respectively 0.76 and 0.74 of M_p . Beam 12A sustained this moment for a short while before fracture.

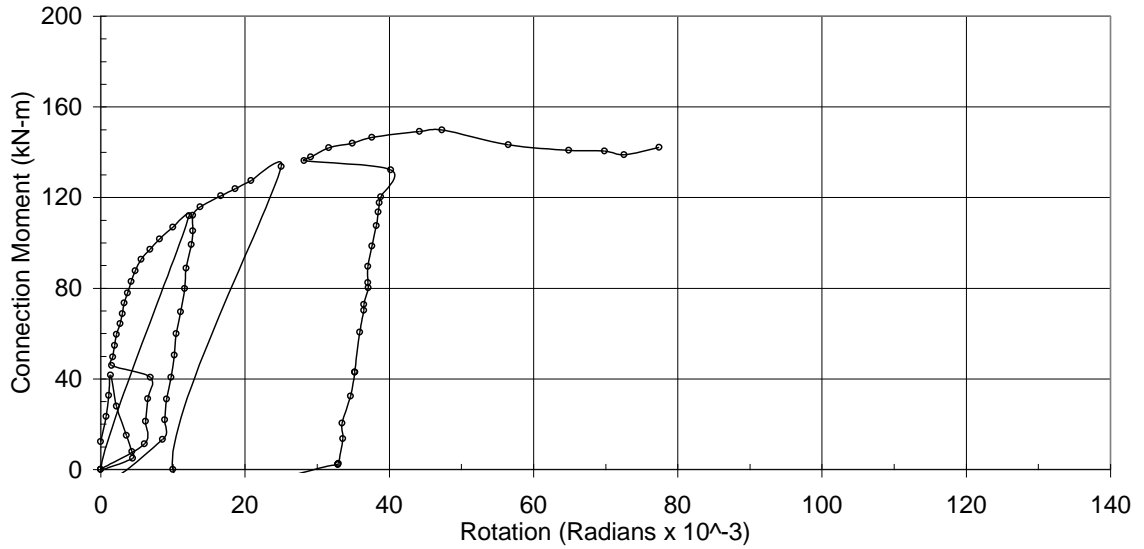


Figure 4.16 – ‘Raw’ Moment Rotation Curve for Beam 12B at joint, Test 2

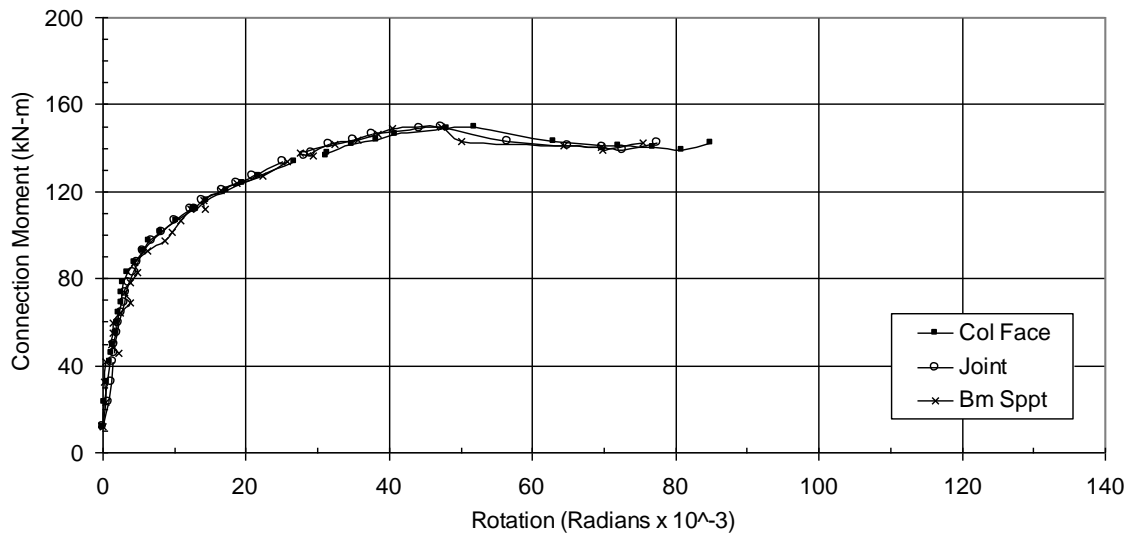


Figure 4.17 – Moment Rotation Curves for Beam 12B, Test 2

When the fracture crack commences in beam 12A, the moment-rotation curve goes through a little loop (see Figure 4.15). This appears to be a measurement error from the ‘shock’. The quasi-static cycling of the loads in Test 2 does not

appear to have had any significant effect on either the outcome of the tests or the behaviour of the connections. This aspect is not studied further in this thesis.

4.2.3 Moment-Rotation Curves for Connection Test 3

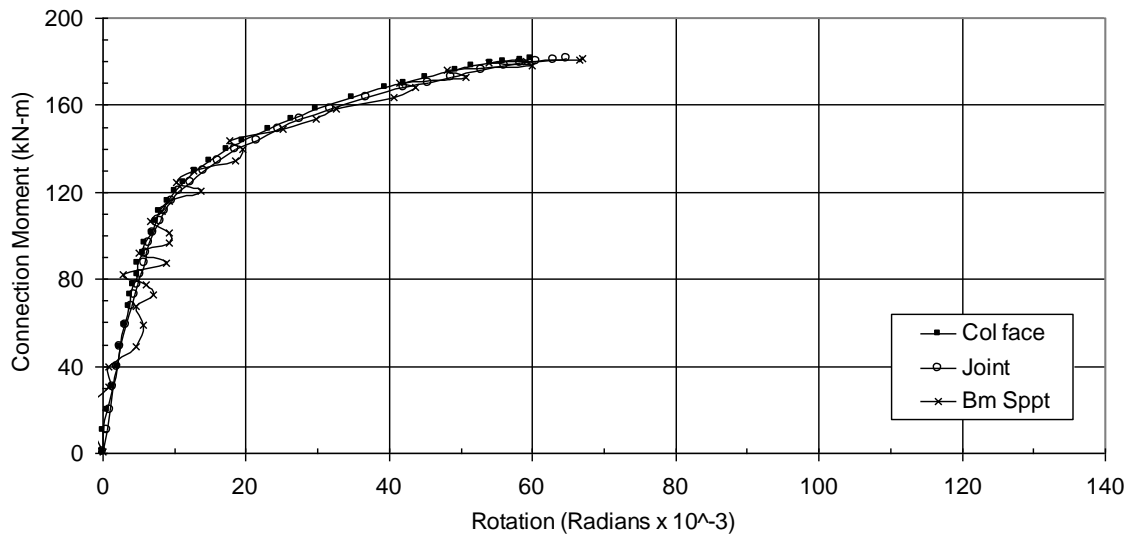


Figure 4.18 – Moment Rotation Curves for Beam 14A, Test 3

Some problems were experienced in Test 3 with voltage fluctuations on the inclinometers, leading to variations in the column face and beam support readings. The test ended when a flush region bolt fractured on beam 14B. At that point the moment on beam 14A was 181.8 kN-m at a rotation of 64.7 milli-radians, while the moment on beam 14B was 181.6 kN-m at 80.2 milli-radians. The swivel moments are 124.6 kN-m on 14a and 120.4 kN-m on 14B. The moment-rotation results are given in Figures 4.18 and 4.19.

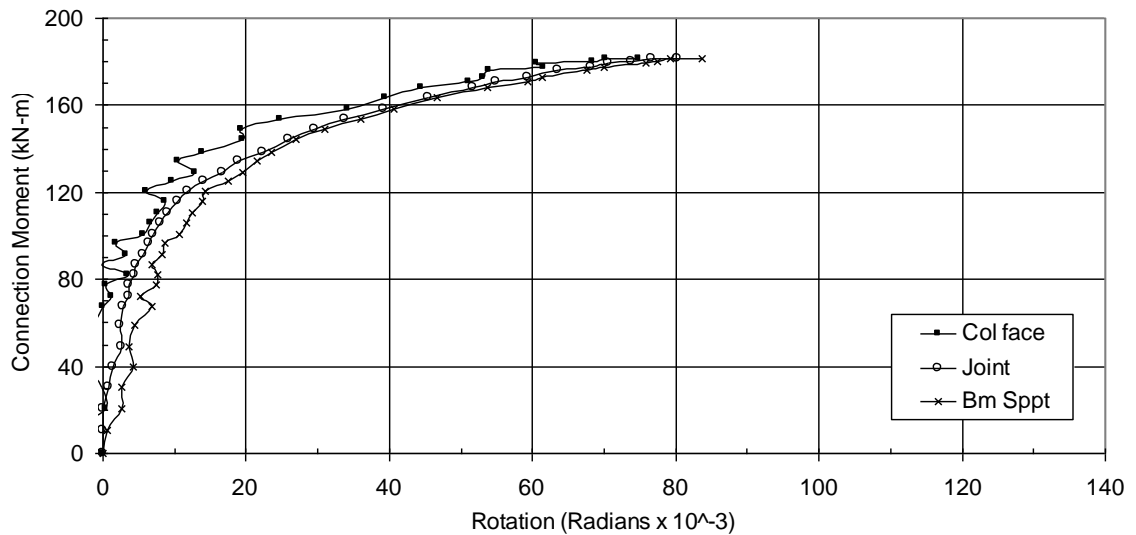


Figure 4.19 – Moment Rotation Curves for Beam 14B, Test 3

4.2.4 Discussion of Test Rotation Data

The moment-rotation curves measured at the joint are all presented in Figures 4.20, 4.21 and 4.22 with both connections in a test per each figure. The Eurocode 3 classification criteria (see Section 1.6) have been superimposed on all three figures, in order to classify the test connections.

To apply the Eurocode 3 stiffness criteria, a beam span is required. For most practical applications beam spans are between 15D to 25D, where D is the beam overall depth. Thus, for the 305 UB 41 I sections tested in this thesis, 6m ($\approx 20D$) would be a practical beam span. The average value of E (Young's modulus) for the beam flanges in the connection tests is 208.4 GPa. Similarly, an average value for I (second moment of area), based on measured dimensions for the beams, is $84.25 \times 10^6 \text{ mm}^4$. Therefore:

$$\begin{aligned}
 25EI_b/L_b &= 73149 \text{ kN-m (Rigid for sway frame)} \\
 8EI_b/L_b &= 23408 \text{ kN-m (Rigid for non-sway frame)} \\
 0.5EI_b/L_b &= 1463 \text{ kN-m (Pinned)}
 \end{aligned}$$

It can be seen therefore that in relation to strength all these connections are partial strength as the strength exceeds the $0.25M_p$ criterion for them to be pinned. In relation to stiffness, none of the tested connections would qualify as rigid in an unbraced frame and so would be considered semi-rigid, but in a braced, non-sway frame the 10B, 12B and 14B connections would all just qualify as rigid. All the connections would qualify as ductile also, as the maximum moment rotations are much larger than 30 millirads (see Surtees & Mann, 1970).

An observable feature in these figures is that there are differences in the moment-rotation curves for nominally identical connections. In test 1 and test 3 (Figures 4.20 and 4.21 respectively), the connections that failed – 10B and 14B – exhibited larger rotations than their counterparts that did not fail. Nevertheless, the connection moments were very similar in 10A and 10B when test 1 was terminated. Likewise, 14A and 14B had similar moments when test 3 was terminated.

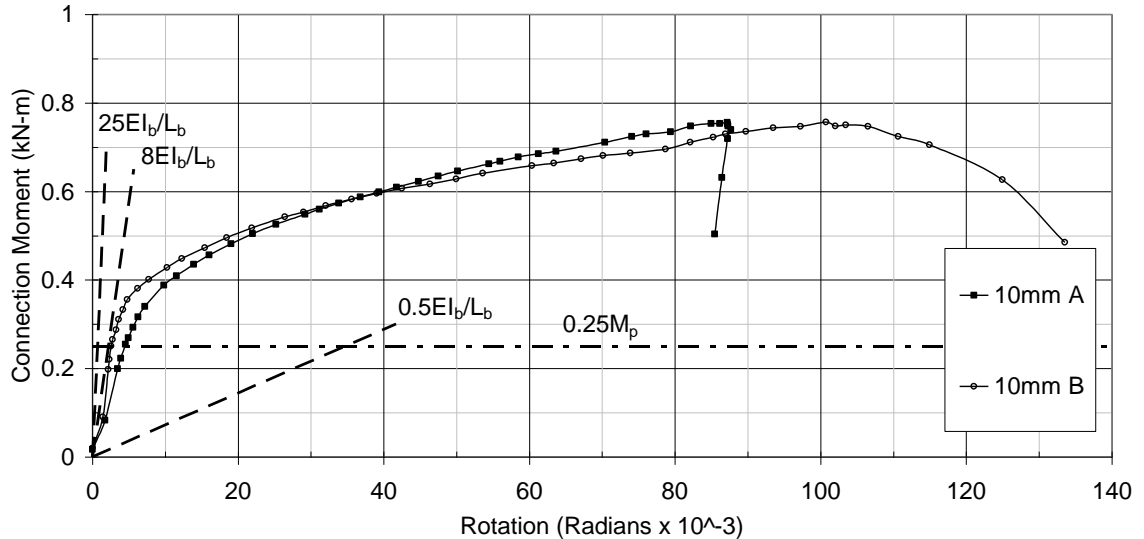


Figure 4.20 – Comparison of Moment Rotation Curves - Beams 10A and 10B

On examination, it can be seen that connections 10B and 14B both had higher initial slopes (stiffness) than connections 10A and 14A respectively. A likely explanation is that connections 10B and 14B had higher bolt pre-tension forces, or a slightly larger bolt diameter. (The turn of the nut method we adopted in this

thesis is known to produce variable results, but it is the method of preference in everyday South African structural steel practice). Other possible reasons include the possibility of slight deviations in weld size from the nominal value, or differences in specimen symmetry between the A and B specimens. The possibility of column rotation was obviated with lateral restraint of the column below the connection level; however, there might be minor differences in the nominally identical specimens. Nevertheless, since the specimens A and B were taken from the same beam length and the endplates were cut from the same plate, any differences in the specimens would be minor. Yet another explanation would be the incidence of higher residual stresses in the stiffer specimens, possibly related to a greater spread of the heat-affected zone adjacent to the welds. It seems then that a higher pre-tension force or a slightly larger bolt diameter in nominally identical connections, as well as differences in the weld-related residual stresses, may lead to a higher initial stiffness, and also seem to lead to greater rotation capacity. This last is a surprising observation as it is counter-intuitive. One would suppose the initially stiffer connection would rotate less.

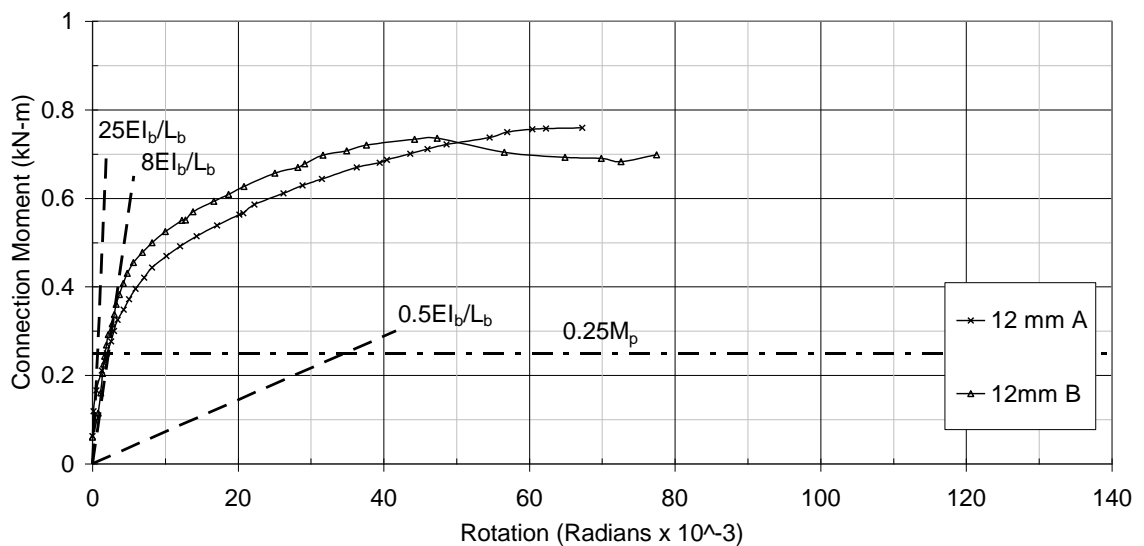


Figure 4.21 – Comparison of Moment Rotation Curves - Beams 12A and 12B

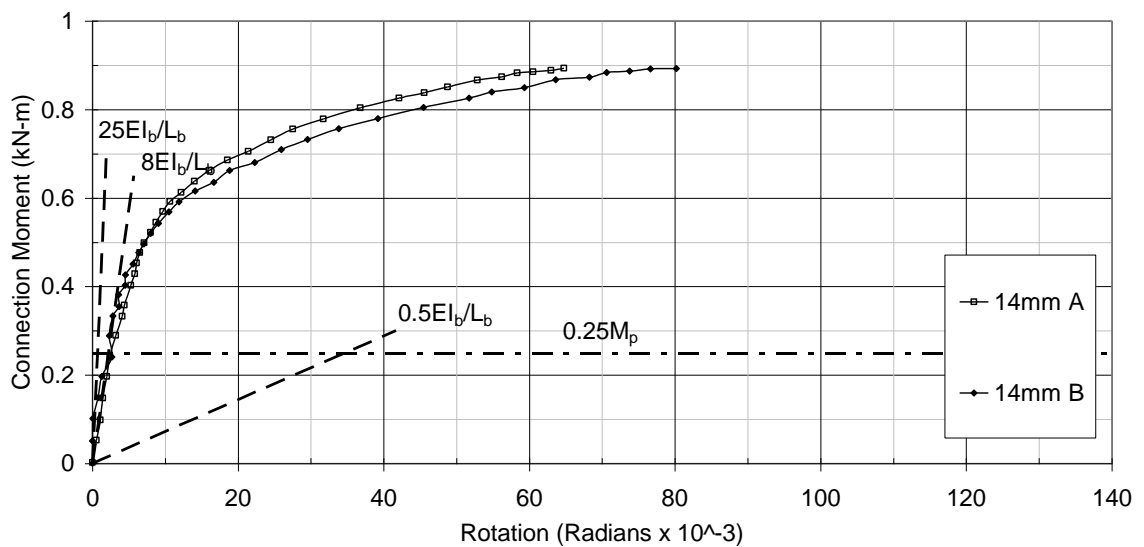


Figure 4.22 – Comparison of Moment Rotation Curves - Beams 14A and 14B

When the individual test readings for tests 1 and 3 are considered however, one observes that at each point in the test prior to failure, the moment applied to each of the A and B connections remains approximately equal. Thus, the difference in initial stiffness does not have an impact on the moment-resisting capacity of the connection, and the difference in rotation behaviour cannot be attributed to differences in applied moments. Again, the onset of yielding sets in at approximately the same level of applied moment for each of the A and B connections in both tests. The superior rotation performance of 10B and 14B compared to their counterparts only starts when the connections have started to yield. A plausible explanation is that the a slightly larger bolt allows the flush or extended tension bolts to restrain the endplate more effectively, so that yielding progresses faster and further in the connections that fail. Thus, the yield line pattern described in the previous section is better developed in the specimen that fails. The reduction in the modulus of elasticity due to widespread yielding is then what leads to the observed improvement in rotation capacity.

In Figure 4.21, beams 12A and 12B do not appear to have conformed to the preceding observations as 12B has a greater initial stiffness than 12A that failed. However, there was an intervening factor in the development of the 12B moment-rotation curve, just after it got to the highest moment attained of $0.74M_p$ or 150

kN-m. This was the point at which the first loud cracking noises were heard during the test when both connections were resisting about 150kN-m. The second cracking noise was when Beam 12A was resisting 154 kN-m. On examination afterwards, it was noticed that both endplates had cracked, and the test terminated when beam 12A fractured. It seems likely then that the crack in beam 12B was severe enough to affect its moment resistance capacity and this explains why connection 12A attained the failure moment first. The curve for 12B does appear to be flattening out just before the crack, and one can speculate that it would have crossed the 12A curve and exhibited greater ductility if the crack had not occurred. We find then that where the connection initial stiffness was sufficiently high enough that the connections behaved in a rigid fashion rather than semi-rigid (at least for a braced frame), the connections exhibited improved rotation capacity. The presence of large residual stresses in the area adjacent to the beam flange weld (heat-affected zone) would explain why this area is susceptible to cracks at large strains.

In Figure 4.23 all six experimental curves are presented together for ease of comparison. The moments resisted by each connection are also given in Table 4.1, together with the corresponding rotations, to facilitate the comparison.

The 'swivel' points in Table 4.1 refer to the point in the moment-rotation curve where the change in slope from the initial stiffness to the second stiffness (leading to the maximum moment) is complete. We notice that the ratio of this swivel moment to the maximum connection moment changes with endplate thickness. The ratio varies from 0.50 for 10B to 0.69 for 14A. The plastic component of the rotation is also determined for each curve in Table 4.1. The plastic moment of resistance of the endplate material is directly proportional to the square of its thickness. Thus, one would expect beam 12A and 12B to fail at higher moments than beams 10A and 10B, given the difference between the 14mm connections and the 12mm connections. It is surprising to note that both of the 10mm endplate connections (10A and 10B) exhibit ultimate moment capacities that are higher than the 12mm endplate connections – even for 12A where the failure mode is identical to 10B. It appears likely then that 12A cracked prematurely due to a loss

in ductility in the heat affected zone of the beam flange weld. Connection 10B failed in the same location, but nominally identical welds may involve varying amounts of heat input, depending on the skill of the welders. The shaded rows in Table 4.1 are ‘summary values’ of moment and rotation for the three tested endplate thicknesses. The swivel values are obtained by averaging the A and B connections, while the maximum values are based only on the failed connection.

Table 4.1 – Moments and rotations in connection tests 1 -3

Connection	Swivel point			Maximum point			Failure Mode
	Rotn.	Moment		Rotn.	Moment		
	m-rads	kN-m	% of M_p	m-rads	kN-m	% of M_p	
Beam 10A	9.8	81.1	38.8	87	157.9	75.6	Did not fail but endplate cracked
Beam 10B	6.2	79.5	38.1	100	158.1	75.7	Endplate fracture
10mm e/plate	8.0	80.3		100	158		
Beam 12A	8.2	95.4	46.9	67	154.5	75.9	Endplate fracture
Beam 12B	6.8	97.1	47.7	47 ¹	149.7	73.6	Did not fail but endplate cracked
12mm e/plate	7.5	96		67	155		
Beam 14A	10.6	124.6	61.2	65	181.8	89.3	Did not fail
Beam 14B	11.9	120.4	59.2	80	181.6	89.2	Flush bolt fracture
14mm e/plate	11.3	123		80	182		

In Figure 4.23 we see that the nominally identical test 1 connections (beam 10A and 10B) have quite different initial stiffnesses. Thus, there is a concern about the predictability of the initial stiffness.

¹ The corresponding rotation to the maximum moment is reported here on the premise that the connection has failed once it begins to shed its moment. However, this definition is not entirely applicable for beam 12B as it sustained moment after the maximum point.

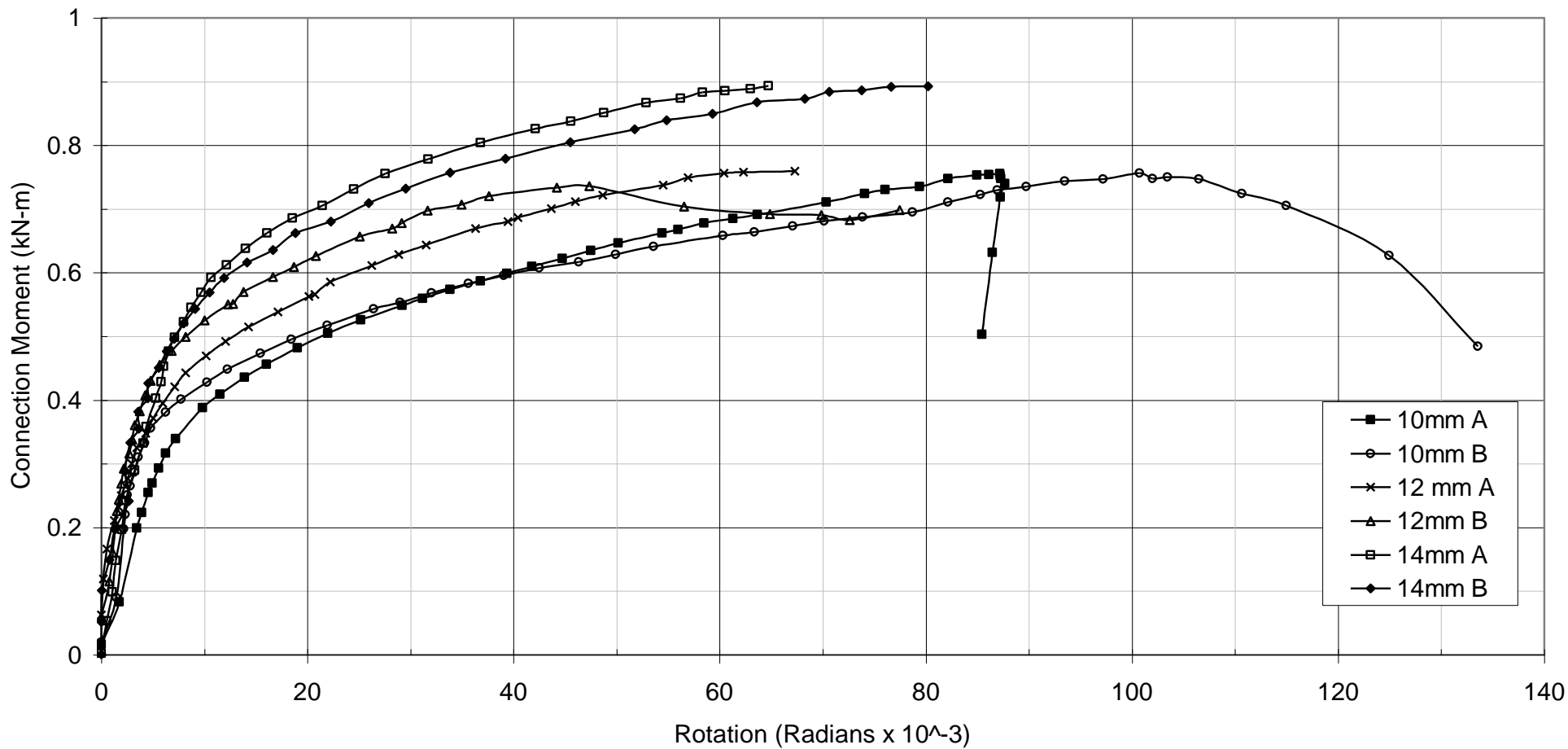


Figure 4.23 – Moment Rotation Curves for Tests 1 – 3 at the ‘Joint’

4.3 BOLT STRAIN GAUGE DATA

4.3.1 Bolt Strains and Bolt Forces Measured in the Connection Tests

In each connection test, the A and B beams each had two bolts instrumented with strain gauges – one bolt in the extended part of the endplate below the tension flange, and the other in the flush region immediately above the tension flange. There were three gauges on each instrumented bolt, aligned at 120 degrees around the bolt shank as shown in Figure 4.24, so that a horizontal line through gauges A and B was parallel to the beam tension flange.

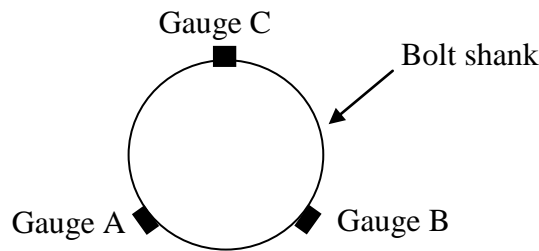


Figure 4.24 - Section through instrumented bolt, with strain gauge positions

Studying the strains recorded for each extended bolt and each flush bolt enables a further understanding of the endplate bending and yielding. In both the extended and flush regions, the endplate deformation tended to bend the bolts both longitudinally and transversely, and the relative proportions of these are evident in the different strains measured. In some instances, the foil gauges peeled from the specimen at high strains before the test was over. Thus, the strain gauge data is incomplete in those areas where gauges failed early. Nevertheless, those gauges that continued to function do allow useful insights.

Gauges A, B and C of Figure 4.24 are referred to in the text as follows: gauge B is the gauge closer to the beam web and is referred to as the web-side gauge, and gauge A is referred to as the edge-side gauge. Gauge C is referred to as the ‘down’ gauge, where ‘up’ and ‘down’ are based on an orientation of the endplate in which the extended region is above the flush. This is illustrated in Figure 4.25.

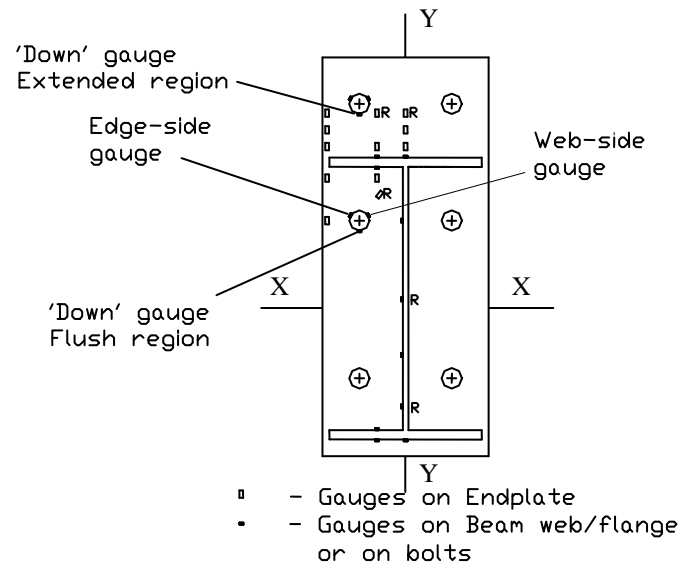


Figure 4.25 – Orientation of Bolt Strain Gauges on Endplate

It is evident that the difference between the web-side and edge-side bolt strains gives an indication of the extent to which the bolt is bending about the axis through the bolt centre, parallel to the beam's minor (Y-Y) axis. I have referred to this as transverse bending of the bolt. In order to obtain a similar indication of the bending of the bolt about an axis through the bolt centre parallel to the beam's major (X-X) axis, I have calculated the strain at the position on the bolt surface opposite the 'down' gauge. The bending of the bolt about this latter axis I refer to as longitudinal bending. Thus, the transverse bending of the bolt is related to deformations of the endplate across its width, while the longitudinal bending of the bolts is related to deformations of the endplate along its longitudinal axis. The calculated strain is referred to as the 'derived down' strain. In test 2 however, up and down were reversed so that the down strain was measured and the 'up' strain was derived.

The derived strain is calculated from the understanding that the strain on the bolt shank at any point has two components – an axial strain due to the axial force, and an elongation or compression due to bending. By considering the bending to be

further decomposable into two moments in orthogonal directions – along the beam X-X and along the beam Y-Y directions – it is possible to calculate the strain at desired positions from the measured strains. This is illustrated in Figure 4.26. The measurement ϵ_{web} is the sum of three components – the axial strain, the X-X bending strain and the Y-Y bending strain. If measurements ϵ_{web} and ϵ_{edge} are averaged, the Y-Y strain would cancel out. Thus the average X-X bending strain in Figure 4.21 is found by averaging ϵ_{web} and ϵ_{edge} and subtracting the axial strain.

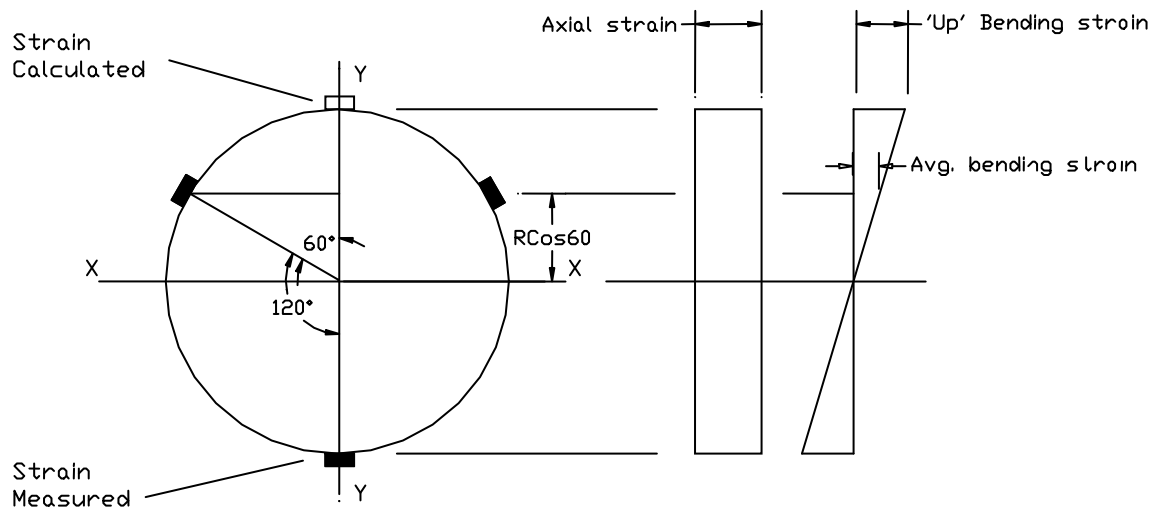


Figure 4.26 – Calculating the bolt ‘down’ strain

The total bolt down strain ϵ_{down} is therefore equal to the average X-X bending strain at the height of the edge and web gauges, multiplied by the bolt radius $R / R \cos 60$, plus the axial strain. The axial strain is simply the average of the three gauge readings – gauges A, B and C (up, edge and web). Thus:

$$\begin{aligned} \epsilon_{down} &= \frac{R}{R \cos 60} \left[\left(\frac{\epsilon_{web} + \epsilon_{edge}}{2} \right) - \left(\frac{\epsilon_{web} + \epsilon_{edge} + \epsilon_{up}}{3} \right) \right] + \left(\frac{\epsilon_{web} + \epsilon_{edge} + \epsilon_{up}}{3} \right) \\ &= 2 \left(\frac{\epsilon_{web} + \epsilon_{edge} - 2\epsilon_{up}}{6} \right) + \left(\frac{\epsilon_{web} + \epsilon_{edge} + \epsilon_{up}}{3} \right) = \frac{1}{3} (2\epsilon_{web} + 2\epsilon_{edge} - \epsilon_{up}) \end{aligned}$$

$$\therefore \quad \varepsilon_{\text{down}} = \frac{1}{3}(2\varepsilon_{\text{web}} + 2\varepsilon_{\text{edge}} - \varepsilon_{\text{up}}) \quad \text{Eqn 4.1}$$

The bolt strains and bolt forces for the three connection tests are presented in the following sections. In the graphs, the legends show how the bolt strains are referred to. Thus, the curve “10mm A Flush Edge” refers to the strains measured by the edge-side gauge for the flush tension region of beam 10A. The point at which the bolt first begins to yield is also indicated where applicable. This point is determined by observing where any strain measurement exceeds the yield strain value measured in the bolt material tests. These values which were previously reported in Table 3.4 are:

10mm plate: Bolt $\varepsilon_y = 3174 \mu\text{strains}$

12mm plate: Bolt $\varepsilon_y = 3266 \mu\text{strains}$

14mm plate: Bolt $\varepsilon_y = 3358 \mu\text{strains}$

Each strain curve has been terminated at the point where it becomes clear that the gauge is no longer functioning correctly. Thus, the termination of a curve may not mean the strains did not exceed the values shown, but that the gauge had ceased to function. In some instances also, the strains recorded exceed the range chosen for display on the graphs.

In several of the bolt strains reported here, there was some initial bending of the bolts, as shown by the fact that the web and edge values differed (transverse bending) at the start of the test, or the up and down strains differed (longitudinal bending) at the start of the test. This is thought to be due to imperfections such as minor welding distortions of the endplate, plate surface roughness, irregular bolt head or nut surfaces, or/and unequal bolt pre-tension.

4.3.2 Bolt Strains in Connection Test 1

On the Beam 10A extended strain curves (Figure 4.27a), the down and up strain initially start at about the same positive value (indicating a strain due to

imperfections and bolt pretension) and then increase at about the same rate, but with the down gauge increasing in tension and the up gauge increasing in compression. Thus, up to about an applied moment of 112 kN-m, the predominant effect in the longitudinal direction is bending i.e. bending about the beam major (X-X) axis.

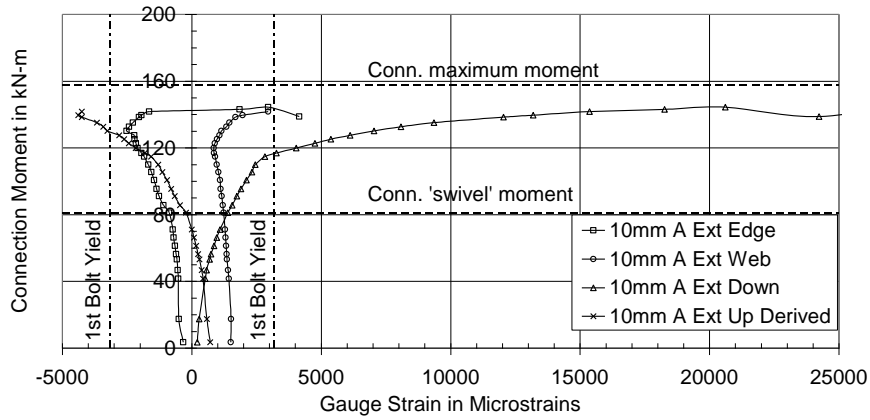
Beyond this point however, the tensile down strains increase rapidly, indicating yielding of the bolt shank in that region. The up strains begin to yield a little later, and the strain curve does not flatten out to the same extent. Thus, there is a tensile axial component in the measured strains at this point.

The edge and web-side strains are quite flat by comparison; they remain fairly parallel indicating little or no transverse bending of the bolt. At about the time the up side of the bolt yields however, the edge and web strains become tensile and increase rapidly, indicating that the entire cross-section is now yielding in tension.

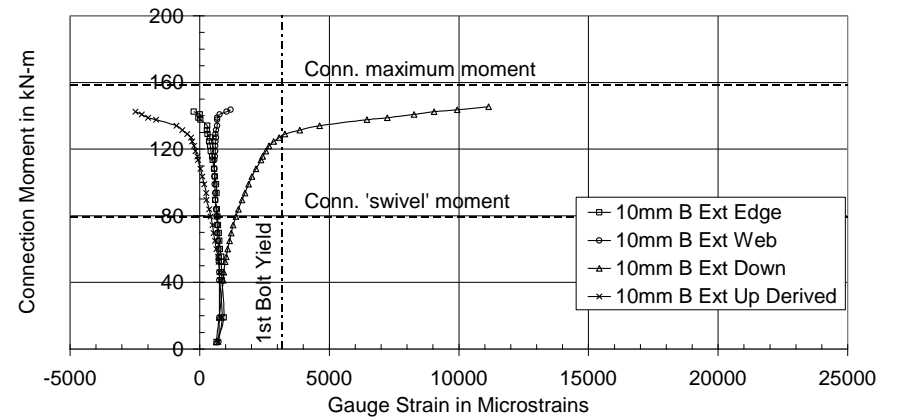
The up and down strains for the extended bolt of Beam 10B exhibit a similar pattern to those for 10A (Figure 4.27b), though the initial yielding takes place at a higher connection moment. The edge and web strains are also similar, and fairly flat, but have almost exactly the same value until the up part of the shank yields.

In summary then, the extended bolts were in combined axial elongation and X-X axis bending, with X-X bending dominating. Each bolt was fully yielded at about a connection moment of 130-140 kN-m.

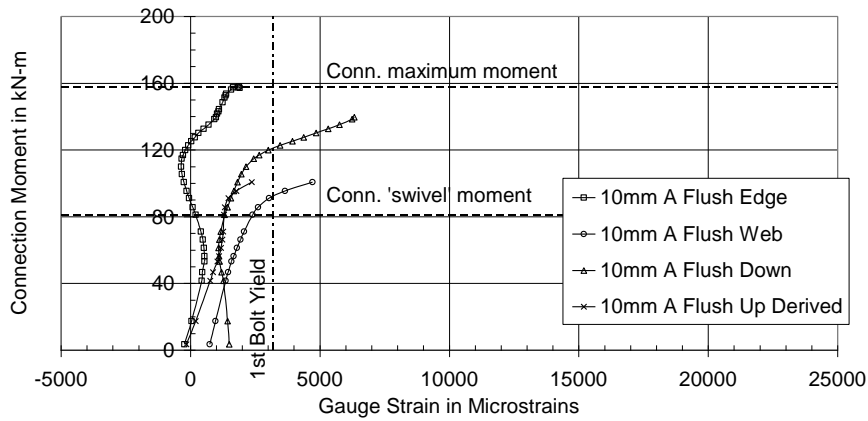
The strain gauges on the flush region bolt of Beam 10B failed prematurely, so that the only data retrieved was for the web-side gauge. The up and web gauges of beam 10A's flush bolt also failed rather early, but the patterns are fortunately still discernible (Figure 4.27c). The up and down strains coincide in the early part of the load cycle and are both tensile throughout. This implies that there is little or no bending about the beam X-X axis (bending in the beam longitudinal plane), and the key effect is axial elongation.



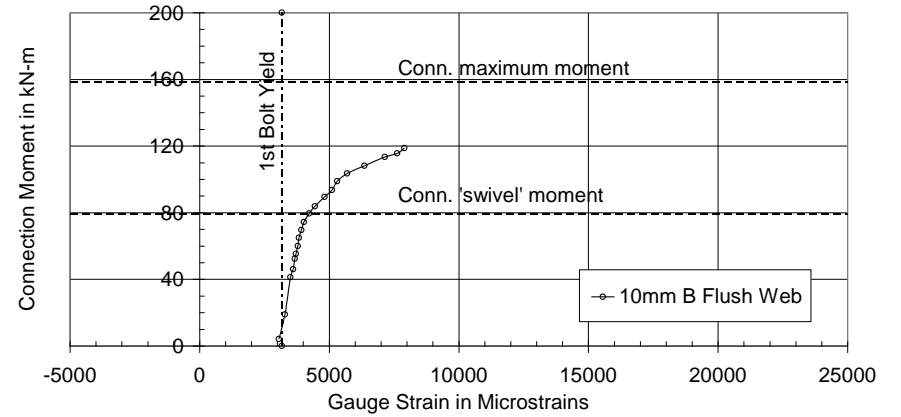
(a) Beam 10A - Extended Bolt Strains



(b) Beam 10B - Extended Bolt Strains



(c) Beam 10A - Flush Bolt Strains



(d) Beam 10B - Flush Bolt Strains

Figure 4.27 – Bolt Strains in Connection Test 1

There is however transverse bending about the beam Y-Y axis (bending in the beam transverse plane), as shown by the edge and web-side strains.

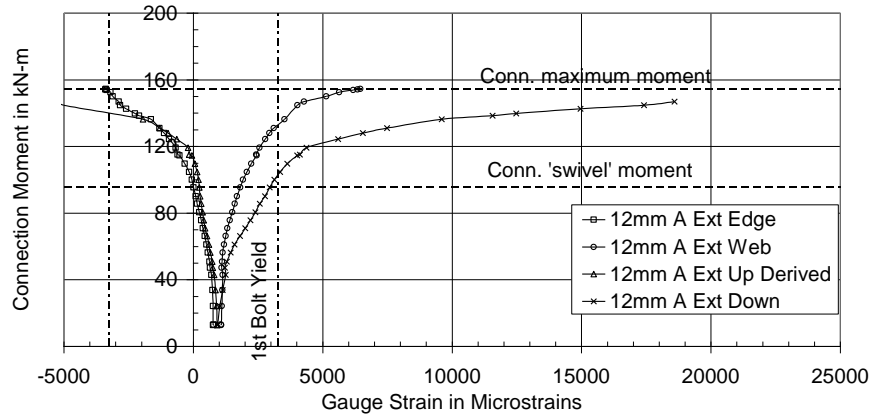
Yielding initiates on the edge side of the bolt as would be expected, and this takes place at only about 90 kN-m - much earlier than in the corresponding extended bolt (112 kN-m). The bolt is fully yielded at about 112 kN-m, and all the strains become tensile, although the edge and web-side strains still differ widely so that there is still transverse bending.

4.3.3 Bolt Strains in Connection Test 2

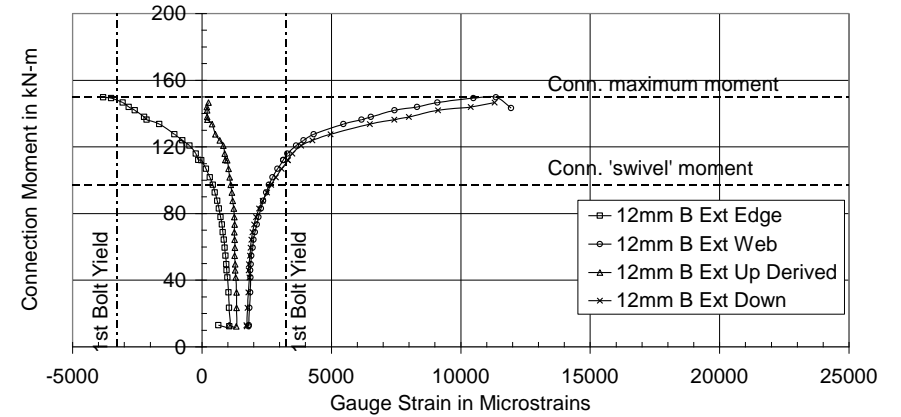
The bolt strains from connection test 2 are given in Figure 4.28. For the extended bolt of beam 12A the down and up strains diverge rapidly (Figure 4.28a), showing that there is considerable bending about the beam major (X-X) axis direction. Longitudinal yielding is initiated at about 120 kN-m on both the down and up sides. In beam 12B the down and up strains also diverge quickly though not to the same degree as in 12A. Yielding is again initiated at about 120 kN-m.

The edge and web-side strains for the extended bolts are clearly quite different from those for beams 10A and 10B – for both 12A and 12B the edge and web-side strains diverge considerably, showing that transverse bending is quite significant here. Beam 12B in fact seems to indicate more transverse bending than longitudinal bending. Thus, the extended bolts in the 12mm tests were bent considerably about both axes.

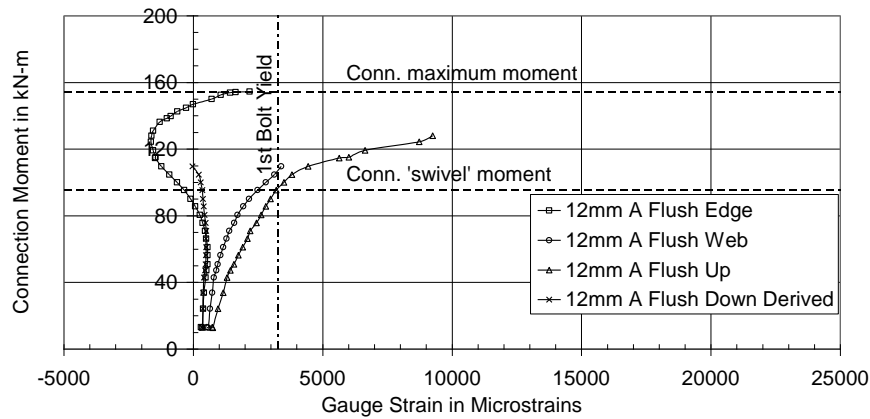
The flush strains for Beam 12A differ even more from those for 10A. Unlike in Beam 10A where there was no longitudinal bending, the flush strains for 12A indicate a significant degree of longitudinal bending besides the transverse bending. The down strain only becomes compressive slowly so there is still an axial effect; but the up and down strains are clearly diverging. Yielding initiates at about 110 kN-m.



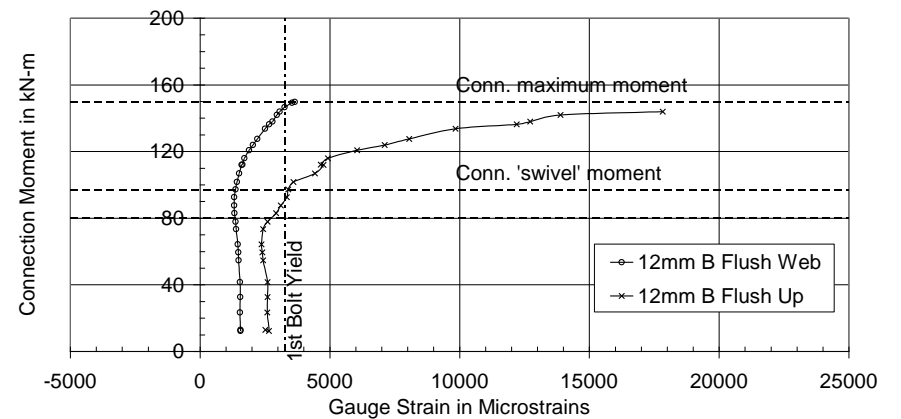
(a) Beam 12A - Extended Bolt Strains



(b) Beam 12B - Extended Bolt Strains



(c) Beam 12A - Flush Bolt Strains



(d) Beam 12B - Flush Bolt Strains

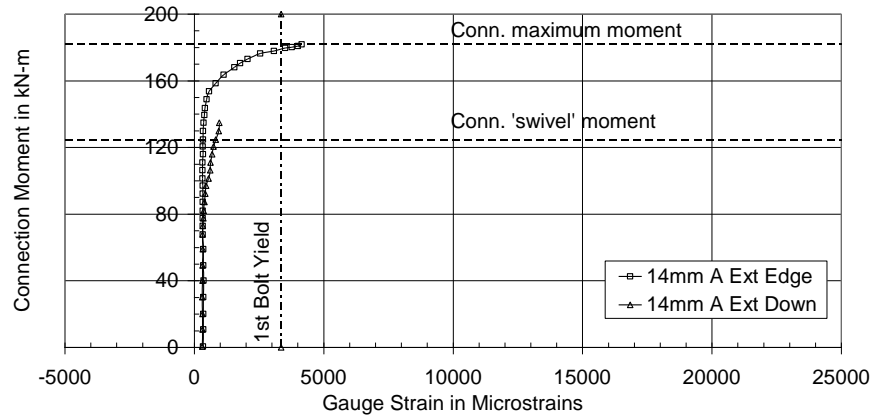
Figure 4.28 – Bolt Strains in Connection Test 2

4.3.4 Bolt Strains in Connection Test 3

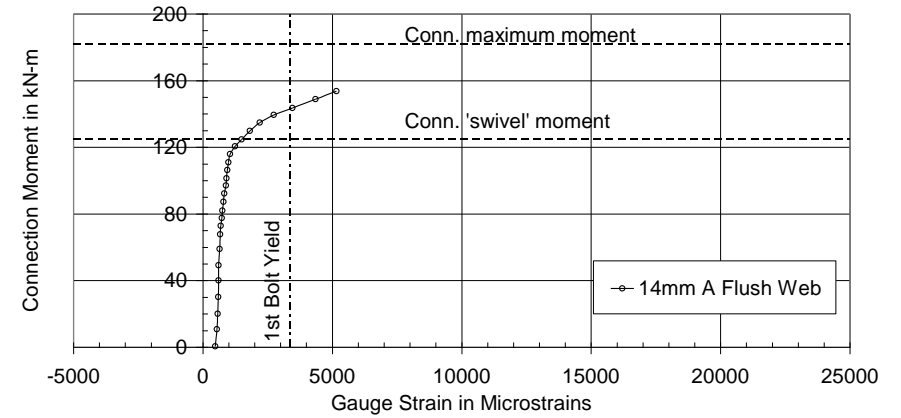
The measured bolt strains from connection test 3 are plotted in Figure 4.29. Only a few gauges were recorded for the extended bolts, and none for the extended bolt of beam 14B. Thus, Figure 4.29b shows the flush bolt strains of beam 14A, 4.29c is the flush strains in beam 14B, and Figure 4.29d is a close-up of part of the latter curve.

The 14mm test strains are all rather small by comparison with the other tests. This reflects the fact that there was considerably less deformation of the endplate (and therefore of the bolts) during the test.

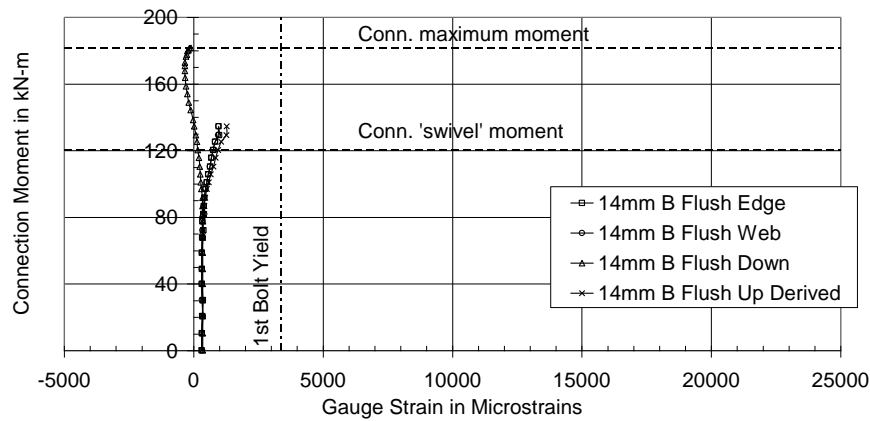
The information from the extended bolts is limited but the edge strain for beam 14A is constant for most of the test, and then yields at a connection moment of about 160 kN-m. This clearly indicates that there is no transverse bending since the edge strain would have to become compressive for transverse bending. There is also no transverse bending in the flush bolt. In Figure 4.29d the edge and web-side strain readings coincide so exactly that they can hardly be distinguished from each other. Thus, the sole effect there is axial tension. There is some bending longitudinally as shown by the up and down strain curves, but this is limited and small in comparison with bending in the 10mm and 12mm tests. In fact, in Figure 4.29 (c) all four strain components coincide exactly till about a connection moment of 80 kN-m. So there is neither longitudinal nor transverse bending till that point in the test. The bolt force curve in Figure 4.32 shows that the bolt force does remain constant at a pre-tension of about 26 kN until a connection moment of 80 kN-m. The bolt does not yield but the curve does begin to bend away from the vertical indicating an increase in axial force along with connection moment.



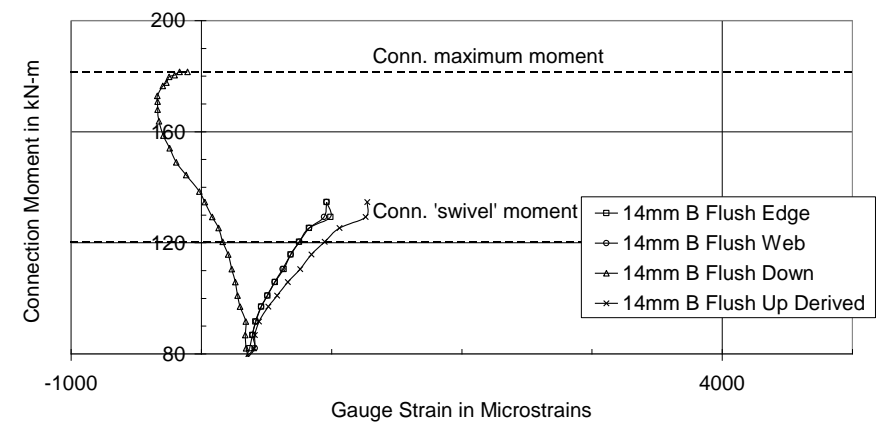
(a) Beam 14A - Extended Bolt Strains



(b) Beam 14A - Flush Bolt Strains



(c) Beam 14B - Flush Bolt Strains



(d) Beam 14B - Flush Bolt Strains (Expanded)

Figure 4.29 – Bolt Strains in Connection Test 3

4.3.5 Bolt Forces in the Connection Tests

The ‘average’ force in each bolt can be calculated from the axial bolt strain. Once the axial strain exceeds the yield strain, the corresponding bolt stress and force must be adjusted to reflect the change from the initial to the strain-hardening slope. Thus, for axial strain ϵ_{axial} :

$$\begin{aligned} \text{If } \epsilon_{axial} \leq \epsilon_y : \quad & \text{axial stress } f_{axial} = E \cdot \epsilon_{axial} \\ \text{If } \epsilon_{axial} > \epsilon_y : \quad & \text{axial stress } f_{axial} = E \cdot \epsilon_y + E_{sh} \cdot (\epsilon_{axial} - \epsilon_y) \end{aligned} \quad \text{Eqn 4.2}$$

where E is the Young’s modulus and E_{sh} is the strain-hardening modulus measured in the bolt material tests.

$$\text{Bolt Force} = f_{axial} \cdot A \quad \text{Eqn 4.3}$$

where A is the measured bolt cross-sectional area.

Bolt forces can only be calculated where all the bolt strains were recorded i.e. where the strain gauges all functioned well. Thus, the flush bolt force for beam 10B could not be calculated for example, since only one gauge functioned. The extended and flush bolt forces for beam 10A and the extended bolt force for 10B are shown in Figure 4.30.

There are four distinct regions in the extended bolt force curves of Figure 4.30. The first is an approximately linear segment where the bolt force increases only very slowly for large increases in the connection moment. There is some initial bedding-in, and then this first segment has a steep slope and is almost vertical. This region seems to indicate the range of connection moment in which the bolt forces are only a little greater than the initial bolt pre-tension force.

In a second region of the extended bolt force curve, the curve flattens out slowly in a ‘knee’. This second region is more apparent in the 10B ext bolt force curve. It can be seen that a straight line through this region would pass more or less through the graph origin. Thus, this second region seems to indicate the range of

connection moment for which the bolt pre-tension has been overcome, so that the bolt force is increasing linearly with connection moment.

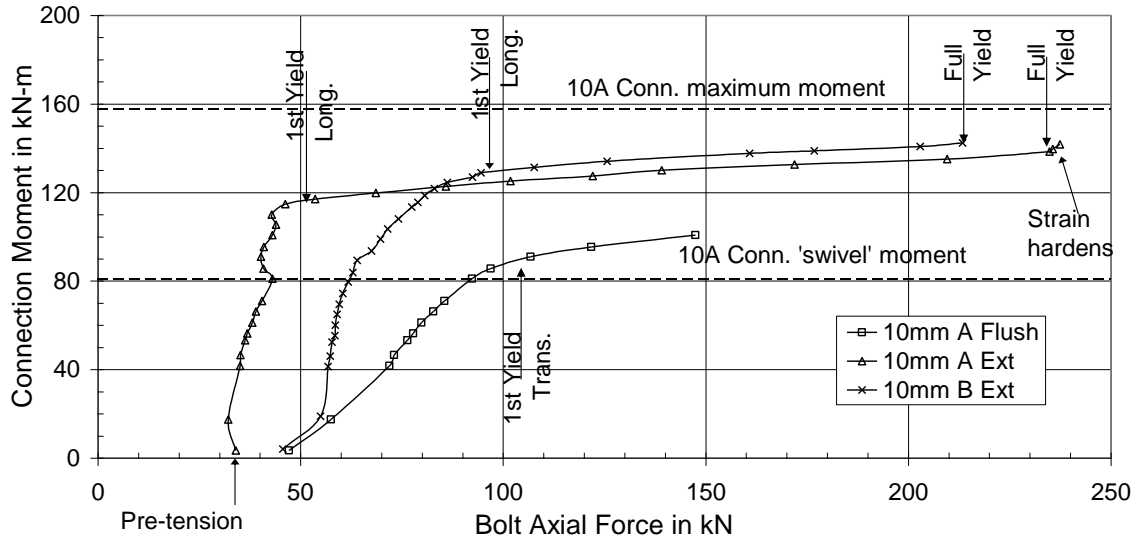


Figure 4.30 – Bolt Forces for Connection Test 1

In a third region of the extended bolt force curve, the curve becomes almost horizontal, and the bolt forces increase considerably with little increase in connection moment. This region seems to be initiated by yielding of the bolts in bending. (The onset of yielding is identified when one of the measured strains first exceeds the yield value – full yielding is where the average axial strain exceeds the yield value). By comparison with Figures 4.27 (a) and (b), we see that the extended bolts are yielding in bending in a longitudinal plane i.e. in a plane parallel to the beam web. Thus, in this third region the bolt is bending to conform to the endplate bending, due to the plate ‘prying’ against the bolt head.

Finally in a fourth region, the slope becomes steeper again. This fourth region clearly corresponds to the attainment of axial yielding, when the entire cross-section appears to be yielding in tension. This region appears in the 10A Ext bolt force curve, but not in the 10A. We assume that the latter strain gauges failed prior to full yield of the bolt.

When the flush and extended bolt forces of Beam 10A are compared, it can be seen that the flush bolt attracts a lot more force than the extended bolt right up to the point where the flush bolt gauges stop recording. When the flush bolt begins to yield at a connection moment of about 90 kN-m, the flush bolt force is 105 kN as compared to 40 kN for the extended bolt. Secondly, whereas the extended bolt force initially remains almost constant at the pre-tension force of approximately 35-40 kN, the flush bolt force increases right from the onset. So initially, the flush region is much stiffer, attracting more force, and the extended region is relatively flexible.

Of the four regions identified for the extended bolts, only regions two and three can be seen clearly for the 10A flush bolt. The first region where the curve is vertical is missing, and the bolt force increases from the pre-tension from the start of the test. The fourth region is also not evident, but this is probably due to the strain gauges failing before the end of the test. From Figure 4.27 we notice that the flush bolt bending is principally in the transverse plane rather than the longitudinal. We also notice that unlike the extended bolts which continue to bend longitudinally till the gauges stop functioning, the transverse bending of the flush bolt gives way to superimposed axial tension.

The bolt forces for test 2 are plotted in Figure 4.31. The extended bolt forces for beam 12A and 12B both exhibit the four regions described above for the bolt forces in connection test 1. An almost vertical pre-tension region is evident, with a pre-tension of approximately 60 kN for 12A and a pre-tension of approximately 90 kN for 12B. The third region after yielding commences is also evident in both extended bolts, with the bolt force increasing rapidly with little increase in connection moment. However, the transition ‘knee’ (second region) is now quite long. As in Figure 4.30 before, the extended bolt forces stop increasing rapidly once the bolt is fully yielded, and the slope of the curve becomes steep.

The flush bolt curve for beam 12A could only be plotted as far as a connection moment of 110 kN-m. In that range however, if one allows for the fact that it

starts at a lower pre-tension compared to the extended region bolt, the two bolt forces run more or less parallel all the way with the flush force being higher by about 10-15 kN.

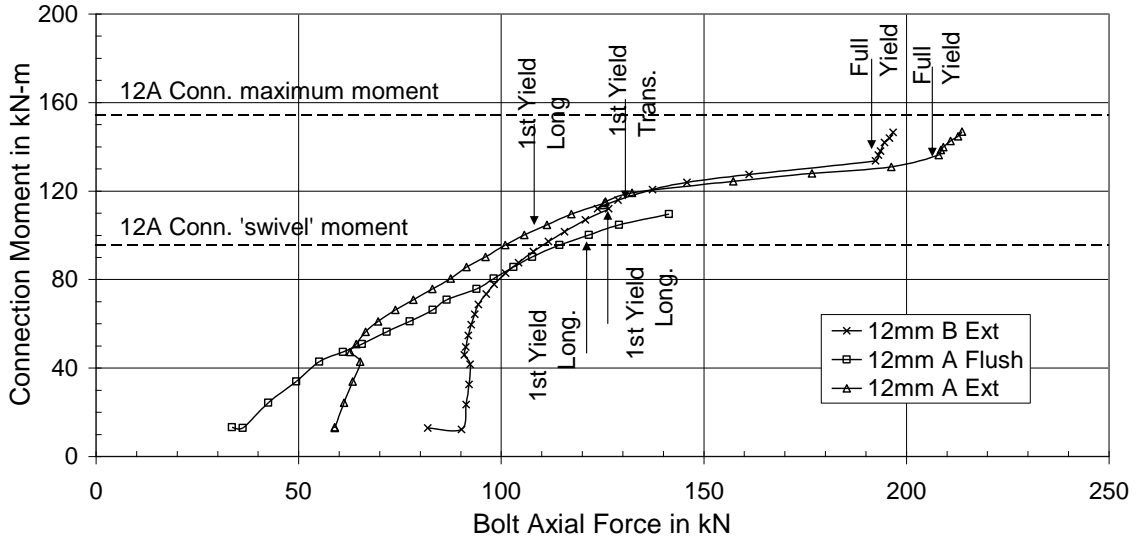


Figure 4.31 – Bolt Forces for Connection Test 2

The flush bolt curve is practically a straight line and is just showing signs of yielding when the gauge readings terminate. When the flush bolt begins to yield at a connection moment of about 100 kN-m, the flush bolt force is 122 kN as compared to 106 kN for the extended bolt. This is a ratio of extended to flush bolt force of 0.87, compared to 40:105 or 0.38 for beam 10A.

Of the four regions identified the 12A flush bolt shows only the second region. The strain gauges have evidently ceased functioning before the third and fourth regions commence.

The flush bolt force in beam 14B is much smaller by comparison with the flush bolt force in beams 12A and 10A. For example, at a connection moment of 100 kN-m, the flush bolt forces for 10A, 12A and 14B are 142, 122 and 34.5 kN respectively. Thus, the flush bolt force at a given connection moment appears to decrease with increasing endplate thickness. By comparison the extended region

work in, and because of the risk of damaging bolt gauge wiring. However, this was not considered as having a major effect on the test results.

In section 4.2.4 it was suggested that the differences in the initial stiffness of the nominally identical A and B beams in a test could be partially explained by a difference in the bolt pre-tension. This hypothesis is supported by Figure 4.30 which shows that the 10B extended bolt had a higher pre-tension than the extended bolt of 10A – 58 kN vs 35 kN. Figure 4.31 also shows that the extended bolt in beam 12B had a higher pre-tension (90 kN) than the corresponding bolt in 12A (60 kN).

In all three connection tests, we notice the presence of a second region in the bolt force curves, where the bolt force increases rapidly with only a little increase in the applied connection moment. It seems then that the mechanism of load transfer/resistance in the connection changes during the test, from one where the bolts are not required to resist large forces to one where they are required to carry large forces.

As described in the previous section, the extended bolt force curves exhibit four regions as follows:

1. An almost vertical region where the bolt pre-tension exceeds the force applied to the bolt by the connection.
2. A mildly sloping transition region, in which the slope is such that the curve could be extrapolated to pass through the origin. The bolt force is increasing elastically and linearly with connection moment in this region.
3. A third region where the bolt force curve is almost horizontal with a very shallow slope. This region is where the bolt is yielding in bending in the longitudinal (beam web) plane.
4. A fourth region where the bolt section is fully yielded in axial tension, so that the slope is once more gentle, though slightly steeper than region 2.

The curves for the flush bolt forces from Tests 1 and 2 are similar to the extended bolt curves, except that the first region is not clearly defined. This would result from the greater stiffness of the flush region in the initial stages of loading, so that the flush bolt forces increase very quickly at first. The other difference is that the flush bolts in these tests bend more in the transverse plane (a plane parallel to the beam flanges), rather than the longitudinal. The flush bolt force curve for the thicker 14mm endplates of test 3 differed however. These flush bolts bent more in the longitudinal plane and behaved more like the extended bolts – at least until the strain gauges ceased to function.

In all three tests, the yielding of the flush bolt in bending was almost coincident with the swivel point in the connection moment-rotation curve. Thus, the endplate was primarily restrained by the end moment due to prying of the bolt head prior to that point, but after that it is restrained more by an axial bolt force than by the bolt moment. One can deduce that the increased bolt force is necessary for the endplate flush region yield-lines to develop properly and hence for the connection rotation to ‘swivel’.

The bending of the flush and extended bolts is due to prying of the endplate against the bolt head. This prying moment will lead to an increase in the axial bolt force, over and above the value due to an average axial strain as given in this section.

As the endplate gets thicker, the ratio of the bolt forces in the extended region to that of the flush region, changes. The change in the ratio of extended bolt force to flush bolt force means the beam tension force is being transferred differently. In the thinner endplates a larger proportion of the beam tension force is transferred via the flush bolts than in the thicker endplates. It seems then that the extended part of the endplate acts as a cantilever to some extent, and when the endplate is thin, the cantilever is not stiff enough to attract as much force as the flush region.

In Figures 4.30, 4.31 and 4.32, we notice that none of the bolt force curves continue to the connection maximum moment. This is because the curves are all terminated prematurely by failure of one or more of the bolt strain gauges. Thus, these are not the maximum bolt forces attained, but the maximum bolt forces measured. In Figure 4.30 for example, we notice that the 10A extended bolt force was measured to 237 kN at about 90 % of the maximum connection moment.

4.4 ENDPLATE STRAIN GAUGE DATA

The strain gauges on the beam and endplate can be divided into four groups:

1. Strain gauges on the extended portion of the endplate, which were intended to allow the estimation of stress gradients along and across the extended region for varying load values.
2. Gauges on the flush tension region of the endplate were included to help to understand the yield and deformation patterns better in that region.
3. The gauges on the beam flanges were intended to allow an estimation of the flange forces.
4. The gauges on the beam web were intended to allow an understanding of the (non-linear) strain distribution across the beam web and to estimate the location of the strain 'neutral axis'.

The data from these four groups are reviewed below. The endplate material properties were previously given in Tables 3.2 and 3.3. For ease of reference however the key properties are re-tabulated in Table 4.2. In the graphs for the gauge strains on the endplates and beam ends, the strain ϵ_y at which the beam/plate begins to yield is shown where relevant.

Table 4.2 – Specimen Material Properties Relevant to Endplate & Beam Strains

	Young's Modulus GPa	ε_y - Yield Strain 10^{-6}	ε_{sh} - Strain Hardening Onset 10^{-6}
Bm flange (1)	209.7	1 547	17 750
Bm web (1)	213.6	1 710	21 100
Bm flange (2)	205.7	1 550	N/A
Bm web (2)	212.1	1 800	14 550
10 mm plate	202.2	1 638	13 450
12mm plate	219.1	1 397	13 500
14mm plate	213.0	1 385	13 600

Note: Beam (2) was used only for test 1

4.4.1 Endplate Strain Gauge Data

Figure 4.33 shows the strain gauge positions in the extended region while Figure 4.34 shows gauge positions in the flush region. The gauges in the extended region are along three vertical (longitudinal) and three horizontal (transverse) gridlines, and each gauge is referred to by these grids. Grid 1 is along the bolt line while grid 3 is along the weld line. Also grid A is along the plate edge while grid C is along the plate centreline. Thus, gauge A1 is on the bolt line by the plate edge.

Gridline 3 is at 12mm from the beam tension flange, which is actually 4mm from the assumed position of the weld line at 8mm from the beam flange surface. This is necessary because of the practical difficulty of fitting in the gauges into the space next to the beam flange weld. Similarly, gridline 1 is offset 10mm from the

bolt centreline towards the beam flange to allow some clearance for the gauge from the bolt head. Gridline 2 is exactly halfway between gridlines 1 and 3.

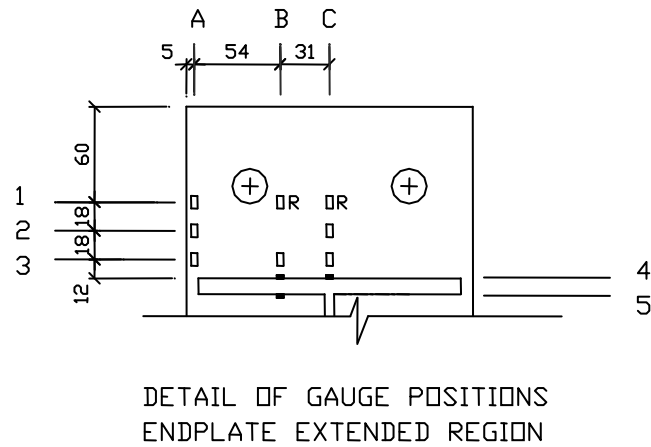


Figure 4.33 – Locations of Strain Gauges in the Endplate Extended Region

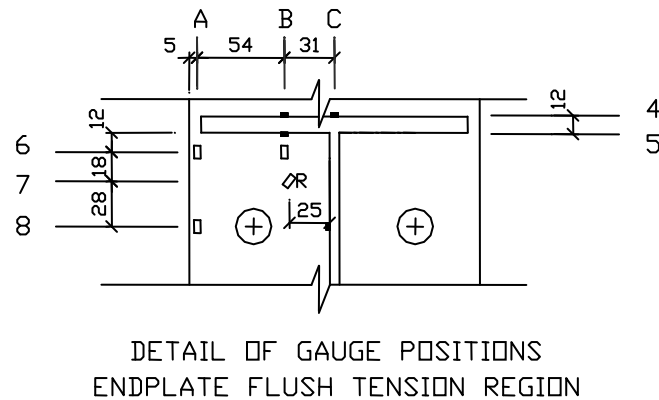
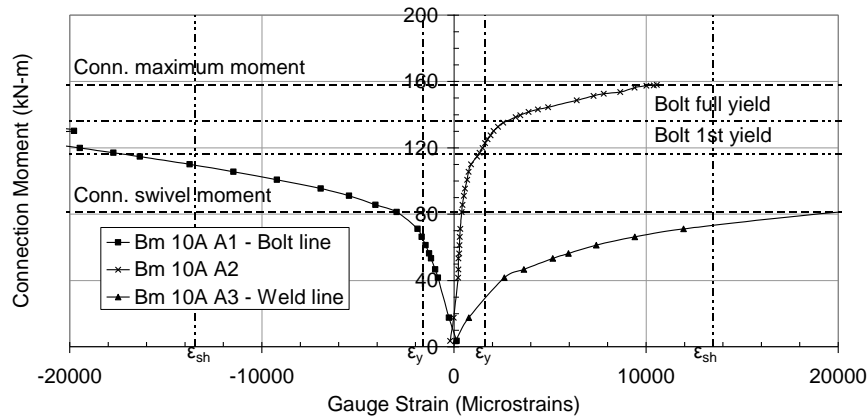
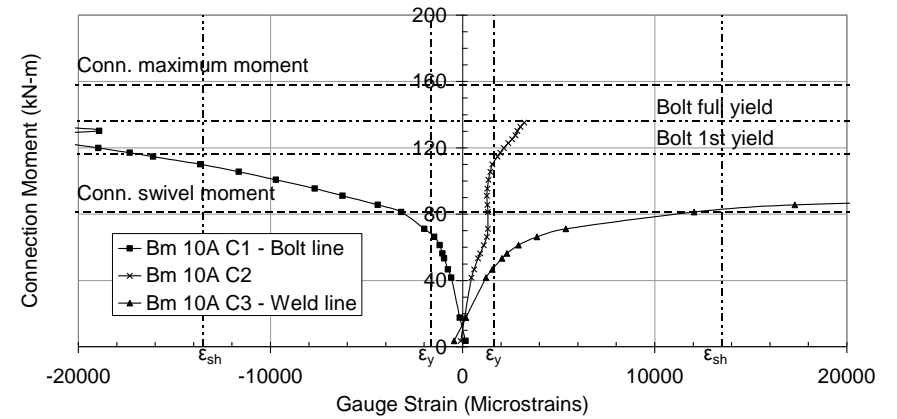


Figure 4.34 – Locations of Strain Gauges in the Endplate Flush Region

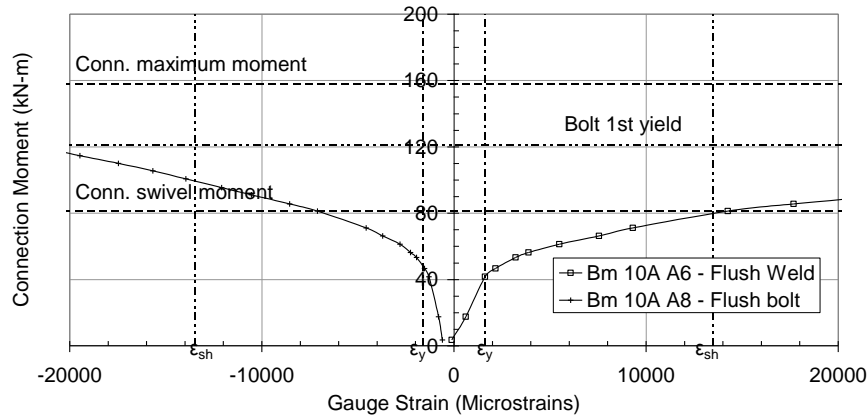
The gauges in the flush region are along the same three longitudinal gridlines, and three transverse gridlines as shown. Grid 6 is on the flush region weld line while grid 8 is on the flush region bolt line. Gauge B7 is a 0-45-90 rosette with a longitudinal (vertical) and a transverse (horizontal) measurement. The third gauge in the rosette is either tangential or radial to a circle with bolt hole as centre. In Figures 4.35 to 4.40 the strain gauge measurements on the endplate are presented for each of the three tests.



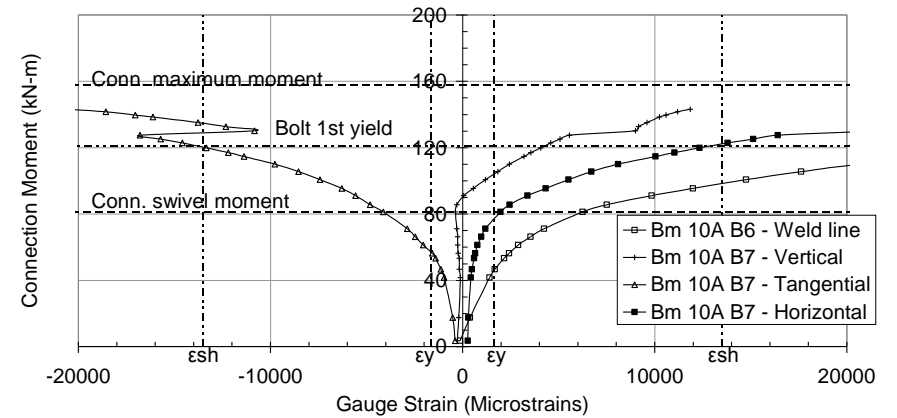
(a) Ext Region Grid A Strains



(b) Ext Region Grid C Strains

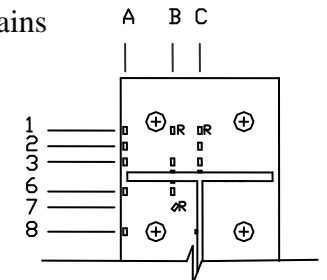


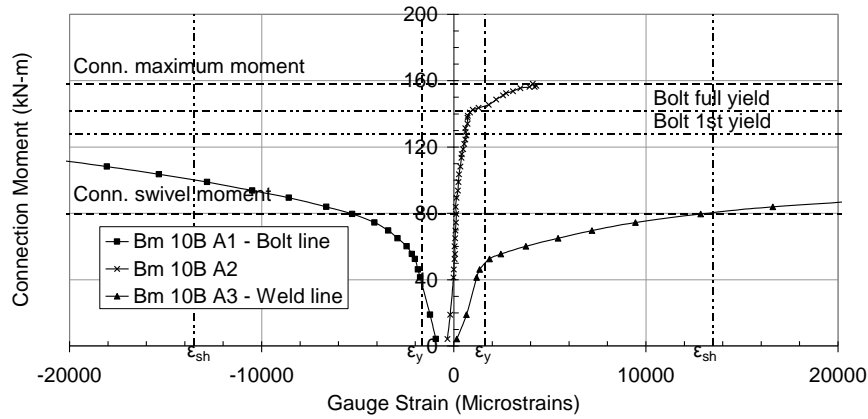
(c) Flush Region Grid A Strains



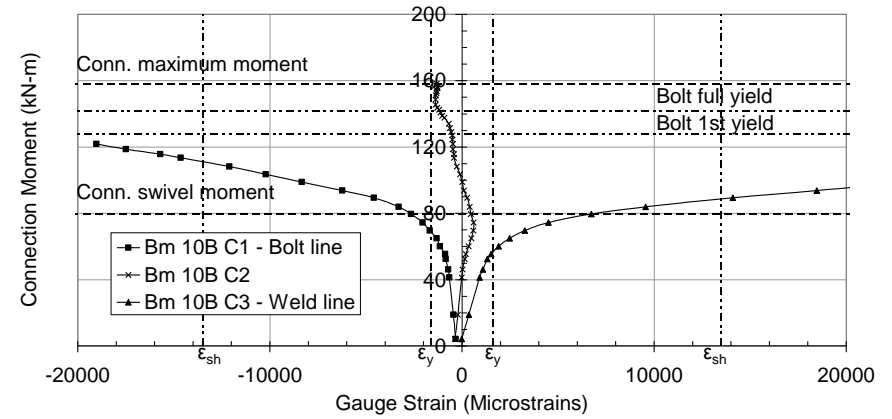
(d) Flush Region Grid B Strains

Figure 4.35 – Endplate Strains in Connection Test 1 – Beam 10A

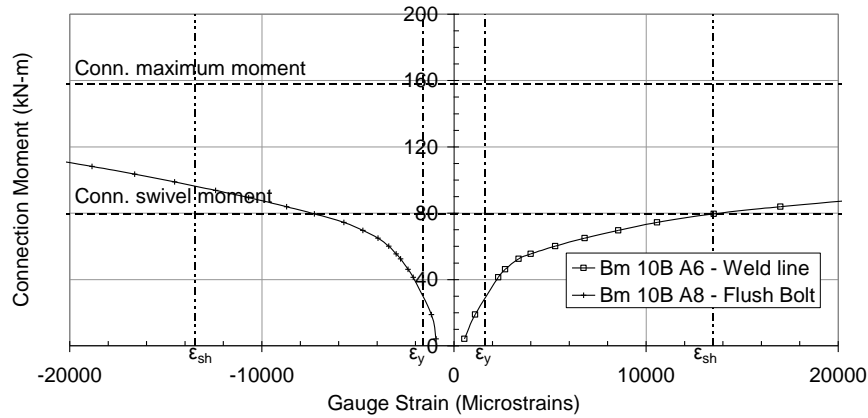




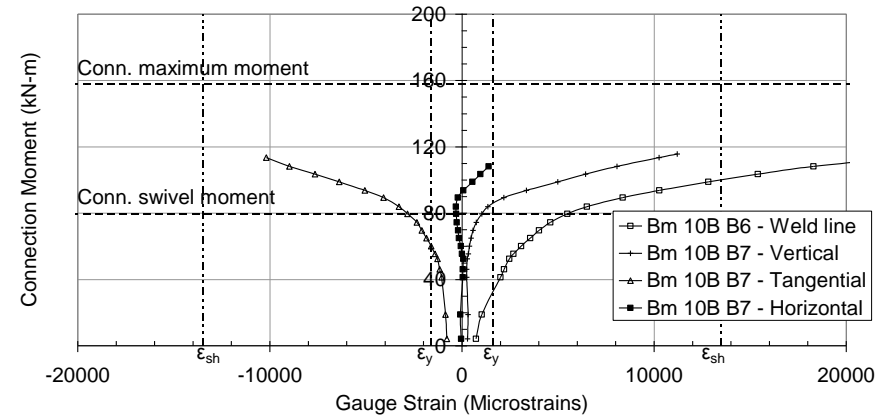
(a) Ext Region Grid A Strains



(b) Ext Region Grid C Strains

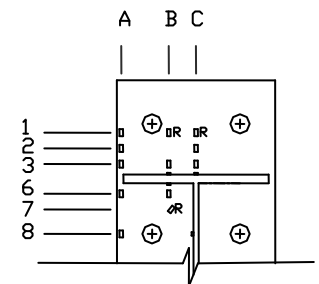


(c) Flush Region Grid A Strains



(d) Flush Region Grid B Strains

Figure 4.36 – Endplate Strains in Connection Test 1 – Beam 10B



The measured strains on the endplate would be impacted by the occurrence of residual stresses in the heat-affected zone from the welding of the beam flanges to the plate, and from possible distortions of the endplate during welding. These residual stresses and distortions were minimized by requiring the use of fillet welds rather than a full-penetration groove weld. The effect of residual stresses would moreover cease to have significant influence once the plate yields. These effects are therefore not considered further in this discussion.

In the extended regions of beams 10A and 10B (Figures 4.35 and 4.36) we see that endplate 10A begins to yield first on the weld line – at 41 kN-m – and only begins to yield on the bolt line at 71 kN-m. The position of yielding is shown approximately by the vertical chain-dotted lines at a strain of $\pm \epsilon_y$, which is the yield strain for the endplate material.

However, the actual strain at which yielding is complete may be slightly offset from ϵ_y due to the occurrence of residual stresses from welding, and is better estimated by the change in slope in the strain curve. Beam 10B yields first on the weld line at 46 kN-m, and then on the bolt line at 69 kN-m. By comparison, yielding in the flush region of beam 10A initiates on the flush weld line at 42 kN-m (gauge A6), and on the flush bolt line at 53 kN-m (gauge A8). Similarly, yielding in the flush region of beam 10B initiates on the flush weld line at 46 kN-m (gauge A6), and on the flush bolt line at 65 kN-m (gauge A8). Thus yielding in the flush region lags behind that in the extended region.

In beams 10A and 10B, the strains on gridline 2 start out being tensile and increasing linearly at a slow rate. This shows that gridline 2 is not at the point of inflexion for the longitudinal strain distribution along the extended region. The tensile stresses on gridline 2 are in approximate agreement with where the point of inflexion would be if the bolt line runs through the bolt centreline.

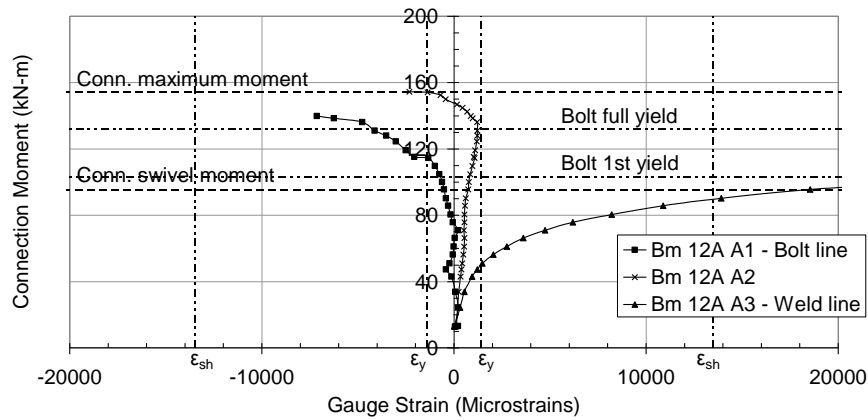
At a connection moment of 110 kN-m, the strain on gauge A2 of beam 10A begins to increase in tension at a higher rate, until it yields in tension at about 132

kN-m. The gauges C2 of beam 10A and A2 of beam 10B exhibit a similar pattern, however gauge C2 of beam 10B inexplicably goes into compression instead. A likely explanation for this is that the fracture in beam 10B began to develop as a crack at that point, in the centre of the weld line. The effect is to reduce the weld line moment, shifting the inflexion point towards the weld line, on gridline C.

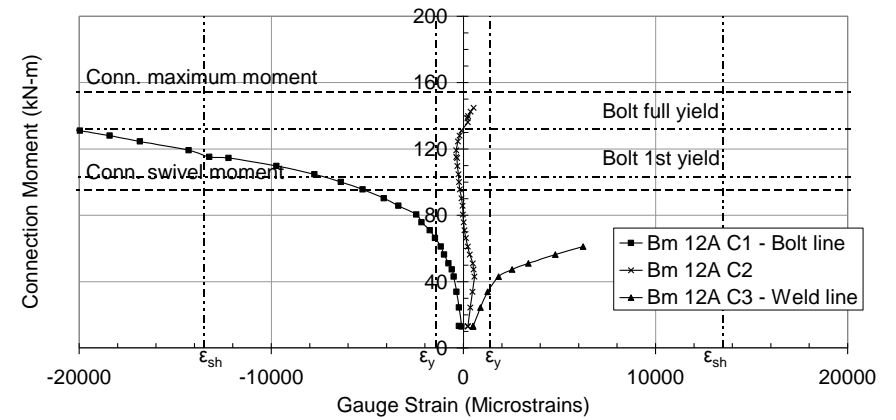
In Figures 4.35d and 4.36d, the rosette at gauge position B7 initially measures almost zero vertical strain and zero horizontal strain. In both cases, at about the connection swivel moment, both the vertical and horizontal components yield in tension and begin to increase rapidly. The similarity between the vertical and horizontal components shows the principal strain is approximately radial to the flush bolt hole centre. The tangential components yielded at 56 kN-m for 10A and 74 kN-m for 10B.

In the extended regions of beams 12A and 12B (Figures 4.37 and 4.38) endplate 12A begins to yield first on the weld line – at 43 kN-m – and begins to yield on the bolt line at 80 kN-m (gridline C). Beam 12B yields on the weld line at 83 kN-m (gridline A), and on the bolt line at 83 kN-m (gridline C). By comparison, yielding in the flush region of beam 12A initiates on the flush weld line at 61 kN-m (gauge A6), and on the flush bolt line at 66 kN-m (gauge A8). Similarly, yielding in the flush region of beam 12B initiates on the flush weld line at 73 kN-m (gauge A6), and on the flush bolt line at 83 kN-m (gauge A8). In general, as one would expect, yielding in the 12mm endplate specimens takes place at higher connection moments than in the 10mm specimens.

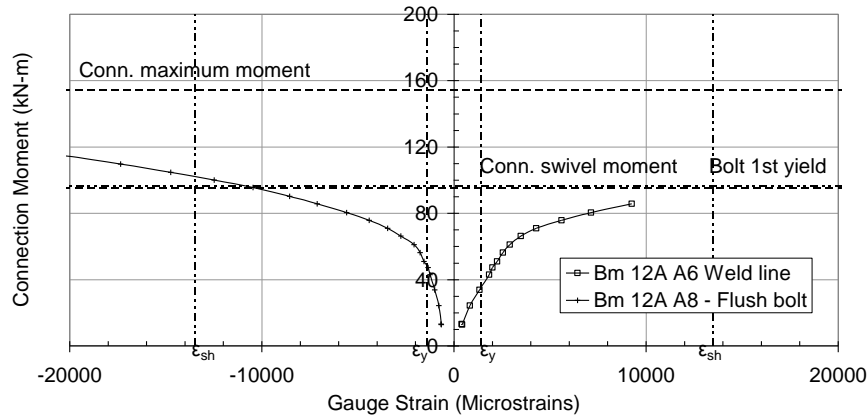
In beams 12A and 12B, the strains on gridline 2 also start out being tensile and increasing linearly at a slow rate (Figures 4.37 and 4.38). Unlike the gridline 2 measurements of test 1 however, these strains don't increase quickly. In beam 12A that fractured, gridline 2 never really yielded, and both the gauges A2 and C2 went into compression before the connection maximum moment. This probably reflects cracking of the endplate on the weld line.



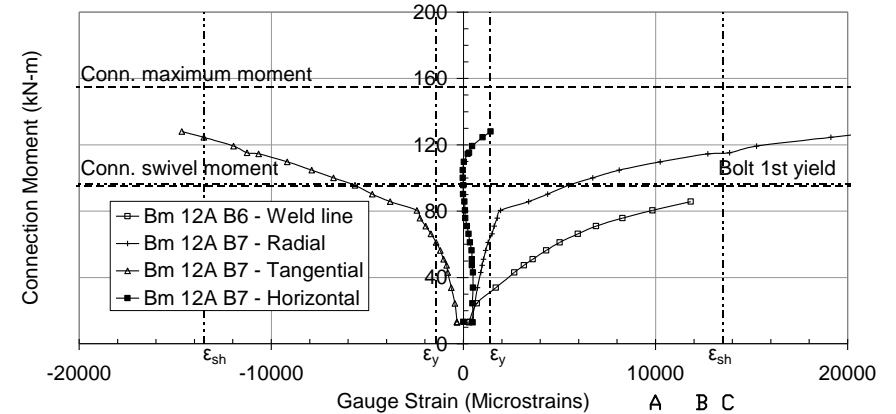
(a) Ext Region Grid A Strains



(b) Ext Region Grid C Strains

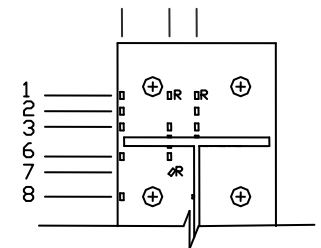


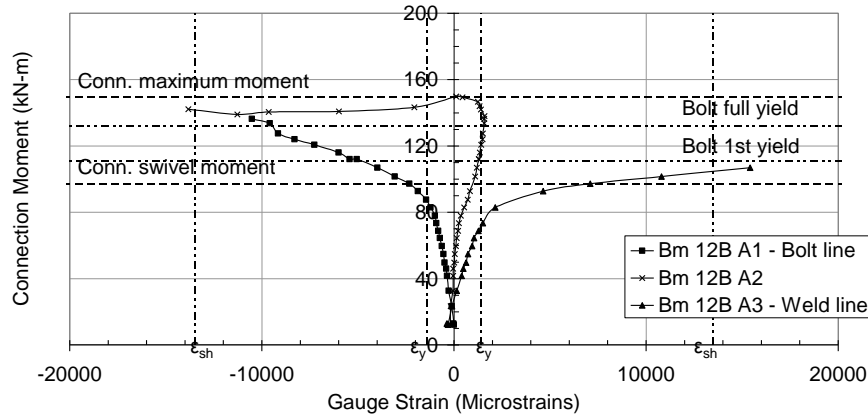
(c) Flush Region Grid A Strains



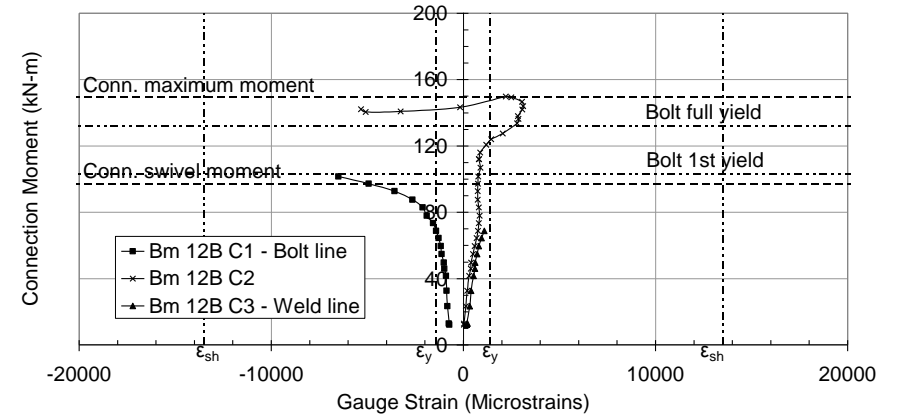
(d) Flush Region Grid B Strains

Figure 4.37 – Endplate Strains in Connection Test 2 – Beam 12A

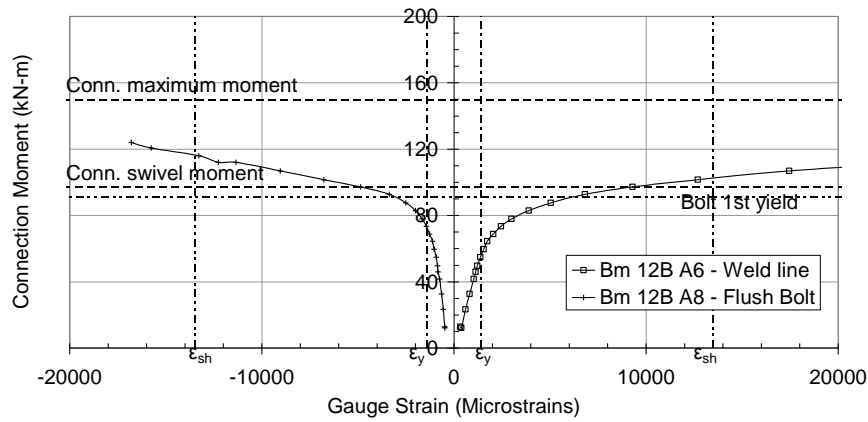




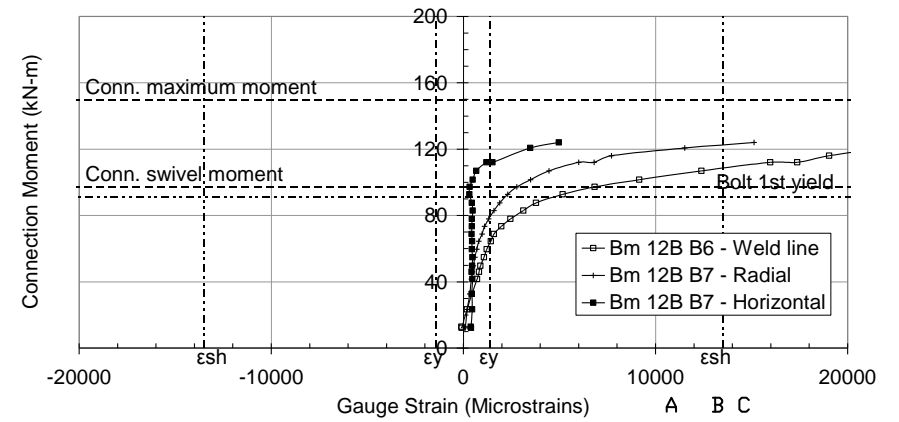
(a) Ext Region Grid A Strains



(b) Ext Region Grid C Strains

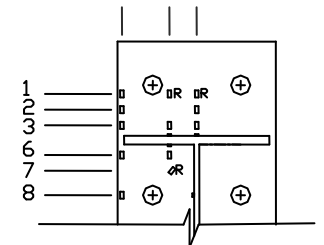


(c) Flush Region Grid A Strains



(d) Flush Region Grid B Strains

Figure 4.38 – Endplate Strains in Connection Test 2 – Beam 12B



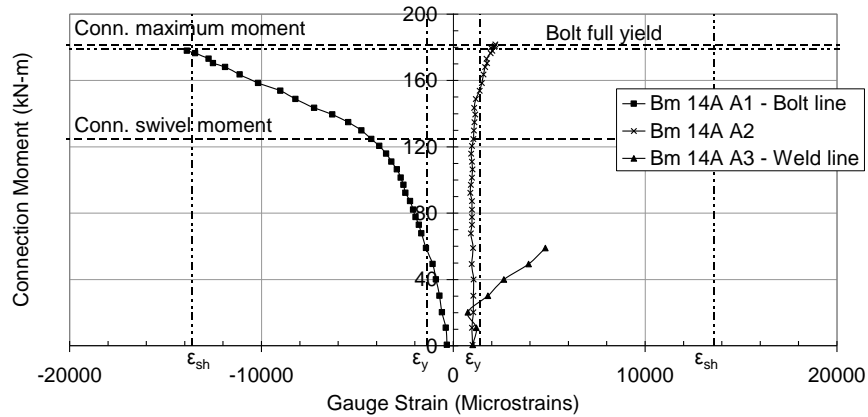
In beam 12B, both A2 and C2 remained tensile till the connection maximum moment, but then became compressive thereafter as the weld line cracked on that beam as well. In connection test 2, the radial and horizontal components were measured at flush gauge B7 rather than the longitudinal component (Figures 4.37d and 4.38d). The radial and tangential components both yielded at about 80 kN-m for beam 12A, and the radial at about 93 kN-m for 12B. As with connection test 1 the flush region lags behind the extended region in yielding.

The endplate strains for connection test 3 are given in Figures 4.39 and 4.40 A. In the extended region of endplate 14A the weld line yielded as early as 30 kN-m, however, the endplate only began to yield on the bolt line at 96 kN-m. Beam 14B yielded first on the weld line at 30 kN-m, and then on the bolt line at 110 kN-m. Yielding in the flush region initiated at 40kN-m on the weld line of beam 14A, but only at 82 on 14B.

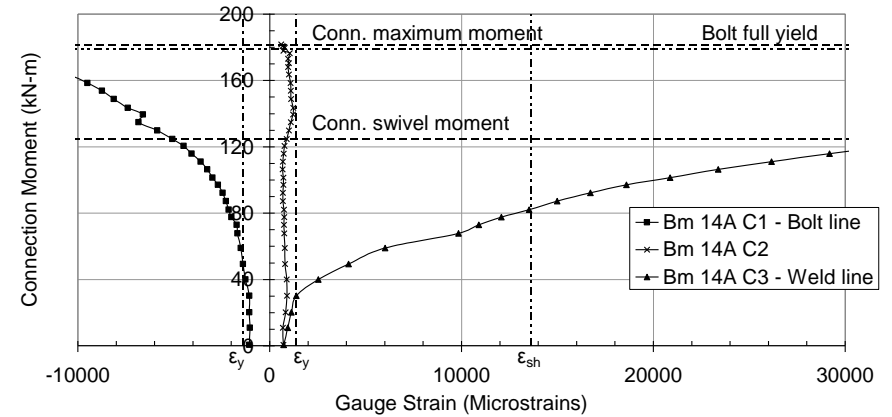
The strains on gridline 2 are once more tensile, reflecting the offset between gridline 2 and the point of inflexion. Unlike in tests 1 and 2 though, there is no evidence of yielding on gridline 2. The only exception to this is at gauge C2 of 14B (Figure 4.40b). In beam 14A, rosette B7 has a larger horizontal component than the radial, showing that the strain is mostly horizontal. This is corroborated by the fact that the vertical strain is compressive. Thus, the bending in that area is mostly transverse, rather than circular as in tests 1 and 2.

4.4.2 Discussion of Endplate Strains

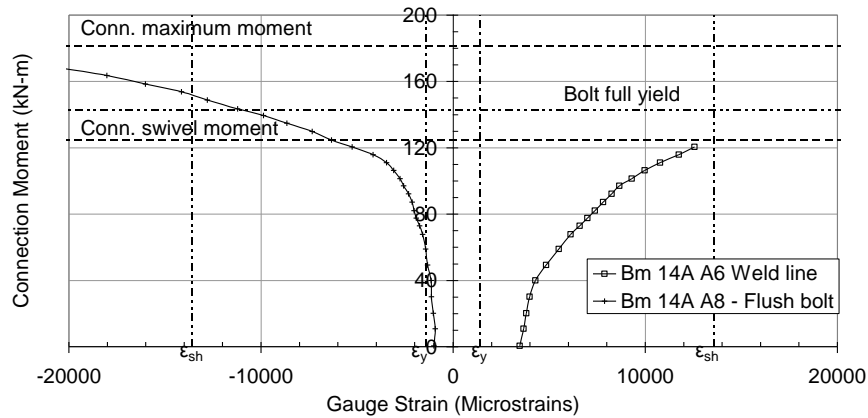
We notice that for both 10A and 10B, the top of the yield 'knee' on the extended region bolt line strains (gauges A1 and C1), coincides more or less with the connection swivel moment. This seems to be consistently true for tests 2 and 3 as well (Figures 4.37 to 4.40). Thus, we infer that the connection swivel starts with yielding on the extended region weld line and ends with full yielding of the extended region bolt line. Between these two is yielding of the flush region.



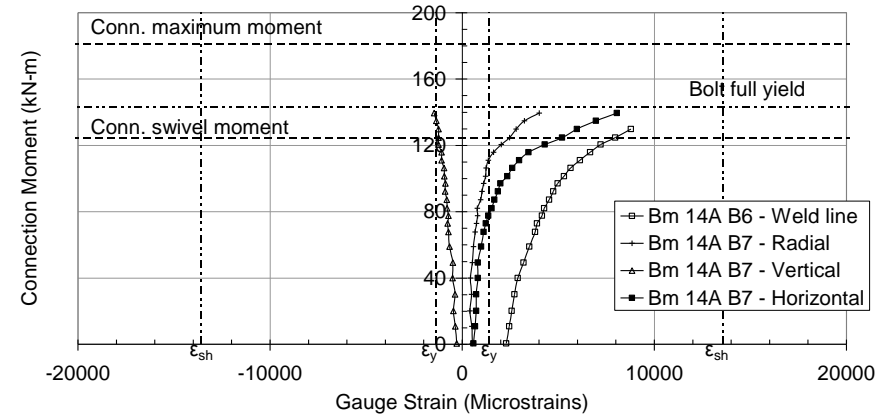
(a) Ext Region Grid A Strains



(b) Ext Region Grid C Strains

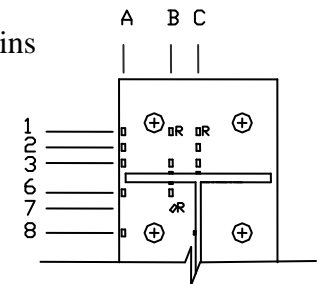


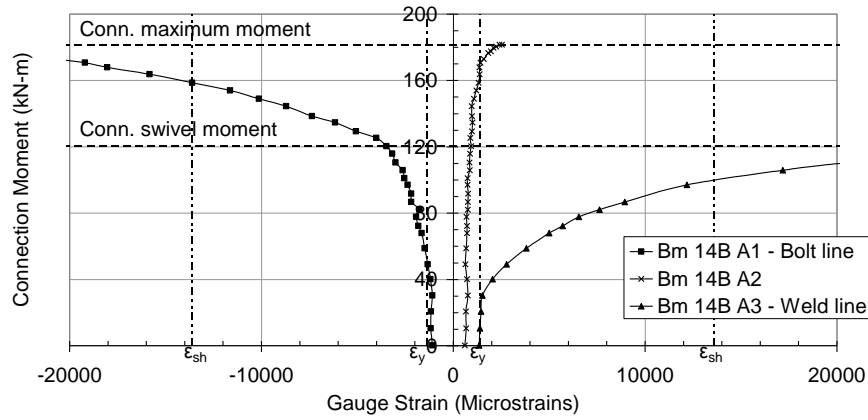
(c) Flush Region Grid A Strains



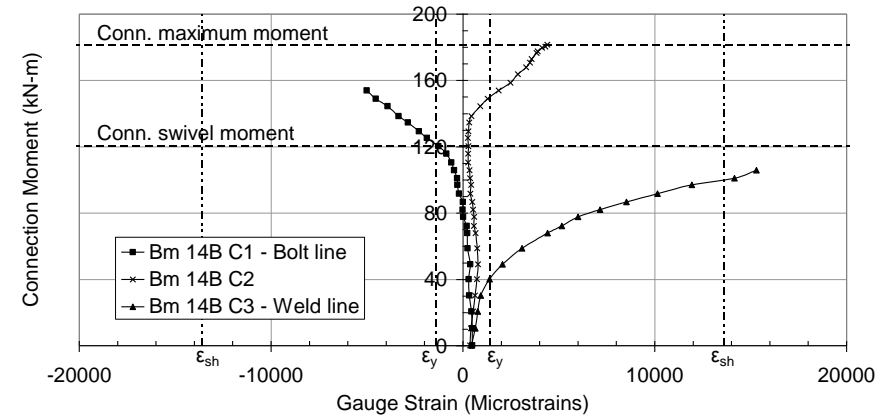
(d) Flush Region Grid B Strains

Figure 4.39 – Endplate Strains in Connection Test 3 – Beam 14A

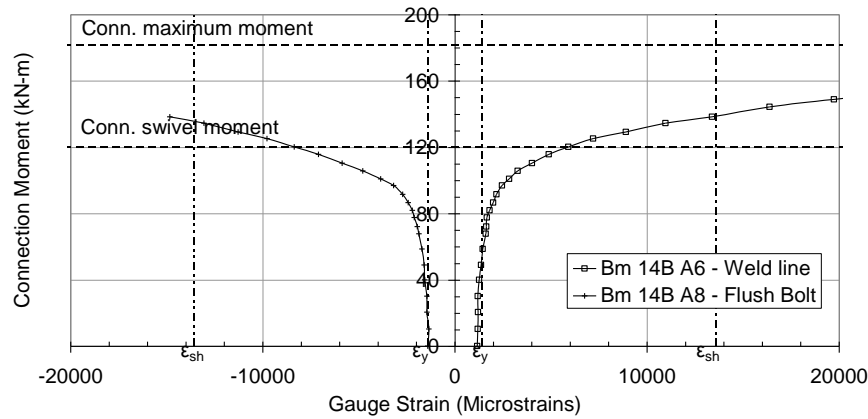




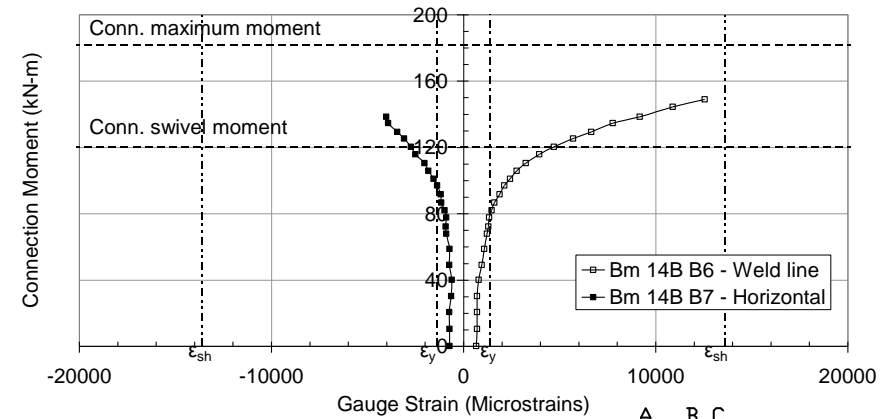
(a) Ext Region Grid A Strains



(b) Ext Region Grid C Strains

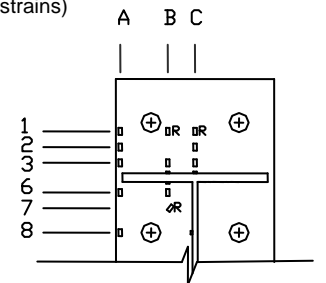


(c) Flush Region Grid A Strains



(d) Flush Region Grid B Strains

Figure 4.40 – Endplate Strains in Connection Test 3 – Beam 14B



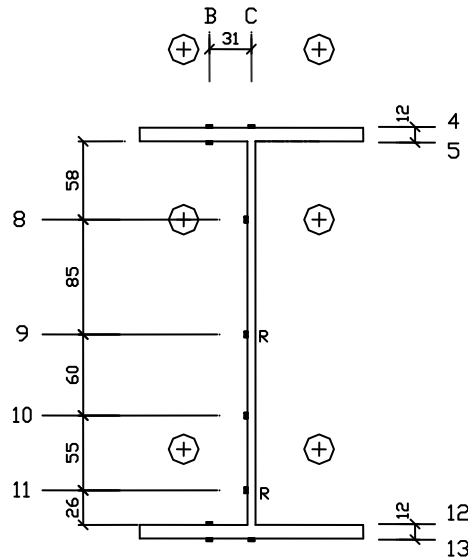
The yielding along gridline 2 in tension in tests 1 and 2 shows that the weld line is really a whole band of yielding extending at least halfway of the distance to the bolt line. Thus, a true plastic hinge develops at the weld line, with substantial strain-hardening adjacent to the beam flange, and with extensive yielding along the endplate to a considerable distance from the beam flange. This continues until cracks develop on the weld line.

The point of inflexion seems to shift closer to the bolt centreline as the yielding develops, possibly either because of a shift in the bolt line away from the flange (due to bolt yielding in bending, with a reduction in prying of the bolt head by the plate), or because of the growth in extent of the plastic moment at the weld line – from a local ‘hinge’ to become a band of plasticity spreading towards the bolt line.

In tests 1 and 2, the yielding of the vertical and horizontal components of the rosette measurements at B7 in the flush region seems to be similar to the behaviour on gridline 2. We surmise that the B7 components yield in tension as a plastic hinge develops on the weld line and on a beam web line adjacent to the beam web. The strains here are clearly radial, with the bolt hole as centre, and hence the tangential component is in compression.

In test 3, the fact that this tension yielding on gridline 2 does appear though on only one gauge (C2 of beam 14B), suggests that the same kind of yielding pattern is developing in the extended region of test 3 as the previous tests. It is clear though that there is a difference in test 3 nevertheless, as the bending at the B7 position of the flush region is transverse rather than radial. It seems then that the 14mm endplates would have the same deformation pattern as the other two tests, but this deformation does not develop before the bolt fractures. We surmise therefore that the bolt is not strong enough to restrain the endplate in either the extended or the flush region, and this is why the deformation pattern does not develop in either region. This should be considered in relation to the observation in section 4.3.5 that the ratio of extended bolt force to flush bolt force increases with endplate thickness.

4.5 STRAIN DATA ON THE BEAM WEBS AND FLANGES



DETAIL OF GAUGE POSITIONS
BEAM WEB AND FLANGES

Figure 4.41 – Locations of Strain Gauges on the Beam Web and Flanges

Figure 4.41 shows the strain gauge positions on the beam web and flanges. These gauges are all positioned to measure strains along the beam length. There are three gauges on each flange, with one pair opposite each other on the flange. The tension flange has gauges B4 and B5 opposite each other, and then C4 on the beam longitudinal centreline. The compression flange has gauges B12 and B13 on gridline B, and C13 on the centreline.

There are four gauges on the beam web – B8 is at the height of the flush tension bolts, B9 is almost exactly on the beam transverse centreline, B10 is 25mm above the centre of the shear bolts, and B11 is approximately halfway from the centroid of the beam compression flange to the level of the shear bolts. All these gauges are positioned 5mm from the edge of the flange or web welds. The test beam web and flange strains are presented in Figures 4.42 to 4.44.

4.5.1 Description of Beam Web and Flange Strain Gauge Data

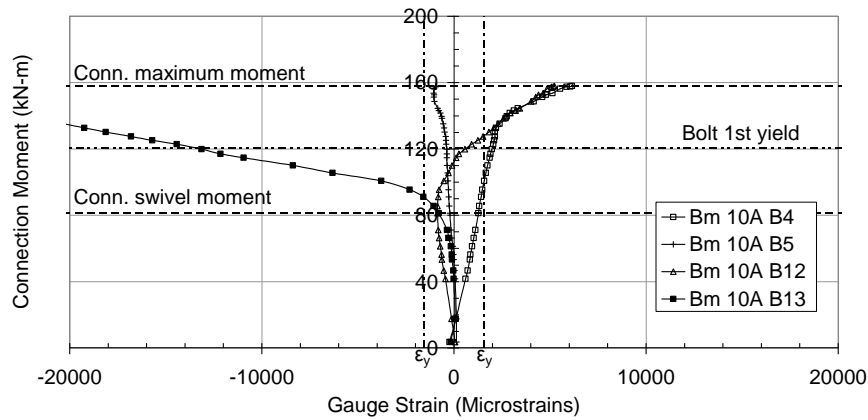
Test 1

In connection test 1 the flange strains for beams 10A and 10B are virtually identical (Figures 4.42a and 4.42b). The strains measured by gauges B4 and B5 on the tension flange are small and are linear until fairly high connection moments. Even though both gauge measurements are linear, B4 is in tension and B5 is in compression, and B4 has larger strain magnitudes than B5. At about 135 kN-m, the tensile strain on B4 begins to increase rapidly – remaining linear but at a new slope.

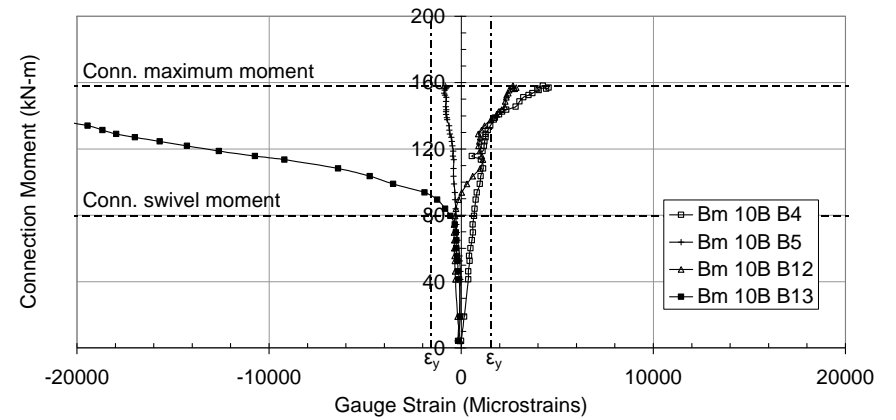
In Figures 4.42a and 4.42b, the compression flange gauges B12 and B13 are in linear compression with virtually the same magnitude up to the connection swivel moment. The initial slope for both gauges is negative i.e. sloping so that the strains become compressive. Just after the connection swivel moment at about 80 kN-m, the slopes change and the strains begin to increase rapidly. B12 reverses direction and becomes tensile, while B13 increases faster in the compression direction. We notice also that the strain magnitudes are much higher in the compression flange (B12 and B13) than the tension flange (B4 and B5). So yielding of the compression flange initiates at about 80 kN-m or 38% of M_p (209 kN-m)

There is a ‘kink’ in the B12 strain curve for beam 10B which is not evident in curve B12 for beam 10A. From a connection moment of 113 kN-m to 139 kN-m, the B12 strain curve changes direction, with the strains reducing in magnitude. At about 139 kN-m it changes direction again and the tensile strains begin to increase once more.

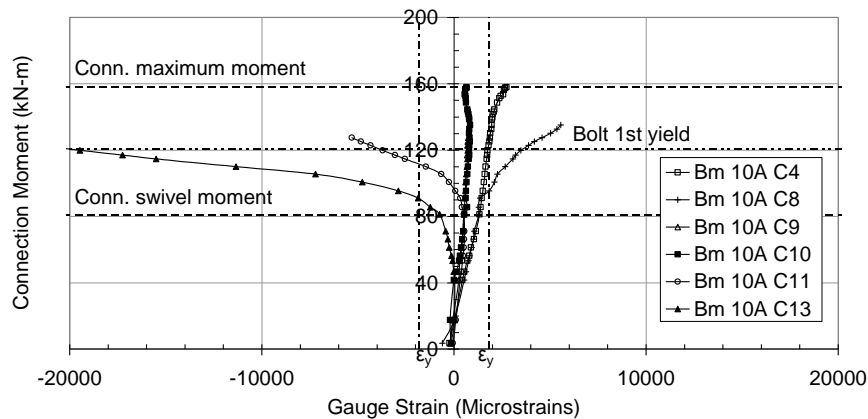
In Figures 4.42c and 4.42d showing the web strains, the curves C4 and C13 are very similar to B4 and B13 respectively for both beams, as would be expected. At a given connection moment however, the C gridline strains are larger than the B gridline strains.



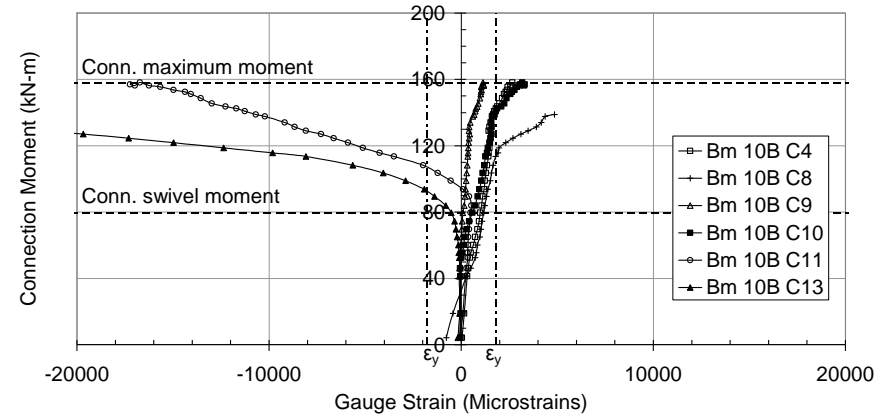
(a) Beam 10A Beam Flange Strains



(b) Beam 10B Beam Flange Strains

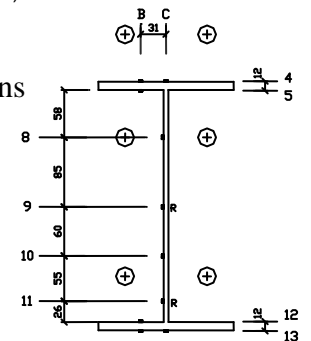


(c) Beam 10A Beam Web Strains



(d) Beam 10B Beam Web Strains

Figure 4.42 – Strains in the Beam Webs and Flanges from Connection Test 1

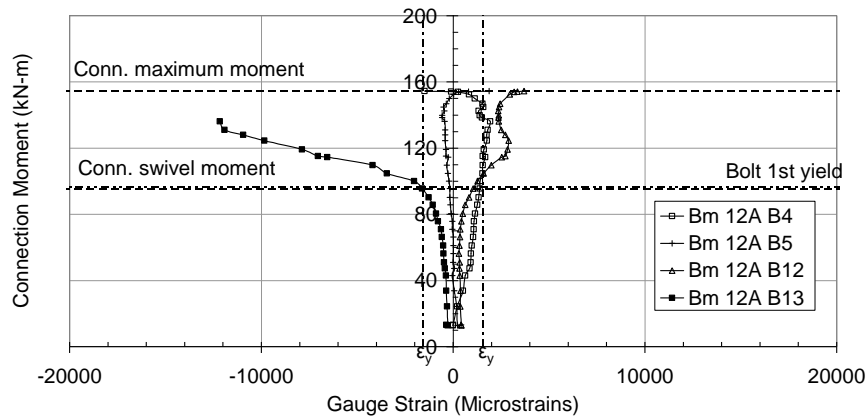


On the beam web, all four measured strains start out as tensile. Initially, strains C9, C10 and C11 are more or less equal in magnitude while strain C8 is larger than the others. In Figure 4.42c, C9 and C10 are identical right through the test and cannot be distinguished from one another. However, at a point in the test, strain C8 begins to increase faster in tension and C11 begins to increase faster in the opposite direction, becoming compressive. Thus, initially only the beam compression flange is in bearing against the column flange, but the compression zone later extends into the web to C11. For beam 10A this change in slope occurs at about 91 kN-m for both strain measurements. For beam 10B the slope change in C8 occurs at about 119 kN-m and the slope change in C11 at about 89 kN-m. C9 and C10 remain linear to the end of the test for both beams.

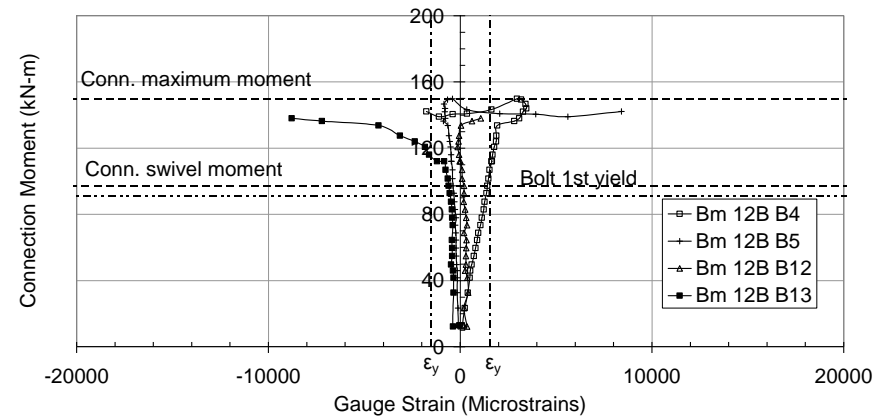
Test 2

In connection test 2 the flange strains for beams 12A and 12B are shown in Figures 4.43a and 4.43b. For both 12A and 12B, strains B4 and B5 on the tension flange are small in magnitude and linear. Only B4 in test 12B shows a definite slope change at a connection moment of about 134 kN-m. In test 12A, both B4 and B5 begin to reduce in magnitude at about 147 kN-m, becoming zero at the connection maximum moment. The reduction in strain at the tension flange is thought to be due to the initiation of cracks in the endplate and the beam flange weld.

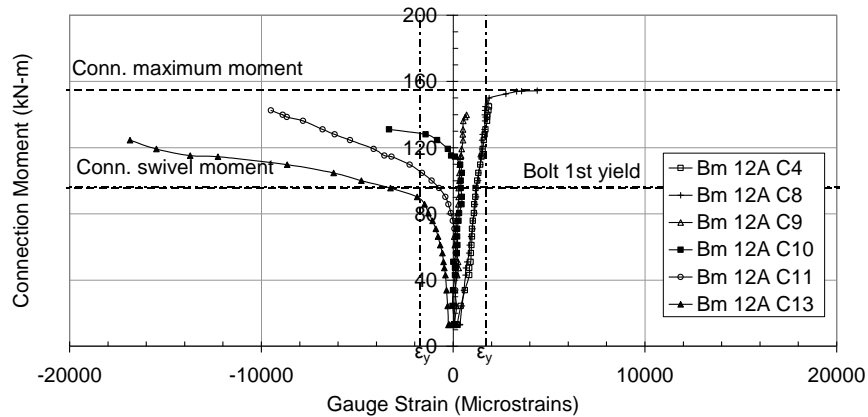
For both beams, from the start of the test, compression flange gauge B12 is in tension and gauge B13 is in tension. Initially both gauges measure linear strains with steep negative slopes and only slight increments in strain. At about 90 kN-m and 112 kN-m respectively for beams 12A and 12B ($0.44M_p$ and $0.55M_p$), the strain on gauge B13 begins to increase faster in the compressive direction with a change in slope. Gauge B12 similarly increases faster in the tensile direction at about 86 kN-m and 134 kN-m for 12A and 12B respectively. As with beam 10B, the B12 curve for beam 12A has a 'change in direction kink' between 119 kN-m and 145 kN-m.



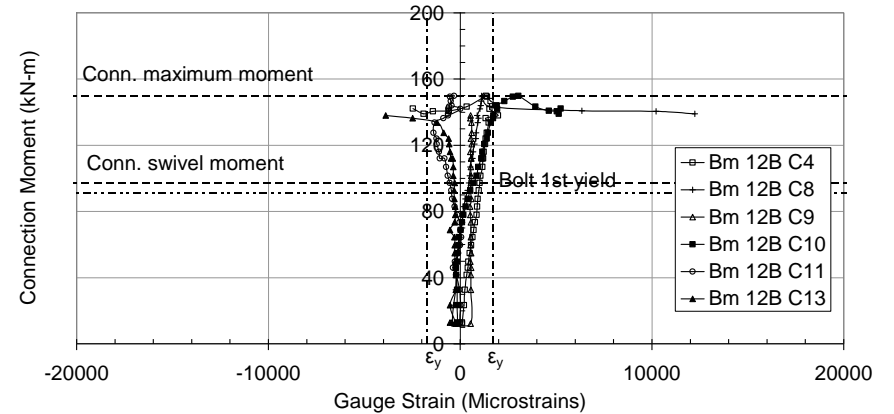
(a) Beam 12A Beam Flange Strains



(b) Beam 12B Beam Flange Strains

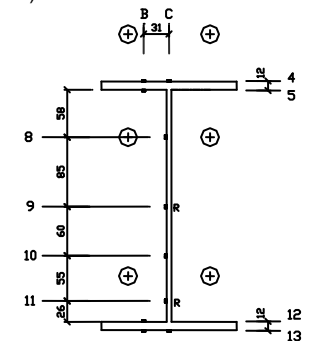


(c) Beam 12A Beam Web Strains



(d) Beam 12B Beam Web Strains

Figure 4.43 – Strains in the Beam Webs and Flanges from Connection Test 2



Figures 4.43c and 4.43d show the web strains in test 2. Strains C4 and C13 are again similar to B4 and B13 but with higher magnitude for a given connection moment.

In the beam webs, at low connection moments (up to 76 kN-m for 12A and 73 kN-m for 12), strains C9, C10 and C11 are about the same magnitude and are increasing linearly in the tension direction with a steep slope. In beam 12B the strains are actually compressive, but this seems to be due to an initial compressive residual stress at the beginning of the test.

On the beam web, all four measured strains start out as tensile. Initially, strains C9, C10 and C11 are more or less equal in magnitude while strain C8 is larger than the others. In Figure 4.42c, C9 and C10 are identical right through the test and cannot be distinguished from one another. However, at a point in the test, strain C8 begins to increase faster in tension and C11 begins to increase faster in the opposite direction, becoming compressive. For beam 12A this change in slope occurs at about 91 kN-m for both strain measurements. For beam 12B the slope change in C8 occurs at about 119 kN-m and the slope change in C11 at about 89 kN-m. C9 and C10 remain linear to the end of the test for both beams.

In test 1, of the four web strains, only C11 changes slope and becomes compressive. In test 12A, both C10 and C11 exhibit this pattern. However, C10 changes slope later in the test than C11. The slope change in C11 is at about 80 kN-m and the slope change in C10 is at about 110 kN-m. In beam 12B, C11 exhibits a slope change at about 73 kN-m. There is however no discernible slope change in C10. In beam 12B, even after the slope change in C11, the rate of strain increase is markedly less than for C11 in beam 12A.

Test 3

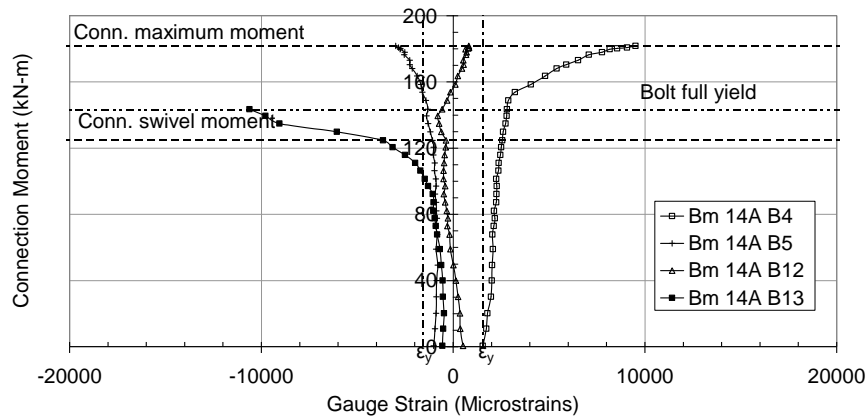
The beam web and flange strains from connection test 3 are given in Figure 4.44. The flange strains measured by gauges B4 and B5 on the tension flange for beams

14A and 14B are similar to tests 1 and 2. The strains are linear and are small until fairly high connection moments. Strain B5 in particular is virtually constant until a connection moment of 143 kN-m and 138 kN-m for 12A and 12B respectively, after which it undergoes a slope change and increases in compression. The corresponding slope changes in B4 are initiated at about 149 kN-m for beam 12A and 116 kN-m for 12B. The compression flange strains B12 and B13 are virtually parallel in the initial part of the test. Gauge B12 is initially tensile while B13 is compressive, but both gauges show a slight slope towards the compression direction. For beam 14A, B12 becomes compressive within that initial linear portion. The same ‘change in direction kink’ that was observed for gauge 12B in beams 10B and 12A, is observable here again for 14B and to a lesser extent for 14A. The change in direction for 14A is from about 125 kN-m to 139 kN-m, and in 14B from about 125 kN-m to about 154 kN-m

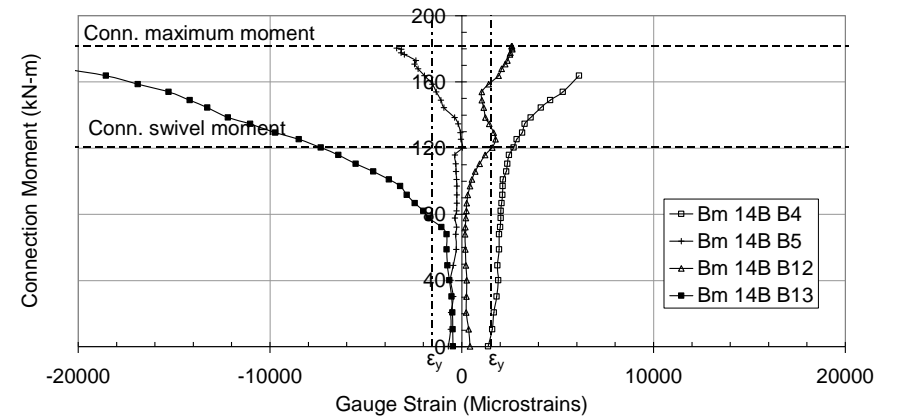
The beam web strains are shown in Figures 4.44c and 4.44d. Gauge C8 is initially linear and tensile with a large slope. In beam 14B, at about 154 kN-m, the strains measured by C8 begin to increase rapidly in tension. This change in slope is not shown on C8 of beam 14A as that gauge failed prematurely before the end of the test.

The strains on gauges C9, C10 and C11 are initially linear with very steep slopes in the early part of the test. At about 135 kN-m in beam 14A, C9 strains show a gentle slope change, with the strains increasing in compression.

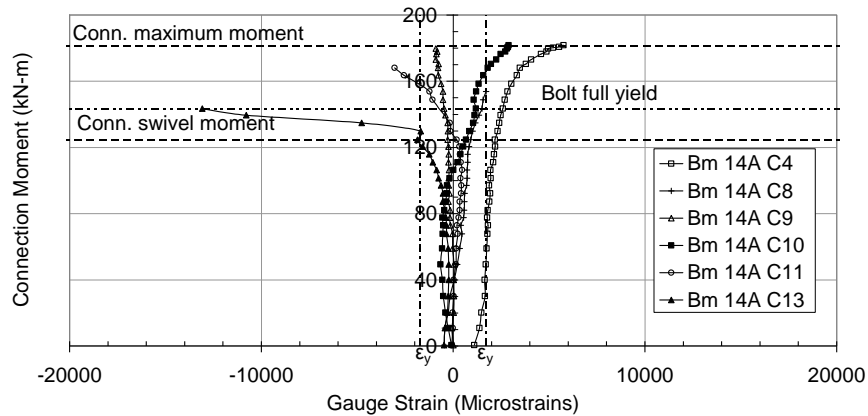
C10 strains also show a slight slope change at about 97 kN-m but increasing in tension, while C11 strains begin to increase in compression at about 120 kN-m. The corresponding moments for beam 14B are 106, 92 and 92 kN-m, for C9, C10 and C11 respectively. In both 14A and 14B, the strain C10 shows a ‘change in direction kink’ at about 143 kN-m and 138 kN-m respectively. At that point the tensile strain begins to decrease with increasing strain, but then resumes increasing again at about 149 kN-m for both beams.



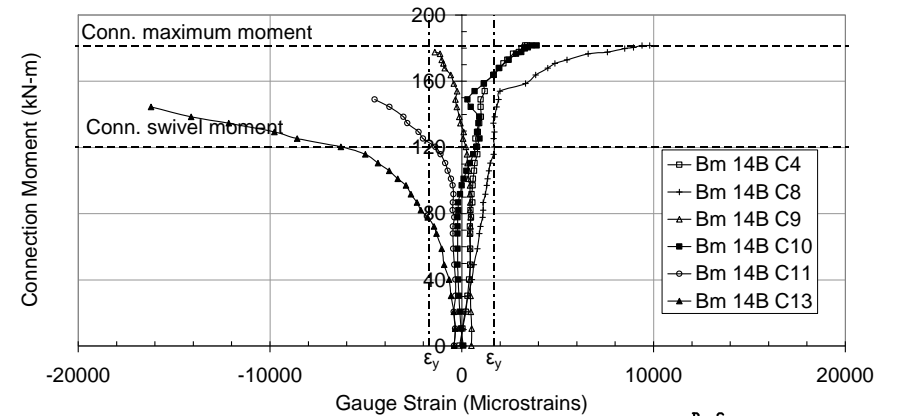
(a) Beam 14A Beam Flange Strains



(b) Beam 14B Beam Flange Strains

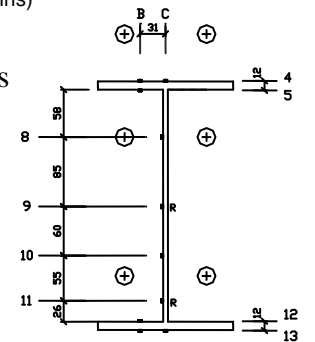


(c) Beam 14A Beam Web Strains



(d) Beam 14B Beam Web Strains

Figure 4.44 – Strains in the Beam Webs and Flanges from Connection Test 3



4.5.2 Discussion of Beam Web and Flange Strain Gauge Data

The differences between the tension flange strains on B4 and B5 suggest that the tension flange is in combined bending and axial (tensile) strain from the onset of testing. In connection test 1, in the initial part of the test, the relative magnitude of strains is such that B4 tensile strains are higher than the B5 compressive strains – from 2.5 to 4 times higher. Thus, there are bending effects superimposed on the dominant axial strains. When the slope of B4 changes and the strains begin to increase faster, this is due to yielding of the flange outermost fibres on the external surface in combined bending and tension.

By comparison, in test 1, bending effects cannot be distinguished in the compression flange strains B12 and B13. Rather, the strains are strongly compressive from the onset of the test. Yielding of the compression flange at approximately 80 kN-m seems to be linked to the connection swivel moment.

The ‘change in direction kink’ that is a feature of strain measurement B12 in all three tests is an interesting observation. We notice that the same change in direction does not occur on other gauges, so that this is unique to the gauge B12 position. We also notice that except in the case of test 3, this change in direction appears only on the beam that failed in that test i.e. beam 10B in test 1 and 12A in test 2. Even in test 3 where it appears on both beams, it is more pronounced on 14B, the beam that failed. We conclude therefore that this ‘change in direction kink’ is the strain gauge picking up the local buckling of the beam flange. It was mentioned already in Section 4.1.4 that physical observation showed that the beam that failed in each test appeared to be the one with the larger local buckle in the compression flange. The ‘change in direction kink’ of strain gauge B12 confirms this visual assessment. There is a regular pattern in the occurrence of the kink – it was at approximately 113 kN-m for beam 10B, 119 kN-m for 12A, and 125 kN-m for 14B. This may not be the moment at which local buckling commences. It is rather the moment at which the local buckle extends to a gauge

position. There was local buckling observed on the beams that did not fail – 10A, 12B and 14A – even if it was less extensive.

In all three tests, we notice that the web strain C8 is relatively large and tensile. This gauge is opposite the flush tension bolts. We conclude therefore that a significant portion of the tension force transfer from the beam profile to the endplate takes place at that level rather than all the forces being transferred via the beam tension flange as is commonly assumed. The point at which the flanges begin to yield is shown by the slope changes in B4, C4, B13 and C13. In all cases, the compression flange yields first, and the compression flange strains are much higher than the tension flange strains at each load level. C8 in the web yields before C4 in the flange. Also C4 and C8 are very similar in magnitude until C8 yields, except for beams 14A and 14B. This substantiates the above supposition that tension force is being transferred via the tension part of the beam web as well. This harmonizes with the cracks observed adjacent to the beam web in the flush tension region in the 10mm and 12mm endplates, and with the observed endplate bending patterns.

In all three tests, the C11 strains generally start out as weak tensile strains, but soon change direction and become compressive, yielding in compression soon after C13. Thus, it seems clear that the ‘neutral axis’ demarcating tensile strains from compressive strains, initially lies in the compression flange, but then moves into the beam web. The latter part of the curves for C13 and C11 are generally of the same shape and approximately parallel, but with C13 deforming more than C11 (see for example Figures 4.42c, 4.43c and 4.44d). It seems then that the compressive strain is loosely linearly distributed across the beam compression flange and the portion of web up to the level of the shear bolts – even after the flange and that portion of web become inelastic. The difference in strain magnitudes actually suggests that the curve is possibly parabolic rather than linear, but it can be approximated as linear here.

In beams 10A, 10B and 12B, the C9 and C10 strains are small in magnitude and are tensile, increasing only slightly as the tests progress, except that in beam 12B the gauge C10 actually yields just before the test ends and begins to increase rapidly. Interestingly, the C10 strain increment is actually a little larger than that of C9 in each of these beams, with moment increase. It seems therefore that the tensile force transfer just above the shear bolt level (C10) may be facilitated by the clamping effect of the shear bolts. This effect is not there at the beam centre (C9), so the C10 strains are higher. This suggestion harmonizes with the observed bulge in the endplate permanent deformation (see section 4.1), between the level of the flush tension bolts and the shear bolts.

The web strain for beam 12A differs from the others, as C10 in 12A is *compressive*, and yields in compression. In beam 12A, C10 follows the curve of C11 and ends up forming a pattern of compressive strains with C11 and C13. Thus, the neutral axis in beam 12A appears to move higher than the level of the C10 gauge (slightly above the shear bolts), and the compressive strain distribution is still linear from the neutral axis to the outermost fibre of the beam compression flange. Clearly, this is not the case in beam 12B discussed in the last paragraph, where the C10 curve remained tensile and yielded in tension. In 12B, the neutral axis remains under the level of the C10 gauge.

It is now possible to infer the strain distribution across the beam profile in tests 1 and 2, and this is sketched in Figure 4.45b. The tensile strains are approximately uniform across the beam tension flange and flush tension region, with a sharp transition or ‘jump’ from the flange into the web. The compressive strains are approximately linear from the compression flange to a point in the beam web – the ‘neutral axis’. The location of this neutral axis is dictated by the endplate thickness for a given endplate geometry. Figure 4.45b shows this assumed strain distribution in an idealised fashion.

Gauge C10 starts out as slightly compressive in beam 14A, while C10 and C11 are both slightly compressive in beam 14B. For both beams, the C9 strains

increase faster in the compressive direction later in the test, but not as fast as C11. However, the C10 strains become tensile. It appears contradictory to have tensile strains at C10 just above the shear bolts but compressive strains at C9 and C11 on either side. The other contradictory observation about C10 in test 3 is that it has a change in direction kink for both beams 14A and 14B. Thus, the C10 gauges are likely quite close to the neutral axis position, so that minor differences between the specimens are sufficient to modify the neutral axis level sufficiently that it is above the gauge position in one case, though below the gauge in other cases.

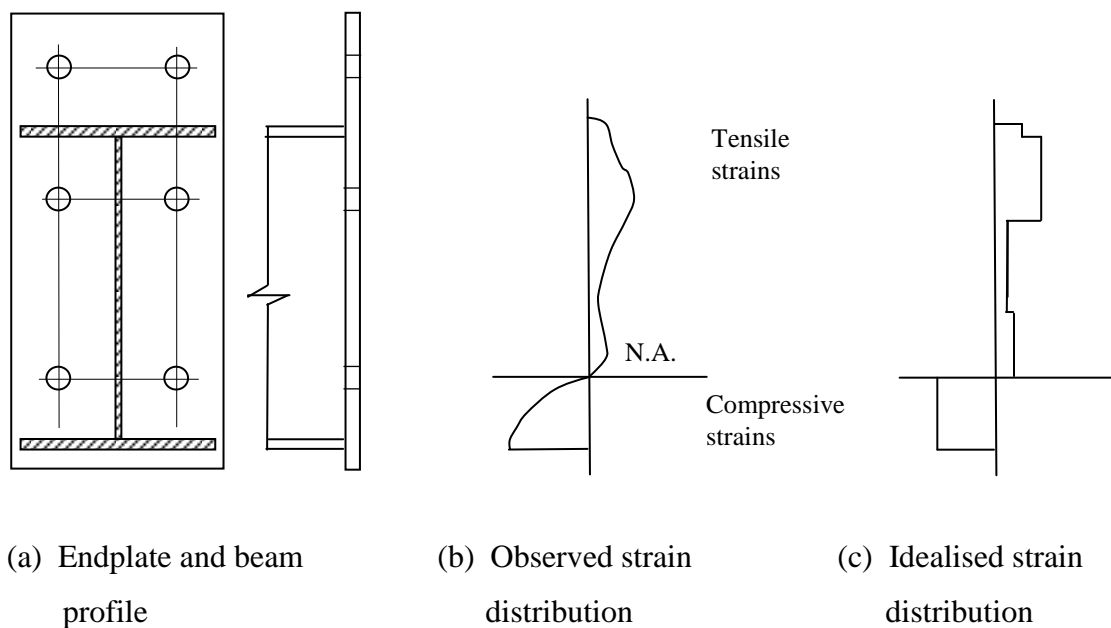


Figure 4.45 – Strain Distribution across Beam Profile in Tests 1 and 2

4.6 SUMMARY OF DEDUCTIONS FROM THE CONNECTION TESTS

Based on the experimental observations and discussions above, the following deductions may be made concerning the behaviour of practical, well-proportioned, thin, partial-strength extended endplates:

1. The deformation of the flush region is initially in a circular pattern, with radial strains around the bolt hole as centre. The circle enlarges until it is constrained

by the beam web and flange, and the pattern then becomes similar to the yield line pattern adopted in this thesis.

2. In the extended region, the region between the beam flange and the bolt line is in double curvature with a point of inflexion between the flange and bolt line. This inflexion point moves towards the bolt line as the applied moment increases.
3. In thinner endplates the flush region deformation pattern is stiffer than the extended region cantilever deformation, and thus the flush bolt forces are initially much higher. Deformation and yielding of the endplate, as well as yielding of the bolts in bending, later leads to a redistribution of forces away from the flush towards the extended region.
4. The weld line extended region of the endplate starts yielding ahead of the flush region, which is probably because of the larger curvatures required for compatibility on the weld line.
5. By the time the stiffer flush region is yielding extensively, the extended region with larger curvatures is already strain hardening. Thus, the swivel point rotation in the moment-rotation curve of the connection is dictated by yielding of the stiffer flush region rather than by the extended region. Nevertheless, the swivel 'knee' is only complete when the extended region bolt line has also yielded.
6. At load levels beyond the swivel point, portions of the flush region also begin to strain harden. When the deformations increase further, both regions also exhibit membrane action, associated with large displacements of the endplate.
7. Cracks in the thin endplate usually develop in the stiffer flush region first, around the bolt-holes and adjacent to the beam web. In deciding on a maximum strain criterion to determine the maximum permissible rotation therefore, it is reasonable to base this on behaviour in the flush region. However, the connection is still able to resist load after these initial cracks, and endplate fracture only occurs when the extended region weld line also cracks and then fractures. Endplate fracture would depend on the endplate strains approaching the ultimate strains in the tensile test, but premature

fracture might occur from the loss of ductility in the heat-affected zone associated with the beam flange weld.

8. At high connection load levels approaching the beam plastic capacity, the beam compression flange undergoes inelastic local buckling accompanied with yielding. This yielding initiates in the beam flange and then spreads to the adjacent area of web.
9. Tension force transfers from the extended bolts via the endplate to the beam section around the level of the beam tension flange, and tension force transfers from the flush bolts via the endplate to the beam section in the upper (tension region) part of the beam web. The tensile strains are highest in the part of the web opposite the flush region tension bolts.
10. Compression force transfer from the beam profile to the endplate takes place across the beam compression flange and the region of web immediately adjacent to the compression flange, with the web contribution commencing at higher load levels.
11. The fulcrum or centre of rotation about which the beam profile rotates is initially at the external edge of the beam compression flange, but at higher connection moments, the centre of rotation shifts into the web and is eventually at about the level of the shear bolts.
12. In the endplate the extent of the compression area is dictated by the presence of shear bolt pre-tension forces that extend the compression area to the level of the shear bolts. The shear bolt pre-tension provides a clamping force that clamps the endplate to the column face between the shear bolts and the beam compression flange. This clamping force is not uniform across the endplate width however, as the portion of the web adjacent to the beam compression flange will exert an outward force to reduce the clamping effect. Thus, bearing of the endplate in compression against the column flange also extends to about the shear bolt level.
13. The shear bolt level may therefore be considered a plastic 'neutral axis' for the change from tension to compression in the endplate, as well as a centre of rotation for the beam profile, at high load levels.

14. Pre-tensioning of the bolts has a beneficial effect on the initial stiffness of the connection as one would expect. Surprisingly however, it also seems to increase the connection rotation capacity. This effect is difficult to take into account however, as current practice leads to variable pre-tension forces.
15. The flush and extended bolts bend significantly during at medium to high levels, and yield in bending prior to yielding axially. Bending of the extended bolts is primarily longitudinal while bending of the flush bolts is primarily transverse. In the 14mm tests however, bending of the flush bolts was also longitudinal.
16. The swivel point in the connection moment-rotation curve appears linked to the yielding of the flush bolts in bending and the development of a yield pattern in the flush region.

5. FE ANALYSES OF CONNECTION TEST ENDPLATES

In this chapter, a finite element analysis is presented for each of the three endplate geometries tested in the experimental programme of Chapter Four. The intention is to isolate and study the fundamental behaviour of the endplate itself, while eliminating material and experimental imperfections such as welding and lack-of-fit residual stresses as well as test specimen dissymmetry.

5.1 FINITE ELEMENT MODELLING APPROACH

The endplates have been modelled with 3-dimensional brick elements using the ANSYS ED software version 9.0. The chosen element was the SOLID 186 – a 3-dimensional 20-node structural solid element, supplemented with the SOLID 187 element, a 10-node tetrahedral. Contact was modelled with CONTA 174 and TARGE 170 contact element pairs. In order to simplify the analysis, only the endplate itself and the flush and extended region bolts were modelled. The effects of bolt pre-tension, as well as column flange deformation and beam bending, were not modelled.

5.1.1. Modelling the Endplate Geometry

Since the endplate geometry is symmetrical about the centreline through the beam web, only half of the width was modelled. Thus, each endplate FEA model comprised half of the endplate on one side of the line of symmetry. This is illustrated in Figure 5.1. The effect of symmetry was modelled by applying a ‘frictionless’ boundary condition to the surface on the line of symmetry, so that perpendicular displacements and rotations on that face are constrained to zero, but

tangential displacements and rotations are permitted. Figure 5.1 shows the coordinate system used.

The column flange was idealised in the FEA models as an unyielding surface. In order to model the endplate interaction with the column flange therefore, a ‘compression-only’ support boundary condition was applied to the ‘far-side’ surface of the endplate, which would be in contact with the column flange. As the name implies, a compression-only support prevents displacement of the surface in the direction implying compression (negative Z direction in this case), but does not resist deformation in the opposite (positive Z) direction. Thus, the compression-only support allows separation of the supported surface from the ‘support’ when tensile stresses develop.

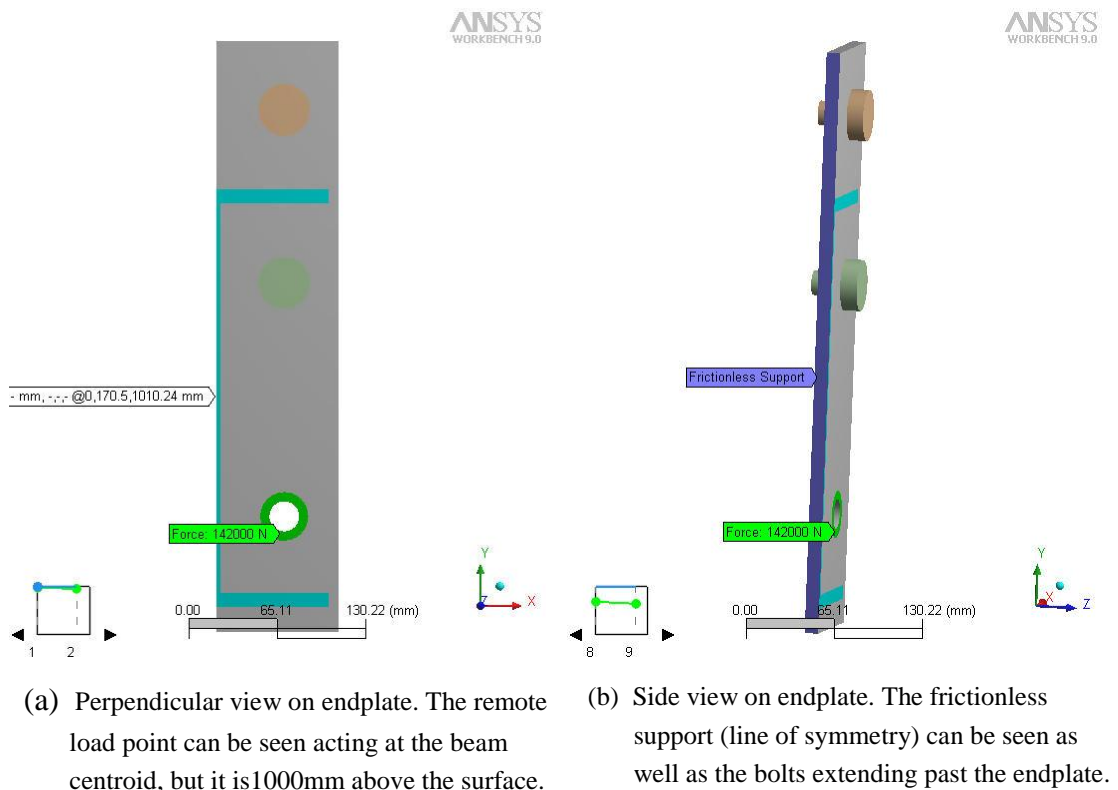


Figure 5.1 – FEA Model of Endplate Geometry

Three surfaces were demarcated to mark the positions where the endplate interacts with bolt-heads. These were each circular annuli, centred around the bolt-holes. The diameter of these ‘contact’ surfaces was taken as the average of the M20

Grade 8.8 HSFG bolt-head width, taken across corners and across flats. The flush and extended region bolts were modelled, with the bolt head exerting pressure on the contact surfaces. The bolt length was taken as grip length, and the width as the thread area diameter. The far end of both bolts away from the endplate had a ‘fixed support’ condition applied to it i.e. zero displacements in the x, y and z directions, as well as zero rotations about the three axes. The shear bolt in the compression area was modelled with a radially-fixed (but axially and tangentially free) support on the inside surface of the bolt hole, and a 142 kN force (the nominal pre-tension for an M20 Grade 8.8S bolt) clamping the endplate to the ‘column flange’ compression-only support.

The contact between the flush and extended bolt shanks and the endplate holes inner surfaces was not modelled. Thus, in the FEA models, the shear component of the applied load was resisted only by the radial fixity at the shear bolt-hole.

The load was applied to the endplate near face by demarcating a surface to match the beam web and flanges (again considering symmetry about the frictionless surface). The load was then applied to a remote point with coordinates matching the actual point of load application i.e. at 1000mm from the endplate surface. The load was then transferred to the demarcated surface by linking the surface to the remote point with rigid links. In this way, the correct ratio of shear force to applied moment was maintained during the load application. Meshing of the FEA models was carried out using the program’s built-in automated meshers.

5.1.2. The FEA Material Models

In the FEA models, the endplate material was modelled using tri-linear stress-strain relationships derived from the experimental endplate samples for each endplate thickness. The flush and extended region bolts were similarly modelled using the bi-linear stress-strain relationships determined experimentally for the bolts under a given grip length (endplate thickness and 14mm column flange).

However, the FEA models require the use of true stress-strain relations rather than the nominal stress and strain values measured experimentally. Thus, the experimental values were adjusted using the following equations:

$$\text{True stress} = f_y (1 + \epsilon_y) \quad \text{Eqn 5.1}$$

$$\text{Log strain} = \ln (1 + \epsilon_y)$$

where f_y is here used as the yield or ultimate stress, and

ϵ_y is used to refer to the yield or ultimate strain.

The bolt tensile test readings were taken on the shank, however, the thread diameter was used to model bolts in the FEA models. Thus, the bolt stress-strain values were further adjusted to account for the difference between the thread diameter and the shank diameter, so as to obtain the same bolt forces at the swivel and bolt fracture points in the bolt bi-linear stress-strain curve. A nominal thread diameter of 16.9mm was used in all the FEA models as this was the average measured thread diameter for the bolts in the tests.

Table 5.1 – Material Properties for FEA Models of Endplate Behaviour

	Young's Modulus GPa	True Yield Stress MPa	True Yield Strain 10^{-3}	True Hard'g Strain 10^{-3}	True Ultimate Stress MPa	True Ultimate Strain 10^{-3}
10mm plate (Test 1)	202.20	331.03	1.637	13.360	537.71	61.360
12mm plate (Test 2)	219.10	305.79	1.396	13.410	537.76	52.608
14mm plate (Test 3)	213.00	294.80	1.384	13.508	503.95	52.234
Bolt for 10mm plate (24mm grip length)	228.53	962.91	4.214	–	1038.95	19.737
Bolt for 12mm plate (26mm grip length)	223.21	969.05	4.341	–	1088.45	21.177
Bolt for 14mm plate (28mm grip length)	215.13	949.85	4.415	–	1043.39	22.363

The true stress-strain values are tabulated in Table 5.1, with the adjusted bolt stresses. The tri-linear material models are based on a secant approximation in the strain hardening region i.e. the ultimate point coincides with the experimentally observed point in terms of ultimate stress and ultimate strain, but the implied value for the Strain hardening Modulus with thus differ from the experimental value, since the strain hardening region is modelled as a linear region.

5.2 RESULTS FROM THE FEA MODELS

5.2.1. The FEA Model Moment-Rotation Curves

The moment-rotation curves derived from the 10mm, 12mm and 14mm endplate FEA models are shown in Figures 5.2 to 5.4, superimposed on the respective test experimental moment-rotation curves. The moment-rotation curves were plotted by applying the remote displacement in incremental steps during the simulation, while calculating the endplate rotation from the geometry of the remote end relative to the endplate. The applied moment was calculated by the software at each load increment.

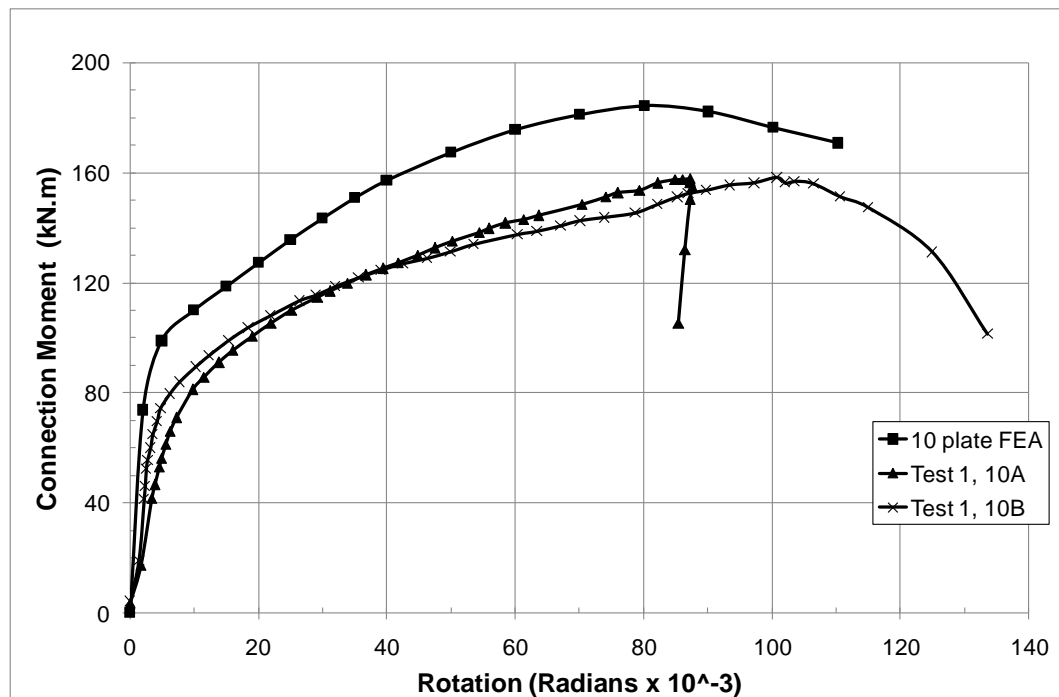


Figure 5.2 – Moment-Rotation Curve for 10mm Endplate FEA Model

It can be seen that there is reasonably good agreement between the 10mm FEA moment-rotation curve and the Test 1 experimental curves in Figure 5.2.

However, the FEA connection is clearly stiffer, getting to the swivel point at 5.1 milli-rads compared with 9.8 and 6.2 milli-rads for the experimental curves 10A and 10B. Similarly, the FEA maximum moment of 184 kN-m occurs at 80 milli-rads, compared to the Test 1 maximum of 157.9 kN-m at 101 milli-rads.

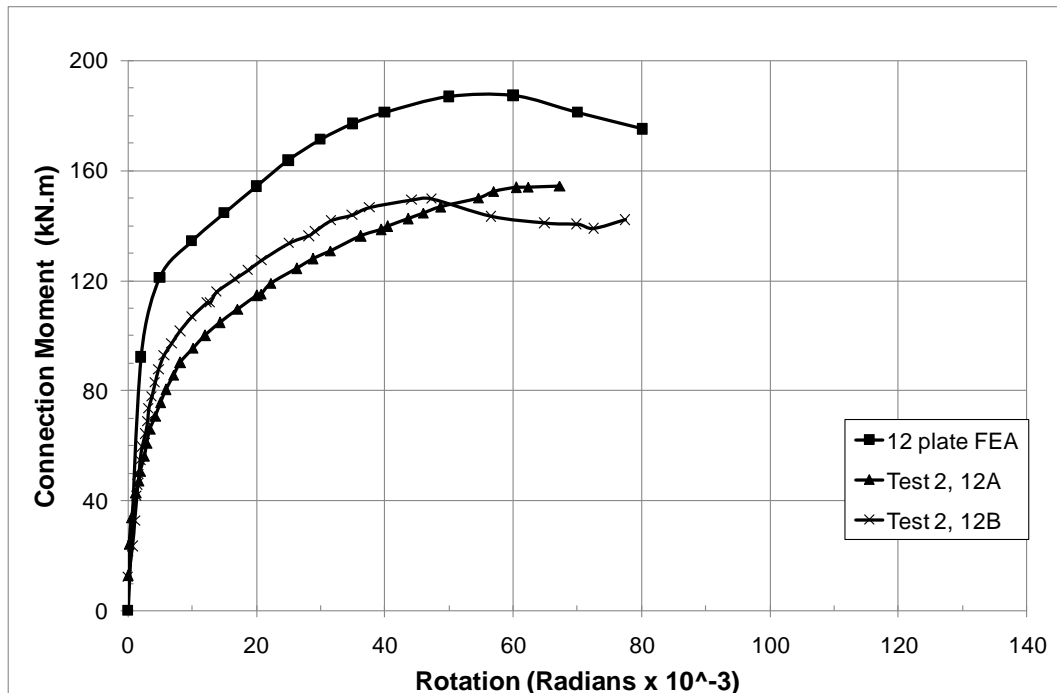


Figure 5.3 – Moment-Rotation Curve for 12mm Endplate FEA Model

In the same way, in Figure 5.3 the moment-rotation curve for the 12mm FEA model shows a good agreement in its shape with the experimental curves, but is stiffer and fails at a higher connection moment. The FEA model swivel takes place at 10 milli-rads compared to 8.2 milli-rads and 6.8 milli-rads for the 12A and 12B test specimens. The maximum moment for the FEA model is 187 kN-m at 60 milli-rads, compared with 154 kN-m at 67 milli-rads in the experiments.

The moment-rotation curve for the 14mm FEA model is given in Figure 5.4. This curve does not match the experimental curves as well as the other two. Swivel takes place at 5 milli-rads compared with the experimental values of 10.6 and 11.9 milli-rads, while the maximum moment is 188.3 kN-m at 35 milli-rads compared to 181.6 kN-m at 80 milli-rads in Test 3.

The greater stiffness of the FEA models as compared to the experiments is largely explained by the omission of the beam from the FEA models. The beam contributes to the rotation in two ways – first by bending of the beam end between

the endplate face, and the joint where the experimental rotation measurements were made. Secondly, the beam contributes to the connection rotation through inelastic deformation of the beam region adjacent to the endplate. This includes inelastic buckling of the compression flange as observed in the experiments. The contribution of beam bending to the total connection rotation increases with endplate thickness, which is why the discrepancy between the FEA model moment-rotations and the experimental moment-rotation curves, also increases with endplate thickness.

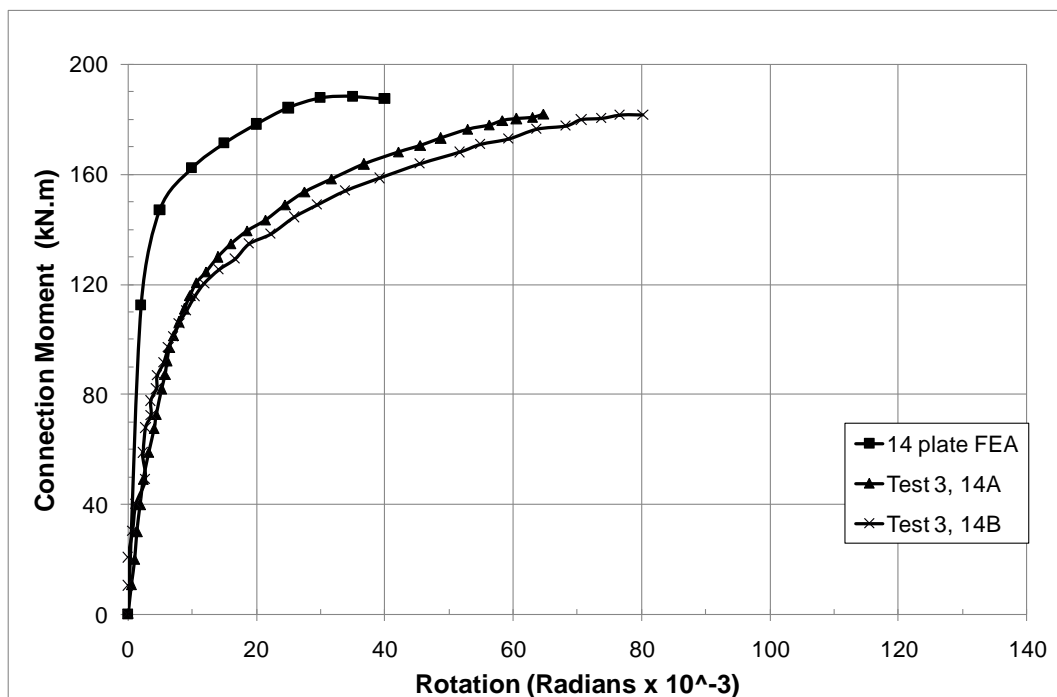
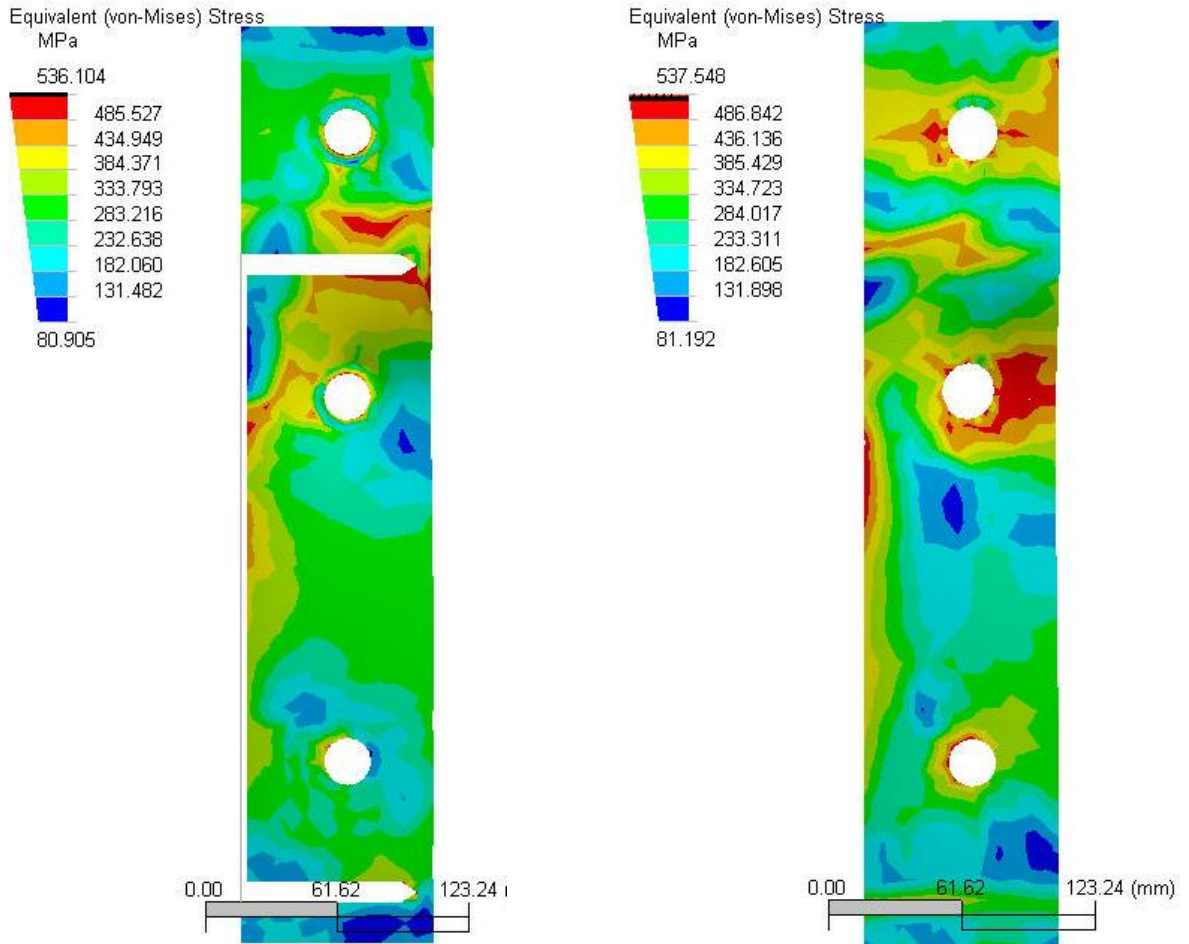


Figure 5.4 – Moment-Rotation Curve for 14mm Endplate FEA Model

5.2.2. Stresses and Deformations in the 10mm Endplate FEA Model

Figure 5.5 shows the stress pattern in the 10mm endplate FEA model at maximum moment. This is the equivalent Von Mises stress plotted in contour bands. Figure 5.5 (a) shows the stresses on the top surface next to the beam, while 5.5 (b) shows the stresses on the bottom surface next to the column flange. The true yield stress in the model (as distinct from the nominal yield stress) is 331 MPa, so that any areas in the figure with stresses above 331 MPa have yielded. The true ultimate stress is 537.7 MPa. It can be seen that the maximum stress has just been attained

on the bottom surface, and the contours in the maximum stress band on both surfaces reveal locations susceptible to stress cracks. These locations agree exactly with the experimental observations.



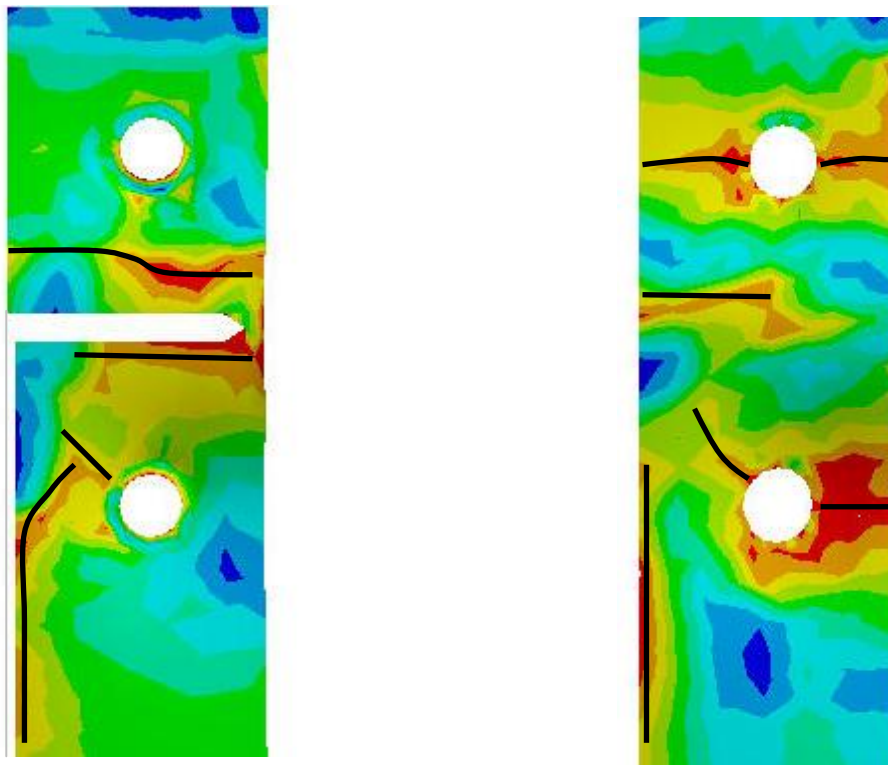
(a) Stresses on top surface (looking from the beam side towards the column flange)

(b) Stresses on bottom surface (looking from the beam side towards the column flange)

Figure 5.5 – FEA Model Stresses in 10mm Endplate at Maximum Moment

In the extended region there are two horizontal bands of yielding – one across a horizontal line through the bolt hole on the bottom surface, and the other on the top surface, parallel and adjacent to the beam tension flange position. These indicate yielding on the bolt line and the weld line respectively – the classical double-curvature of the extended region.

In the flush region of the endplate, the positive yield-lines on the top surface are two essentially straight lines. The first is adjacent and parallel to the beam tension flange position while the second is adjacent and parallel to the beam web position. Three negative yield lines can be discerned on the bottom side. The first is horizontal through the bolt line, but only on the plate edge side. The second is along the beam web, and the third is radial from the bolt hole upwards. Figure 5.6 is a close-up view of the 10mm endplate FEA stresses, with the yield-lines superimposed.



(a) Stresses on top surface with inferred yield-lines superimposed

(b) Stresses on bottom surface with inferred yield-lines superimposed

Figure 5.6 – Yield-lines inferred from FEA Stresses in 10mm Endplate

It appears then that there are essentially two yield-lines in the extended region – both horizontal, with one at the bolt line and the other at the weld line. And there are four distinct yield-lines in the flush region – a vertical one by the beam web, a horizontal one by the beam flange, a second horizontal one through the bolt line

but only on the outer edge of the plate, and a fourth one which is diagonal from the bolt hole to the corner between the beam web and beam flange.

At those yield-lines where the yielding is on both surfaces and the plate curvatures are large, the plate is predominantly subject to bending stresses. However, at the bolt line in the extended region and the partial bolt line in the flush region, as well as the horizontal weld line in the flush region below the beam flange, the yielding is extensive on one surface but insignificant on the other. It would seem therefore that membrane stresses are superimposed on the bending stresses in those regions.

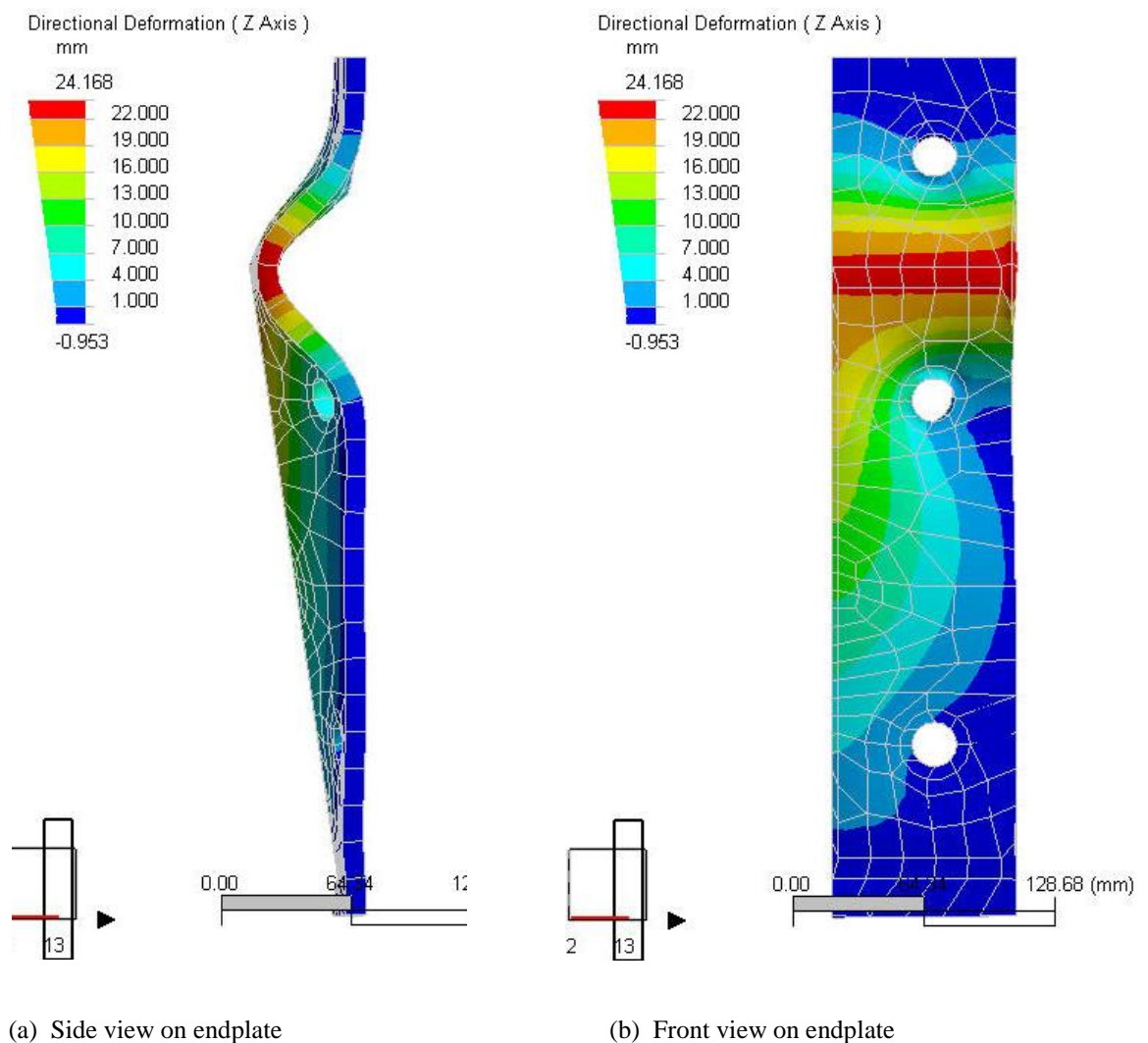


Figure 5.7 – FEA Model Deformations in 10mm Endplate at Max Moment

Figure 5.7 shows the deformations of the 10mm endplate FEA model at maximum connection moment. The contours are directional i.e. are based on deformation components in the Z direction along the beam axis.

A side elevation is shown in Figure 5.7 (a) where it can be seen that the beam profile rotates as a single piece. This is linked to the finite element formulation as the beam end is modelled with non-deformable rigid links. In Figure 5.5 (b), even though it is partly obscured by the ruler, it is possible to see that there is a region of high stress on the bottom surface of the endplate, opposite where the compression flange bears against the top endplate surface.

This does not imply however that the compression of the endplate against the column flange is confined to the region opposite the beam compression flange. A second region of high compressive stresses is visible in Figure 5.5 (b), around the shear bolt. This is due to the clamping effect of the pre-tension in the shear bolt. By virtue of the plate geometry, the shear bolt could resist high shear forces, but would only resist low to moderate axial forces when the connection is subjected to bending moment. Thus, the clamping force is not overcome under load.

In Figure 5.7 (b) it can be seen that the part of the endplate below the level of the shear bolt does not deform away from the column flange, and remains more or less in contact with the column flange. This also applies to a narrow strip along the free edge of the endplate. Thus, in terms of the prying of the endplate flush region against the column flange, a 'neutral axis' can be discerned, approximately at the level of the shear bolts. This refers to where the endplate, beam and bolt interaction with the column flange changes from a force on the endplate towards the column flange surface, to a net force on the endplate to pull away from the column flange surface. In Figure 5.5 it can be seen that above the shear bolt level, the beam web acts on the endplate to exert a force away from the column flange.

5.2.3. Stresses and Deformations in the 12mm Endplate FEA Model

The stress pattern in the 12mm endplate FEA model is very similar to that in the 10mm endplate FEA model at the maximum moment. The true yield stress used in the tri-linear material model for the simulation is 306 MPa, and the true ultimate stress is 537.8 MPa.

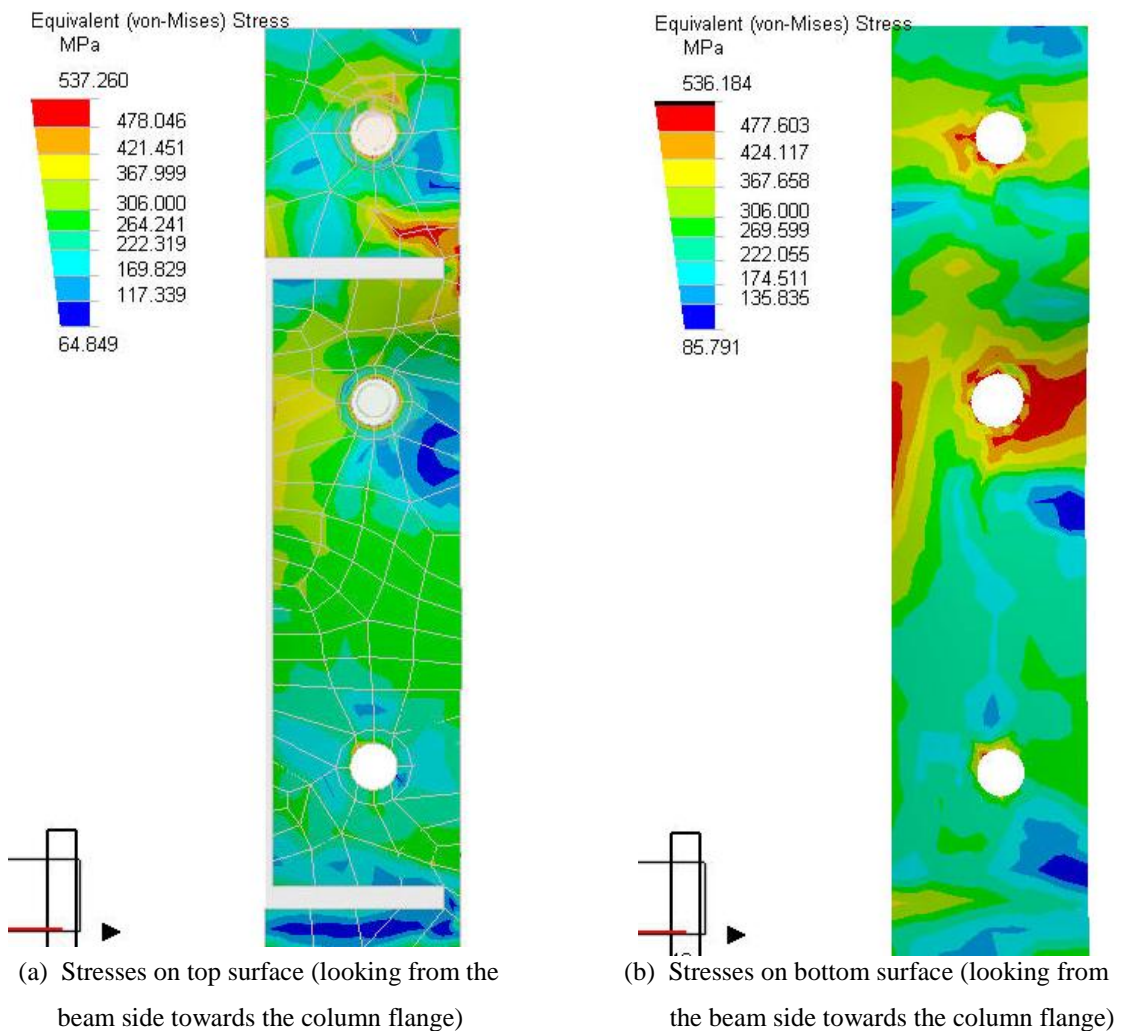


Figure 5.8 – FEA Model Stresses in 12mm Endplate at Maximum Moment

In Figure 5.8, the same double curvature patterns on the bolt line and weld line can be seen in the extended region. Similarly, in the flush region, the same yield-line bands are discernible, though not as pronounced on the top surface.

Figure 5.9 shows the FEA stress pattern in the 12mm endplate at the swivel moment. Most of the yield-lines that appear at the maximum moment can be seen to be emerging already at swivel, though the stresses are still below yield value.

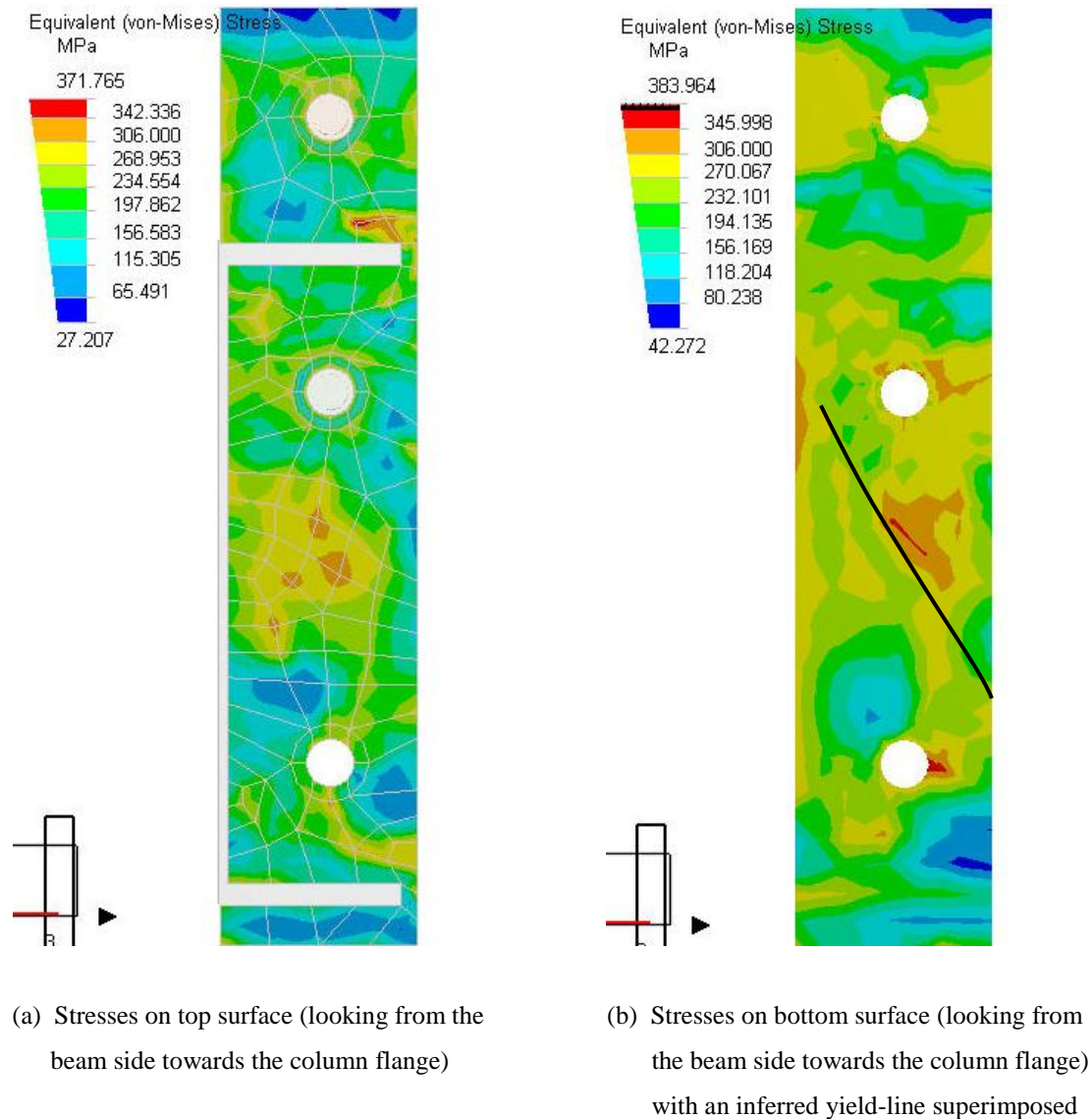


Figure 5.9 – FEA Model Stresses in 12mm Endplate at Swivel Moment

However, a difference between the yield and swivel patterns can be seen in the flush region, halfway between the flush and shear bolt positions. There is an additional inclined yield-line apparent in this region, running from the web side at flush bolt level towards the plate edge at shear bolt level. This is marked up on the bottom surface in Figure 5.9. It can also be noticed that the incipient yielding in

the flush region at the beam web – beam flange junction is more widespread than at the maximum moment. These differences in the swivel from the maximum stress pattern are in harmony with the experimental observations where the yield pattern at swivel was seen to be different from that at maximum moment.

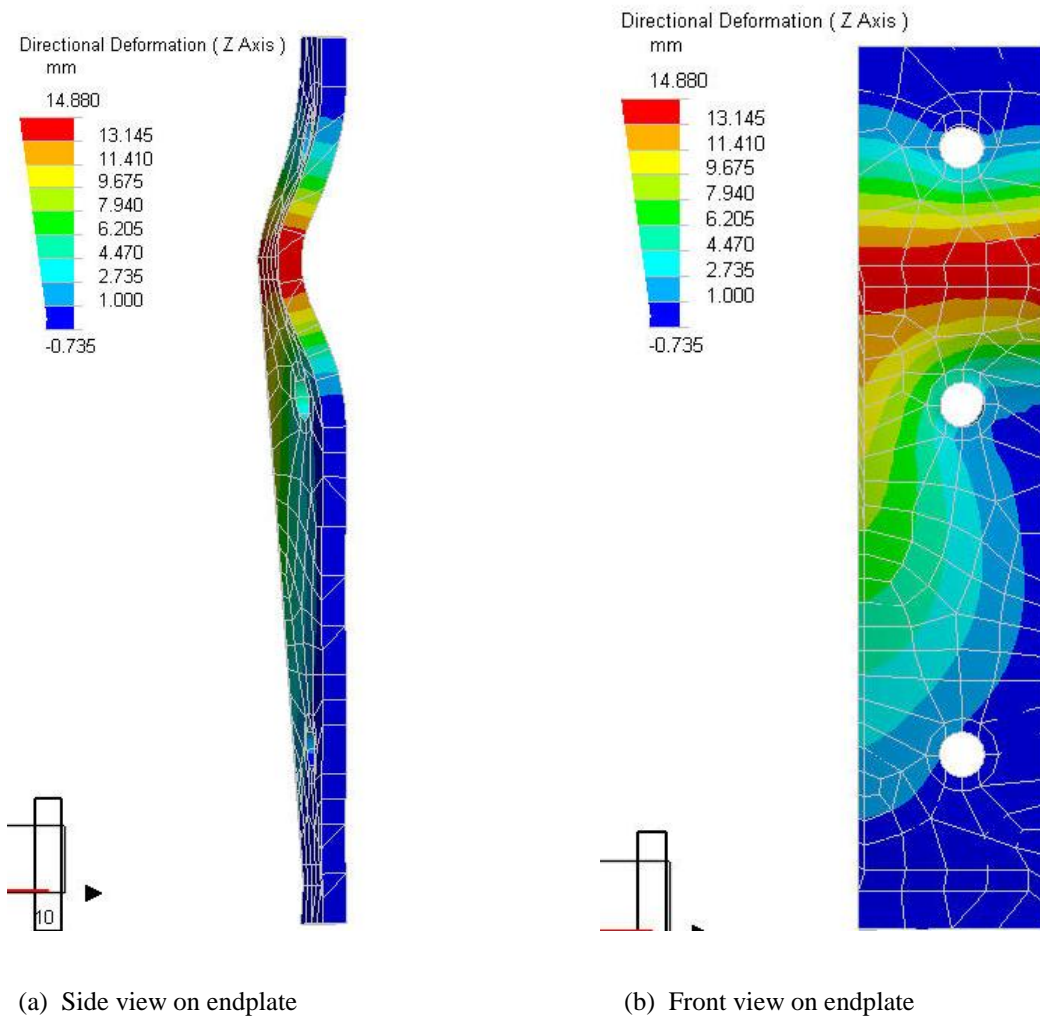


Figure 5.10 – FEA Model Deformations in 12mm Endplate at Max Moment

The deformation of the 12mm endplate FEA model at maximum moment is shown in Figure 5.10. It can be seen that the deformation pattern and contours are identical to those for the 10mm endplate FEA model in Figure 5.7. However, the absolute values differ. Thus, the maximum deformation in the z axis direction for the 10mm model was 24.2mm, while the same value for the 12mm endplate model is 14.9mm. This is again in harmony with the experimental observations.

5.2.4. Stresses and Deformations in the 14mm Endplate FEA Model

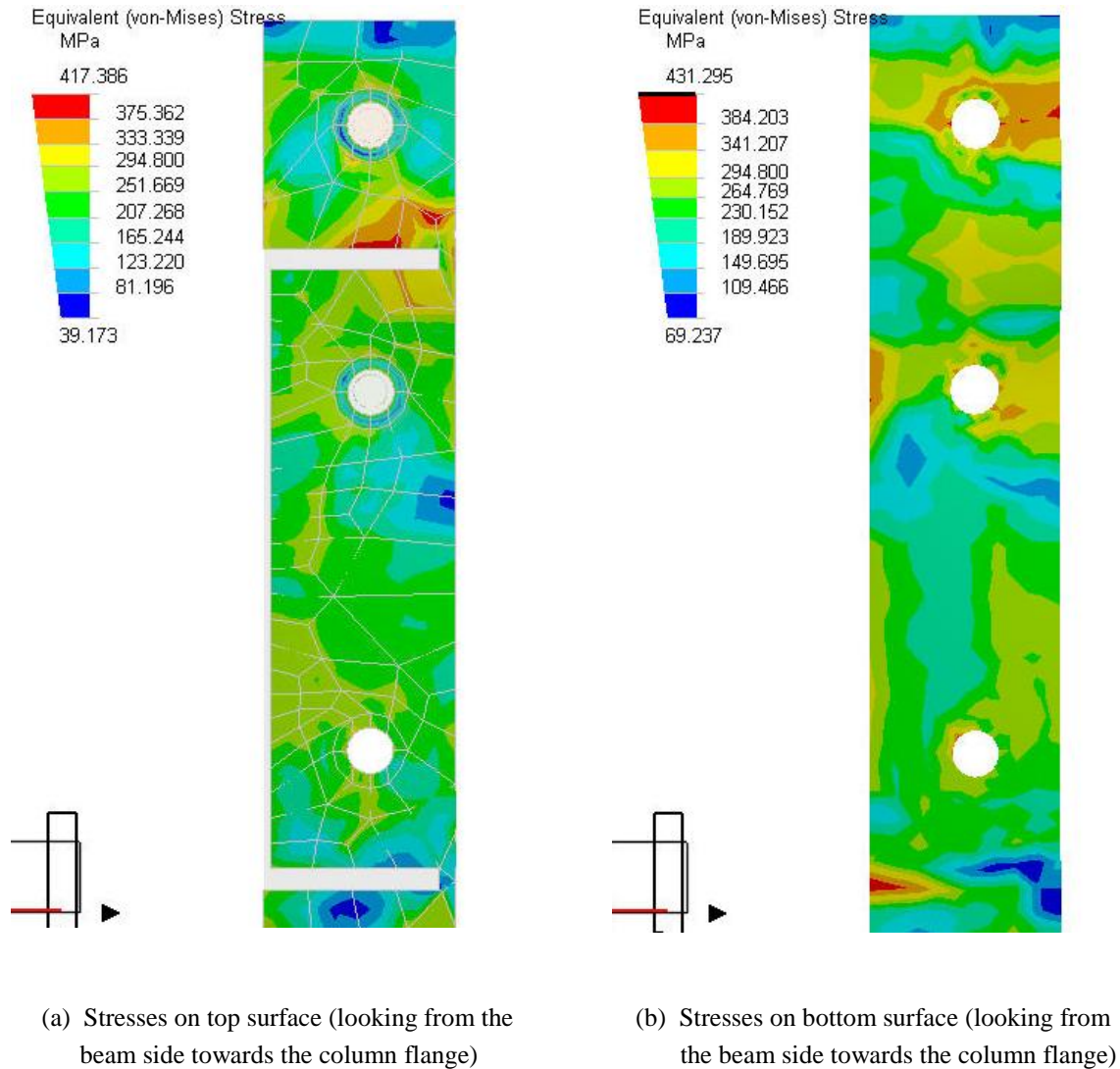


Figure 5.11 – FEA Model Stresses in 14mm Endplate at Maximum Moment

The stress patterns of the 14mm endplate FEA model are shown in Figure 5.11. In Figure 5.11 the familiar double-curvature yield-lines can be seen in the extended region. However, in the flush region, only one of the four yield-lines observed for the 10mm and 12mm models is fully developed. This is the horizontal yield-line on the bolt line from the bolt hole to the edge of the plate. There is yielding apparent parallel to and adjacent to the beam web, but only over a short length. Again, there is yielding parallel to and adjacent to the beam flange, but only for a short length also.

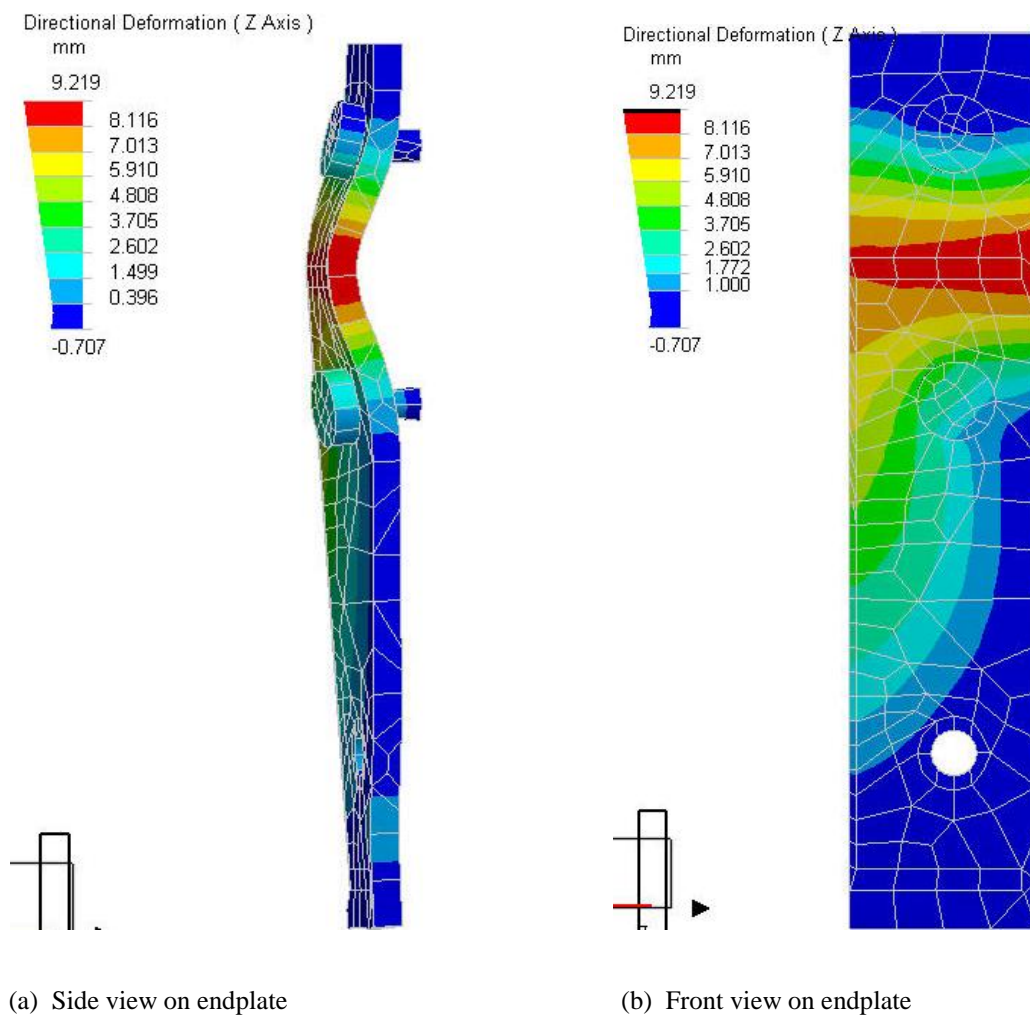


Figure 5.12 – FEA Model Deformations in 14mm Endplate at Max Moment

The maximum stress of 431 MPa in the 14mm endplate at maximum connection moment, is much less than the value of 504 MPa for the ultimate stress of the material. This is different from the 10mm and 12mm models where the maximum

connection moment corresponded to the ultimate stress, but it is in accordance with the experimental observations. In the experiments, the 10mm and 12mm endplates were susceptible to fracture, while the 14mm endplate did not fail by plate fracture but by bolt fracture. The deformation pattern for the 14mm endplate model in Figure 5.12 is similar to that for the 10mm endplate and 12mm endplate models.

5.3 DISCUSSION OF FEA MODELS

The FEA models allow us to confirm the fundamental behaviour of the endplates apart from possible influences of residual stresses from welding or lack of fit. As observed in the experiments, it can be seen that the deformation of the flush region is initially in a circular pattern, and then becomes similar to the yield line pattern suggested in this thesis. The circular pattern would be applicable at the beginning of the swivel ‘knee’ in the moment-rotation curve, just before the flush region deformation becomes significant. Our interest however, is at the top of the swivel ‘knee’ when the yield-line pattern has changed to that suggested in this thesis..

The FEA models accurately predict the locations susceptible to high stresses and cracks at ultimate connection moments. The models confirm that the endplate remains in bearing against the column flange to the level of the shear bolts, so that the endplate ‘neutral axis’ is at the shear bolt level.

The bending behaviour of the bolts is confirmed qualitatively, as the longitudinal and transverse bending of the extended and flush bolts respectively is similar to the experimental observations.

As could be seen from the experimental strains, the high stresses in the FEA models reveal the occurrence of strain hardening on the extended region weld line close to the plate edge; and more widespread strain hardening on the extended

region bolt line right across the plate. The models also show strain hardening taking place in the flush region on the yield line adjacent and parallel to the beam web, and on the flush bolt line, especially from the plate edge to the bolt hole.

The FEA models for the 10mm and 12mm endplate show in addition that membrane stresses occur in the extended region on the bolt line, and in the flush region on the partial bolt and the weld line.

A comparison is made in Table 5.2 between the experimental results and the FEA model values, for the connection moment-rotation curve. We notice that the FEA models consistently overestimate the connection ultimate moment and consistently underestimate the connection rotation. In the FEA models the beam end is modelled with non-deformable rigid links. This has the effect of increasing the initial stiffness, and increases the apparent stiffness of the flush region of the endplate, thus leading to higher ultimate moment resistance. Table 5.2 shows that the FEA overestimate is consistently about 25% at swivel, but varies from 21% to 3% at the maximum moment.

Table 5.2 – Comparison between FEA Results and Experimental Values

		Moment values (kN-m)			Rotation values (rads x 10 ⁻³)		
		Expt	FEA	FEA/Expt	Expt	FEA	FEA/Expt
10mm endplate	Swivel	80	99	1.24	8.0	5.1	0.64
	Maximum	158	184	1.16	100	80	0.80
12mm endplate	Swivel	96	121	1.26	7.5	10.0	1.33
	Maximum	155	187	1.21	67	60	0.90
14mm endplate	Swivel	123	147	1.20	11.3	5.0	0.44
	Maximum	182	188	1.03	80	35	0.44

The underestimate of connection rotation is due to the omission of the beam end contribution to rotation in the FEA models. In the tests of Bernuzzi et al (1991), the IPE 300 beam end contributed over 50% of the total rotation at the maximum point in a test on a 15mm endplate connection, while the contribution was about

20% for a 12mm endplate connection. Thus, the FEA/Experimental ratios of 0.80 and 0.44 respectively, for the maximum point rotation of the 10mm and 14mm endplates, show excellent agreement with the observations of Bernuzzi et al. The value of 0.80 implies a 20% contribution by the beam end for the 10mm endplate, while a value of 0.44 implies a 56% contribution by the beam end for the 14mm endplate.

We suggested in the previous chapter that the 12mm experimental endplate probably fractured prematurely, possibly due to loss of ductility in the heat-affected zone. This supposition is supported by the FEA/Experiment ratios at maximum point, as the 12mm experimental maximum moment and rotation do not fit the patterns suggested by the 10mm and 14mm endplate values. Lower values for the maximum moment and rotation FEA/Experimental ratios (implying larger maximum moment and rotation in the experiments), would be more consistent with the 10mm and 14mm endplate ratios.

6. A MODEL OF ENDPLATE DUCTILITY

6.1. INTRODUCTION

In this chapter a model is presented for predicting the ductility of a partial-strength extended endplate connection with four tension bolts symmetrically disposed about the beam tension flange. The interactions between three key areas are considered – the flush region of the endplate between the flanges, the extended region of the endplate beyond the tension flange, and the portion of the beam immediately adjacent to the connection, which properly forms part of the joint. Bending of the column flange and shear panel deformation are not included in this model.

The moment-rotation behaviour of the connection can be idealized as a bi-linear curve. Thus, the ductility model proposed here is based on identifying the connection moments and rotations at two points in the moment-rotation curve. These two points are referred to as the ‘swivel point’ where the two lines of the bi-linear model intersect, and the ‘maximum point’ where the maximum moment is predicted to occur. This is illustrated in Figure 6.1.

In the model to be developed, the swivel point is taken as the point at which the yield lines in the flush region are fully developed, so that the flush region is about to start strain-hardening. The maximum point is taken as the point at which the strains in the flush region reach a maximum permissible strain level, or as the point at which the force in either the flush or extended tension bolts attains to the ultimate bolt capacity in tension, F_{ub} .

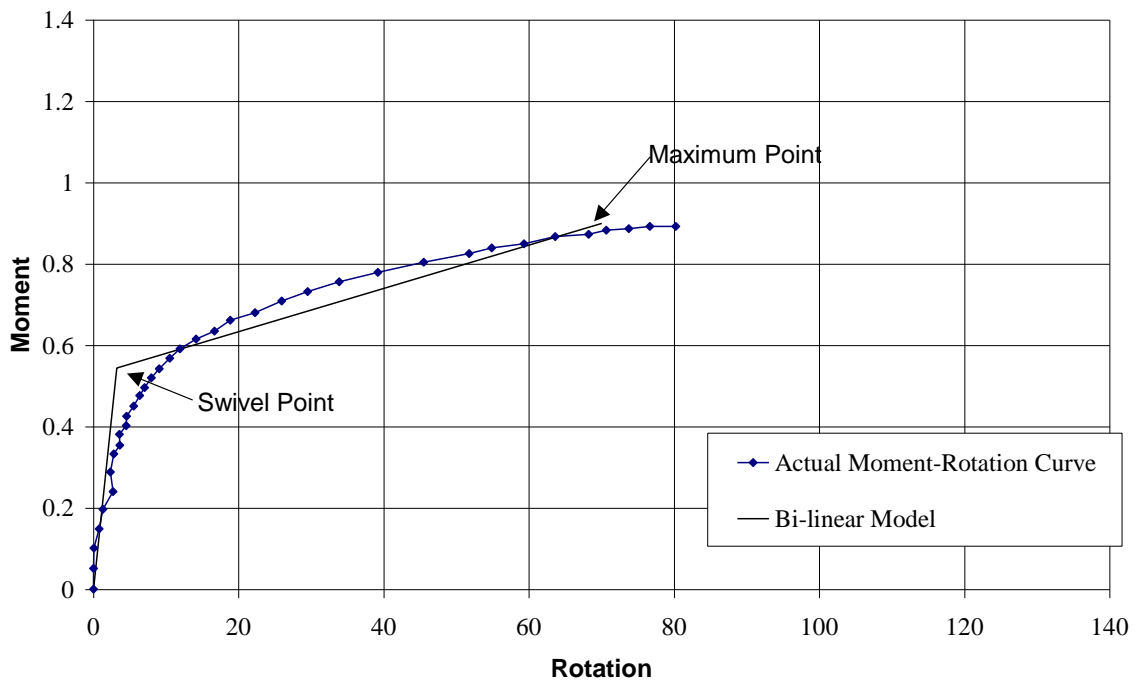


Figure 6.1 – Typical Bilinear Model of a Moment-Rotation Curve

In order to determine the moments at the swivel and maximum points, the tension bolt forces in the extended and flush regions must be calculated. The tension bolt force in the flush region at swivel is based on a yield-line analysis of the flush region, using a well-established yield-line model.

The rotation of the connection at both the swivel and maximum points is based on the deformation of the stiffer flush region. The flush region deformation is assessed using a mechanical model of a simply supported square plate with a central point load. The model provides a relationship between the applied force and the plate deflection, including membrane action, and also a relationship between the plate deflection and the maximum strain in the plate. Strain hardening is catered for at the maximum point by adjusting the plate bending stiffness from a function of E to a function of E_{sh} , for the force increment from the swivel point to the maximum point.

The square plate model is used to obtain the flush region deformation at the swivel point, with the point load taken as the previously calculated flush tension

bolt force at swivel. The same square plate model is used to obtain the flush region deflection at the maximum point, by setting the maximum strain in the plate at the maximum permissible strain level. The flush tension bolt force at maximum point can then be calculated from the flush region deformation at maximum point.

The extended region deflections at swivel and maximum points are obtained from the corresponding flush region deflections at those points, by considering compatibility of deformation. A conceptual model of the extended region as a simply-supported beam is then used to provide a relationship between the extended region bolt force and the extended region deflection. Strain hardening and membrane action are included in this model. Thus, the extended bolt tension forces can be calculated from the extended region deflections, at both the swivel and maximum points.

Once the extended and flush tension bolt forces are all known, the connection moments and rotations can be calculated using a stress-block approach.

It is necessary however, to first establish a material behaviour model for the endplate in terms of its moment-curvature relationship. This forms the basis for the material assumptions in the development of the model. Thus, before considering the model development further, the next section deals with the endplate material model to be adopted.

6.2. THE ENDPLATE MATERIAL MODEL

6.2.1. The Endplate Stress-Strain Curve in Uniaxial Tension

The measured material properties for the connection test members were reported earlier in Table 3.2. In Table 6.1 these same material properties are presented again but as dimensionless ratios. The ultimate strain in this latter table has been calculated from the ultimate stress and the strain-hardening modulus.

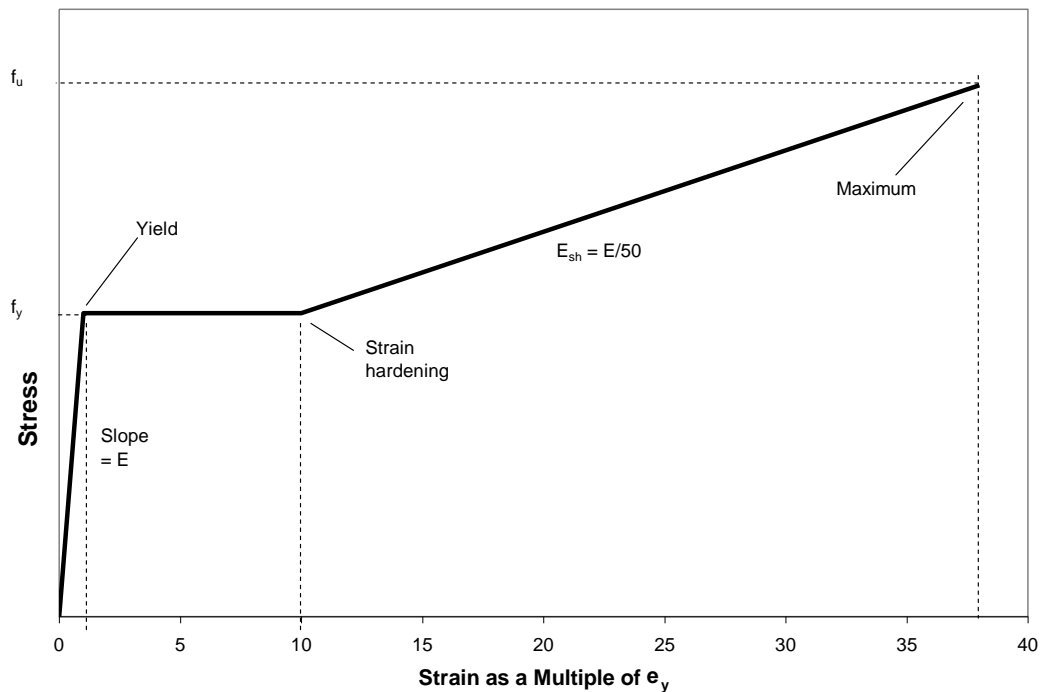


Figure 6.2 – Idealized Material Stress-Strain Curve

The ratios in Table 6.1 lead to average values for the E/E_{sh} ratio of 50.43, for ϵ_{sh}/ϵ_y of 9.83, and for $\epsilon_{ult}/\epsilon_y$ of 36.57 in the endplates. These values agree closely with typical averages of 50 and 10 for E/E_{sh} and ϵ_{sh}/ϵ_y , reported for steels produced in South Africa and North America (Kemp, 1988 and Galambos & Ravindra, 1978). Thus, it is reasonable to idealize the material uniaxial stress-strain curve as a tri-linear curve with a linear elastic region, a perfectly plastic region to a strain of $10\epsilon_y$, and then with a strain-hardening region at a slope of $E/50$. This simplified representation is shown in Figure 6.2. For the endplates only, a reasonable assumption of the ultimate strain would be $38\epsilon_y$.

Table 6.1 – Material Properties in Connection Tests as Dimensionless Parameters

	Young's Modulus GPa	Yield stress MPa	Yield Strain 10^{-3}	Harden'g Strain 10^{-3}	Harden'g Modulus GPa	Ultimate Stress MPa	Ultimate Strain 10^{-3}	E/E _{sh}	ϵ_{sh}/ϵ_y	$\epsilon_{ult}/\epsilon_y$
	(E)	(f _y)	(ϵ_y)	(ϵ_{sh})	(E _{sh})	(f _{ult})	(ϵ_{ult})			
Col flange	209.60	299.10	1.427	16.600	3.82	483.00	64.741	54.90	11.63	45.37
Col web	201.90	333.90	1.654	12.200	4.01	494.70	52.300	50.35	7.38	31.79
Bm flange (1)	209.70	324.40	1.547	17.750	5.09	494.90	51.247	41.20	11.47	33.13
Bm web (1)	213.60	365.30	1.710	21.100	3.91	525.40	62.046	54.60	12.34	36.28
Bm flange (2)	205.71	318.89	1.550	N/A	N/A	493.67	N/A	N/A	N/A	N/A
Bm web (2)	212.12	381.77	1.800	14.550	3.88	534.63	53.946	54.67	8.08	29.97
10 plate (pilot)	212.10	304.50	1.436	11.600	5.84	537.60				
12 plate (pilot)	219.10	306.00	1.397	13.500	5.04	510.20				
10 mm plate	202.20	331.30	1.638	13.450	3.50	505.71	63.281	57.77	8.24	38.63
12mm plate	219.10	306.00	1.397	13.500	5.04	510.20	54.016	43.47	9.66	38.67
14mm plate	213.00	295.00	1.385	13.600	4.58	478.30	53.622	46.51	9.82	38.72
Averages								50.43	9.83	36.57

6.2.2. The Endplate Moment-Curvature Relation

Given the rectangular section shown in Figure 6.2 with breadth b and depth $2d$, and subjected to a bending moment M , then the theoretical plastic moment of resistance M_{pth} for the section is bd^2f_y – where f_y is the yield stress. If the tri-linear stress-strain curve of Figure 6.2 is assumed, then the stress distribution across the section changes with increasing load, from a linear elastic stress distribution to an inelastic stress distribution, and finally to an inelastic stress distribution with strain-hardening. The section would eventually fracture with cracks developing at the outermost fibres. These three stages are shown in Figure 6.3.

Even when a large portion of the section is inelastic and already strain-hardening, there will still be a small central core of linear elastic strains less than ϵ_y . The next region bounding the elastic core on either side is inelastic but without strain-hardening. The outermost fibres are however strain-hardening in tension and compression.

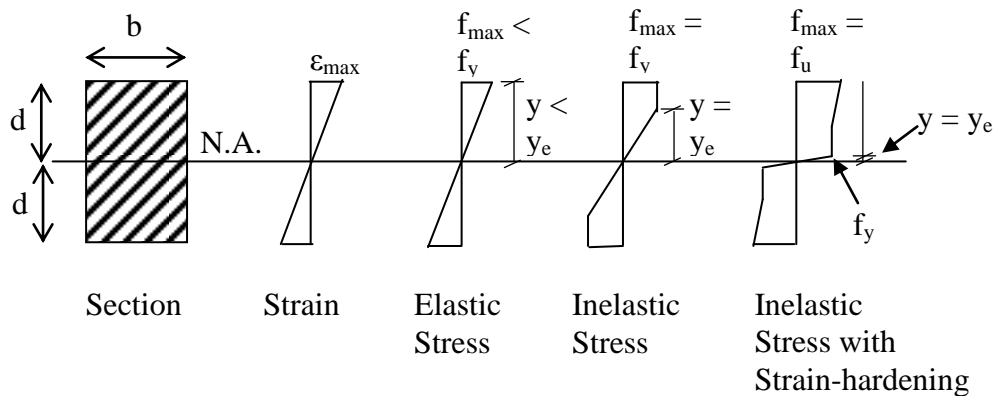


Figure 6.3 – Changes in Stress Distribution on Member Section under Increasing Bending Moment

If curvature is denoted as k , the strain in the outermost fibre is denoted as ϵ_{max} , and the subscripts y , sh and ult (or u) are used to denote values at yield, strain-hardening and ultimate strains respectively, the moment-curvature relations are determined as follows:

When the maximum stress $f_{\max} < f_y$, the strain $\varepsilon_{\max} < \varepsilon_y$ (section entirely elastic).
 The beam curvature $k = \varepsilon_{\max}/d$, and when the outermost fibre yields, $k = k_y = \varepsilon_y/d$
 ($d = y_e$). Calculating the moment of the forces:

$$M = \frac{2}{3}bd^2 \cdot f_{\max} = \frac{2}{3}bd^2 \cdot E\varepsilon_{\max} = \frac{2}{3}bd^3 \cdot Ek = \frac{2}{3}bd^3 \cdot \frac{f_y}{\varepsilon_y} k = \frac{2}{3}M_{\text{pth}} \cdot \frac{k}{k_y} = \frac{2}{3}M_{\text{pth}} \cdot k'$$

Eqn 6.1

$$\text{when } \varepsilon = \varepsilon_y, \text{ then } k = k_y \text{ and } M = M_y = 2M_{\text{pth}}/3$$

For the range $f_y \leq f_{\max} \leq f_{\text{sh}}$, then $\varepsilon_y \leq \varepsilon_{\max} \leq \varepsilon_{\text{sh}}$. The inner elastic core is still obeying elastic relations, but there is an additional moment of resistance due to the plastic regions on either side. The curvature is of course the same for the elastic and inelastic zones, but the elastic relations for curvature are only true in the elastic zone. The moment of resistance is:

$$\begin{aligned} M &= \frac{2}{3}by_e^3 \cdot Ek + bf_y(d - y_e)(d + y_e) \\ k &= \frac{\varepsilon_y}{y_e} \Rightarrow y_e = \frac{f_y}{Ek} \Rightarrow f_y = Eky_e \quad \therefore M = \frac{2}{3}by_e^3 \cdot Ek + by_e Ek(d^2 - y_e^2) \\ \Rightarrow M &= bf_y \left(d^2 - \frac{f_y^2}{3E^2k^2} \right) = M_{\text{pth}} - \frac{bf_y \varepsilon_y^2}{3k^2} = M_{\text{pth}} - \frac{bf_y \varepsilon_y^2 d^2}{3\varepsilon_y^2} = M_{\text{pth}} \left(1 - \frac{1}{3k'^2} \right) \end{aligned} \quad \text{Eqn 6.2}$$

$$\text{When } \varepsilon = \varepsilon_{\text{sh}}, \text{ then } k = k_{\text{sh}} \text{ and } \varepsilon_{\text{sh}} = 10\varepsilon_y, \text{ then } M = M_{\text{sh}} = 299M_{\text{pth}}/300 = 0.997M_{\text{pth}}$$

For $\varepsilon_{\text{sh}} \leq \varepsilon \leq \varepsilon_{\text{ult}}$

$$\begin{aligned} M &= bf_y \left(d^2 - \frac{f_y^2}{3E^2k^2} \right) + 2 \left[\frac{b}{2}(d - 10y_e)(f_u - f_y) \right] \times \left[\frac{2}{3}(d - 10y_e) + 10y_e \right] \\ f_u &= E_{\text{sh}}(\varepsilon_{\text{ult}} - 10\varepsilon_y) + f_y = \frac{Ek}{50}(d - 10y_e) + f_y \\ \therefore M &= bf_y \left(d^2 - \frac{f_y^2}{3E^2k^2} \right) + bf_y \left(\frac{Ekd^3}{75f_y} - \frac{d^2}{5} + \frac{20f_y^2}{3E^2k^2} \right) \\ \Rightarrow M &= \frac{4}{5}bf_y d^2 + bf_y \left(\frac{Ekd^3}{75f_y} + \frac{19f_y^2}{3E^2k^2} \right) = \frac{4}{5}M_{\text{pth}} + bf_y \left(\frac{Ekd^3}{75f_y} + \frac{19f_y^2}{3E^2k^2} \right) \end{aligned}$$

$$= \frac{4}{5} M_{pth} + bf_y \left(\frac{E\varepsilon d^2}{75f_y} + \frac{19f_y^2 d^2}{3E^2 \varepsilon^2} \right) = \frac{4}{5} M_{pth} + bf_y d^2 \left(\frac{\varepsilon}{75\varepsilon_y} + \frac{19\varepsilon_y^2}{3\varepsilon^2} \right)$$

$$\therefore M = M_{pth} \left(\frac{4}{5} + \frac{k'}{75} + \frac{19}{3k'^2} \right) \quad Eqn 6.3$$

For the endplates, $\varepsilon_{ult} = 38\varepsilon_y$ from Table 6.1, therefore $M_u = 1.311M_{pth}$

In terms of the dimensionless constant $M' = M/M_{pth}$ these equations would become:

$$\begin{aligned} \varepsilon \leq \varepsilon_y \quad (k' \leq 1) & \quad M' = \frac{2}{3} k' \\ \varepsilon_y \leq \varepsilon \leq \varepsilon_{sh} \quad (1 \leq k' \leq 10) & \quad M' = 1 - \frac{1}{3k'^2} \\ \varepsilon_{sh} \leq \varepsilon \leq \varepsilon_{ult} \quad (10 \leq k' \leq 38) & \quad M' = \frac{4}{5} + \frac{k'}{75} + \frac{19}{3k'^2} \end{aligned} \quad Eqn 6.4$$

Following Kemp et al (2002), a simple bi-linear approximation to the moment-curvature curve may be adopted, with the slope of the elastic portion as EI_x and the slope of the inelastic portion as $E_{sh}I_x$. By plotting the line of best fit for the inelastic and strain-hardening region, the inelastic region is found to have a slope of E/e , where e ranges from a lower limit of 75 to an upper limit of 60, and has a mean value of 65. The line of best fit intersects the linear elastic line at $0.92M_{pth}$. For simplicity, this intersect is taken here as $0.9M_{pth}$. The upper limit of $e = 60$ is adopted here. The resulting bi-linear approximation is shown in Figure 6.4 along with the full theoretical moment-curvature curve.

The curvature k_p at the swivel point is taken as $0.9M_{pth}/EI$, so that $k_p = 1.35k_y$, where k_y is the curvature at first yield, as in the equations above. The maximum moment ratio in the bi-linear approximation is 1.307 at a maximum strain of $28.15k_p$ ($38k_y$). The slope of the strain-hardening segment is taken as $E_{sh}I_x$ but with E_{sh} now set at a limiting value of $E/60$ rather than the tri-linear average value of $E/50$. The equation for the bi-linear curve in Figure 6.4 may then be written as follows:

$$\begin{aligned} \text{when } \frac{M}{M_{pth}} \leq 0.9 & \quad \frac{M}{M_{pth}} = 0.9 \frac{k}{1.35k_y} \\ \text{when } \frac{M}{M_{pth}} > 0.9 & \quad \frac{M}{M_{pth}} = \frac{0.9}{60} \left(\frac{k}{1.35k_y} - 1 \right) + 0.9 \end{aligned}$$

Eqn 6.5

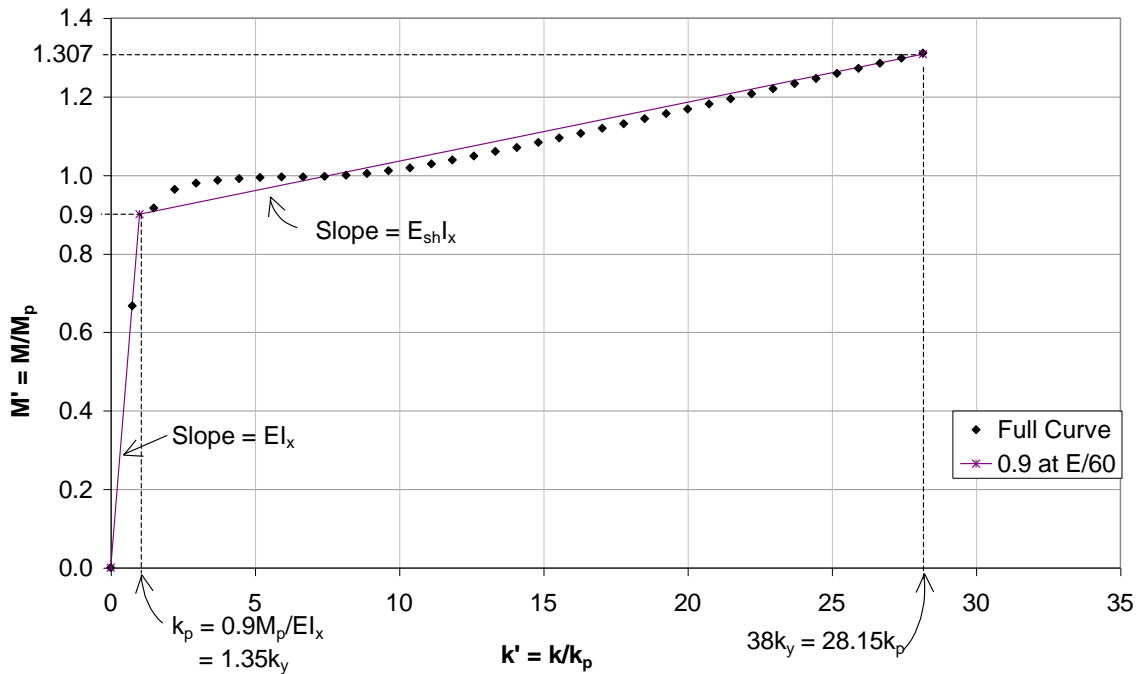
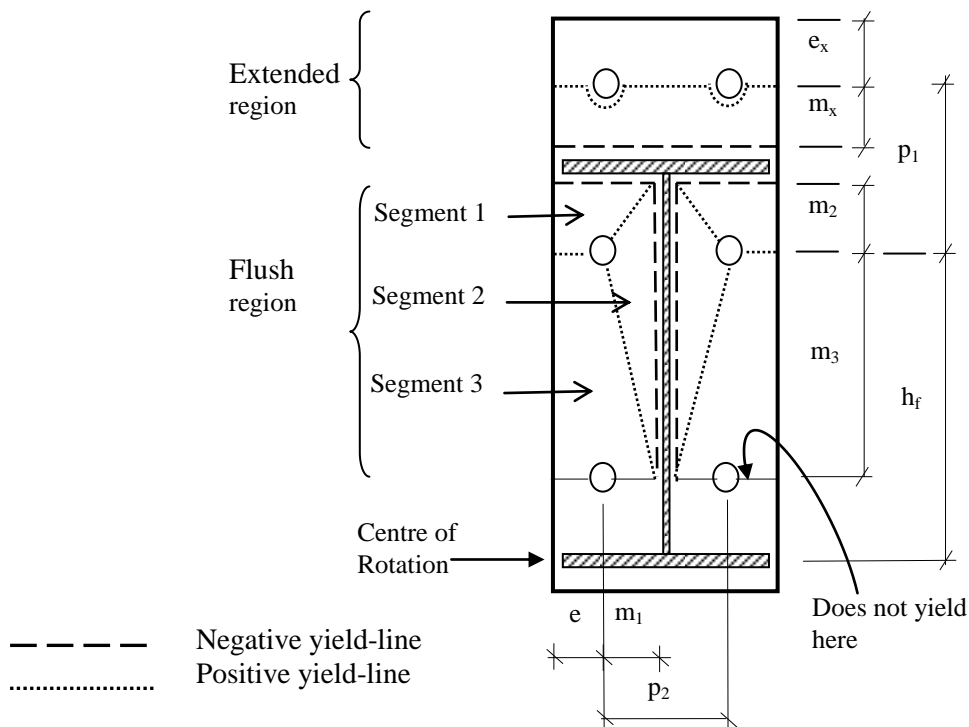


Figure 6.4 – Proposed Bi-linear Moment-Curvature Relation for the Endplate Material

6.3. DEVELOPING THE DUCTILITY MODEL EQUATIONS

6.3.1. The Endplate Flush Region at the Swivel Point

Following the evidence of the experimental observations in this study and recommendations in Zandonini and Zanon (1988), the flush region is conceptualized as a plate supported on three sides resisting a point (bolt) force. The connection swivel point occurs when a yield-line collapse mechanism is fully developed in the flush region. Based on experimental observations, the yielding pattern is initially circular around the bolt-head; however, as the yielding develops, it changes into the pattern shown in Figure 6.5. This is essentially the thin-plate pattern proposed in Bernuzzi et al (1991).



**Figure 6.5 – Idealized Yield-line Pattern Adopted for Flush Region at Swivel
Adapted from Bernuzzi et al, 1991**

A key difference here though is that the line at the base of segment 3 in Figure 6.5 is not considered to be a proper yield-line. The reasoning behind that change is as follows: The connection forces are applied via the beam web and tension flange. However, segment 3 is clamped against the column flange by the tension and shear bolt pre-tension forces, and is continuous with the portion of endplate adjacent to the beam compression flange.

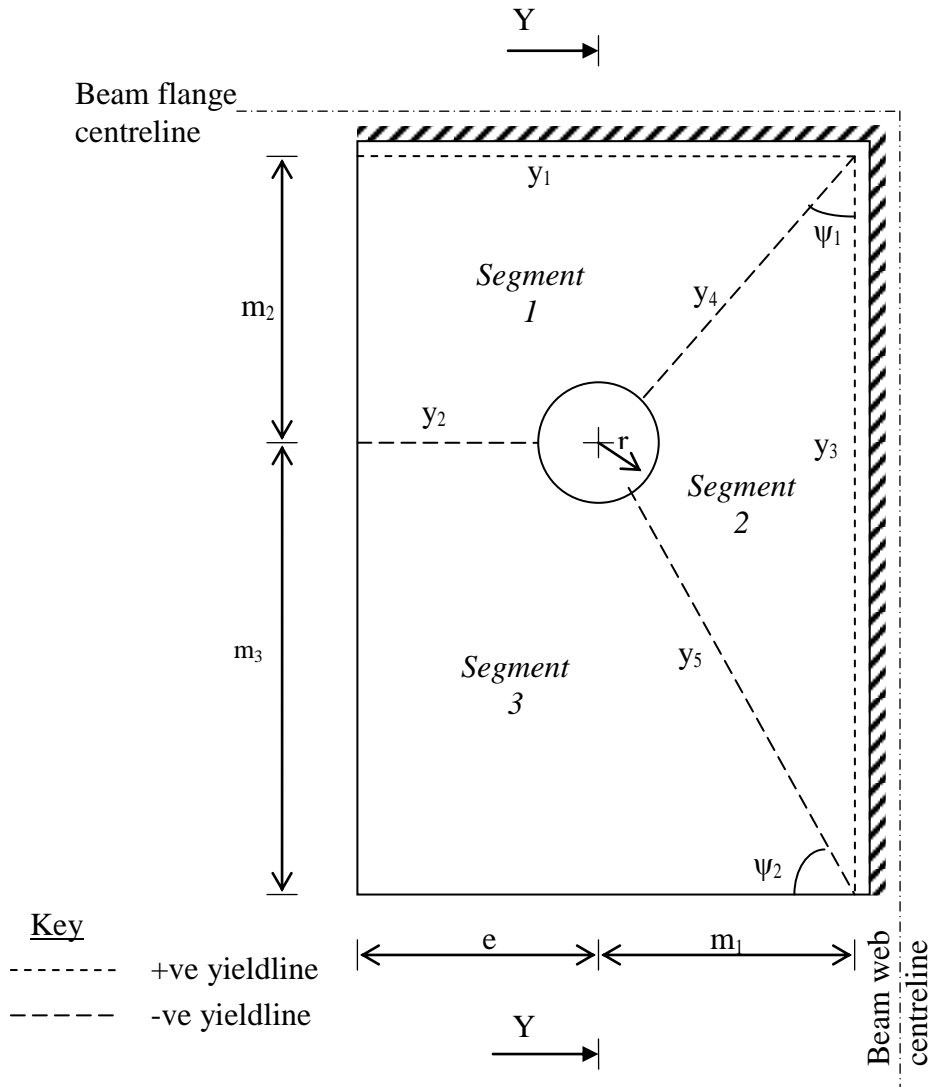


Figure 6.6 – Detail of Assumed Yield-line Pattern

The deformation of segments 1 and 2 away from the column flange is sufficient to allow the beam profile to rotate more or less as a straight line from the tension flange to the compression flange level, but is not sufficient to allow a fully

developed yield-line at the base of segment 3. Thus, segment 3 only deforms a little, and yielding at the base of segment 3 is assumed negligible. In fact, if the shear bolt pre-tension has not been exceeded, the plate remains clamped against the column flange at the shear bolt level.

Bolt force

In order to determine the tension bolt forces at the swivel point, a yield-line analysis is carried out using the well-established yield-line pattern of Figure 6.5b. Figure 6.5a shows the observed positions of yield-lines in the experiments, while 6.5b shows the idealized positions used in the analysis.

The endplate geometry is described using the dimensions shown in Figure 6.5b, following the notation of SCI (1995) and Eurocode 3 (2005). Thus, m_1 and m_2 are the distances from the bolt-hole centre to the face of the web and flange respectively, less 0.8 times the respective fillet weld leg length. The edge distance is e , and the bolt-hole radius is r . m_4 is measured to the face of the beam compression flange less 0.8 times the fillet weld leg length. The tension bolts are at a pitch of p_1 and a gauge of p_2 , and the flush tension bolts are at a height of h_f above the base of the compression flange. Other symbols used in the model are E for Young's modulus, b_p and t_p for the endplate width and thickness respectively; f_y for the endplate yield strength, and m_{pth} for the theoretical plastic moment per unit length of plate.

The yield-line pattern is shown in close-up for one side of the endplate in Figure 6.6.

The lengths of the yield-lines in Figure 6.6 are:

$$\begin{aligned}
 y_1 &= e + m_1 & y_4 &= (m_1^2 + m_2^2)^{1/2} - r \\
 y_2 &= e - r & y_5 &= (m_1^2 + m_3^2)^{1/2} - r \\
 y_3 &= m_2 + m_3
 \end{aligned}
 \tag{Eqn 6.6}$$

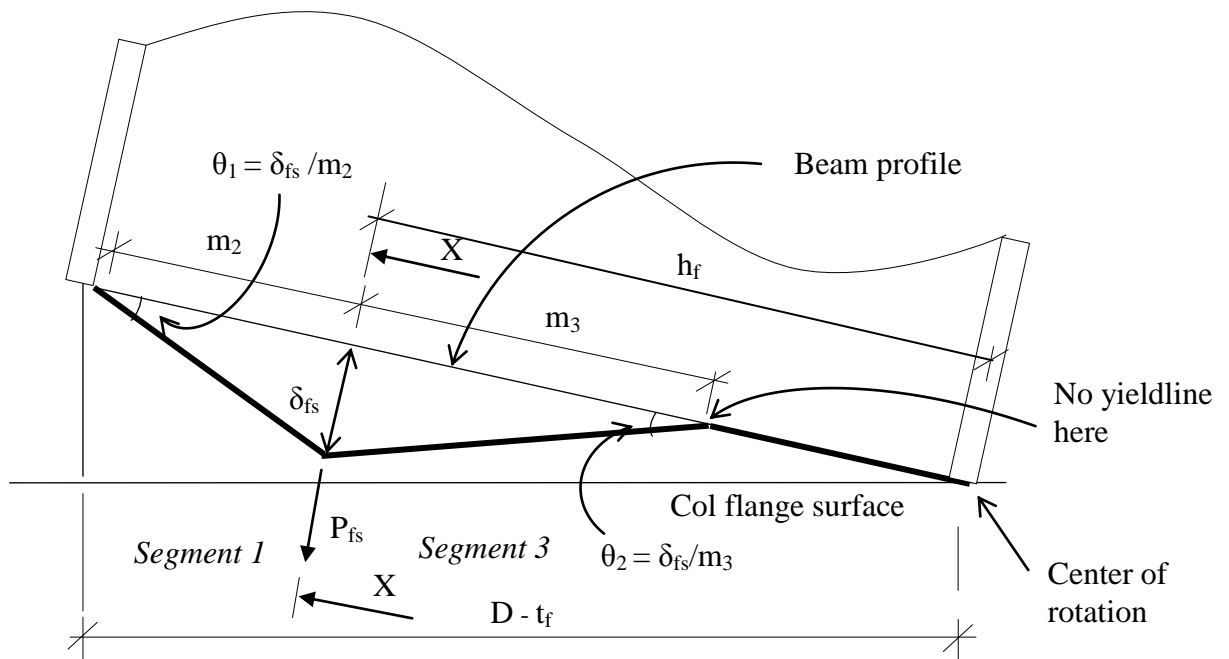


**Figure 6.7 – Longitudinal Section through Flush Region at Swivel
(Sect. Y-Y in Fig 6.6)**

It is assumed that the flush tension bolts will bend/deform sufficiently so that the plate is not closely clamped against the flange, which is why a circular yield-line is not included immediately around the bolt head. This is consistent with the experimental observations and the literature. It was observed that there was initially widespread yielding around the bolt-head, but at higher rotations the prying of the bolt-head led to inelastic deformation of the bolt in bending so that the clamping effect was reduced.

In Figure 6.7 showing a longitudinal section through the endplate, segments 1 and 3 on the plate, which would have been in line with the beam profile, can be seen to rotate through θ_1 and θ_2 respectively, away from the beam profile. Deflection δ_{fs} is the movement of the endplate away from the bolt-head on the column flange, measured in a direction perpendicular to the endplate. The last subscript s denotes that this is at the swivel point. As explained previously, the beam profile is assumed to rotate about the compression flange at swivel.

The internal work done by unit resistance moments m_{p1} and m_{p2} (kN-mm/mm width) on yield-lines y_1 and y_2 respectively, will be:

$$y_1 : \quad m_{p1} \cdot y_1 \cdot \frac{\delta_{fs}}{m_2} = m_{p1} \cdot (e + m_1) \cdot \frac{\delta_{fs}}{m_2} = m_{p1} \delta_{fs} \cdot \frac{(e + m_1)}{m_2} \quad \text{Eqn 6.7}$$

$$\begin{aligned} y_2 : \quad m_{p2} \cdot y_2 \cdot \left(\frac{\delta_{fs}}{m_3} + \frac{\delta_{fs}}{m_2} \right) &= m_{p2} \cdot (e - r) \cdot \left(\frac{\delta_{fs}}{m_3} + \frac{\delta_{fs}}{m_2} \right) \\ &= m_{p2} \delta_{fs} \cdot (e - r) \cdot \left(\frac{m_2 + m_3}{m_2 m_3} \right) \end{aligned} \quad \text{Eqn 6.8}$$

There is no yield-line at the bottom end of segment 3 as indicated in the figure. In the figure, P_{fs} is the component of the bolt force that is perpendicular to the beam profile and so parallel to the beam tension flange at the joint. The external work done by the bolt in causing the plate rotation is therefore:

$$\text{External Work} = P_{fs} \cdot \delta_{fs} \quad \text{Eqn 6.9}$$

Figure 6.8 is a transverse section through the endplate, but taken at an angle so that the section shown is perpendicular to the beam profile (X-X in Figure 6.7).

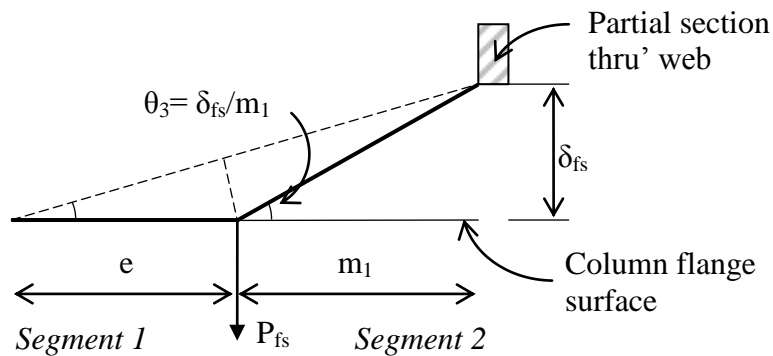


Figure 6.8 – Transverse Section through Flush Region (Sect. X-X in Fig 6.7)

In Figure 6.8, we see that yield-line y_3 has rotated through the angle θ_3 . The internal work done on yield-line y_3 by unit moment of resistance m_{p3} is:

$$y_3 : \quad m_{p3} \cdot y_3 \cdot \frac{\delta_{\text{fs}}}{m_1} = m_{p3} \cdot (m_3 + m_2) \cdot \frac{\delta_{\text{fs}}}{m_1} = m_{p3} \delta_{\text{fs}} \cdot \frac{(m_3 + m_2)}{m_1} \quad \text{Eqn 6.10}$$

The rotation θ_4 on yield-line y_4 is the sum of the components of the slopes (relative to the beam profile) for segments 1 and 2 i.e. $\theta_1 \cdot \text{Cos } \psi_1 + \theta_3 \cdot \text{Sin } \psi_1$ (see Figure 6.6 for definitions of ψ_1 and ψ_2). Similarly, the rotation θ_5 on yield-line y_5 is the sum of the components of the slopes for segments 2 and 3 i.e. $\theta_3 \cdot \text{Cos } \psi_2 + \theta_2 \cdot \text{Sin } \psi_2$. The internal work done on yield-lines y_4 and y_5 by the moments of resistance m_{p4} and m_{p5} respectively is:

$$\begin{aligned} y_4 : \quad & m_{p4} \cdot y_4 \cdot \left(\frac{\delta_{\text{fs}}}{m_2} \cdot \text{Cos} \psi_1 + \frac{\delta_{\text{fs}}}{m_1} \cdot \text{Sin} \psi_1 \right) \\ & = m_{p4} \cdot \left[(m_1^2 + m_2^2)^{1/2} - r \right] \cdot \left(\frac{\delta_{\text{fs}}}{m_2} \cdot \text{Cos} \psi_1 + \frac{\delta_{\text{fs}}}{m_1} \cdot \text{Sin} \psi_1 \right) \end{aligned} \quad \text{Eqn 6.11}$$

$$\begin{aligned} y_5 : \quad & m_{p5} \cdot y_5 \cdot \left(\frac{\delta_{\text{fs}}}{m_1} \cdot \text{Cos} \psi_2 + \frac{\delta_{\text{fs}}}{m_3} \cdot \text{Sin} \psi_2 \right) \\ & = m_{p5} \cdot \left[(m_1^2 + m_3^2)^{1/2} - r \right] \cdot \left(\frac{\delta_{\text{fs}}}{m_1} \cdot \text{Cos} \psi_2 + \frac{\delta_{\text{fs}}}{m_3} \cdot \text{Sin} \psi_2 \right) \end{aligned} \quad \text{Eqn 6.12}$$

From Figure 6.6,

$$\begin{aligned} \text{Cos} \psi_1 &= m_2 \cdot (m_1^2 + m_2^2)^{-1/2}; \quad \text{Sin} \psi_1 = m_1 \cdot (m_1^2 + m_2^2)^{-1/2} \\ \text{Cos} \psi_2 &= m_1 \cdot (m_1^2 + m_3^2)^{-1/2}; \quad \text{Sin} \psi_2 = m_3 \cdot (m_1^2 + m_3^2)^{-1/2} \end{aligned}$$

Therefore the work equations for y_4 and y_5 may be written as:

$$y_4 : \quad m_{p4} \delta_{\text{fs}} \cdot \left[\sqrt{m_1^2 + m_2^2} - r \right] \cdot \left(\frac{2}{\sqrt{m_1^2 + m_2^2}} \right) = m_{p4} \delta_{\text{fs}} \cdot \left(2 - \frac{2r}{\sqrt{m_1^2 + m_2^2}} \right) \quad \text{Eqn 6.13}$$

$$y_5 : \quad m_{p5} \delta_{\text{fs}} \cdot \left[\sqrt{m_1^2 + m_3^2} - r \right] \cdot \left(\frac{2}{\sqrt{m_1^2 + m_3^2}} \right) = m_{p5} \delta_{\text{fs}} \cdot \left(2 - \frac{2r}{\sqrt{m_1^2 + m_3^2}} \right) \quad \text{Eqn 6.14}$$

Thus, the virtual work equation is:

$$\begin{aligned}
P_{\text{fs}} \cdot \delta_{\text{fs}} &= m_{p1} \delta_{\text{fs}} \cdot \frac{(e + m_1)}{m_2} + m_{p2} \delta_{\text{fs}} \cdot (e - r) \cdot \left(\frac{m_2 + m_3}{m_2 m_3} \right) + m_{p3} \delta_{\text{fs}} \cdot \frac{(m_3 + m_2)}{m_1} \\
&+ m_{p4} \delta_{\text{fs}} \cdot \left(2 - \frac{2r}{\sqrt{m_1^2 + m_2^2}} \right) + m_{p5} \delta_{\text{fs}} \cdot \left(2 - \frac{2r}{\sqrt{m_1^2 + m_3^2}} \right) \\
\Rightarrow P_{\text{fs}} &= m_{p1} \cdot \frac{(e + m_1)}{m_2} + m_{p2} \cdot (e - r) \cdot \left(\frac{m_2 + m_3}{m_2 m_3} \right) + m_{p3} \cdot \frac{(m_3 + m_2)}{m_1} \\
&+ m_{p4} \cdot \left(2 - \frac{2r}{\sqrt{m_1^2 + m_2^2}} \right) + m_{p5} \cdot \left(2 - \frac{2r}{\sqrt{m_1^2 + m_3^2}} \right)
\end{aligned}$$

At the swivel point, the unit moments of resistance $m_{p1} - m_{p5}$ in the flush region are equal to $0.9m_{\text{pth}}$ (see Section 6.1.2). Therefore, the virtual work equation can be written as:

$$P_{\text{fs}} = 0.9m_{\text{pth}} \cdot \left[\frac{e + m_1}{m_2} + (e - r) \cdot \frac{m_2 + m_3}{m_2 m_3} + \frac{m_2 + m_3}{m_1} + 4 - \frac{2r}{\sqrt{m_1^2 + m_2^2}} - \frac{2r}{\sqrt{m_1^2 + m_3^2}} \right] \quad \text{Eqn 6.15}$$

The dimensions m_1 and m_2 are usually in the range of 40 – 60 mm, and so are typically much larger than the bolt-hole radius r , which is 11 or 13 mm for M20 or M24 bolts respectively. The dimension m_3 is of course even larger than m_2 . Thus, the last two terms in the virtual work equation above will be of the order of 10%, so that for simplicity it was decided to eliminate these terms. Therefore the equation for P_{fs} can be simplified to obtain:

$$P_{\text{fs}} = 0.9m_{\text{pth}} \cdot \left[\frac{e + m_1}{m_2} + (e - r) \cdot \frac{m_2 + m_3}{m_2 m_3} + \frac{m_2 + m_3}{m_1} + 4 \right] \quad \text{Eqn 6.16}$$

Flush region deflection

To obtain the flush region deflection, each half of the flush region of the endplate may be conceptualised as a rectangular plate with a concentrated load due to the bolt force, and with fixed supports on the adjacent edges where it is bordered by the beam web and flange. The third ‘edge’ is at a line through the shear bolts, and

that edge is simply-supported since the restraining moment there is very small. The fourth edge is free. This is illustrated in Figure 6.9a. An exact solution for the deflection of a rectangular plate with this particular combination of loading and supports has not been identified. However, an approximate solution may be obtained by considering the case of a simply-supported square plate under a concentrated load, as shown in Figure 6.9b.

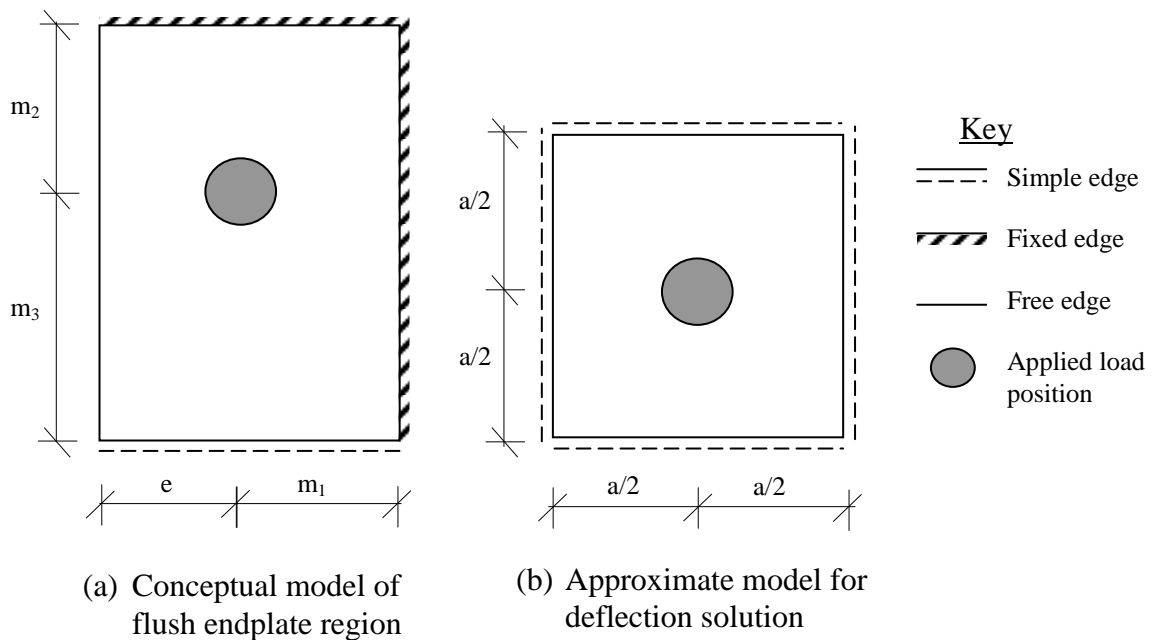


Figure 6.9 – Square plate model for flush region deflection

In Figure 6.9 a simple support means the plate is restrained from in-plane and out of plane translation, while a fixed support is additionally also rotationally restrained. A free edge is not supported at all.

When the plate is not subject to an initial deflection due to its own self-weight, Roark (1965: 247) gives a solution for the simply-supported square plate of Figure 6.9b, described in equations 6.17 and 6.18 as follows:

$$\frac{12Pa^2(1-\nu^2)}{Et^3} = \delta \left[\varphi_1 + \varphi_2 \left(\frac{\delta_t}{t} \right)^2 \right] \quad \text{Eqn 6.17}$$

This first equation is a relationship between the applied force and the plate deflection, and it includes an allowance for membrane action, which is catered for by the term including ϕ_2 on the right-hand side. P is the applied concentrated force, δ is the deflection at the point of load application, and t is the thickness of the plate. The plate width/breadth is a , and E and ν are Young's modulus and Poisson's ratio respectively. The coefficients ϕ_1 and ϕ_2 are 87 and 28 for a plate that is simply-supported on all four sides, and are 192 and 36 respectively for a plate with fixed edges. At the swivel point, there is already yielding along the two 'fixed edges' in the idealized model of Figure 6.9a, and so a simply-supported solution model is considered more appropriate.

The plate is considered to have an initial deflection δ_i due to pre-applied loads, so that the total deflection $\delta_t = \delta + \delta_i$.

$$\text{Secondly } f_{\text{center}} = \alpha E \left(\frac{\delta_t^2 - \delta_i^2}{a^2} \right) \quad \text{Eqn 6.18}$$

This second equation is a relationship between the maximum membrane stress f_{center} at the centre of the plate, and the deflection δ . Coefficient α is 1.6 for simply-supported edges and 2.9 for fixed edges.

In order to apply these equations to the endplate deflection at the swivel point, we consider that there is no strain-hardening or membrane action yet in the flush region at the swivel point, and there is no initial self-weight deflection δ_i . Thus, using the notation adopted in this thesis, equation 6.17 simplifies to:

$$\frac{12P_{\text{fs}} a^2 (1 - \nu^2)}{Et_p^3} = 87\delta_{\text{fs}} \Rightarrow \delta_{\text{fs}} = \frac{12P_{\text{fs}} a^2 (1 - \nu^2)}{87Et_p^3} = P_{\text{fs}} \cdot \frac{a^2}{8Et_p^3}$$

where $a = 2 m_1$ and Poisson's ratio is taken as 0.3.

The square plate approximation to the actual flush region geometry has been investigated using an FEA model in Chapter 7. The FEA model results show that a reasonable agreement is obtained between the deflection of the original geometry and the square plate deflection, if the square plate width ‘a’ is taken as $a = 2m_1$ (the lesser dimension of m_1 and m_2), and the square plate deflection at swivel is multiplied by a factor of 3. Therefore:

$$\Rightarrow \delta_{\text{fs}} = P_{\text{fs}} \cdot \frac{a^2}{8Et_p^3} = 3P_{\text{fs}} \cdot \frac{m_1^2}{2Et_p^3} = 1.5P_{\text{fs}} \cdot \frac{m_1^2}{Et_p^3} \quad \text{Eqn 6.19}$$

Therefore the connection rotation θ_{cps} due to endplate deformation at the swivel point, is given by:

$$\theta_{\text{cps}} = \frac{\delta_{\text{fs}}}{h_f} = 1.5P_{\text{fs}} \cdot \frac{m_1^2}{Et_p^3 h_f}$$

which assumes the beam profile to rotate about the centroid of the beam compression flange at the swivel point. Ignoring the contributions of the beam end and the bolt extensions, then the total connection rotation $\theta_{\text{cs}} = \theta_{\text{cps}}$, and θ_{cs} is given by:

$$\theta_{\text{cs}} = \frac{\delta_{\text{fs}}}{h_f} = 1.5P_{\text{fs}} \cdot \frac{m_1^2}{Et_p^3 h_f} \quad \text{Eqn 6.20}$$

6.3.2. The Endplate Flush Region at the Maximum Point

The ‘maximum point’ is dictated by the occurrence of either of two events – the tension force in either the flush or extended region bolts attains a limiting value, or the occurrence of a limiting strain in the endplate flush region. The limiting bolt force is chosen here as the bolt ultimate strength F_{ub} , though a safety factor would doubtless be included in practical design. Similarly, the limiting endplate strain is chosen to limit the likelihood of endplate cracks to acceptable values. For the endplates tested in this study, a suitable limit would be $38\varepsilon_y$ (see section 6.2.1). The first endplate cracks appear around the bolt-hole.

At the maximum point, the flush region of the endplate is undergoing both strain-hardening and membrane effects. The solution model of Roark (1965) may still be used as an approximate basis for a solution; however, the elastic modulus E is now relaxed to the value for strain-hardening, E_{sh} in equations 6.17 and 6.18. This is justified from the understanding that at the maximum point, yielding would be widespread over most of the flush region, and the plate bending stiffness would have deteriorated.

At a limiting endplate strain of $38\epsilon_y$ the limiting endplate stress is given approximately by f_u , where

$$f_u = E_{sh} (\epsilon_{ult} - 10\epsilon_y) + f_y = \frac{E \cdot \epsilon_y}{60} (38 - 10) + f_y = 1.47f_y$$

Therefore $f_u = 1.47f_y$.

At the maximum point, we are effectively considering the endplate deflection as consisting of two steps – an initial elastic deflection given by δ_{fs} and the plastic or inelastic increment in deflection. Thus, $\delta_i = \delta_{fs}$ and the total stress at the plate centre will increase from a maximum of f_y at swivel, to a maximum of $1.47f_y$ at the maximum point – an increment of $0.47f_y$. Equation 6.18 gives the membrane plate stress at the plate centre. At the maximum point therefore, the membrane plate stress will equal the increment of $0.47f_y$ as we have assumed the membrane stress to be zero at swivel in the flush region. Hence,

$$f_{center} = \alpha E_{sh} \left(\frac{\delta_{fms}^2 - \delta_{fs}^2}{a^2} \right) = 0.47f_y \quad \Rightarrow \quad \delta_{fms} = \sqrt{\left(\frac{0.47a^2 f_y}{\alpha E_{sh}} + \delta_{fs}^2 \right)}$$

where α is 1.6 (simply-supported), and δ_{fms} refers to the flush region deflection at the maximum point as calculated by the limiting strain criterion.

The elastic deflection δ_{fs} is small, so that the square may be neglected. Thus, the equation simplifies to:

$$\delta_{fms} \approx \sqrt{\frac{0.47a^2 f_y}{1.6E_{sh}}} = \sqrt{\frac{a^2 f_y}{3.4E_{sh}}}$$

However, our maximum stress does not occur at the plate centre but, allowing for stress concentrations, on the bolt-hole radius r . This may be accounted for with a linear approximation so that

$$\delta_{fms} = a \sqrt{\frac{f_y}{3.4E_{sh}}} \times \left(1 - \frac{2r}{a}\right) = a \sqrt{\frac{60f_y}{3.4E}} \times \left(1 - \frac{2r}{a}\right) \approx 4.2(a - 2r) \cdot \sqrt{\frac{f_y}{E}} \quad \text{Eqn 6.21}$$

Equation 6.17 can be re-written for the maximum point to obtain:

$$\frac{12\Delta P_f a^2 (1 - \nu^2)}{E_{sh} t_p^3} = (\delta_{fms} - \delta_{fs}) \left[87 + 28 \left(\frac{\delta_{fms}}{t_p} \right)^2 \right]$$

where ΔP_f refers to the increment in the flush region tension bolt force from the swivel point to the maximum point. This may be simplified to:

$$\frac{655.2\Delta P_f a^2}{E t_p^3} = (\delta_{fms} - \delta_{fs}) \left[87 + 28 \left(\frac{\delta_{fms}}{t_p} \right)^2 \right]$$

Again neglecting δ_{fs} for simplicity,

$$\Delta P_f = \frac{87}{655.2} \cdot \frac{E t_p^3 \delta_{fms}}{a^2} + \frac{28}{655.2} \cdot \frac{E t_p \delta_{fms}^3}{a^2} = \frac{E t_p^3 \delta_{fms}}{7.53a^2} + \frac{E t_p \delta_{fms}^3}{23.4a^2} \quad \text{Eqn 6.22}$$

$$\text{and } P_{fm} = \Delta P_f + P_{fs} \quad \text{Eqn 6.23}$$

However, the limiting bolt force criterion is that neither the flush region nor extended region tension bolt forces may exceed the bolt ultimate capacity in tension.

$$\text{Thus, } P_{fm} \leq F_{ub} \quad \text{Eqn 6.24}$$

If P_{fm} as calculated with equations 6.22 and 6.23 is greater than F_{ub} , then make $P_{fm} = F_{ub}$, and δ_{fmb} , the flush region deflection at the maximum point using the bolt

force criterion, must be calculated. This is obtained by substituting δ_{fmb} for δ_{fms} and F_{ub} for P_{fm} in equations 6.22 and 6.23. This leads to a cubic equation in δ_{fmb} which can be solved by trial and error. In a design situation however, where the designer wishes to avoid failure of the connection from bolt fracture, a governing limiting bolt force criterion would indicate the need to change to a larger bolt or a thinner endplate.

In a similar manner to equation 6.20, the connection rotation θ_{cpm} due to endplate deformation at the maximum point, is given by:

$$\theta_{cpm} = \frac{\delta_{fm}}{m_3}$$

which assumes the beam profile to rotate about the level of the shear bolts at the maximum point.

At maximum point the contributions of the beam end and the bolt extensions are significant, therefore the endplate contribution is increased by a factor of 1.33 to account for these. This empirical factor is based on test results published in Bernuzzi et al (1991) as explained in chapter seven. Thus, the total connection rotation at the maximum point θ_{cm} is taken as:

$$\theta_{cm} = \frac{4}{3} \cdot \frac{\delta_{fm}}{m_3} \tag{Eqn 6.25}$$

6.3.3. The Endplate Extended Region Flange Force

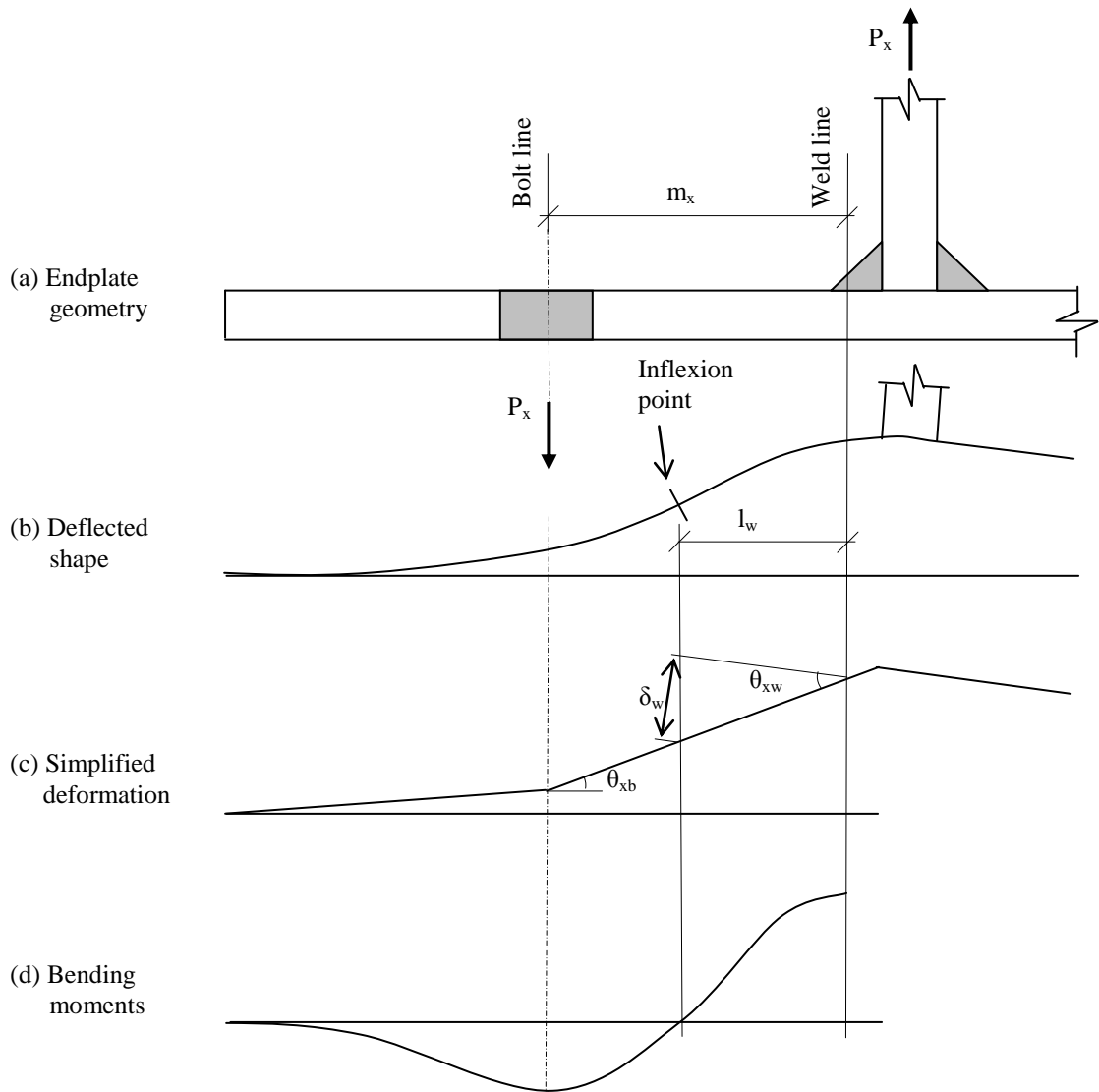


Figure 6.10 – Bending Moment Distribution across extended region

For a thin endplate with reasonable dimensions and typical proportions, experimental observations show that the extended region of the endplate, from the beam tension flange to the bolts, is in double-curvature. Maximum moments occur adjacent to the beam tension flange weld (referred to here as the weld line), and close to the centreline of the two bolts in the extended region (referred to as the bolt line). This is shown in Figure 6.10 (d). There is an inflexion point between

the bolt line and the weld line, and because the weld line moment exceeds the bolt line moment, this inflexion point is closer to the bolt line.

Figure 6.10 depicts a cross-section through the extended region of a thin endplate, with the geometry and deflected shape shown in parts (a) and (b). Part (c) shows a simplified, linearized version of the deflected shape, while (d) shows the bending moment distribution across the cross-section. Bending and membrane action in the extended region of the endplate is due to an applied force P_x at the beam tension flange as shown in Figure 6.10. This force excludes any flange forces resisted by the flush region, and also excludes the self-equilibrating prying action forces in the endplate. From equilibrium P_x is also the bolt force at the bolt line, minus prying action.

In SCI (1995) and EN 1993-1-8 (Eurocode 3, 2005) the weld line is offset from the beam flange face by 80% of the flange weld leg length s_{wf} , as in the flush region. This is due to the much greater stiffness of the portion of endplate underlying the weld.

Following the notation in Eurocode 3, the dimensions m_x and e_x shown in Figure 6.11 are taken as:

e_x = distance from bolthole centre to plate edge

m_x = distance from bolthole centre to face of tension flange – $0.8s_{wf}$.

At the swivel point in the connection moment-rotation curve, it is assumed here that yield-lines are just fully developed at the bolt line and the weld line. Yield-line y_6 in Figure 6.11 is the negative yield-line on the weld line while y_7 is positive and is on the bolt line. At the maximum strain point in the moment-rotation behaviour, these yield-lines have grown to become bands of plastic material with an elastic zone between.

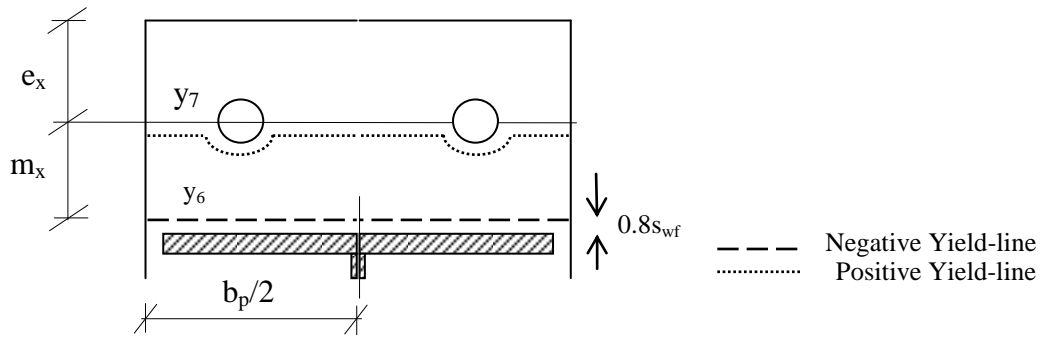


Figure 6.11 – Location of yield-lines in Extended Region

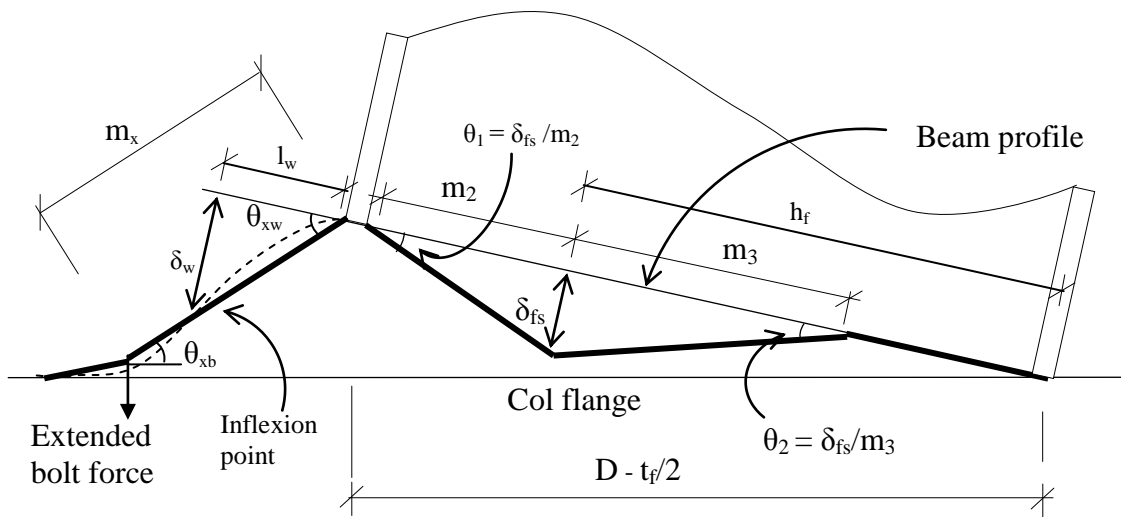


Figure 6.12 – Longitudinal Section through Endplate at Swivel

Bolt force P_{xs} at Swivel

In order to establish the extended bolt force at swivel, consider Figure 6.12 which is a longitudinal section through the endplate at swivel. The flush region is shown as well to clarify how the beam profile rotation affects the rotation of the extended region about the weld line. The plate deflected shape is clearly non-linear between the bolt and weld lines, since the bending moments are non-linear and there is also plastification around the yield-lines. However, a linear simplification may be usefully adopted to establish approximately the point of inflexion.

The rotation on the bolt line is defined as θ_{xb} and the rotation on the weld line is θ_{xw} . It can be seen that the weld line rotation must exceed the bolt line rotation, so

that the weld line moment must exceed the bolt line moment. For the simplified linear deformation shown,

$$\theta_{xw} = \theta_{xb} + \theta_{cp}$$

where θ_{cp} is the rotation of the beam profile due to plate deformation (θ_{cps} or θ_{cpm} as the case may be).

Then from similar triangles, θ_{xb} is given at swivel by

$$\theta_{xb} = \theta_{cps} \cdot \frac{D - t_f/2}{m_x} \approx \theta_{cps} \cdot \frac{D}{m_x}$$

$$\text{Thus, } \theta_{xw} = \theta_{xb} + \theta_{cps} = \theta_{cps} \cdot \left(1 + \frac{D}{m_x}\right) \quad \text{Eqn 6.26}$$

Thus, l_w in Figures 6.10 and 6.12 is given as

$$l_w \approx m_x \cdot \frac{\theta_{xw}}{\theta_{xw} + \theta_{xb}} = m_x \cdot \frac{m_x + D}{m_x + 2D} \quad \text{Eqn 6.27a}$$

If we consider the length l_w from the inflexion point to the weld line as half of a simply-supported beam with the support at the point of inflexion, the central deflection of this beam equals the deviation δ_w of the weld line from the point of inflexion, which is given for the simplified deformation as:

$$\delta_w = \theta_{xw} \cdot l_w = m_x \cdot \frac{\theta_{xw}^2}{\theta_{xw} + \theta_{xb}} = \frac{\theta_{cps}^2 (m_x + D)^2}{m_x + 2D} \quad \text{Eqn 6.27b}$$

Since θ_{cps} has previously been obtained at the swivel point from equation 6.20, equation 6.27b allows us to calculate δ_w at the swivel point.

This conceptual model is illustrated in Figure 6.13. The simply-supported beam is restrained axially at the ends so that axial membrane forces develop as would actually occur in the endplate due to the restraint at the bolt line and weld line. The force P acting at the beam centre to produce the same deflection δ_w as in the

extended region of the endplate will be twice the force P_x acting on the endplate. This model is statically equivalent to the endplate extension from the weld line to the inflexion point, regardless of whether or not yielding is occurring, as long as the second moment of inertia and the material model are the same as for the extended region.

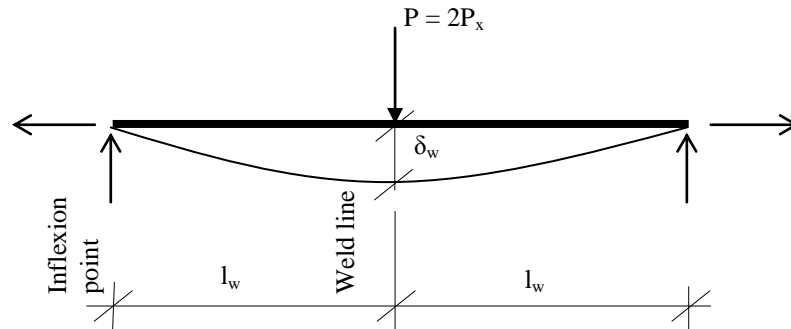


Figure 6.13 – Conceptual Model of Extended Region

Sherbourne and Lu (1993) present a solution for establishing the central point load P acting on an axially restrained, simply supported beam which undergoes large deflections, similar in magnitude to its own depth or greater, and where the central force is sufficient to cause inelastic strains in the beam fibre so that the beam yields and strain hardens significantly at the centre. This matches the behaviour of the conceptual model above. In their solution, Sherbourne and Lu assume a rigid – linear strain hardening material model, so that elastic strains are neglected. For our endplate extended region, the elastic strains are negligible by comparison with the inelastic strains so that this is acceptable. In non-dimensional form, the solution of Sherbourne and Lu is given below as Equation 6.28.

$$p = 1 + 4w^2 + \frac{h}{2} \sqrt{2\lambda w(1 + 6w^2) \cdot [\pi + 4(\pi - 4)w^2]} \quad \text{Eqn 6.28}$$

where w is the ratio of central deflection to the endplate thickness = δ_w / t_p

h is the ratio of thickness to half the span length = t_p / l_w

λ is the hardening factor - a measure of the material strain-hardening behaviour

$$\text{and } \lambda = \frac{E_{sh}}{3f_y} = \frac{E}{180f_y} \text{ for our material model.}$$

$p = P/P_0$ and is the ratio of P to the theoretical plastic collapse load P_0

For a simply-supported beam with span L ,

$$P_0 = \frac{4M_p}{L} = \frac{2M_p}{l_w}$$

where M_p is the beam fully plastic moment. In the material model adopted in this thesis, the plastic moment is taken as 0.9 of the theoretical value (moment-

$$\text{curvature relation of Section 6.2), so that } P_0 = \frac{0.9M_{pth}}{l_w} = \frac{0.9m_{pth}b}{l_w} \quad \text{Eqn 6.29}$$

where M_{pth} is the theoretical plastic moment for bending across the entire endplate width, m_{pth} is the theoretical plastic moment per unit width, and b is the endplate width. Only half the endplate is considered here (for one extended region bolt), hence a factor of 0.9 has been used in equation 6.29 rather than 1.8.

In Equation 6.28, the second term represents an amplification of the collapse load due to axial membrane effects, while the third term represents amplification due to strain hardening. For the connections tested in this thesis the effect of strain hardening was to increase the effect of collapse load plus membrane by a factor that was consistently about 25%. Thus, for simplicity, the strain hardening term may be replaced with a multiplier k_{es} where $k_{es} = 1.25$, and the equation becomes:

$$p = k_{es}(1 + 4w^2) = P/P_0 = 2P_x/P_0$$

$$\Rightarrow P_{xs} = \frac{k_{es}}{2} P_0(1 + 4w^2) = \frac{k_{es}}{2} P_0 \left(1 + \frac{4\delta_w^2}{t_p^2}\right) = \frac{k_{es} m_{pth} b}{2.2l_w} \left(1 + \frac{4\delta_w^2}{t_p^2}\right) \quad \text{Eqn 6.30}$$

Equation 6.30 gives the magnitude of the swivel bolt force P_{xs} in our extended region of the endplate.

In order to apply equation 6.30 it is necessary to know δ_w . However, we have found an approximate solution for δ_w in equation 6.27b. Thus, equations 6.27 and 6.30 together provide a solution for the flange force due to bending and membrane action in the endplate extended region, which is to the swivel point. Note that P_{xs} cannot exceed the bolt ultimate capacity F_{ub} since the bolt would fracture first.

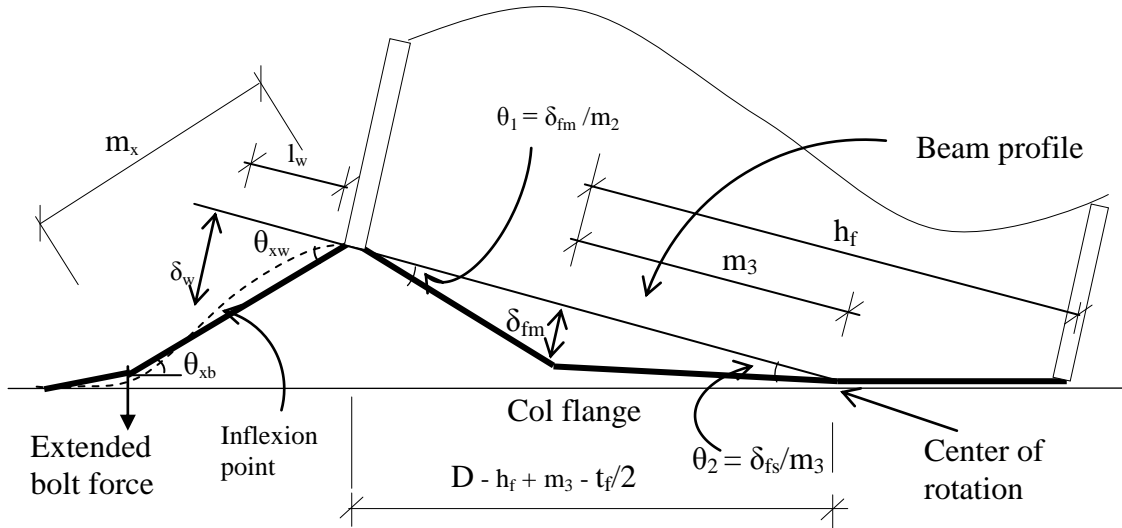


Figure 6.14 – Longitudinal Section through Endplate at Swivel

Bolt force P_{xm} at Maximum Point

The above analysis for the extended bolt force at swivel applies also to the maximum point, except that the beam flange now rotates about the shear bolt level rather than the compression flange centroid. This is shown in Figure 6.14.

The previous equations already defined will still apply, except that the lever arm for beam rotation is no longer D but D' where

$$D' = D - h_f + m_3 - t_f/2$$

$$\text{Then } l_w = m_x \cdot \frac{m_x + D'}{m_x + 2D'} \tag{Eqn 6.27c}$$

$$\text{and } \delta_w = \frac{\theta_{cpm} (m_x + D')^2}{m_x + 2D'} \tag{Eqn 6.27d}$$

Since θ_{cpm} has previously been obtained at the maximum point, equation 6.27d allows us to calculate δ_w at the maximum point. The rest of the analysis is identical to that for the swivel point, and thus

$$P_{\text{xm}} = \frac{k_{\text{es}} m_{\text{pth}} b}{2.2I_w} \left(1 + \frac{4\delta_w^2}{t_p^2} \right) \quad \text{Eqn 6.30a}$$

When this equation was applied to the connection tests in this thesis, the membrane term returned reasonable values, however the strain-hardening term (represented by k_{es}) fluctuated for minor differences in endplate thickness, at the 10mm endplate values. Thus, the k_{es} term appears less well-conditioned at large deflections. The average value for k_{es} at the maximum point was about 1.50. However, due to the large fluctuations and for simplicity, it has conservatively been retained at the swivel value of 1.25.

In setting a practical limit for P_{xm} , cognisance should be taken of the occurrence of prying forces as well, since these are not included in the model.

6.4. AN ENDPLATE DUCTILITY MODEL

6.4.1. The Stress-block Approach

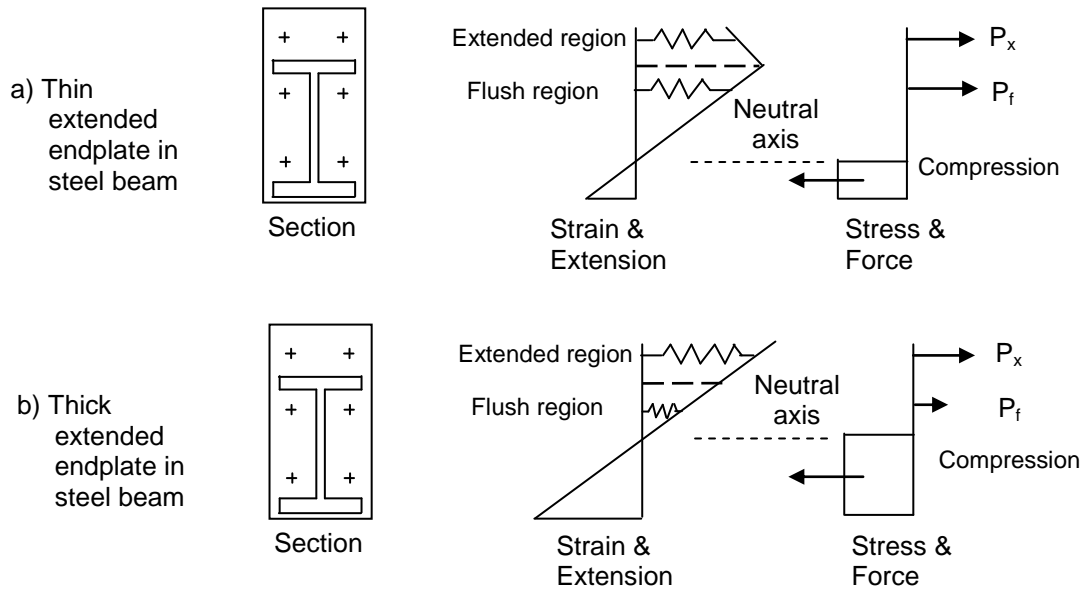


Figure 6.15 – Forces and Stresses across the endplate in the Stress-block approach, based on Brown & Anderson (2001)

The approach taken here to estimating the connection moments at the swivel and maximum points is similar to the stress-block/spring approach of Brown and Anderson (2001) for composite beams, but includes strain-hardening of the endplate and membrane action in the endplate, rather than strain-hardening of the steel section and yielding of the reinforcement as proposed by Brown and Anderson.

In our model the plastic ‘neutral axis’ reflects the level of zero compression strain in the stress blocks of the steel beam adjacent to the connection. In the steel beam and extended endplate assembly, the force components are the tension forces P_f and P_x developed by the tension bolts in deforming the endplate, and the balancing compression forces in the bottom flange and the adjacent web of the steel section. Figure 6.15 illustrates how smaller compression forces are required

for thin extended endplates, and how these compression forces increase as there is an increase in stiffness/thickness of the extended endplate. Along with the progression in increased compression forces, the neutral axis position moves higher.

For the thin endplates considered here, the plastic neutral axis in the beam profile is assumed to be within the compression flange centroid at the swivel point, and at the level of the shear bolts at the maximum point. Thus, the centroid of the area in compression is at the centroid of the beam compression flange at the swivel point, but is halfway between the level of the shear bolts and the external face of the compression flange at the maximum point.

The connection moment is determined from the forces acting on the endplate due to the flush tension and extended region bolts. The effective line of action of force P_x is therefore taken to act at the level of the extended region bolts, while the force P_f is taken to act at the level of the flush tension bolts.

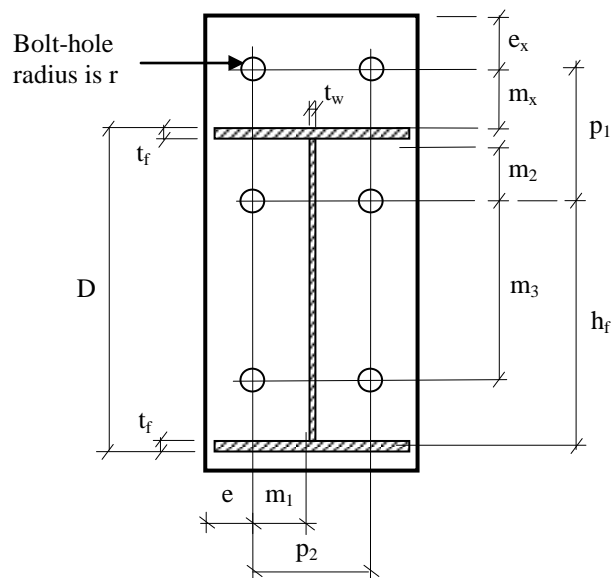


Figure 6.16 – Nomenclature for endplate geometry in ductility model

Thus, once P_f and P_x are determined, the connection moment M can be calculated as:

$$M_{cs} = 2[P_{fs} \cdot h_f + P_{xs} \cdot (h_f + p_1)] \quad \text{at the swivel point} \quad \text{Eqn 6.31}$$

$$\begin{aligned} M_{cm} &= \left[P_{fm} \cdot \left(h_f + m_3 + \frac{t_f}{2} \right) + P_{xm} \cdot \left(h_f + m_3 + \frac{t_f}{2} + 2p_1 \right) \right] \\ &= 2[P_{fm} \cdot h_m + P_{xm} \cdot (h_m + p_1)] \quad \text{at the maximum point} \quad \text{Eqn 6.32} \end{aligned}$$

where h_f , m_3 , p_1 , and t_f are dimensions in the endplate geometry as shown in Figure 6.16, and $h_m = \frac{1}{2}(h_f + m_3 + t_f/2)$. The subscripts s and m refer to the swivel and maximum values respectively.

The ‘swivel point’ in a moment-rotation bi-linear model is where the two lines of the bi-linear approximation intersect, as the connection stiffness reduces from one approximately constant level to a second approximately constant level, in a manner reminiscent of Young’s modulus and the strain-hardening modulus in mild steel. The maximum moment will be determined by imposing a maximum acceptable strain level on the endplate beyond which it is considered that fracture is likely to occur, AND by imposing a maximum bolt force beyond which bolt failure is likely to occur.

6.4.2. A Summary of the Ductility Model

The model is then as follows:

1. At swivel, the flush region swivel bolt force P_{fs} and the swivel connection rotation θ_{cs} are determined from endplate geometry using equations derived in section 6.3 as:

$$P_{fs} = 0.9m_{pth} \cdot \left[\frac{e + m_1}{m_2} + (e - r) \cdot \frac{m_2 + m_3}{m_2 m_3} + \frac{m_2 + m_3}{m_1} + 4 \right] \quad \text{and} \quad \text{Eqn 6.16}$$

$$\theta_{cs} = 1.5P_{fs} \cdot \frac{m_1^2}{Et_p^3 h_f} \quad \text{Eqn 6.20}$$

E refers to Young's modulus, t_p is the endplate thickness and m_{pth} is the theoretical plastic moment for the endplate, per unit length of plate. The other variables describe the endplate geometry.

2. The endplate deflection δ_{fm} at the flush bolt position at maximum point, is:

$$\delta_{fm} = 4.2(a - 2r) \cdot \sqrt{\frac{f_y}{E}} \quad \text{Eqn 6.21}$$

3. The corresponding flush region bolt force P_{fm} and connection rotation θ_{cm} at maximum strain are given by:

$$P_{fm} = P_{fs} + \frac{Et_p^3 \delta_{fm}^3}{7.53a^2} + \frac{Et_p \delta_{fm}^3}{23.4a^2} \quad (\text{but } P_{fm} \leq F_{ub}) \quad \text{Eqn 6.22}$$

where F_{ub} is the bolt ultimate capacity in tension.

$$\text{And } \theta_{cm} = \frac{4}{3} \cdot \frac{\delta_{fm}}{m_3} \quad \text{Eqn 6.25}$$

Note that if $P_{fm} > F_{ub}$ then we need to increase the bolt capacity (bolt size or grade) or reduce the endplate thickness, to avoid the bolt fracture failure mode. Alternatively, if bolt fracture is considered acceptable, then P_{fm} is taken as equal to F_{ub} , and deflection δ_{fm} is obtained by substituting P_{fm} in equation 6.22 and solving by trial and error.

4. At the swivel point, the extended region variables for estimating the region deflection at the beam flange-to-endplate weld are:

$$\delta_w = \frac{\theta_{cs} (m_x + D)^2}{m_x + 2D} \quad \text{and} \quad l_w = m_x \cdot \frac{m_x + D}{(m_x + 2D)} \quad \text{Eqn 6.27a,b}$$

where D is the beam depth and θ_{cs} is the connection rotation at swivel ($\theta_{cps} = \theta_{cs}$). The extended region bolt force acting at the weld line is then calculated for the swivel point from:

$$P_{xs} = \frac{k_{es} m_{pth} b}{2.2l_w} \left(1 + \frac{4\delta_w^2}{t_p^2} \right) \quad \text{Eqn 6.30}$$

where b_p is the endplate width, k_{es} is the strain-hardening multiplier, and $k_{es} = 1.25$.

5. At the maximum point, the extended region variables for estimating the region deflection at the beam flange-to-endplate weld are:

$$\delta_w = \frac{0.75\theta_{cm} (m_x + D')^2}{m_x + 2D'} \quad \text{and} \quad l_w = m_x \cdot \frac{m_x + D'}{(m_x + 2D')} \quad \text{Eqn 6.27c,d}$$

where $D' = D - h_f + m_3 - t_f/2$

and θ_{cm} is the connection rotation at the maximum point ($\theta_{cpm} = 0.75\theta_{cm}$). The extended region bolt force acting at the weld line is then calculated for the maximum point from:

$$P_{xm} = \frac{k_{es} m_{pth} b}{2.2l_w} \left(1 + \frac{4\delta_w^2}{t_p^2} \right) \quad (\text{but } P_{xm} \leq F_{ub}) \quad \text{Eqn 6.30a}$$

with $k_{es} = 1.25$ as before.

Note that where $P_{xm} > F_{ub}$, then we make $P_{xm} = F_{ub}$, which implies extended region bolt fracture as the failure mode. As for the flush bolt; we can increase the bolt size (or reduce the endplate thickness) to avoid this failure mode.

6. The connection moments are then calculated at the swivel and maximum points from equations 6.31 and 6.32:

$$M_{cs} = 2[P_{fs} \cdot h_f + P_{xs} \cdot (h_f + p_1)] \quad \text{at swivel, and}$$

$$M_{cm} = 2[P_{fm} \cdot h_m + P_{xm} \cdot (h_m + p_1)] \quad \text{at maximum strain.}$$

and $h_m = 1/2(h_f + m_3 + t_f/2)$.

7. DISCUSSION OF DUCTILITY MODEL

7.1. JUSTIFICATION OF ASPECTS OF THE DUCTILITY MODEL

7.1.1. Introduction

In the experiments on extended endplate connections carried out as part of this research and reported here, it was found that relatively thin endplates deform considerably under conditions where bolt and weld failure is precluded, leading to high connection rotations. The ductility model developed in Chapter five provides a means of assessing the deformation of ‘thin’ and intermediate endplates, and uses that assessment of deformation to estimate the connection rotation under load.

The model is based on two premises: The first is that even for a ‘thin’ endplate, the scale of endplate thickness to endplate planar dimensions/geometry is such that thick plate effects such as strain hardening cannot be overlooked in endplate deformation. For the connection to be ductile, the endplate deformations must be large and inelastic, and large inelastic rotations require strain hardening of the endplate material. A second premise is that the magnitude of deformation is such that the applied forces will develop significant components in the plane of the endplate, so that the endplate resistance includes membrane action. The underlying philosophy applied is that the connection swivel point is the point at which the flush region yield-lines are fully defined but are just beginning to strain-harden, and the connection maximum point is the point at which the endplate has reached some limiting strain or a bolt has fractured.

7.1.2. The Endplate Yield-line Pattern

The forces acting on the endplate are transferred via the bolts, and in order to understand the endplate deformation we need to calculate the bolt forces. In the

flush region the tension bolt force is calculated using a yield-line approach. The yield-line pattern for the flush region shown in Figure 7.1 is well-established, having been used by Surtees & Mann (1970), Zandonini & Zanon (1988), Bernuzzi & Zandonini (1990), Bernuzzi et al (1991), and Abel & Murray (1992) but with slight differences between these various researchers.

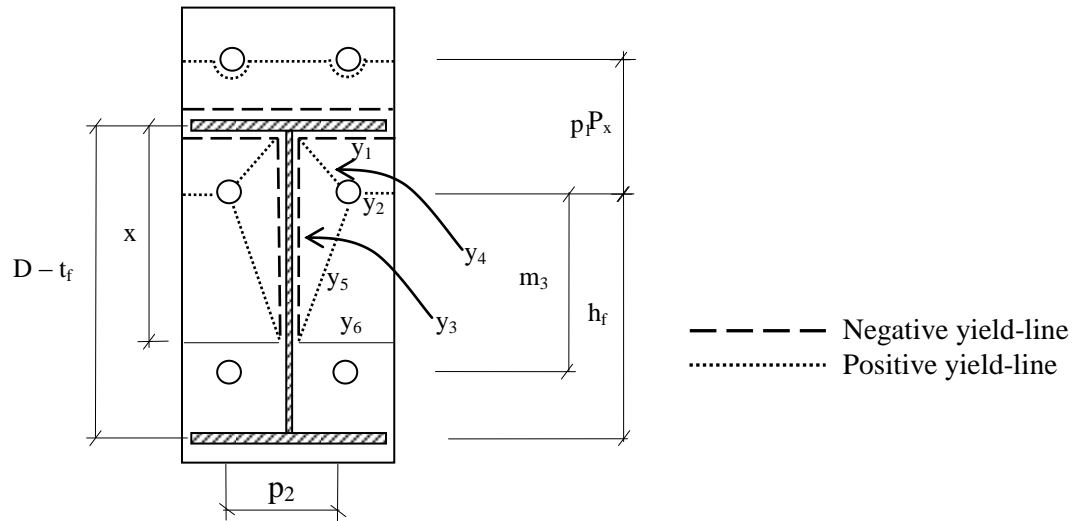


Figure 7.1 – The Governing Yield-line Pattern for the Endplate

In Surtees & Mann’s original yield-line pattern, the line marked ‘ y_6 ’ in Figure 7.1 was not included as a yield line, and the dimension marked ‘ x ’ was taken at half the beam depth so that $x = 0.5(D - t_f)$.

When Zandonini and his colleagues at Trento first applied this yield-line mechanism in Zandonini & Zanon (1988), they introduced an additional yield-line at y_6 and changed the position so that dimension $x = 0.6(D - t_f)$. In their later publication – Bernuzzi & Zandonini (1990) – they kept the yield-line but moved the position to the inside face of the compression flange so that dimension $x = D - 1.5t_f$, where t_f is the flange thickness. In Bernuzzi et al (1991), they again revised the position of y_6 , placing it on the centreline of the shear bolts and making the dimension $x = m_3$.

Abel & Murray (1992) kept the additional yield-line at y_6 but based the position on a minimum energy calculation. Their equation would result in an expression for x such that $x = 0.5p_1 + 0.5(b.p_2)^{0.5}$. For the specimens tested in this thesis, with $D - t_f = 293.6\text{mm}$, $b = 180\text{mm}$, and p_1 and $p_2 = 126\text{mm}$ and 100mm respectively, the Abel & Murray expression would give $x = 130\text{mm}$ i.e. 40mm above the level of the shear bolts – or $x = 0.443(D - t_f)$.

We see then that the location of the dimension x and the presence of a yield-line at y_6 , or not, has been considered differently by previous researchers. In this thesis the position of dimension x was established at m_3 from both the experimental observations and FEA models. I have however gone back to the thinking of Surtees & Mann in excluding a yield-line at position y_6 . This is based on the argument that the endplate segment above y_6 is clamped against the column flange by the tension and shear bolt pre-tension forces, and so is continuous with the portion of endplate between y_6 and the beam compression flange. Thus, the endplate cannot yield at y_6 .

Surtees & Mann correctly made the assumption in their paper that the line y_6 would coincide with the neutral axis in the beam profile. They assessed the neutral axis position by measuring the strain distribution across the beam end. However, their endplates were relatively thick, ranging from $\frac{3}{4}"$ to $1.125"$ (19mm to 28.6mm). Thus, the neutral axis would be higher up in the beam profile than for the thin endplates considered in this thesis. (It should also be borne in mind that yielding in the endplate along its edges may extend further down than the observed neutral axis position, as the neutral axis was estimated based on strain measurements at the beam web only). In this thesis therefore, I have set the dimension x at $x = m_3$, which value is based on my experimental observations for thin endplates. This agrees with the value for x in the last publication of Zandonini and his colleagues (Bernuzzi et al, 1991) on the subject, for endplates of similar thickness.

The Abel and Murray approach is probably a good way of determining the value of x more accurately. However, their formula would need to be corrected to exclude the yield-line they assumed at y_6 . For the thin range of endplates, our approach here was considered sufficiently accurate.

7.1.3. The Deflection of the Flush Region

In order to determine the flush region deformation at the bolt position, we used square plate deflection formulae taken from Roark (1965). Roark attributed the formulae to Sturm & Moore (1937).

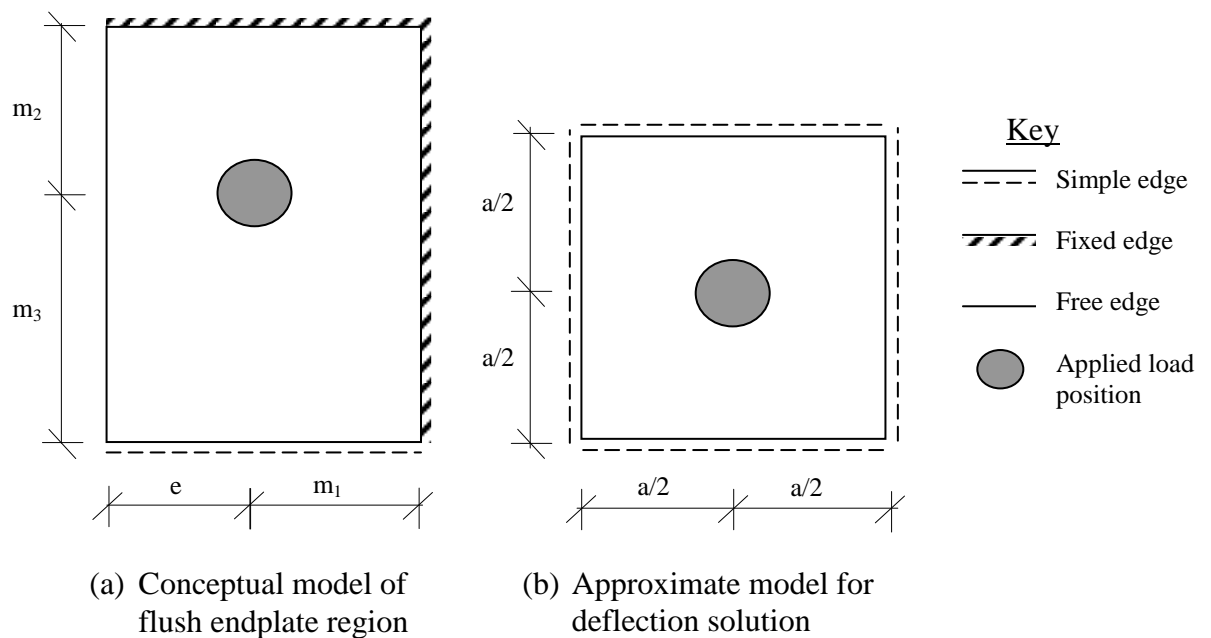


Figure 7.2 – Square plate model for flush region deflection

Each half of the flush region of the endplate is conceptualised as a rectangular plate with a concentrated load due to the bolt force, and with fixed supports on the adjacent edges where it is bordered by the beam web and flange. The third ‘edge’ is at a line through the shear bolts, and that edge is simply-supported since the moment there is negligible. The fourth edge is free. To apply Roark’s formula we

approximate the flush region into a square plate with all four sides simply-supported and with sides ' a ' = $2m_1$. The assumption of simple supports where the flush region is actually 'fixed' is compensated for in part by the use of a simple support where the flush region edge is really free. It is further justified by the fact that our definitions of the connection swivel and maximum points require the fixed supports to be fully yielded anyway, so that they are no longer 'fixed'. The approximation is illustrated in Figure 6.9 reproduced here as Figure 7.2.

To ensure that the square plate approximation of Figure 7.2 (b) leads to similar deformations as the actual rectangular flush plate behaviour of Figure 7.2 (a), the square plate has been empirically 'calibrated' using FE analysis.

FEA calibration procedure

In the FEA calibration of the square plate, FEA models of Figure 7.2 (a) and Figure 7.2 (b) were prepared for the endplate geometry tested in this thesis, for the 10mm, 12mm and 14mm endplate tests. Loads were then applied to each model as a pressure over the bolt-hole area, to simulate the flush bolt force at swivel and maximum strain points.

In the development of the ductility model, in order to apply Roark's square plate formulae at the maximum point, we treated the deformation of the flush region as consisting of two consecutive steps – a first step up to the swivel point in which the deformations are mostly elastic within the flush region but become inelastic on the boundaries. Then a second step in which the yielding has spread over wide bands with attendant strain hardening, so that most of the endplate is now resisting loads inelastically. This implies a bi-linear model of the endplate stress-strain relationship with a slope of E up to yield, and a slope of E_{sh} after yield. In the FEA calibration models therefore, the square plate is tested in two load steps as per the derived equations with a different material model for each step. In the first step up to swivel, the material model is linear elastic with a stress-strain slope of E (elastic Young's Modulus). In the second step from swivel to the maximum point, the material model is again linear elastic but with a stress-strain slope of E_{sh}

(Strain-hardening Modulus assumed to be $E_{sh} = E/60$). Thus, the deflection observed in the second FEA step is taken as the increment in deflection from swivel to the maximum strain point. This agrees exactly with our approach to deriving Equations 6.21 and 6.22 in Section 6.3.2.

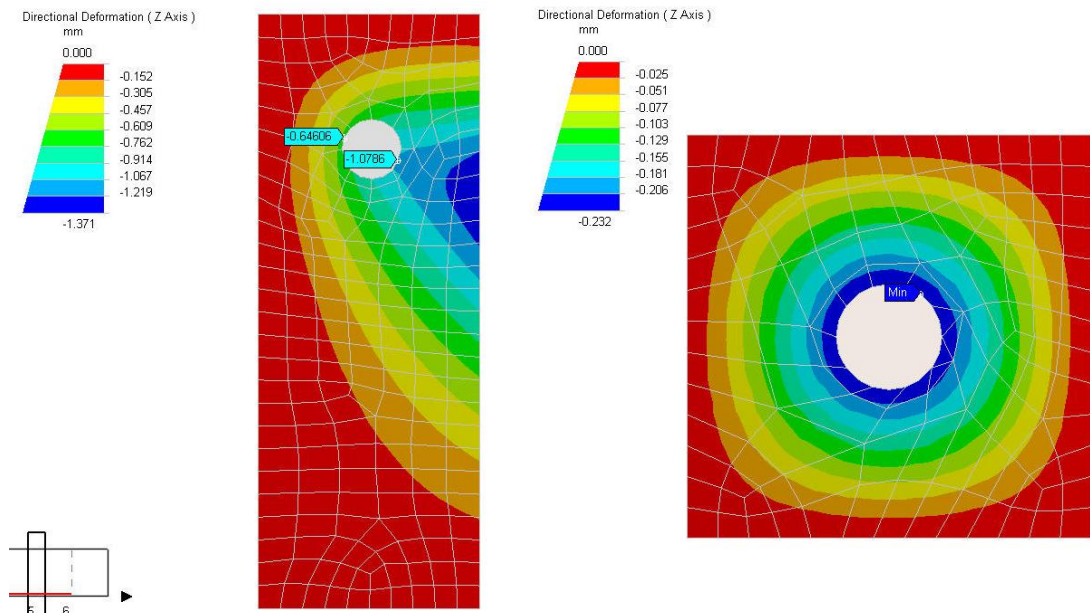
By contrast, the FEA rectangular plate deflection models are based on a full bi-linear endplate material model, with the same material model used at both swivel and maximum load points. The slope of the strain-hardening portion will not achieve the same ultimate strain at the maximum stress as would be achieved with the experimental tri-linear material models of Chapter Three. However it should lead to a better estimate of the deflection. In Table 7.1, these bi-linear material models are presented along with the linear elastic models used for the square plate FEA models.

Table 7.1 – Material Properties for FEA Deflection Models

	Bi-linear Model for Rectangular Plates			Linear elastic models for Square Plates	
	Young's Modulus GPa	True Yield Strain 10^{-3}	Strain Hard'g Modulus GPa	Young's Modulus (deflection at Swivel) GPa	Strain Hard'g Modulus (Swivel to Max increment) GPa
10mm plate (Test 1)	202.20	1.637	3.37	202.20	3.37
12mm plate (Test 2)	219.10	1.396	3.65	219.10	3.65
14mm plate (Test 3)	213.00	1.384	3.55	213.00	3.55

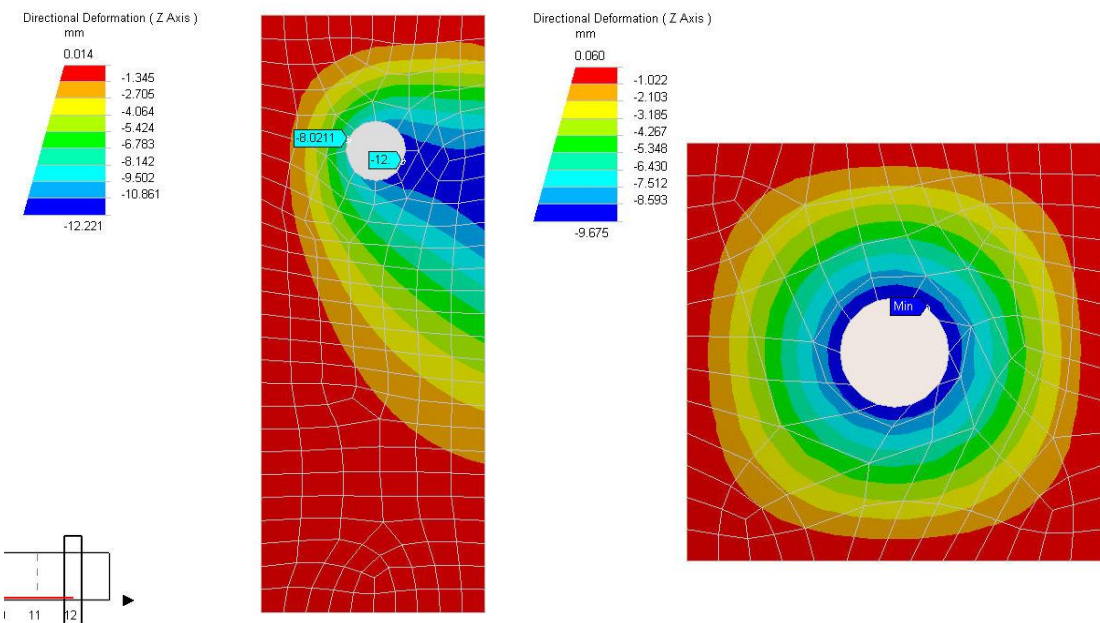
In the FEA models the swivel bolt force was based on the measured values in the test data, while the maximum strain bolt force was taken as the ultimate bolt force F_{ub} . The deflection on the bolt load annulus was then measured at each of the two bolt force levels, for both the rectangular and the square plates. In order to confirm the swivel bolt force, the load was applied in uniform steps from zero to

F_{ub} and a graph of load versus deflection was plotted. Thus, we could confirm the swivel point for the flush region deflection.



(a) 10mm rectangular plate deflection at swivel

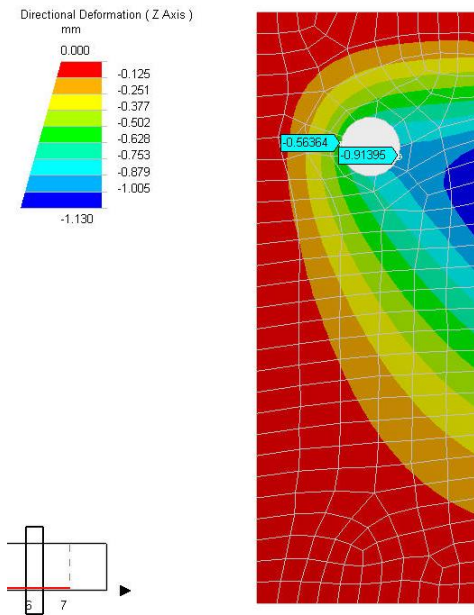
(b) 10mm square plate deflection at swivel



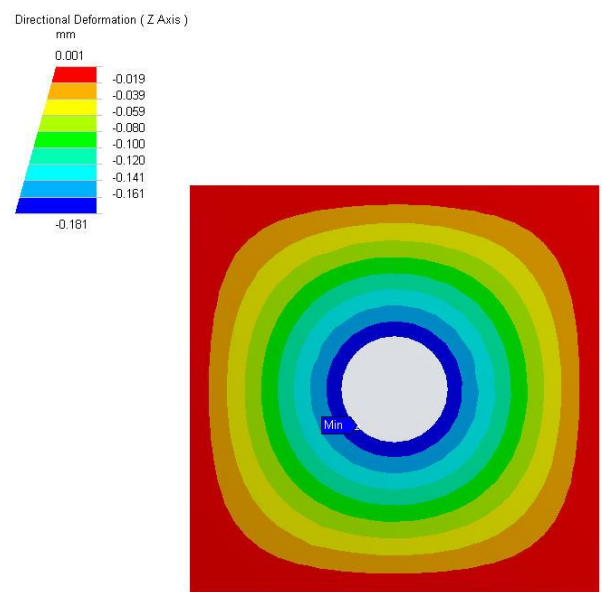
(c) 10mm rectangular plate deflection at maximum point

(d) 10mm square plate deflection at maximum point

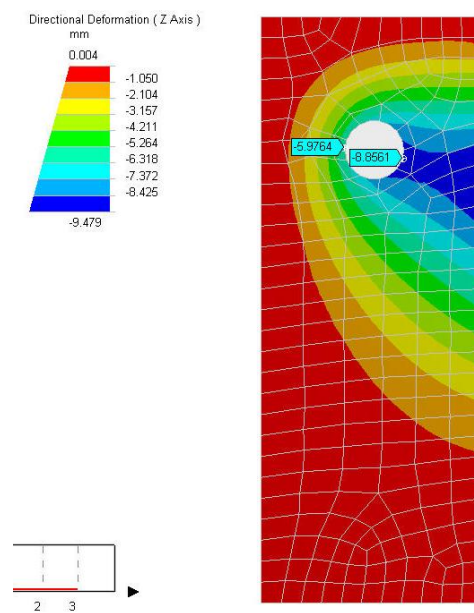
Figure 7.3 – Deflections for 10mm rectangular and square plate models



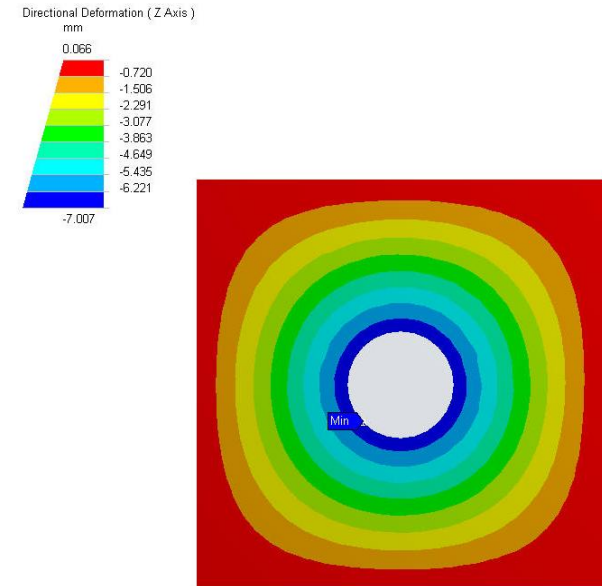
(a) 12mm rectangular plate deflection at swivel



(b) 12mm square plate deflection at swivel

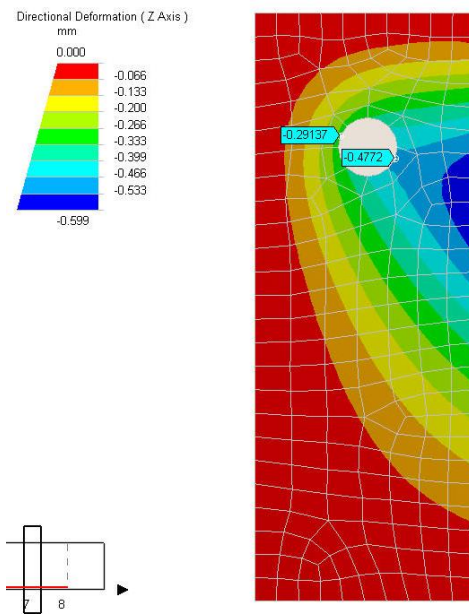


(c) 12mm rectangular plate deflection at maximum point

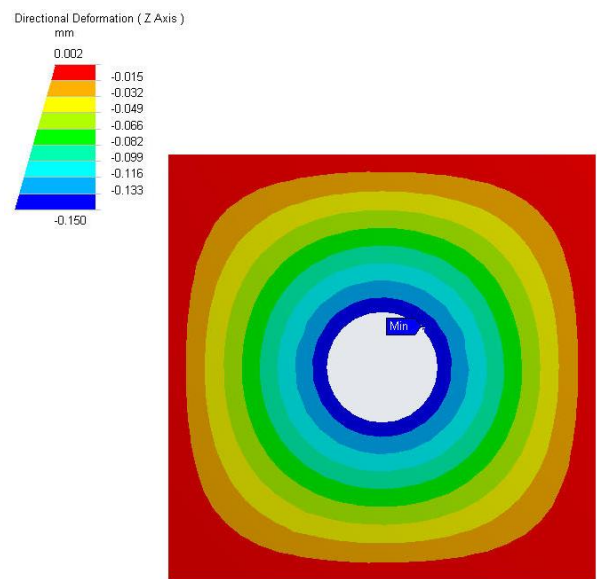


(d) 12mm square plate deflection at maximum point

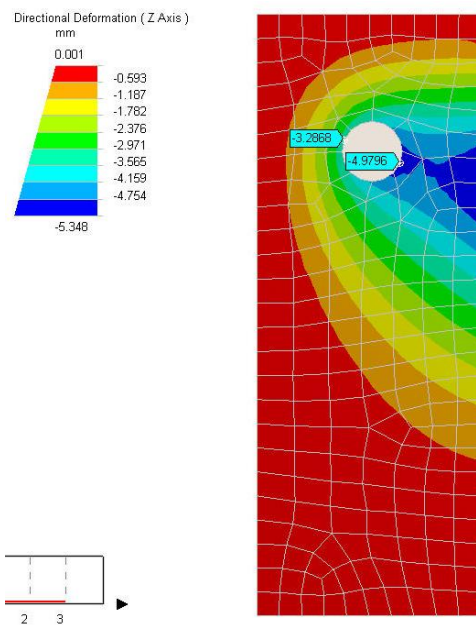
Figure 7.4 – Deflections for 12mm rectangular and square plate models



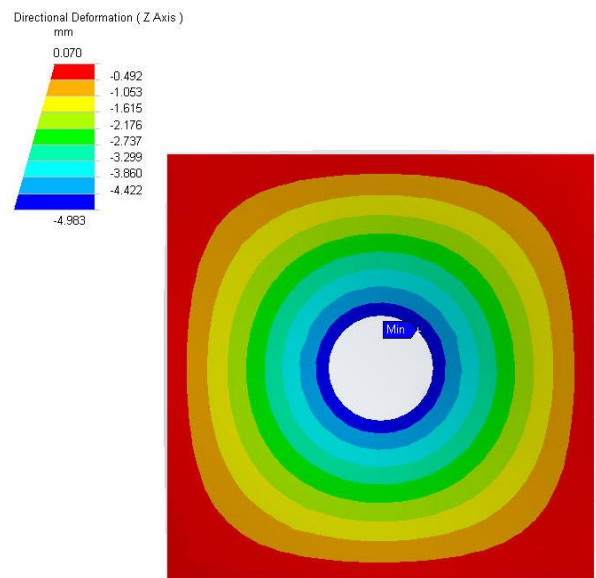
(a) 14mm rectangular plate deflection at swivel



(b) 14mm square plate deflection at swivel



(c) 14mm rectangular plate deflection at maximum point



(d) 14mm square plate deflection at maximum point

Figure 7.5 – Deflections for 14mm rectangular and square plate models

Figures 7.3, 7.4 and 7.5 show the deflection patterns for each endplate thickness, for both the rectangular and square plates. For the rectangular plates the bolt holes slope under load at an angle of approximately 45 degrees to the vertical edges. Thus, the deflection was measured at two positions – the maximum and minimum deflections on the bolt hole perimeter – and the average was taken for each load case. The measured deflections are summarised in Table 7.2.

Table 7.2 – Deflections Measured for Rectangular and Square Plate FEA Models

	Assumed Bolt Force	Rectangular Plate Model			Square Plate Model		Ratio of rectangle to square deflectn
		Min deflectn	Max deflectn	Average deflectn	Deflectn	Swivel to Max Increment	
	kN	mm	mm	mm	mm	mm	
10mm Swivel	95	0.646	1.079	0.862	0.232		3.71
10mm Max	228	8.021	12.000	10.011	9.907	9.675	1.01
12mm Swivel	114	0.564	0.914	0.739	0.181		4.08
12mm Max	228	5.976	8.856	7.416	7.188	7.007	1.03
14mm Swivel	133	0.291	0.477	0.384	0.150		2.56
14mm Max	228	3.287	4.980	4.133	5.133	4.983	0.81
Average at Swivel Point							3.45
Average at Maximum Point							0.95

The results in Table 7.2 show that the deflection of a simply-supported square plate, with sides $2m_1$, gives a reasonable approximation to the deflection of the endplate flush region, if the square plate deflection at swivel is multiplied by 3. This is based on the assumptions about material behaviour i.e. elasticity modulus of E before swivel, and modulus of E_{sh} for increment from swivel to max.

In reality, a neat partition between the case where the plate is inelastic only at boundaries, and the case where the plate is inelastic on most of the surface, is unlikely. It is however, a convenient abstraction to deal with the complex reality.

7.1.4. The Beam End and Bolt Contributions to Connection Rotation

The model developed provides an accurate representation of the connection strength – swivel and maximum moments – but only models the endplate contribution to the connection rotation. The other components that could contribute significantly to the connection rotation are the beam end and the tension bolts. The beam end refers to that portion of the beam adjacent to the endplate up to a distance of a beam depth, and this portion is part of the connection as defined in this thesis. It contributes to the connection rotation through elastic and inelastic rotation, along with local buckling of the compression flange. The tension bolts contribute through their extension, particularly the extension of the flush bolts. Deformation of the column flange could also contribute significantly, but this thesis is limited to the case where the column flange is relatively thick or is stiffened.

Table 7.3 – Relative Contributions of Connection Components to Maximum Rotation, in Bernuzzi et al (1991)

Test ID		Contributing component						Total
		Endplate		Bolts		Beam end		Rotn
		m-rads	%age	m-rads	%age	m-rads	%age	m-rads
EP1-1	12.0 mm E/plate	75	75	5	5	20	20	100
EP1-2	15.6 mm E/plate	39	42	7	7	48	51	94

In Bernuzzi et al (1991), they tested 15mm and 12mm endplate connections with similar geometry to that adopted here, and distinguished the contributions of the beam end, the endplate and the bolt extension. From their graphical results, the

relative contributions of the three components are as given in Table 7.3. These values are measured off their graphs, but are reasonably accurate.

We see that the joint contribution of the beam end and bolts in the Bernuzzi et al tests was 25% of the total for their 12mm test, or 33% of the endplate contribution. Similarly, in their 15mm test the beam end and bolts contributed 56% of the total or 133% of the endplate contribution. The 12mm value is taken as an 'average' thickness value for a thin endplate. Thus, in order to reflect the beam end and bolt contributions, the endplate model values are multiplied by a factor of 1.33 or $4/3$. This factor is empirical and so it applies best to connections with similar beam and bolt sizes and material characteristics, to those tested in Bernuzzi et al (1991). There is a need for further work to quantify this factor better, especially in relation to the beam end contribution.

7.2. PARAMETERS INFLUENCING ENDPLATE BEHAVIOUR

In Adegoke & Kemp (2006), we reported on the parameters seen to influence the modes of failure, ultimate moments, and end rotations at maximum moment:

These are listed below as follows:

- *Endplate thickness & neutral axis height*

The thicker the endplate, the larger the flush (and extended) tension force that is required to develop the endplate mechanism. For a given beam section size therefore, the larger compression force required for equilibrium in a ‘thick’ plate causes the plastic neutral axis to move higher into the beam web. Once the neutral axis is significantly higher than the level of the shear bolts the compression zone begins to inhibit the development of the yield-line mechanism above the neutral axis.

However, the endplate mechanism has to develop sufficiently for inelastic redistribution of forces, or else the flush bolts could fracture prematurely. A thick endplate in this context then is one in which the level of the neutral axis moves significantly higher than the level of the shear bolts before the yield-line mechanism is fully developed. The calculated flush bolt force at swivel P_{fs} would then exceed the ultimate bolt capacity F_{ub} . The ductility model in this thesis is applicable to ‘thin’ endplates only, for which $P_{fs} < F_{ub}$.

- *Yielded length of beam adjacent to end connection*

Good ductility and large connection rotations require an extended length of yielding in the steel beam compression flange. If the elastic moment at onset of beam yielding, M_e , is significantly less than the observed maximum beam moment, M_u , inelastic curvature will occur over a longer length of beam adjacent to the connection. The yielded length of beam is directly proportional to the extent of local buckling observed. For the connections tested in this thesis, yielding of the beam compression flange initiated at between $0.45M_p$ to

$0.55M_p$ (see section 4.5). Adegoke and Kemp (2006) recommended that the ratio, M_e/M_u , should be less than 0.8. Assuming M_u to be about $1.1M_p$, the ratio M_e/M_p , should then be less than say 0.85.

- *Local buckling*

For a given endplate thickness, limited local buckling of the compression flange and adjacent web of the steel section, together with a large zone of yielding, is required to move the neutral axis up into the web to the level of the shear bolts. This is the ideal neutral axis position for the development of the yield-line mechanism assumed in this thesis. Thus, some local buckling in the compression flange is desirable prior to connection failure, as long as the beam continues to sustain the load. The connection must be a partial strength connection for inelastic local buckling of the compression flange to take place. A ‘pinned’ connection would not cause the beam to yield.

To achieve large inelastic rotations at maximum moment, Kemp et al (1995) recommended an upper limit to the plastic neutral axis, and proper evaluation of lateral buckling in cases of long negative moment regions (pattern loading).

- *The size of the tension bolts*

The thickness of an endplate is also relative to the size of the bolts, as the flush tension bolts must be strong enough to restrain the endplate and develop the yield-line mechanism. Otherwise the flush tension bolts would fracture before the neutral axis has moved high enough to the level of the shear bolts. The rule-of-thumb given in Eurocode 3 (Eurocode 3, 2005) is that the endplate thickness t_p should not exceed $0.36d (f_{ub}/f_y)^{0.5}$, in order for the plate to behave as ‘thin’. d and f_{ub} are the bolt diameter and ultimate strength respectively. For the connection tests in this thesis, with bolts standardized at M20 Grade 8.8 HSF8 (average measured f_{ub} in tests was 788 MPa), and Grade 300W steel (average measured f_y of 311 MPa), this would impose an upper limit of 11,5mm on the endplate thickness. The corresponding limit for M24 bolts with the same value for f_{ub} would be 13,8mm. With Grade 350W steel at a nominal

f_y of 350 MPa and nominal f_{ub} of 800 MPa, the limits for t_p decrease to 10,9mm and 13,1mm respectively. The test 2 and 3 results in this thesis show that these values are conservative as those connections were all ductile (rotation $> 30 \times 10^{-3}$ radians). There is a need to investigate further to establish a better limit.

- *The degree of bolt pretension*

An unexpected result from the connection tests was the observation that not only the initial stiffness, but also the ductility, is affected by the bolt pretension. Surtees and Mann (1970) investigated the effect of different degrees of bolt pretension on the connection stiffness in the working range (up to $0.6M_p$), and found that there was no change from hand-tight to one-third pretension. The stiffness typically increased by about 50% at two-thirds pretension and 100% at full pretension. There is a need for further work to investigate the effect of pretension on the connection ductility. However, bolt pretensions are difficult to establish and guarantee in practical steel erection conditions.

- *Endplate Geometry*

In order to ensure that the connection initial stiffness is high, the bolt spacing around the beam tension flange must be as compact as possible i.e. endplate geometry parameters m_1 and m_2 should be kept to a minimum. The steel industry in South Africa has standardized on bolt pitch and gauge for a given bolt diameter for shear connections, but not for moment connections. There is a need for further work to recommend specific values for bolt and pitch that take the ductility model in this thesis into consideration.

The effect of the column flange was not investigated in this thesis, but in experiments reported here, stiffeners were provided across the column flanges at the beam flange levels. The column flange must be at least as strong as the endplate in order for the endplate yield-line mechanism to develop, or a column yield-line mechanism would develop instead. There would also be a

need to prevent column web buckling. A useful approach would be to limit the endplate thickness to some fraction of the column flange thickness when the column is not stiffened. For values of bolt pitch and gauge for the flush and extended bolts similar to those used in the tests in this thesis (pitch of 126mm and gauge of 100mm), a suggested value might be to limit the endplate thickness t_p to 0.6 times the column flange thickness if the connection is unstiffened, and to 0.9 times the column flange thickness if the connection is stiffened.

As already discussed above, the thickness of the plate must be limited relative to the beam section as well, so the neutral axis does not move too high above the shear bolt level. The bolt diameter must also be chosen so that the bolts can restrain the stiffer endplate flush region.

- *Prying of the Extended Region Bolts*

The bolt force P_x calculated for the extended region bolts does not include an allowance for prying. Thus, to ensure that bolt fracture does not occur, one could consider that the bolt force should be limited to some fraction of the bolt ultimate capacity F_{ub} . For example, if we adopted the recommendation of Surtees & Mann (1970) to assume prying forces as 30% of the total extended bolt force, we would need to limit P_x to about $0.77F_{ub}$. However, it should be borne in mind that prying forces are small at the high connection load levels approaching failure in a well-proportioned thin endplate (see for example Bernuzzi et al, 1991). Thus, this refinement is not considered necessary in the ductility model presented here.

7.3. DUCTILITY MODEL COMPARISON WITH THE THESIS EXPERIMENTS

Table 7.4 summarizes the endplate geometric variables required to apply the ductility model developed in chapter five for the specimens tested in this thesis. For ease of reference, the nomenclature is repeated in Figure 7.6.

Table 7.4 – Connection Test Endplate Geometry for the Ductility Model

MEASURED VARIABLES			Test 1	Test 2	Test 3
Endplate geometry (430 x 180 endplate)	t_p	mm	10.24	11.83	13.86
	m_1	mm	42.08	42.26	42.26
	m_2	mm	49.91	50.03	50.03
	m_3	mm	170	170	170
	m_x	mm	49.9	50.0	50.0
	h_f	mm	230.6	230.6	230.6
	e	mm	40	40	40
	p_1	mm	126	126	126
	b_p	mm	180	180	180
	r	mm	11	11	11
Endplate material	f_y	MPa	331.3	306.0	295.0
	E	GPa	202.2	219.1	213.0
Bolt material (M20 Gr 8.8 HSF)	F_{ub}	kN	238.3	239.5	229.9
Beam variables (305 UB 41 beam)	D	mm	303.8	303.8	303.8
	M_p	kN-m	209.0	203.4	203.4

The endplate geometry variables tabulated in Table 7.4 are based on the actual measured values for the connection rather than nominal values. The exceptions are the bolt ultimate capacities F_{ub} , which are based on the bolt test results of section 3.3. The actual connection bolts obviously could not be tested to destruction.

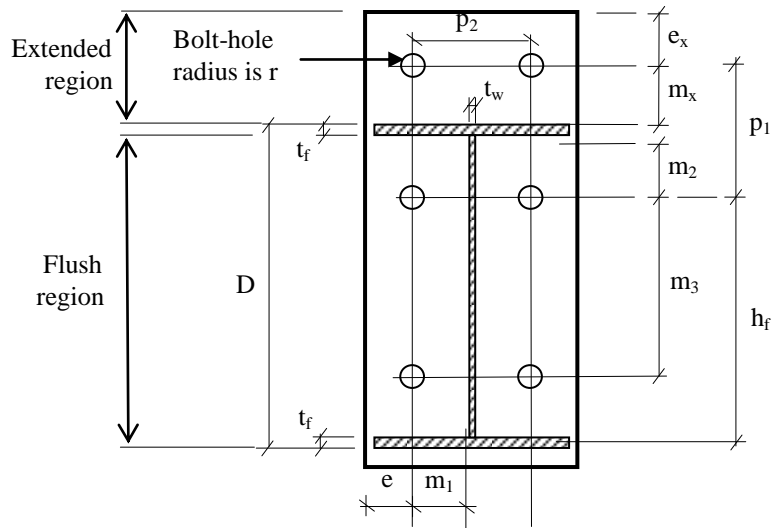


Figure 7.6 – Nomenclature for endplate geometry in ductility model

Table 7.5 – Results of the Ductility Model for the Connection Tests

MODEL RESULTS			Test 1	Test 2	Test 3
Swivel flush bolt force	P_{fs} - Eqn 6.16	kN	90.84	111.79	147.93
Swivel connection rotation	θ_{cs} - Eqn 6.20	mrads	4.81	3.57	3.03
Flush bolt deflection at max	δ_{fm} - Eqn 6.21	mm	10.57	9.81	7.90
Max point flush bolt force	P_{fm} - Eqn 6.22	kN	148.60	192.61	240.00*
Max connection rotation	θ_{cm} - Eqn 6.25	mrads	82.88	76.69	62.00
Swivel extended bolt force	P_{xs} - Eqn 6.30	kN	33.81	40.83	53.69
Max extended bolt force	P_{xm} - Eqn 6.30a	kN	149.90	133.21	110.97
Swivel connection moment	M_s - Eqn 6.31	kN-m	67.35	82.32	108.69
Max connection moment	M_m - Eqn 6.32	kN-m	158.97	165.85	170.46
Failure Component			Endplate	Endplate	Flush bolt

*This is the bolt ultimate capacity value.

The results of the ductility model for the connection test specimens are given in Table 7.5. The predicted failure mode for tests 1 and 2 is endplate fracture. This

agrees with the experimental observations for test1 where beam 10B failed in mode 1 at 158 kN-m. It is also in agreement with the experimental result for test 2 where beam 12A failed in mode 1 at 154.5 kN-m. The predicted failure mode for test 3 is endplate yield + eventual bolt fracture (mode 2 of SCI, 1995 and Eurocode 3, 2005). This was again the observed failure mode for beam 14B which failed at 181.6 kN-m.

Table 7.6 – Comparison between Ductility Model and Connection Test Results

Test	Failed Connection	Experiment results			Thesis ductility model		
		M_u kN-m	θ_u 10^{-3} rad	Failure Mode	M_m/M_u	θ_{cm}/θ_u	Failure Mode
Test 1	Beam 10B	158.1	100	Endplate	1.01	0.83	Endplate
Test 2	Beam 12A	154.5	67	Endplate	1.07	1.14	Endplate
Test 3	Beam 14B	181.6	80	Endplate + flush bolt	0.94	0.78	Endplate + flush bolt

Table 7.6 gives a comparison between the key experimental values from the connection tests, for those connections that actually failed (10B, 12A and 14B), and the model results. The ratios show that the model predictions for ultimate capacity are within 7% of the experimental values. The maximum rotations are conservative except for the 12mm endplate of test 2.

In Figures 7.7 to 7.9 the ductility model results are superimposed onto the experimental moment-rotation curves for connection tests 1, 2 and 3. The connection moments in those figures are normalized by the beam M_p .

Figures 7.7 – 7.9 show that there is a good agreement between the ductility model and the experimental results in terms of the swivel and maximum rotations, and also in terms of the swivel and maximum moments. The rotation for test 1 is an underestimate when compared with 10B that failed, but gives a good prediction for 10A. Thus, the model prediction is slightly conservative for test 1. In Figure 7.8, the model appears to overestimate the rotation for 12A that failed. We note however that 12B did continue to resist the connection moment to a larger rotation than 12A. Thus, the overestimate is not as significant as it first appears. From all indications, 12A appears to have failed prematurely. The ductility model results are again slightly conservative for test 3.

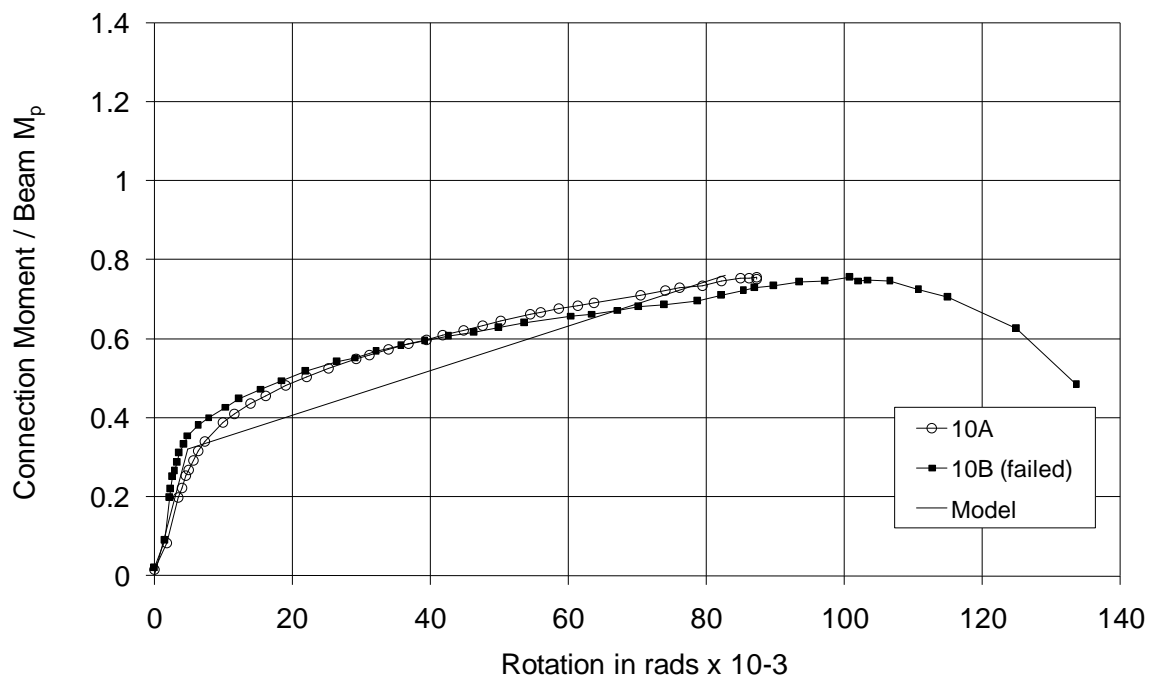


Figure 7.7 – Ductility Model Results for Connection Test 1

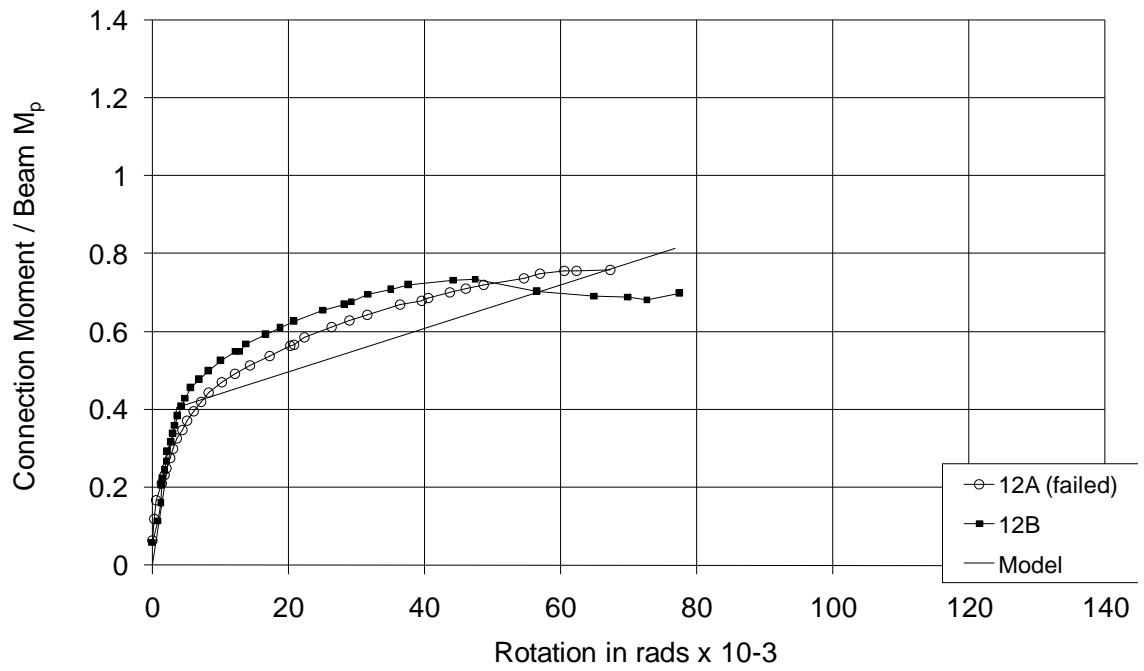


Figure 7.8 – Ductility Model Results for Connection Test 2

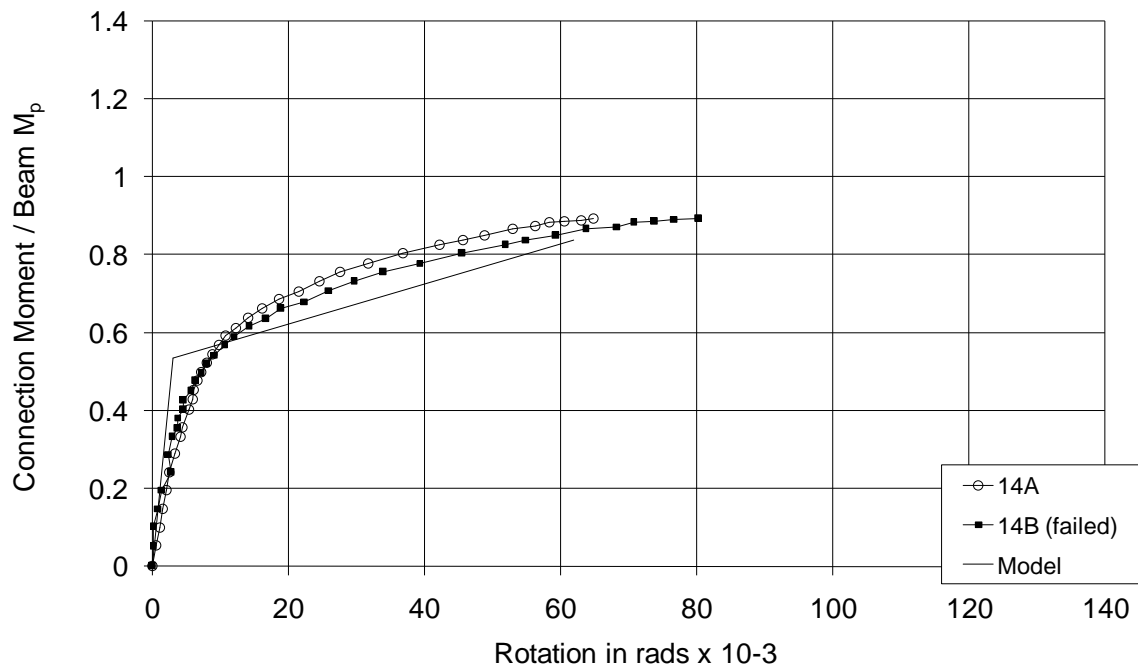


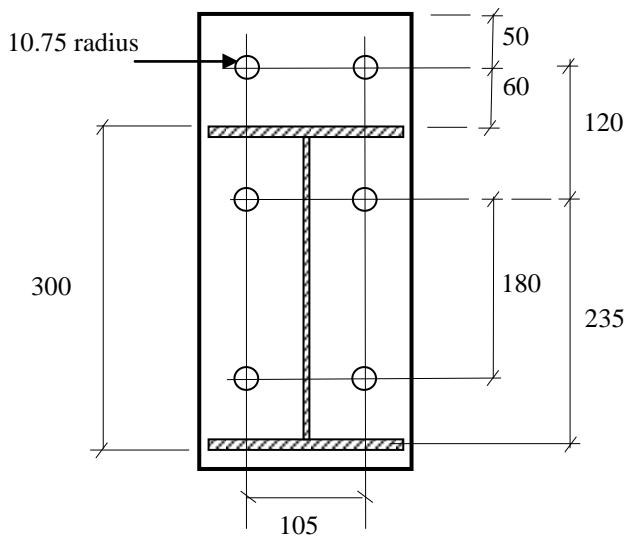
Figure 7.9 – Ductility Model Results for Connection Test 3

7.4. MODEL COMPARISON WITH PUBLISHED TEST RESULTS

7.4.1. Comparison with Test Results from Bernuzzi et al (1991)

Bernuzzi et al (1991) and Zandonini & Zanon (1988) reported results from five connection tests on endplates extended on one side as in this thesis, with varying thickness. The key geometric parameters for the connections tested by Bernuzzi et al are given in Figure 7.10.

Their tests were single sided, but with the endplate connected to a ‘counter-beam’ rather than a column. This counter-beam was attached to a strong floor along its entire length. Thus, there was no panel shear or column rotation. The ‘column’ effectively behaved like an internal column with equal moments on either side, as in the connection tests reported here in this thesis. The counter-beam was stiffened at intervals so there was also no risk of web yielding or buckling.



Endplate:	420 long x 180 wide		
Beam:	IPE 300 – single-side test		
Column:	Counter-beam		
Bolts:	6 ~ M20 Grade 8.8		
	Endplate t_p (mm)	Endplate f_y (MPa)	Bolt F_{ub} (kN)
Test EP 1-1	12.0	321.0	261
Test EP 1-2	15.6	300.0	261
Test EP 1-3	18.6	292.0	261
Test EP 1-4	21.8	221.0	261
Test EP 1-5	25.7	210.7	261

All dimensions in mm

Figure 7.10 – Endplate Geometry in Bernuzzi et al (1991)

In order to apply the ductility model, I have assumed 8mm fillet welds at the beam flange, and 6mm welds at the web. I have also assumed nominal values for the endplate modulus of elasticity (E), the bolt area and the beam depth (D).

The model results are plotted against the experimental moment-rotation curves in Figures 7.11 and 7.12 for test EP 1-1 (12mm endplate) and EP 1-2 (15mm endplate) respectively. We see that the model gives good results for the 12mm endplate and reasonable results for the 15mm endplate. For test EP 1-1, the ductility model predicts failure due to endplate yielding and eventual fracture (mode 1 of Eurocode 3, 2005), while for test EP 1-2, the predicted failure mode is fracture of the flush bolt after extensive endplate yielding (mode 2 of Eurocode 3, 2005). The difference in rotation at maximum point in the 15m test is mainly because the ductility model underestimates the beam end contribution for the thicker endplates.

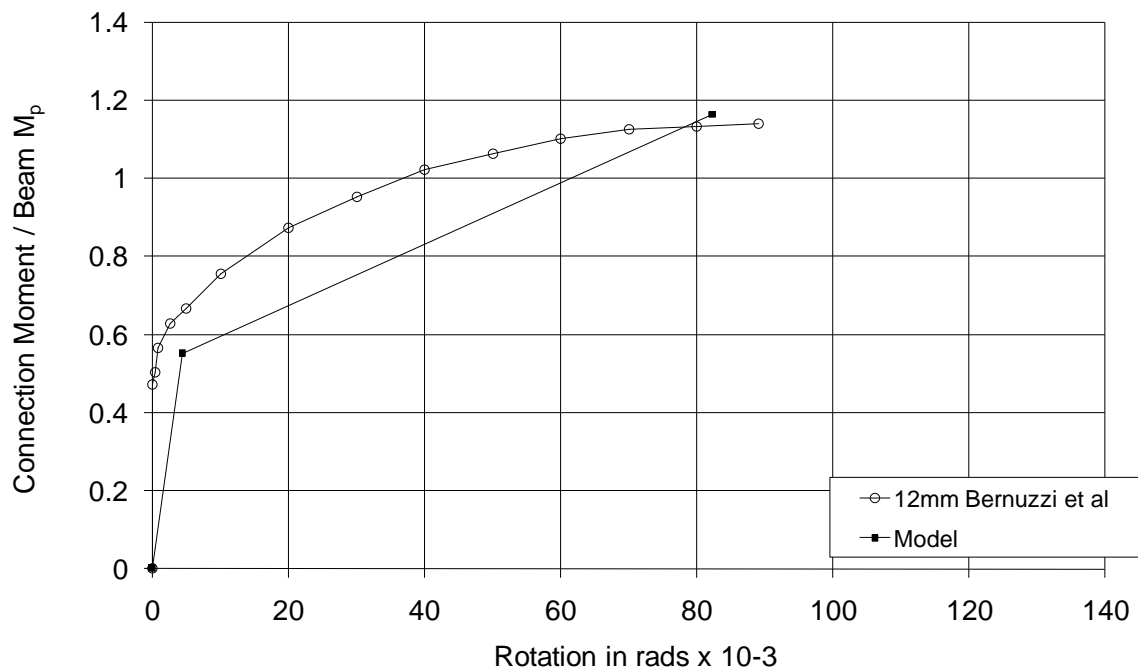


Figure 7.11 – Comparison of Ductility Model with Test EP 1-1 of Bernuzzi et al, 1991

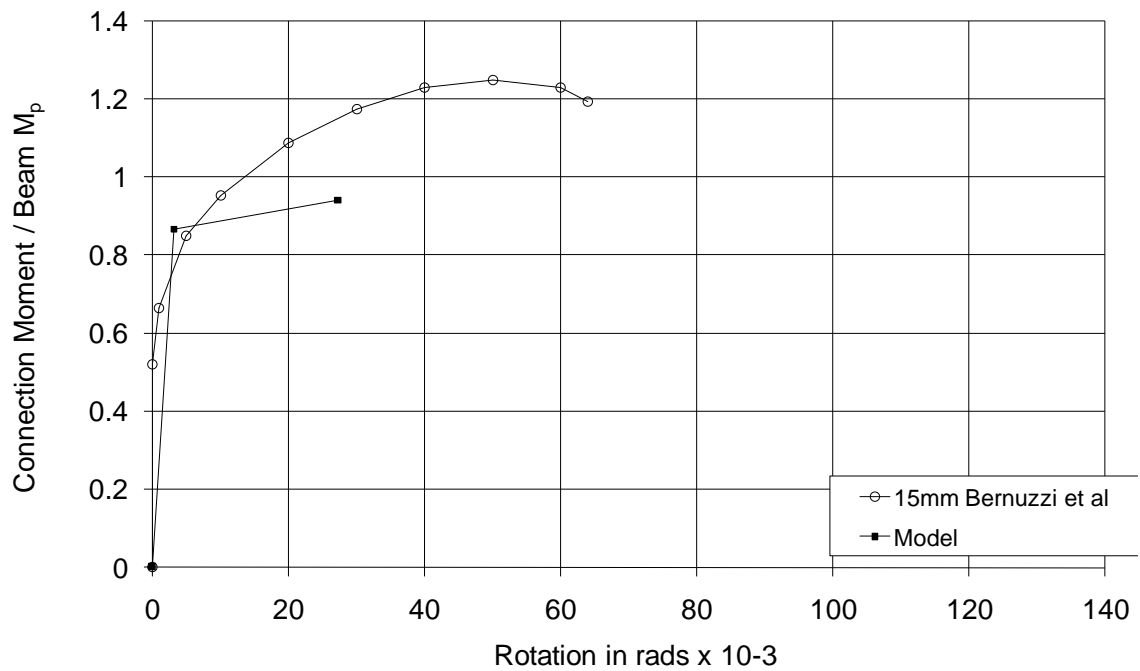


Figure 7.12 – Comparison of Ductility Model with Test EP 1-2 of Bernuzzi et al, 1991

For tests EP 1-3 (18mm endplate), EP 1-4 (22mm endplate) and EP 1-5 (25mm endplate), the ductility model predicted fracture of the flush bolt *before* the flush region is fully yielded. In other words the endplate is ‘thick’. (This would correspond to mode 3 of Eurocode 3, 2005). Thus, it is possible to estimate an ultimate connection moment from the model (from $P_{fs} = F_{ub}$ and calculating the corresponding value of P_{xs}), but not to predict rotations or a moment-rotation curve. The predicted ultimate moments for those three tests are included in the next section.

7.4.2. Comparison of Ductility Model with Eurocode 3 Model Predictions

In Table 7.7, a comparison is made between the predictions of the ductility model in this thesis, and the models of SCI (1995) and Eurocode 3 (2005). This

comparison is made for the connection tests in this thesis, but also for the published test results of Bernuzzi et al.

The difference between the models of SCI (1995) and Eurocode 3 (2005) is that Eurocode 3 provides an alternative formula for calculating the mode 1 bolt forces, along with the original formula given in SCI (1995). This alternative typically leads to higher bolt forces. In Table 7.7, the maximum moments predicted using the SCI and the Eurocode 3 models are presented as ratios of the experimental measured moments. The SCI model is calculated using the original formula for mode 1 while the Eurocode 3 model is calculated with the alternative formula.

Table 7.7 – Comparison between Ductility Model and Eurocode 3 Model Predictions

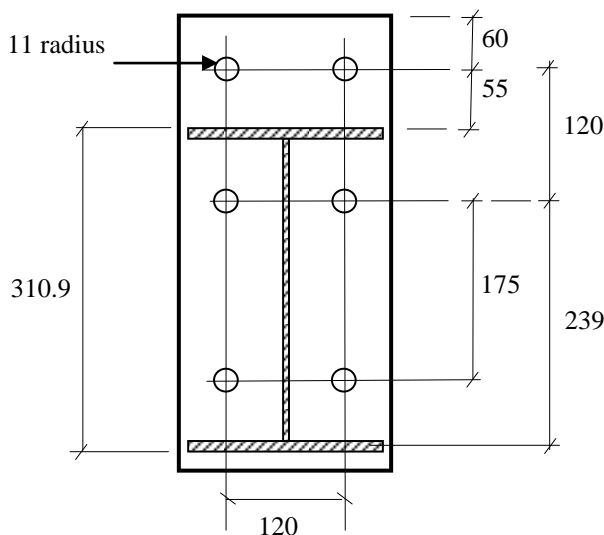
Nominal endplate thickness	Ref.	Experiment results		Thesis ductility model			SCI (1995) model		Eurocode 3 model
		M_u kN-m	θ_u 10^{-3} rad	M_m/M_u	θ_{cm}/θ_u	Fail Mode	M_{SCI}/M_u	Fail Mode	$M_{Eurocode3}/M_u$
10	Test 1	158.1	100	1.01	0.83	1	0.42	1	0.50
12	Test 2	154.5	67	1.07	1.14	1	0.53	1	0.63
12	EP 1-1	181.5	81	1.02	1.02	1	0.48	1	0.55
14	Test 3	181.6	80	0.94	0.77	2	0.59	2	0.63
15	EP 1-2	199.5	46	0.75	0.59	2	0.60	2	0.64
18	EP 1-3	204.4	30	0.88*	N/A*	3	0.74	2	0.79
22	EP 1-4	222.4	20	0.82*	N/A*	3	0.70	2	0.75
25	EP 1-5	225.7	20	0.90*	N/A*	3	0.83	2	0.89

* The model predicts flush bolt fracture prior to flush region yielding, therefore ductility calculation does not apply.

SCI (1995) is very conservative for the thin endplates, predicting ultimate capacities of only about 50% of the observed strength. Even for the 22 and 25mm endplates, the results are still quite conservative at about 70 – 80% of the observed

strength. The Eurocode 3 model with the alternative mode 1 formula does better, with 80 – 90 % predictions for the thicker endplates, but only 50 – 65% predictions for the thinner endplates. Thus, the model Eurocode 3 predictions are also very conservative. This highlights the importance of including strain-hardening and membrane action effects for thinner endplates. To our knowledge, the model in this thesis is the only model for extended endplate connections that explicitly includes these effects. When compared with the Eurocode 3 and SCI models, the thesis ductility model gives far superior predictions for the ultimate moment for the Bernuzzi tests as well as the connection tests in this thesis - even for the connections which are predicted to fail in mode 3. Test EP 1-3 with the 18mm endplate just meets the ductile criteria of 30 milli-radians, so it could be considered a ductile connection. It would however, be considered non- ductile under Eurocode 3 (2005).

7.4.3. Comparison with Test Results from Jenkins et al (1986)



Endplate:	440 long x 200 wide		
Beam:	305 UB 54 – cruciform test		
Column:	254 UC 132		
Bolts:	6 ~ M20 Grade 8.8		
	Endplate t_p (mm)	Endplate f_y (MPa)	Bolt F_{ub} (kN)
Test 4	12	302.5	235
Test 9	15	302.5	235
Test 15	12	302.5	235
Test 4 is 'hand-tight' and test 15 is torqued to proof load			

All dimensions in mm

Figure 7.13 – Endplate Geometry in Jenkins et al (1986)

In this section, the ductility model predictions are compared with experimental test results from Jenkins et al (1986). Jenkins et al reported on six tests with flush endplates and 12 tests with extended endplates. Jenkins et al did not report the moment-rotation curves for some of those extended endplate tests and those are excluded here. In addition, I have excluded the tests with un-stiffened columns since the rotations would include web bucking deformation effects. I have also excluded those tests where the connection failed (prematurely) from tension flange weld fracture, or where the endplate was clearly relatively thick. Of the 12 extended endplate tests therefore, three are presented below for comparison purposes.

The endplate geometries for the tests in Jenkins et al (1986) are given in Figure 7.13. Unfortunately, the endplate yield stress is not reported by the authors; however the material is reported as Grade 43. Grade 43 has a nominal strength of 275 MPa. For hot-rolled sections, I have assumed that the actual strength will be in the order of 115% of the nominal value. Similarly, the bolt ultimate capacity has been assumed based on the grade. The flange and web welds have been assumed as 8mm and 6mm fillet welds.

All three tests are for 305x165x54 beams with 254x254x132UC columns with M20 Grade 8.8 bolts. Test 9 (15mm endplate) failed by flush bolt fracture, while test 4 (12mm endplate, snug-tight bolts) failed by tension flange weld fracture. Test 15 (12mm endplate and pre-tensioned bolts) failed by “plate bending”.

In Figure 7.14 the ductility model prediction is compared with the moment-rotation curves for tests 4 and 15; and the model is compared with the curve for test 9 in Figure 7.15. A difficulty encountered with the published results of Jenkins et al was that the published moment-rotation curves did not extend as far as the reported ultimate connection moment. Thus, the final point in each curve has been extrapolated.

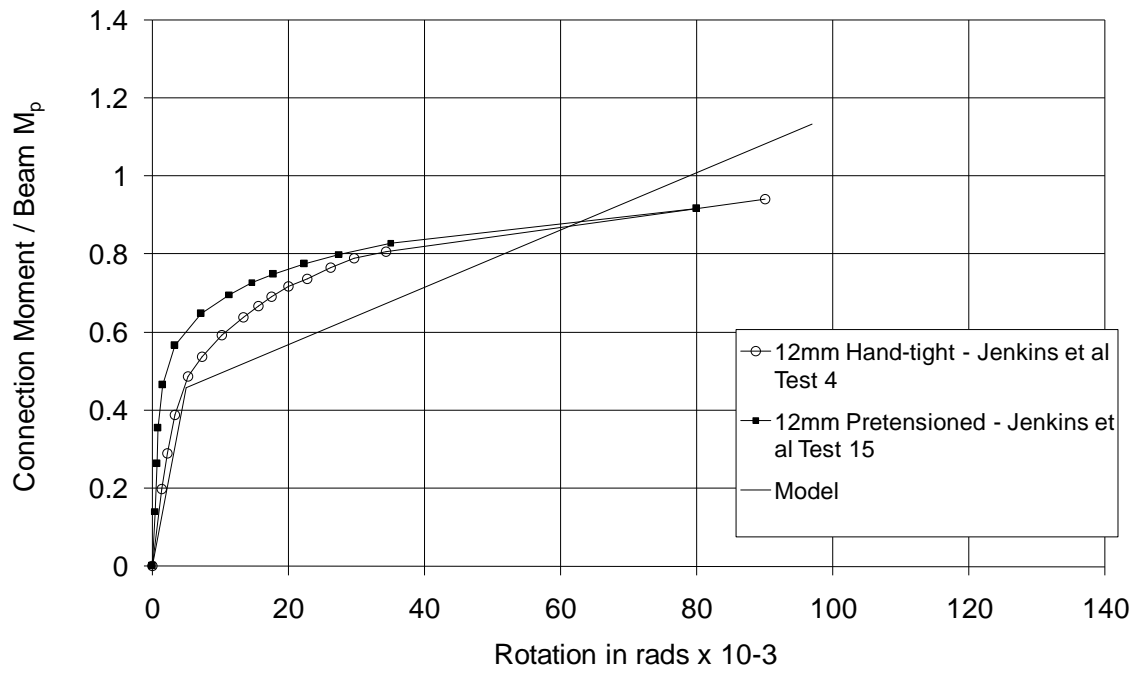


Figure 7.14 – Comparison of Ductility Model with Tests 4 & 15 of Jenkins et al, 1986

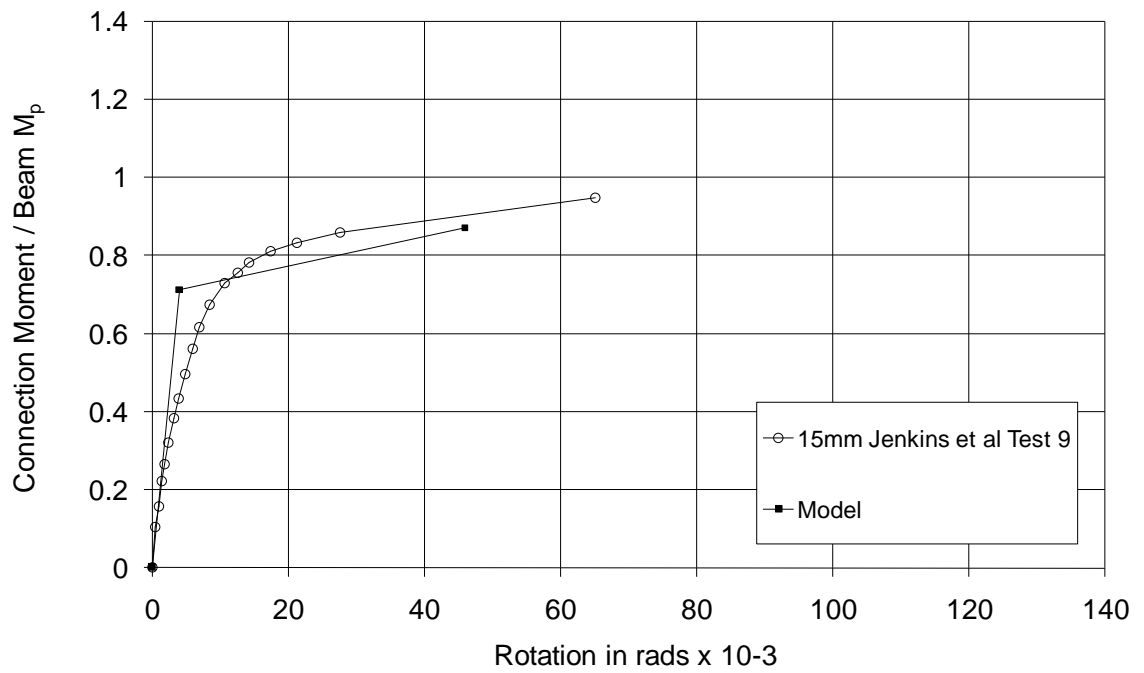


Figure 7.15 – Comparison of Ductility Model with Test 9 of Jenkins et al, 1986

The ultimate rotation is not known with exactitude since it was extrapolated. Nevertheless, the ductility model provides a good prediction of the estimated ultimate rotation in all three tests, as can be seen in Table 7.8.

Table 7.8 – Comparison between Ductility Model and Jenkins et al Test Results

Nominal endplate thickness	Jenkins et al reference	Experimental results			Thesis ductility model		
		M_u kN-m	θ_u 10^{-3} rad	Fail Mode	M_m/M_u	θ_{cm}/θ_u	Fail Mode
12	Test 4	190.5	90	Weld fracture	1.20	1.08	1
12	Test 15	185.5	80	Endplate 'bending'	1.24	1.21	1
15	Test 9	220.0	65	Flush bolt fracture	0.80	0.70	2

Table 7.8 shows that there is some correspondence between the ductility model predictions and the observed ultimate strength in the tests. The correspondence here is not as good as for the other test results available, but this may be because the yield strength value and thicknesses in the model are nominal rather than the actual values. The ductility model however correctly predicts the failure mode for tests 15 and 9. We can infer that if tension weld fracture had not intervened, Jenkins' test 4 would probably have failed by endplate deformation and fracture as well, which is the mode predicted by the model.

8. CONCLUSION

8.1. SUMMARY

A model of the extended endplate behaviour has been developed in this thesis, which allows the prediction of the endplate contribution to the connection rotation in terms of the connection strength (moment capacity) and ductility (rotation capacity). The model presents this prediction as a moment-rotation curve. The extended endplate strength model developed in this thesis is unique in that it addresses the possibility of strain hardening and membrane action in the endplate. These phenomena have been shown in the thesis to be critical for the ductility and strength of thin endplates, but they have not previously been modelled by other researchers of extended endplates. Because the leading models of the day such as the Eurocode model (Eurocode 3, 2005) have not catered for these effects, they seriously underestimate the strength of ‘thin’ extended endplates. Thus, the ductility model leads to the possibility of using much thinner endplates, such as would be appropriate for partial-strength connections.

The model is bi-linear, with the strength and ductility evaluated at two points – the swivel and maximum strain points. The flush region strength behaviour is based on a yield-line analysis of the endplate flush region at the swivel point, and an analysis for a plate supported on three sides and with a central point load, at the maximum strain point. The deformation of the flush region is based on the plate model. The strength and deformation of the extended region is based on uni-axial double-curvature bending of the portion between the bolt line and the weld line, for both the swivel and maximum strain points.

Strain hardening and membrane action are catered for in the model by adjusting the material properties from elastic values to strain-hardening values, and by

applying solutions for the deformation that takes account of large deflections and thick member theory. This makes the model developed here unique.

This thesis model is also unique in that the ductility of the endplate is measured directly by the model in a mechanical analogy. There are existing FEA and mathematical models of the moment-rotation curve, but these tend to be mostly empirical and completely opaque to the user. There are other existing mechanical models of connection strength and stiffness such as Eurocode 3 (2005), but there is currently no direct mechanical model of connection ductility that this researcher is aware of. The mathematical models in the literature that generate moment-rotation curves do provide an indication indirectly of ductility, but these models were not developed specifically for ductility. The Eurocode 3 strength and stiffness models for example, when taken together, can be used to generate a moment-rotation curve. Nevertheless, the authors of Eurocode 3 do not attempt to establish ductility from that curve, but rather introduce a rule of thumb for the adequacy of ductility. Based on the literature, a value of 30×10^{-3} radians was used here to confirm the adequacy of ductility.

The comparisons with the connection tests and published test results in chapter six show that the ductility model provides an excellent assessment of the ultimate rotations of a thin extended endplate connection. As a 'by-product', the model also provides a bi-linear approximation to the moment-rotation curve. The bi-linear approximation to the moment-rotation curve is again quite good for thin endplates with typical geometries. The bi-linear curve cannot be established for thick endplates failing in mode 3, but the ultimate connection moment can still be estimated with reasonable accuracy.

The model developed in this thesis is based on the mechanical elastic and inelastic interaction between the extended endplate, the tension bolts and the beam end adjacent to the endplate. The contributions of the column flange and column web are not taken into account. Thus, the endplate must be 'thin' relative to the column flange, for this model to apply. Similarly, column web buckling and panel shear

must be excluded by the column choice or design of the connection. Bose & Hughes (1995) have shown that when column web buckling supervenes, it leads to non-ductile failure patterns on connections that would otherwise have failed in a ductile manner. The endplate must also be thin relative to the tension bolts for the connection ductility to be maximized and for failure to occur in a safe manner through fracture of the endplate. Nevertheless, an admirable characteristic of the ductility model presented here is that it still provides a means to establish the connection ductility under mode 2 conditions i.e. when there is fracture of either the extended or the flush bolts, after yielding of the flush region.

There are obviously limitations to the endplate geometry for which this ductility model will be applicable, but these are not onerous. The dimensions used for bolt pitch (p_1) and gauge (p_2) around the four tension bolts, in the tested connections, are typical of South African practice. These dimensions, along with the yield strength f_y of the endplate, will tend to have the greatest influence on the connection ductility for a given beam size. Within the middle range of beam sizes (say 203 – 457 depth) on which the test were conducted, and the limitations of typical bolt pitches (90 – 120mm) and gauges (70 – 100mm), the ductility model can be applied with confidence. For these beam sizes, the use of four M20 or M24 tension bolts is probably still feasible in a partial strength connection. It would however depend on such variables as the load, load pattern and the span, as well as the frame layout.

8.2. AREAS FOR FURTHER STUDY

Everyday design is based on nominal values of the endplate and beam yield strength. There is a need for a sensitivity study to establish how the inaccuracies introduced in this manner affect the model predictions, and to establish a means of catering for this when this model is applied to partial-strength frame analysis. The model was based on endplates being thin compared to the column flange, or the column flange being stiffened as in my tests. There is a need to investigate the

column flange thickness limit, for the case where the column flange is not stiffened.

There is a need for further research into the effects of the bolt grip length and such issues as thread diameter versus bolt shank diameter, in estimating the bolt contribution to the connection rotation.

The contribution of the beam end to the joint rotation can be significant, and at the upper limit of thin endplates can even exceed the plate contribution. In this thesis the beam end contribution was added on as an empirical factor. There is a need for further research in this area to determine the beam end contribution, especially after inelastic buckling as would commonly occur in typically sized connections.

There is a need to conduct research and tests for connections of larger beam sizes, say from 533mm depth upwards. The use of only four tension bolts may no longer be feasible for these connections, even at size M30, and the assumed yield line patterns may then no longer apply. Thus, a different model may be required for these larger beam sizes.

The effect of the heat-affected zone in reducing ductility in the region adjacent to the beam flanges was noted in Test 2 in this thesis. There is a need for this aspect to be studied further to estimate what is a reasonable factor of safety to apply to the calculated ductility, in order to adequately cater for this effect.

REFERENCES

Abel, M.S. & Murray, T.M. (1992), “*Analytical and Experimental Investigation of the Extended Unstiffened Moment End-plate Connection with Four Bolts at the Beam Tension Flange*”, Research Report CE/VPI-ST-93/08, Blacksburg, Virginia: Virginia Polytechnic Institute & State University. As revised in 1994.

Adegoke, I.O. and Kemp, A.R., (2006), “Available Ductility in Extended Endplate Connections of Continuous Steel Beams”, *Steel 50 Conference*, Southern African Institute of Steel Construction, Sandton, Johannesburg, 8th-9th November.

Agerskov, H., (1976), “High-Strength Bolted Connections Subject to Prying”, *ASCE Journal of the Structural Division*”, Vol. 102, January, pp. 161-175.

Bahia, C.S., Graham, J. & Martin, L.H., (1981), “Experiments on Rigid Beam to Column Connections Subject to Shear and Bending Forces”, In *Joints in Structural Steelwork*, (Ed. by J.H. Howlett, W.M. Jenkins & R. Stainsby), Pentech Press, London.

Bernuzzi, C. & Zandonini, R. (1990), “Moment-Rotation Response of Extended End Plate Connections”, *Final Report of the International Colloquium on Stability of Steel Structures*, Budapest, Hungary, 155-162.

Bernuzzi, C., Zandonini, R. & Zanon, P. (1991), “Rotational Behaviour of End Plate Connections”, *Costruzioni Metalliche*, n.2, 3-32.

Bose, B. & Hughes, A.F. (1995), “Verifying the Performance of Standard Ductile Connections for Semi-Continuous Steel Frames”, *Proceedings of the Institution of Civil Engineers, Structures & Buildings*, Vol. 110, Nov., pp 441-457.

Brown, N.D. and Anderson, D.A., (2001), “Structural Properties of Composite Major-Axis End-Plate Connections”, *Journal of Constructional Steel Research*, Vol. 57, pp. 327-349.

BS 5950: Part 1 (1990), *Structural use of steelwork in building: Code of practice for design in simple and continuous construction – hot rolled sections*”, British Standards Institution, London.

Dekker, N.W. (1986), “Prediction of the Rotational Stiffness of Endplate Connections” Unpublished M.Eng. thesis, University of Pretoria.

Douty, R.T. and McGuire, W., (1965), “High Strength Bolted Moment Connections”, *ASCE Journal of the Structural Division*”, Vol. 91, April, pp. 101-128.

EN 10002 (1990), Part 1, *Metallic Materials – Tensile Testing – Part 1: Method of test (at ambient temperature)*, CEN, Brussels.

Eurocode 3 (1992), DD ENV 1993-1-1, *Eurocode 3: Design of Steel Structures Part 1.1 General Rules and Rules for Buildings*, British Standards Institute, London.

Eurocode 3 (2005), BS EN 1993-1-8, *Eurocode 3: Design of Steel Structures Part 1-8 Design of Joints*, British Standards Institution, London.

Frye, M.J. and Morris, G.A., (1975), “Analysis of Flexibly Connected Steel Frames”, *Canadian Journal of Civil Engineering*, Vol. 2, (3), pp. 280-291.

Galambos, T.V., and Ravindra, M.K., (1978), “Properties of Steel for use in LRFD”, *ASCE Journal of the Structural Division*”, Vol. 104, September, pp. 1459-1468.

Grundy, P., Thomas, I.R., & Bennetts, I.D., (1980), "Beam-to-Column Moment Connections", *ASCE Journal of the Structural Division*", Vol. 106, January, pp. 313-330.

Jenkins, W.M., Tong, C.S., & Prescott, A.T. (1986), "Moment Transmitting Endplate Connections in Steel Construction, and a Proposed Basis for Flush Endplate Design", *The Structural Engineer*, Vol. 64A, (5), May, pp 121-132.

Kemp. A.R., (1988), "Simplified Modelling of Material Non-linearity in Structural Frames", *The Civil Engineer in South Africa*, Vol. 30, 9, September, pp 425-432.

Kemp, A.R., Dekker, N.W., and Trincherro, P., (1995) "Differences in Inelastic Properties of Steel and Composite Beams", *Journal of Constructional Steel Research*, Vol. 34, No. 2, pp. 187-206.

Kemp, A.R., Byfield, M.P. & Nethercot, D.A. (2002), "Effect of strain hardening on flexural properties of steel beams", *The Structural Engineer*, 80 (8), 29-35.

Krishnamurthy, N. (1978), "A fresh look at bolted end-plate behavior and design", *Engineering Journal*, AISC, Vol. 15, (2), pp. 39-49.

Krishnamurthy, N., Huang, H., Jeffrey, P.K., & Avery, L.K., (1979), "Analytical M- θ curves for end-plate connections", *ASCE Journal of the Structural Division*", Vol. 105, ST1, pp. 133-145.

Krishnamurthy, N., & Oswalt, R.E. (1981), "Bolt head and weld effects in steel connection behaviour", In *Joints in Structural Steelwork*, (Ed. by J.H. Howlett, W.M. Jenkins & R. Stainsby), Pentech Press, London.

Jaspart, J.P. and Maquoi, R., (1992), "Plastic Capacity of End-Plate and Flange Cleated Connections – Prediction and Design Rules", In *Connections in Steel*

Structures II: Behaviour, Strength & Design, (Ed. by R. Bjorhovde, G. Haaijer & J.W.B. Stark), Chicago: American Institute of Steel Construction, pp. 225-235.

Murray, T.M. & Borgsmiller, J.T. (1996), "Strength of Moment End-plate Connections with Multiple Bolt Rows at the Beam Tension Flange". In *Connections in Steel Structures III: Behaviour, Strength & Design*, (Ed. by R. Bjorhovde, A. Colson & R. Zandonini), Oxford: Pergamon.

Nair, R.S., Birkemoe, P.C., & Munse, W.H., (1974), "High Strength Bolts Subject to Tension and Prying", *ASCE Journal of the Structural Division*", Vol. 100, February, pp. 351-372.

Packer, J.A. and Morris, L.J., (1977), "A Limit State Design Method for the Known Region of Bolted Beam-Column Connections", *The Structural Engineer*, 55 (10), 446-458.

Revised Annex J (1994), "*Eurocode 3 Part 1.1 – Revised Annex J: Joints and Building Frames*", European Committee for Standardization, Document CEN/TC 250/SC3-N419E, Brussels.

Roark, R.J. (1965), *Formulas for Stress and Strain*, 4th Ed., McGraw-Hill, New York.

SAISC (1997), *Southern African Steel Construction Handbook*, The Southern African Institute of Steel Construction, 3rd Ed.

SANS 10162 (2005), *The Structural Use of Steel: Part 1- Limit-states design of hot-rolled steelwork*, South African Bureau of Standards, Pretoria.

SANS 2001 (2005), *Construction Works: Part CSI- Structural steelwork*, South African Bureau of Standards, Pretoria.

SCI (1995), “*Joints in Steel Construction: Moment Connections*”, The Steel Construction Institute & The British Constructional Steelwork Association Ltd, Ascot.

Sherbourne, A.N. (1961), “Bolted Beam to Column Connexions”, *The Structural Engineer*, June, pp 203-210.

Sherbourne, A.N. & Lu, F. (1993), “Effect of Axial Restraints on the Deflection of Strain Hardening Beams”, *International Journal of Mechanical Science*, Vol. 35, No. 5, pp. 397-413.

Steel Structures Research Committee (1936), *Final Report*, Dept of Industrial & Scientific Research, HMSO.

Steenhuis, M. (1992), “Frame Design and Economy”, *Proceedings, 1st COST C1 State of the Art Workshop*, Strasbourg, France.

Sturm, R.G., & Moore, R.L. (1937), “The Behaviour of Rectangular Plates under Concentrated Load”, *Journal of Applied Mechanics*, ASME, Vol. 4, (2), Paper A-75.

Surtees, J.O. & Mann, A.P. (1970), “End Plate Connections in Plastically Designed Structures”, Conference on Joints in Structures, University of Sheffield, July.

Tarpy, T.S. and Cardinal, J.W., (1981), “Behavior of Semi-rigid Beam-to-Column End Plate Connections”, In *Joints in Structural Steelwork*, (Ed. by J.H. Howlett, W.M. Jenkins & R. Stainsby), Pentech Press, London.

Timoshenko, S., (1959), *Theory of Plates and Shells*, McGraw-Hill, New York.

Truby, S.F., (1995), "The Development of a Mathematical Model for the Design of Extended End-Plate Connections", Unpublished M.Sc. Eng. Project Report, University of the Witwatersrand.

Weynand, K., Jaspart, J.P., & Steenhuis, M., (1996), "The Stiffness Model of Revised Annex J of Eurocode 3". In *Connections in Steel Structures III: Behaviour, Strength & Design*, (Ed. by R. Bjorhovde, A. Colson & R. Zandonini), Oxford: Pergamon.

Whittaker, D. and Walpole, W.R., (1982), "Bolted End-Plate Connections for Seismically Designed Steel Frames", *Research Report 82-11*, Department of Engineering, University of Canterbury, New Zealand.

Yee, Y.L. and Melchers, R.E., (1986), "Moment-Rotation Curves for Bolted Connections", *ASCE Journal of the Structural Division*", Vol. 112, March, pp. 615-635.

Zandonini, R. & Zanon, P. (1988), "Experimental Analysis of End Plate Connections". In *Connections in Steel Structures: Behaviour, Strength & Design*, (Ed. by R. Bjorhovde, J. Brozzetti & A. Colson), London: Elsevier Applied Science.

Zoetemeijer, P., (1974), "A Design Method for the Tension Side of Statically Loaded, Bolted Beam-to-Column Connections", *Heron*, 20 (1), Delft University, pp. 1-59.

ANNEXURE A

TEST SPECIMEN MATERIAL TESTS

A.1 MATERIAL TEST DATA

Material properties were required for the test sections - the 305 UB 41 and 203 UC 60 sections, as well as for the 10mm, 12mm and 14mm endplates. With the exception of the 10mm connections, the materials all came from single section lengths or plate. Thus, there was a need to determine only one set of properties for each section size/ plate thickness, except the 10mm endplate specimen for Test 1. Off cuts were obtained therefore and used to determine the material properties in tensile tests. Coupons were taken from material off-cuts, flame cutting large pieces then sawing smaller pieces out, and then machining these to the coupon dimensions. Cognisance was taken of the direction of rolling in cutting plate coupons, so that transverse and longitudinal coupons were cut i.e. perpendicular to the rolling grain or parallel to it respectively. Two coupons were taken per beam or column flange (for each flange), and two coupons per beam web. Also four coupons were taken per plate – two in the longitudinal direction and two from the transverse direction.

The tensile tests were carried out in accordance with EN 10002 (1990), using rectangular test pieces conforming to Annex C of that code. Strain was measured using an extensometer with a 100mm gauge length, and the specimens were tested in an Amsler Universal Testing Machine with a force-extension plotter attached. The stress rate was kept at about 3 MPa/sec up to yield, and the strain was kept to about 0.0025/s from the yield point to fracture. We were unable to measure the strain-weakening behaviour because of the likelihood of causing damage to the extensometer, however we did determine the fracture load and so the ultimate stress in each test. The material constants were determined from the graphs, and these are reported here in Table A.1 and summarized in Table 3.2 in chapter 3.

Table A.1 – Test Specimen Material Properties from Tensile Tests

	Coupons				Yield	Yield	Yield	Hard'g	Ult.	Ult.	Young's	Hard'g
	No.	Width	Thick	Area	Load	Stress	Strain	Strain	Load	Stress	Mod E	Mod E _{sh}
		mm	mm	mm ²	kN	MPa	millistrain	millistrain	kN	MPa	GPa	GPa
Column - 203 UC 60												
Flange 1	1	12.76	14.33	182.85	55.0	300.8	1.6	16.6	87.6	479.1	202.4	4.00
	2	12.70	13.97	177.42	51.0	287.5	1.6	13.5	85.0	479.1	208.5	4.10
Flange 2	1	12.60	14.08	177.41	54.0	304.4	1.5	18.6	86.8	489.2	214.7	4.03
	2	12.55	13.65	171.31	52.0	303.5	1.7	17.5	83.0	484.5	212.7	3.23
Web	1	20.27	8.83	178.98	57.5	321.3	1.6	13.6	87.7	490.0	201.1	3.55
	2	20.36	8.93	181.81	63.0	346.5	2.4	10.7	90.8	499.4	202.6	4.46
Beam 1- 305 UB 41												
Flange 1	1	12.60	10.15	127.89	42.0	328.4	1.6	20.6	62.9	491.8	200.4	5.51
	2	12.66	10.41	131.79	42.0	318.7	1.6	15.6	65.8	499.3	210.8	5.84
Flange 2	1	12.55	9.74	122.24	40.0	327.2	1.5	18.8	60.1	491.7	228.2	4.09
	2	12.58	10.34	130.08	42.0	322.9	1.7	16.0	64.6	496.6	199.4	4.91
Web	1	20.62	5.95	122.69	44.0	358.6	1.7	18.8	63.7	519.2	207.5	3.76
	2	20.61	5.95	122.63	45.0	367.0	1.7	23.0	64.8	528.4	213.5	3.88

	Coupons				Yield	Yield	Yield	Hard'g	Ult.	Ult.	Young's	Hard'g
	No.	Width	Thick	Area	Load	Stress	Strain	Strain	Load	Stress	Mod E	Mod E _{sh}
		mm	mm	mm ²	kN	MPa	millistrain	millistrain	kN	MPa	GPa	GPa
Web contd.	3	20.45	5.97	122.09	46.0	376.8	2.0	23.2	64.5	528.3	214.2	3.90
	4	20.48	5.99	122.68	44.0	358.7	1.9	19.3	64.5	525.8	219.1	4.08
10mm	T1 ¹	12.17	9.88	120.24	35.0	291.1	3.0	9.1	63.9	531.4	222.5	6.60
Endplate	T2	13.14	9.88	129.82	39.3	302.3	2.0	11.7	69.0	531.5	217.3	5.66
(Pilot)	L1	12.12	10.01	121.32	38.3	315.7	2.5	13.3	64.9	534.9	195.8	5.52
	L2	12.43	9.45	117.46	36.3	308.6	2.2	12.2	65.1	554.2	212.8	5.57
10mm	L1	20.30	10.15	206.05	69.3	336.3	1.4	13.0	105.3	511.1	199.8	3.36
Endplate	L2	20.28	10.27	208.28	70.0	336.1	1.3	13.3	105.2	505.1	215.8	3.47
(Test 1)	L3	20.42	10.29	210.12	67.5	321.2	2.0	14.1	105.2	500.7	191.1	3.58
12mm	T1	9.48	12.06	114.33	35.0	306.1	1.8	13.7	60.4	528.3	230.0	3.60
Endplate	T2	12.22	11.41	139.43	45.0	322.7	2.0	14.0	74.2	532.2	225.9	5.28
	T3	13.22	11.98	158.38	46.5	293.6	2.0	13.9	78.3	494.4	223.1	4.65
	L1	10.13	12.02	121.76	38.0	312.1	1.8	18.2	60.8	499.3	202.6	4.89

	Coupons				Yield Load kN	Yield Stress MPa	Yield Strain millistrain	Hard'g Strain millistrain	Ult. Load kN	Ult. Stress MPa	Young's Mod E GPa	Hard'g Mod E _{sh} GPa
	No.	Width	Thick	Area								
		mm	mm	mm ²								
12mm contd.	L2	9.47	11.47	108.62	37.0	340.6	1.7	15.1	61.3	564.3	222.2	5.42
	L3	12.81	11.94	152.95	46.5	304.0	1.7	12.6	77.1	504.1	214.8	5.09
	L4	13.01	11.91	154.95	47.0	303.3	1.9	13.3	79.0	509.8	215.1	5.12
14mm	T1	12.90	13.86	178.79	52.0	290.8	1.1	11.6	85.9	480.4	284.3	4.47
Endplate	T2	12.11	13.87	167.97	51.0	303.6	1.2	16.8	80.0	476.5	238.1	4.80
	L1	12.50	13.84	173.00	51.0	294.8	1.8	14.6	82.5	476.9	265.9	3.91
	L2	12.42	13.86	172.14	50.0	290.5	1.8	11.1	82.5	479.3	213.0	5.10

¹T and L in the coupon number represent coupons taken transversely or longitudinally respectively i.e. perpendicular or parallel to the steel rolling direction.